ABSTRACT

Title of Dissertation: LIFETIME AND DISTRIBUTION OF OZONE AND RELATED POLLUTANTS IN THE EASTERN UNITED STATES

Daniel L. Goldberg, Doctor of Philosophy, 2015

Dissertation directed by: Professor Russell R. Dickerson and Professor Ross J. Salawitch, Department of Atmospheric and Oceanic Science

Most major cities in the eastern United States have air quality deemed unhealthy by the EPA under a set of regulations known as the National Ambient Air Quality Standards (NAAQS). The worst air quality in Maryland is measured in Edgewood, MD, a small community located along the Chesapeake Bay and generally downwind of Baltimore during hot, summertime days. Direct measurements and numerical simulations were used to investigate how meteorology and chemistry conspire to create adverse levels of photochemical smog especially at this coastal location.

Ozone (O_3) and oxidized reactive nitrogen (NO_y), a family of ozone precursors, were measured over the Chesapeake Bay during a ten day experiment in July 2011 to better understand the formation of ozone over the Bay and its impact on coastal communities such as Edgewood. Ozone over the Bay during the afternoon was 10% to 20% higher than the closest upwind ground sites. A combination of complex boundary layer dynamics, deposition rates, and unaccounted marine emissions play an integral role in the regional maximum of ozone over the Bay.

The CAMx regional air quality model was assessed and enhanced through comparison with data from NASA's 2011 DISCOVER-AQ field campaign. Comparisons show a model overestimate of NO_y by +86.2% and a model underestimate of formaldehyde (HCHO) by –28.3%. I present a revised model framework that better captures these observations and the response of ozone to reductions of precursor emissions. Incremental controls on electricity generating stations will produce greater benefits for surface ozone while additional controls on mobile sources may yield less benefit because cars emit less pollution than expected.

Model results also indicate that as ozone concentrations improve with decreasing anthropogenic emissions, the photochemical lifetime of tropospheric ozone increases. The lifetime of ozone lengthens because the two primary gas-phase sinks for odd oxygen ($O_x \approx NO_2 + O_3$) – attack by hydroperoxyl radicals (HO_2) on ozone and formation of nitrate – weaken with decreasing pollutant emissions. This unintended consequence of air quality regulation causes pollutants to persist longer in the atmosphere, and indicates that pollutant transport between states and countries will likely play a greater role in the future.

LIFETIME AND DISTRIBUTION OF OZONE AND RELATED POLLUTANTS IN THE EASTERN UNITED STATES

by

Daniel L. Goldberg

Thesis submitted to the Faculty of the Graduate School of the
University of Maryland, College Park, in partial fulfillment
of the requirements for the degree of
Doctor of Philosophy
2015

Advisory Committee:
Professor Russell R. Dickerson, Chair
Research Assistant Professor Timothy P. Canty
Professor Sheryl H. Ehrman, Dean's representative
Adjunct Professor Kenneth E. Pickering
Professor Ross J. Salawitch
Associate Professor Maria Tzortziou

Dedication

To my grandfather, Mark Gurtman, who passed away during my time as a Ph.D. student. Hope this makes you proud!

Acknowledgments

I can't possibly thank every single person involved in this 5-year effort, but I will certainly try!

To my family, Rich Goldberg, Dr. Fran Gurtman, and Ben Goldberg, for their enduring support through this tedious process. To my girlfriend, (almost Dr.) Tracy Singer, for her patience and great attitude that has kept me in good spirits during my time in graduate school.

To my advisors, Dr. Russ Dickerson, Dr. Ross Salawitch, and Dr. Tim Canty for their wisdom and guidance. They provided a tough, but enlightening project that sparked an interest I didn't even know I had.

To the Maryland Department of the Environment, especially George "Tad" Aburn, Michael Woodman, Jennifer Hains, and Joel Dreessen, for financial support for this project. To Susan Wierman and Julie McDill at the Mid-Atlantic Regional Air Management Association (MARAMA), for providing emission datasets that were used to initialize my model simulations.

To all scientists involved in the DISCOVER-AQ Maryland field campaign, especially project investigator Dr. Jim Crawford and project scientist Dr. Ken Pickering.

To the elder graduate students including but not limited to Dr. Hao He, Dr. Chris Loughner, and Dr. Stefan Cecelski for providing guidance towards completing my dissertation. To my classmate Steve Baxter for his guidance and help in my classes. To my fellow graduate students Tim Vinciguerra, Linda Hembeck, Dan Anderson, and Kyle Hosley who have been co-authors on my publications.

To the research staff including, but not limited to Dr. Xinrong Ren, Dr. Dale Allen, Dr. Jeff Stehr, Dr. Lackson Marufu, Dr. Glenn Wolfe, and Dr. Maria Tzortziou for helping me in all aspects of this project.

And last but not least, to the IT support staff, Jeff Henrikson and Dave Yanuk, who have helped troubleshoot computer issues at all hours of the day.

Table of Contents

Table of Figures

Table of Tables

1. Introduction

Tropospheric ozone, in high enough concentrations, causes the premature aging of lungs [Bell et al., 2004], exacerbates asthma in children [McConnell et al., 2002], and stunts the growth of plants [Sandermann, 1996]. To protect human health and agriculture, EPA limits ambient ozone to an 8-hour daily maximum mixing ratio of 70 parts per billion by volume (ppbv) [EPA, 2015a]. Several health studies show deleterious effects from ozone even at low concentrations [Bell et al., 2006; Jerrett et al., 2009; Anenberg et al., 2010; Fann et al., 2011]. Figure 1-1 shows that exposure to mixing ratios above 40 ppbv causes a statistically significant increase in mortality risk.

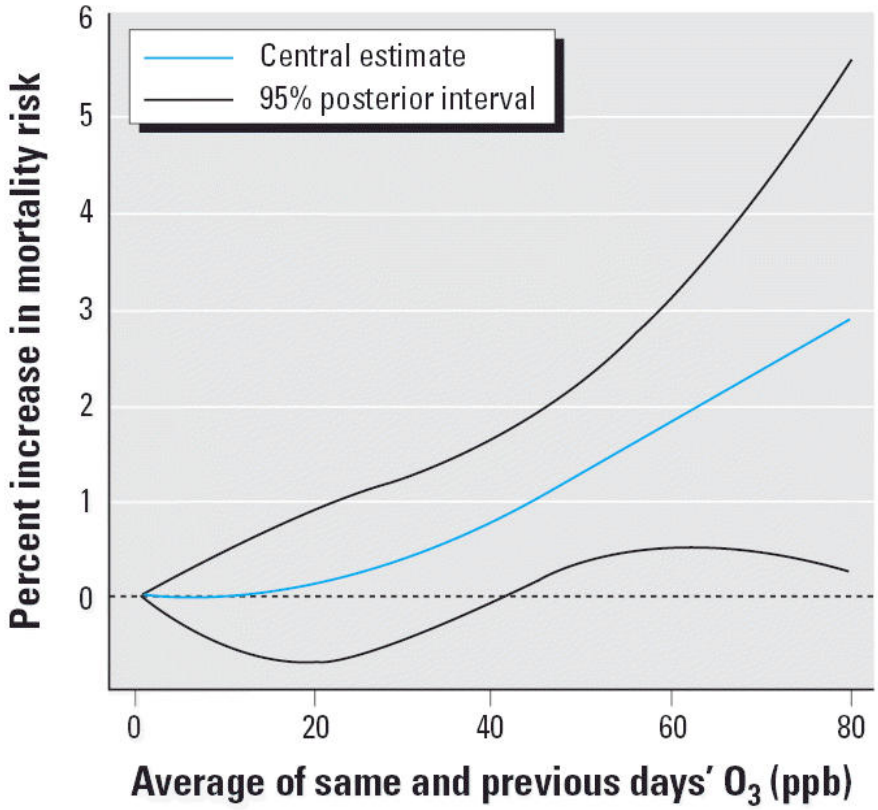

Figure 1-1. Percentage increase in daily non-accidental mortality at various ozone (O_3) mixing ratios. Figure 3 from Bell et al. [2006].

1.1 Current EPA Regulations and Designations

1.1.1 Surface Ozone

Surface ozone air pollution has been a long-standing health issue in the eastern United States [Seinfeld and Pandis, 2006]. Most major cities in the eastern United States including Baltimore, Maryland currently have air quality deemed unhealthy by the EPA under a set of regulations known as the National Ambient Air Quality Standards (NAAQS) [EPA, 2014a]. To be in compliance of the NAAQS for ozone, a metropolitan region may not have an ozone monitor register above 70 parts per billion by volume (ppbv) during the 4th highest annual maximum daily 8-hour average [EPA, 2015a]. The standard was recently revised from 75 ppbv [EPA, 2008] to 70 ppbv in October 2015 [EPA, 2015a]. Most urban and suburban monitors in the northeastern United States exceed the 70 ppbv standard; monitors in southern Connecticut, downwind of New York City exceed 80 ppbv, as shown in Figure 1-2.

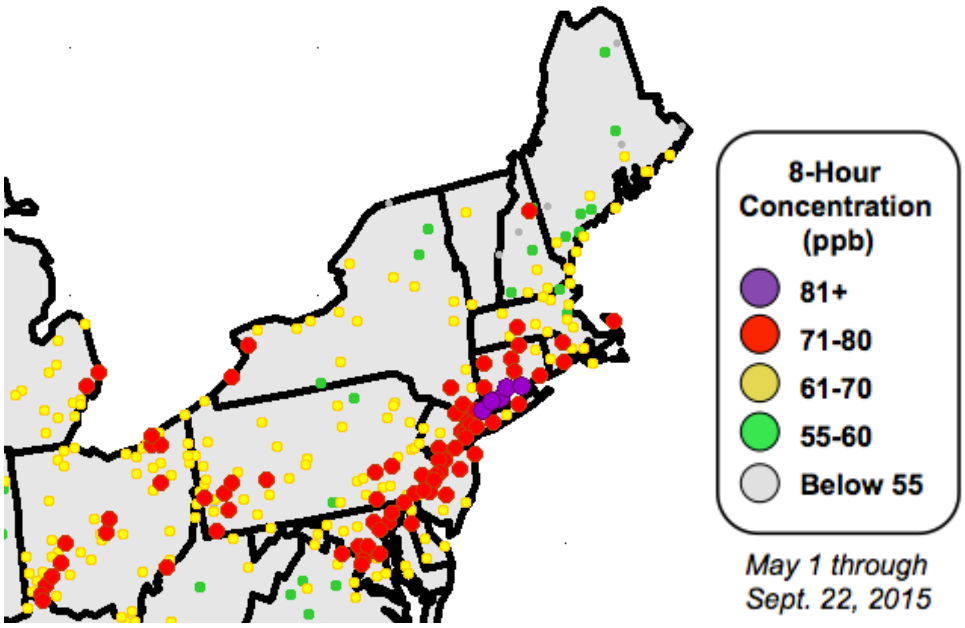

Figure 1-2. Preliminary 2015 4th highest 8-hour maximum ozone mixing ratios at monitors in the northeastern United States. Figure courtesy of Jeff Underhill, NH DES.

In 2011, EPA determined that the Baltimore, MD region is in "moderate non-attainment" of the 75 ppbv ozone 2008 NAAQS [EPA, 2014a]. EPA defines a moderate non-attainment area as a region that has an ozone design value – a 3-year running mean of the 4th highest annual maximum daily 8-hour average – between 86 and 100 ppbv [EPA, 2008]. In 2011, the highest ozone design value for the Baltimore region was 93 ppbv [EPA, 2015b]. EPA required the State of Maryland to demonstrate that the non-attainment region will be in attainment of the NAAQS (i.e., 75 ppbv) within six years of being designated – in this case, by the end of 2017 – by submitting a State Implementation Plan (SIP) [EPA, 2014a].

As of October 2015, there was a clean data determination for the area when all monitors registered ozone design values below the 75 ppbv standard; the Baltimore metropolitan area is no longer in violation of the NAAQS for ozone [Michael Woodman, personal communication]. The recently revised standard, from 75 ppbv [EPA, 2008] to 70 ppbv in October 2015 [EPA, 2015a], places the metropolitan area back into non-attainment. Preliminary 2015 ozone design values as of September 30, 2015 are shown in Table 1-1.

Table 1-1. Observed 2011 and 2015 (preliminary) ozone design values (ppm) for monitoring sites located in Maryland. Red shading indicates that the site is in non-attainment of the 70 ppbv NAAQS for ozone; green indicates attainment. Table courtesy of Michael Woodman, Maryland Department of the Environment.

Monitor Location	2011 Design Value (ppm)	2015 Preliminary Design Value (ppm)
Davidsonville	0.087	0.069
Padonia	0.082	0.071
Essex	0.084	0.068
South Carroll	0.079	0.067
Fair Hill	0.086	0.073
Southern Maryland	0.083	0.066
Frederick Airport	0.079	0.067
Edgewood	0.090	0.071
Aldino	0.082	0.070
Millington	0.082	0.069
Rockville	0.077	0.068
Hagerstown	0.075	0.065
PG Equestrian Center	0.087	0.069
Piney Run	0.075	0.064
Calvert	0.083	0.068
HU-Beltsville	0.082	0.068
Furley	0.075	0.065

1.1.2 Particulate Matter

Particulate matter with a diameter less than 2.5 micrometers (PM2.5) poses a similar health hazard. Microscopic particles can infiltrate deep inside a human's lungs; potential symptoms include increased respiratory symptoms, decreased lung function, aggravated asthma and sometimes more serious effects such as heart attacks [EPA, 2013a]. Franklin et al. [2007] observed a 1.21% increase in all-cause mortality with a 10 $\mu g/m^3$ increase in previous day's PM2.5. The magnitude of these associations is more than triple than recently reported for PM10, suggesting that combustion and traffic related particles are more toxic than larger sized particles [Franklin et al., 2007]. PM2.5 can also contribute to haze and reduced visibility, a concern at national parks and wilderness areas [EPA, 2013a]. The current standard for PM2.5 is 12 $\mu g/m^3$ annual mean

averaged over three years and 35 μg/m^3 in the 98% percentile averaged over three years [EPA, 2013a]. While PM2.5 can be a serious issue, the Baltimore-Washington metropolitan region is in attainment with EPA's 2006 standard [EPA, 2014c]. PM2.5 still remains an issue for the nearby Philadelphia and New York City metropolitan areas as well as the San Joaquin Valley in California and the Salt Lake Valley in Utah [EPA, 2014c].

1.2 Trends in Air Quality

There has been a dramatic decline in the number of days exceeding the NAAQS for ozone in the eastern United States, as seen in Figure 1-3. In the early 1980's, the Baltimore metropolitan region exceeded a 75 ppbv threshold between sixty and eighty days per year – essentially every other day during the summer months. By 2014, the same region exceeded a 75 ppbv threshold less than ten days per year.

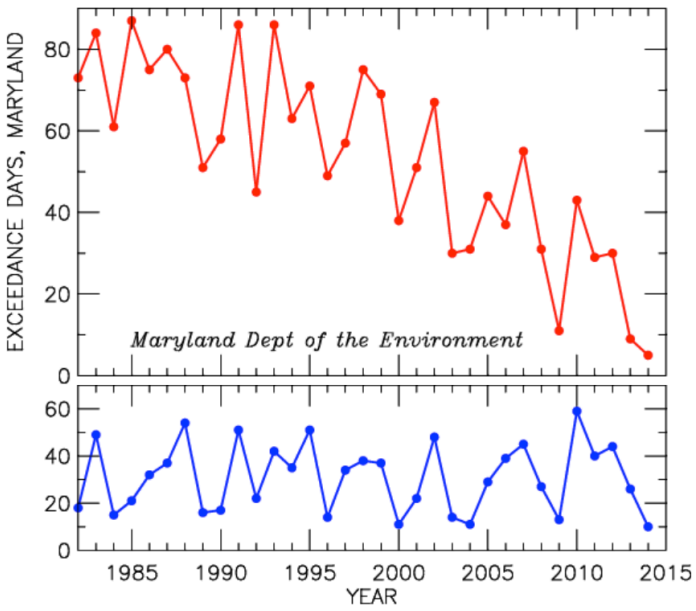

Figure 1-3. Data from the Maryland Department of the Environment (MDE) showing (top) the number of days per year when 8-hour maximum daily ozone exceeds a 75 ppbv threshold and (bottom) the number of days per year when temperature at the BWI airport is above 90° F (32.2° C). Figure courtesy of Ross J. Salawitch.

The sharp decline in exceedance days is a result of successful emission reduction strategies enforced by EPA under the Clean Air Act. These policies initiated a decline in the ambient concentrations of the NO_x (NO_x=NO+NO_2) and volatile organic compounds (VOCs); a few of the most successful policies are outlined here. In 1990, the Clean Air Act Amendments imposed regulations that required car manufacturers to improve the efficiency of catalytic converters in cars and gasoline refineries to reformulate gasoline to contain fewer VOCs [EPA, 1991]. In 2002, EPA capped emissions of NO_x from power plants under the NO_x SIP Call [EPA, 2002]. When the legislation expired in 2008, a similar program under the Clean Air Interstate Rule (CAIR) was enacted [SourceWatch, 2010]; this program is responsible for the significant decline in SO_2 emissions in the late 2000s. The Cross-State Air Pollution Rule (CSPR) is scheduled to replace CAIR [EPA, 2015c]. Figure 1-4 shows the reductions in the emission of SO_2, NO_x, and CO_2 since 1995 in Maryland and Pennsylvania.

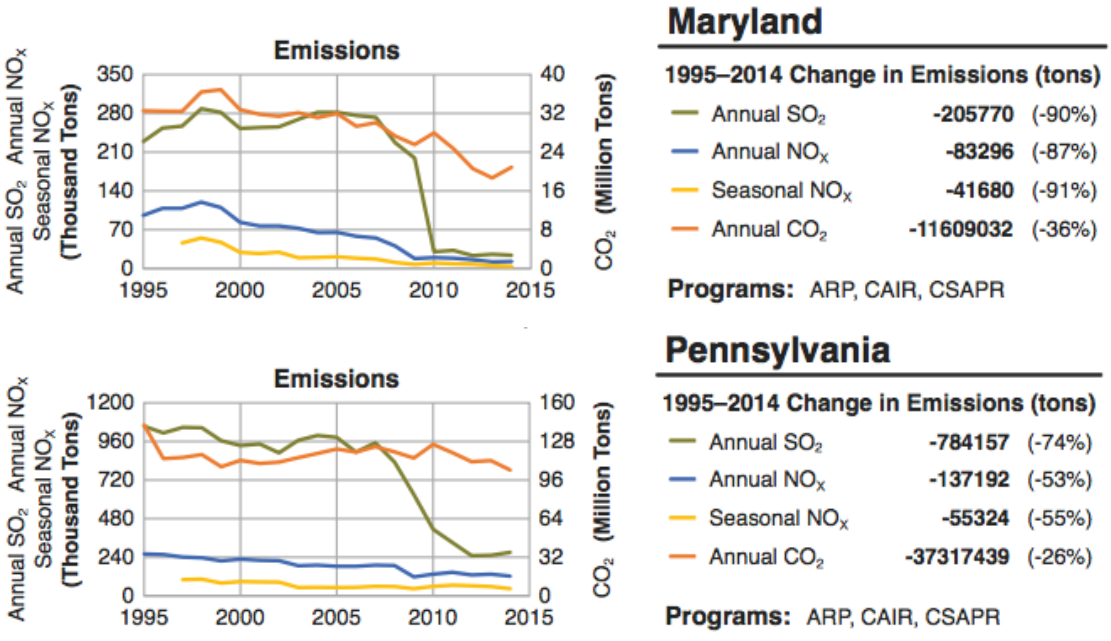

Figure 1-4. Changes in Emissions of SO_2, NO_x, Seasonal (Mar – Oct) NO_x, and CO_2 from power plants in Maryland and Pennsylvania between 1995 and 2014. Figure obtained from: http://www2.epa.gov/airmarkets.

1.3 Surface Ozone Photochemistry & Air Pollution Meteorology

High concentrations of surface ozone typically occur due to favorable meteorological conditions – hot temperatures, clear skies, and a subsidence inversion – and substantial ozone precursor (i.e., NO_x and VOC) emissions, generated locally as well as advected to the region during strong westerly transport conditions [Ryan et al., 1998; He et al., 2013a]. Peaks in surface ozone are highest just downwind of major metropolitan areas due to the enhanced emissions from the metropolitan city centers [Kleinman et al., 2000]. This has been shown in many air quality model simulations [Yegorova et al., 2011; Castellanos et al., 2011] and has been verified by ground monitoring stations [EPA, 2015b]. In the Baltimore-Washington region there are complex interactions that arise with the influence of the Chesapeake Bay breeze [Loughner et al., 2011; Stauffer et al., 2012; Stauffer and Thompson, 2013; Goldberg et al., 2014; Loughner et al., 2014], which will be discussed in Chapter 2.

NOx and VOCs emitted by natural and anthropogenic sources, photochemically react to create ozone [Crutzen, 1970; Seinfeld and Pandis, 2006]. This classifies ozone at the surface as a secondary pollutant: a chemical produced in the atmosphere rather than emitted directly into it [Jacobson, 2002]. The first step of surface ozone formation is the oxidation of VOCs or CO by the hydroxyl radical (OH) – primarily a product of $O(^1D)$ reacting with water – to create the peroxy radical (HO_2); $O(^1D)$ is generated from the photolysis of ozone. Table 1-2 displays the global budget of the OH radical.

Table 1-2. Free Tropospheric Budget for OH radicals. From Table 3 of Ridley et al. [1992].

Reaction	Rate, 10^5 cm^{-3} s^{-1} 24-hour Average	%	Solar Noon	%
Production				
$H_2O + O(^1D) \rightarrow OH + OH$	4.73	39.8	18.88	47.8
$HO_2 + NO \rightarrow OH + NO_2$	2.79	23.4	8.15	20.6
$H_2O_2 + h\nu \rightarrow OH + OH$	2.04	17.1	6.02	15.2
$HO_2 + O_3 \rightarrow OH + 2O_2$	1.98	16.6	5.45	13.8
$CH_3(OOH) + h\nu \rightarrow CH_3O + OH$	0.36	3.0	1.04	2.6
Destruction				
$OH + CO \rightarrow CO_2 + H$	5.82	49.0	19.21	48.7
$OH + CH_4 \rightarrow CH_3 + H_2O$	2.11	17.8	6.95	17.6
$OH + CH_3(OOH) \rightarrow CH_3O_2 + H_2O$	0.84	7.1	2.77	7.0
$OH + H_2O_2 \rightarrow HO_2 + H_2O$	0.77	6.5	2.55	6.5
$OH + CH_2O \rightarrow CHO + H_2O$	0.66	5.4	2.10	5.3
$OH + H_2 \rightarrow H + H_2O$	0.59	5.0	1.94	4.9
$OH + HO_2 \rightarrow H_2O + O_2$	0.54	4.5	2.11	5.3
$OH + O_3 \rightarrow HO_2 + O_2$	0.51	4.3	1.68	4.2
$OH + NO_2 (+M) \rightarrow HNO_3 (+M)$	0.05	0.4	0.16	0.4

Once the HO_2 radical is formed, it can react with a NO molecule to oxidize it to NO_2. At wavelengths hν < 420 nm (i.e., primarily ultraviolet radiation), NO_2 will photodissociate into NO and $O(^3P)$. The $O(^3P)$ atom will quickly react with O_2 to create O_3. The rate-limiting step for ozone formation is the HO_2 + NO reaction. A summary of ozone formation reactions from CO and CH_4 are shown below [Seinfeld and Pandis, 2006].

	$CH_4 + OH \rightarrow CH_3 + H_2O$	
	$CH_3 + O_2 + M \rightarrow CH_3O_2 + M$	
	$CH_3O_2 + NO \rightarrow CH_3O + NO_2$	
	$CH_3O + O_2 \rightarrow HCHO + HO_2$	
	$HCHO + h\nu \rightarrow H + HCO$	
$CO + OH \rightarrow CO_2 + H$	$HCO + O_2 \rightarrow HO_2 + CO$	
$H + O_2 + M \rightarrow HO_2 + M$	$H + O_2 + M \rightarrow HO_2 + M$	
$HO_2 + NO \rightarrow NO_2 + OH$	$3\ (HO_2 + NO \rightarrow NO_2 + OH)$	
$NO_2 + h\nu \rightarrow NO + O(^3P)$	$4\ (NO_2 + h\nu \rightarrow NO + O(^3P)$	
$O_2 + O(^3P) \rightarrow O_3$	$4\ (O_2 + O(^3P) + M \rightarrow O_3 + M)$	
Net: $CO + 2O_2 + h\nu \rightarrow CO_2 + \boldsymbol{O_3}$	$CH_4 + 8O_2 + h\nu \rightarrow CO + H_2O + 2OH + \boldsymbol{4O_3}$	

The stratospheric-tropospheric exchange (STE) of ozone can be an important contributor to the natural background ozone concentrations. The natural background for surface ozone in the eastern United States is between 10 – 20 ppbv during the summer months [Mickley et al., 2001].

1.4 Chemical Transport Models

Scientists use air quality models such as the Community Multiscale Air Quality (CMAQ) model [Byun and Schere, 2006] and the Comprehensive Air Quality Model with Extensions (CAMx) [ENVIRON, 2014] to simulate tropospheric ozone. Both models can successfully predict summertime 8-hour maximum tropospheric ozone mixing ratios to within 20% in the United States [Koo et al., 2015].

Policymakers use air quality models to determine if certain regulation scenarios will allow certain locations to be in future compliance with the air quality regulations. It is therefore critical to verify that the models are accurately simulating the atmosphere. We can analyze the reproducibility of the models by comparing observations to the model simulations.

1.5 Observational Data

1.5.1 Surface data: MDE and CASTNET Monitoring Networks

The Maryland Department of Environment (MDE) currently operates twenty-six air-monitoring sites measuring ground-level concentrations of criteria pollutants and air toxics. Although monitoring takes place statewide, most of the stations are concentrated in urban/industrial areas, which have the highest population and number of pollutant sources. For a list of monitoring locations in Maryland, see Figure 1-5 on the next page.

Figure 1-5. Monitoring Locations. Figure courtesy of MDE

In addition, EPA's CASTNET (Clean Air Status and Trends Network) [AMEC, 2013] program operates two sites in Maryland: at the USDA Beltsville Agricultural Research Center (BARC) and Blackwater at the Blackwater National Wildlife Refuge (NWR) on the Eastern shore; both are denoted as white circles on Figure 1-5. As of January 2013, there are 90 CASTNET sites located in or near rural areas or sensitive ecosystems across 39 states and Ontario, Canada. These sites measure ambient ground-level ozone concentrations as well as dry deposition fluxes of nitrogen and sulfur species.

1.5.2 DISCOVER-AQ

During the month of July 2011, the National Aeronautics and Space Administration (NASA) conducted a comprehensive air quality field study, Deriving Information on Surface conditions from COlumn and VERtically resolved observations relevant to Air Quality (DISCOVER-AQ) [Crawford et al., 2014], in the States of Maryland, Delaware and Virginia to investigate air quality with the primary goal of providing data to better interpret observations from current and future satellites for air

quality applications. In conjunction with DISCOVER-AQ, NASA conducted the oceanographic field campaign GEO-CAPE CBODAQ (Geostationary Coastal and Air Pollution Events-Chesapeake Bay Oceanographic Campaign with DISCOVER-AQ), to address questions related to both estuarine biogeochemical processes as well as atmospheric pollution over the Chesapeake Bay urban estuarine environment [Tzortziou et al., 2013]. A depiction of the field campaign is shown in Figure 1-6 and a detailed description of the modes, locations, types, and days of observations is provided in Table 2-1 in Chapter 2.

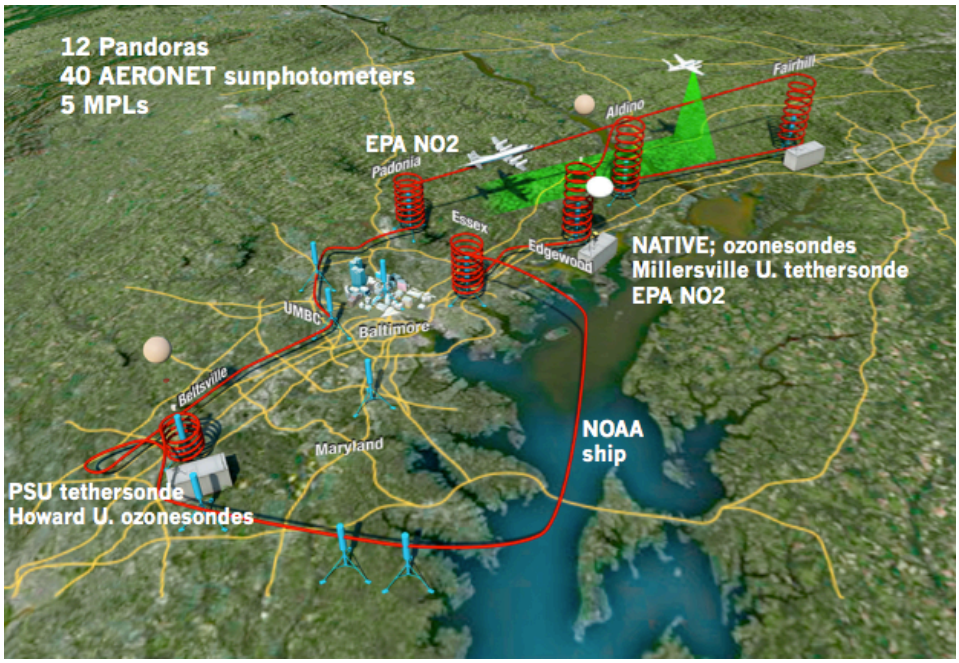

Figure 1-6. The DISCOVER-AQ Maryland field experiment during July 2011. Figure courtesy of Kenneth Pickering, NASA GSFC and James Crawford NASA LaRC.

1.5.3 RAMMPP

The Regional Atmospheric Measurement, Modeling and Prediction Program (RAMMPP) is a joint mission between the University of Maryland and MDE to understand the regional air quality in Maryland. A Cessna 402B aircraft leased by the

University of Maryland measures concentrations of trace gases (O_3, SO_2, NO_2, CO), aerosol optical depth, black carbon concentration and meteorology (temperature, relative humidity, pressure) between the surface and 3000 m during particularly poor air quality days in the Maryland region [He et al., 2013a]. The ultimate goal of this program is to understand the chemistry and transport of atmospheric pollutants into the Maryland region.

1.5.4 NASA Satellites

Satellite sensors can play an important role measuring column content in large spatial dimensions. Satellites are becoming increasingly useful due to improved retrieval algorithms. The Ozone Monitoring Instrument (OMI) on the Aura satellite can measure atmospheric constituents such as vertical column O_3, NO_2, SO_2, BrO, OClO, and aerosol characteristics from its low-Earth orbit (NASA) [Levelt et al., 2006]. Satellite data can be extraordinarily useful for understanding spatial patterns in atmospheric composition, particularly using a combination of different satellite sensors flying on different orbits and integration of satellite data with ground-based observations and air-quality models.

1.6 Description of Surface Measurements

1.6.1 Ozone

At ground-based measurement sites, such as the MDE air monitoring network, ozone is typically measured by UV absorption [Bowman and Horak, 1972; Oltmans, 1981]. A UV photometric analyzer determines ambient concentration by measuring the attenuation of UV radiation emitted at 254 nm by a mercury (Hg) lamp (i.e., Beer-Lambert Law). There are two optical benches in the analyzer: one measures the attenuation of the sample gas, while the other establishes a “zero” using a reference gas

that is scrubbed of O_3; refer to Figure 1-7 for a schematic. The solenoid switches every 10 seconds to rotate which optical bench is measuring the sample gas. Typical mixing ratios at the surface during the summer in the Baltimore / Washington region vary from 5 ppbv pre-sunrise to 120 ppbv during the afternoons of the most polluted days. Typical 8-hour maximums can often exceed the 70 ppbv EPA standard.

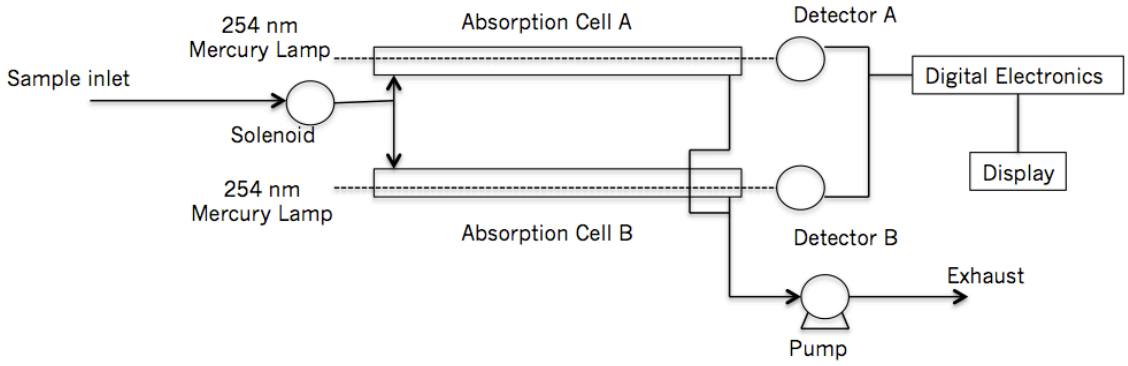

Figure 1-7. Schematic of the UV absorption technique used to measure ozone concentrations

1.6.2 Reactive oxidized nitrogen (NO and NO_y)

Nitric oxide (NO) is typically measured via a chemiluminescence technique [Fehsenfeld et al., 1987]. The NO in the sample gas reacts in a chamber with excess O_3 to form NO_2 in an excited state. The excited NO_2 releases a photon as it reverts to the ground state. A detector is able to identify the strength of the emission and correlates it to a concentration of excited NO_2 and via the stoichiometric 1:1 ratio. If available, an external molybdenum catalyst heated to 350° C can be added. At the high temperature, the catalyst reduces all reactive oxidized nitrogen species (NO_2, NO_3, HNO_3, $2 \times N_2O_5$, HONO, peroxyacetyl nitrates (PANs), organic nitrates ($RONO_2$), and particulate nitrate) to NO and non-reactive byproducts [Fehsenfeld et al., 1987]. Using a solenoid, sample air bypasses the molybdenum converter every 10 minutes measuring NO, while the following 10 minutes it passes through the molybdenum converter measuring NO_y. To

obtain a zero, the sample gas is diverted to a zeroing chamber, where the NO_2 releases a photon before being directed into the measuring chamber. The NO/NO_y analyzer is usually zeroed for a small portion of each hour to adjust the instrument calibration based on the drift of the instrument. The NO/NO_y analyzer can also be calibrated in-situ using a NO, NO_2, and n-propyl nitrate (NPN) standard reference material (SRM). Typical concentrations of NO at the surface during the summer in the Baltimore / Washington region vary from 0.1 ppbv during the late afternoon to 1.5 ppbv after the morning rush hour around 9 AM. Typical concentrations of NO_y vary from 1 ppbv during the late afternoon to 10 ppbv after the morning rush hour.

2. Chesapeake Bay Ozone

2.1 Introduction

Air quality models such as the CMAQ model indicate decidedly higher ozone near the surface of large interior waters bodies such as the Great Lakes and Chesapeake Bay (e. g., [Godowitch et al., 2008]). In order to test the validity of the model output and to determine whether coastal areas have worse air quality, we performed surface measurements of ozone (O_3) and total reactive nitrogen (NO_y) on the 26-m Delaware II NOAA Small Research Vessel experimental (SRVx), deployed in the Chesapeake Bay for ten daytime cruises in July 2011. This work has been published in the February issue of *Atmospheric Environment*. The objectives of this section are to:

- Compare ozone observations over the Bay to nearby land areas
- Determine if ozone concentrations are indeed higher over the Bay
- Determine if known meteorological and chemical processes can explain the observed differences
- Investigate whether model grid resolution plays a role in determining the simulated surface ozone concentrations over the Bay
- Investigate NO_y observations to determine if this group of precursors is accurately predicted by the model simulations

2.1.1 Previous Field Campaigns over Interior Water Bodies

A study by Angevine et al. [2004] showed the importance of ozone transport along coastal regions. Measurements of ozone over the southern Great Lakes during a 2007 summer field campaign show higher concentrations of ozone over the lakes than

over the adjacent land with the biggest difference detected at night [Levy et al., 2010]. A similar study was conducted over Lake Michigan in the summers of 1990 and 1991, where O_3 and NO_x were monitored from aircraft [Luria et al. 1992]. High levels of ozone were shown only at the lowest levels of the boundary layer, which they attribute to a lack of vertical mixing over the lake [Dye et al. 1994]. An experiment in 2003 measured ozone at the Chesapeake Bay Lighthouse, located on an island 15 miles (~25 km) to the east of the entrance to the Chesapeake Bay, as a means to test ozone monitoring on ocean buoys and towers [Hintsa et al., 2004]. This field campaign found ozone at the surface consistently exceeding 80 ppbv during an air quality episode from June 24 - 28, 2003. Wentworth et al., [2015] analyzed the impact of the Lake Ontario breeze on ozone and nitrogen oxide mixing ratios in the Toronto metropolitan area; the study found that days with lake breezes enhanced surface ozone mixing ratios.

2.1.2 DISCOVER-AQ and GEO-CAPE CBODAQ field campaigns

During the month of July 2011, the National Aeronautics and Space Administration (NASA) conducted a comprehensive air quality field study, DISCOVER-AQ [Crawford et al., 2014], in the Washington, DC – Baltimore, MD metropolitan area and over the Chesapeake Bay to investigate air quality with the primary goal of providing data to better interpret observations from current and future satellites for air quality applications. In conjunction with DISCOVER-AQ, NASA conducted the oceanographic field campaign GEO-CAPE CBODAQ (Geostationary Coastal and Air Pollution Events-Chesapeake Bay Oceanographic Campaign with DISCOVER-AQ), to address questions related to both estuarine biogeochemical processes as well as atmospheric pollution over the Chesapeake Bay urban estuarine environment [Tzortziou et al., 2013]. There were

seven instrument platforms during the field campaign. A detailed description of the modes, locations, types, and days of observations is provided in Table 2-1.

Table 2-1. Modes of measurement during Phase I of the DISOVER-AQ campaign in the Baltimore-Washington region.

Mode of Measurement	Trace Gases Measured	Location	Days in which Active during July 11, 2011 through July 20, 2011
NASA P3-B	O3, NO, NO2, PNs, ANs, HNO3, NOy, CO, CH4, CH2O, CO2, VOCs		July 11, July 14, July 16, July 20
UC-12 King Air	Column O3, NO2, CH2O		July 11, July 14. July 20
Cessna 402B	O3, SO2, CO, NO2		July 11, July 18, July 20
MDE Ground Stations	O3, NO, NOy, PM2.5, CO, SO2	Aldino, MD, Beltsville, MD, Edgewood, MD, Essex, MD, Fairhill, MD, Padonia, MD	Every day
Pandora	Column NO2	Aldino, MD, Beltsville, MD, Edgewood, MD, Essex, MD, Fairhill, MD, Padonia, MD, College Park, MD, Catonsville, MD, SRVx NOAA Vessel	Every day
Ozonesondes	O3	Edgewood, MD	Every day
SRVx NOAA Research Vessel	O3, NO, total NOy	see Figure 1	Every day

This paper focuses on observations from the 26-m Delaware II NOAA Small Research Vessel experimental (SRVx; also referred to as "boat") deployed in the Chesapeake Bay as part of the CBODAQ campaign from July 11 - 20, 2011.

2.2 Materials and Methods

2.2.1 Measurements description

The SRVx was equipped with a Thermo Environmental Model 49 UV photometric ozone (O_3) analyzer and a modified Thermo Environmental Model 42C chemiluminescence nitric oxide (NO) analyzer retrofitted with an external molybdenum catalyst to also measure total reactive nitrogen (NO_y) [Delany et al., 1982]. The NO_y analyzer was zeroed for 10 minutes each hour during the campaign and measurements were adjusted based on the drift of the instrument. The NO_y analyzer was calibrated in-situ by Dr. William Thorn III on July 19, 2011 using a NO_2 standard reference material (SRM) from the National Institute of Standards and Technology (NIST).

2.2.2 Model description

In this study, we use EPA's Community Multiscale Air Quality (CMAQ) [Byun and Schere, 2006] model Version 5.0, driven off-line by output from the Weather Research and Forecasting (WRF) model Version 3.3 [Skamarock et al., 2008] to simulate

the state of the atmosphere covering the entire months of June and July 2011; Dr. Christopher Loughner performed the simulations. Passing the meteorology into an air quality model at a high temporal resolution or running the chemistry online within a meteorological model is preferable, but requires significantly more computational resources [Grell et al., 2004].

The WRF and CMAQ model simulations are at 36, 12, 4, and 1.33 km resolution in the area of interest with 34 verticals levels from the surface to 100 mbar and 16 levels within the lowest 2 km in order to accurately simulate boundary layer processes. The four model domains are shown in Figure 2-1. The 1.33 km model domain covers the Baltimore-Washington metropolitan region and nearby Chesapeake Bay.

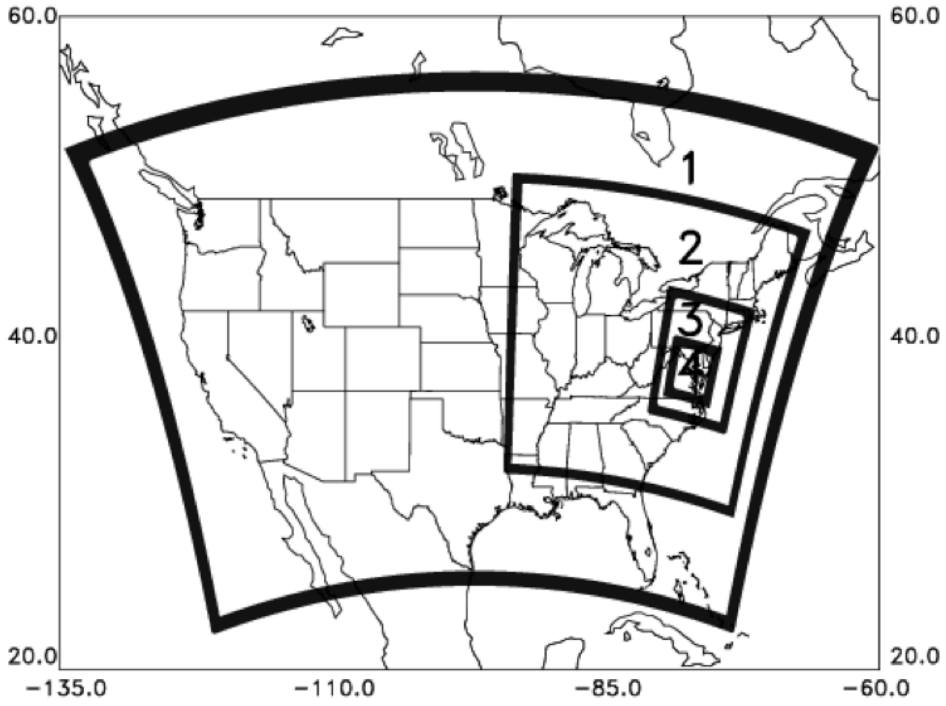

Figure 2-1. CMAQ and WRF model domains. (1) 36 km, (2) 12 km, (3) 4 km, (4) 1.33 km

The North American Regional Reanalysis (NARR) is used for the model initial and outermost lateral boundary conditions in WRF. The Multi-scale Ultra-High

Resolution (MUR) dataset was used to set the sea surface temperatures. The WRF model was re-initialized every 3 days and run in 3.5 day increments. The first 12 hours of each simulation was thrown out (i.e., not passed to CMAQ). WRF model output is input into the Meteorology-Chemistry Interface Processor (MCIP; Otte and Pleim, 2010) to create meteorological input fields for CMAQ. Chemical initial and boundary conditions come from a MOZART-4 simulation [Emmons et al., 2010]. The Carbon-Bond-05 (CB05) gas-phase chemical mechanism [Yarwood et al., 2005] was used in CMAQ. The CMAQ and WRF simulations began May 24, 2011, which allows ample spin-up time for our comparison in mid-July.

Anthropogenic emissions input files for CMAQ are created with the Sparse Matrix Operator Kernel Emissions (SMOKE) modeling system [Houyoux and Vukovich, 1999]. We use a projected 2012 emissions inventory because a 2011 emissions inventory was not yet available when the simulations were performed. Annual projected point and countywide area emissions are temporally distributed based on the time of day, day of the week, and season based on temporal surrogates from the EPA. Mobile emissions estimates from cars, trucks, and motorcycles are computed with the Motor Vehicle Emission Simulator (MOVES 2010a) [Kota et al., 2012]. Point sources are vertically distributed based on the meteorology, stack height, and the temperature and velocity of the emissions exiting the stack. Biogenic emissions are calculated using Biogenic Emissions Inventory System (BEIS) and lightning NO_x emissions and based on Allen et al. [2012]; both are calculated in-line within the CMAQ model. BEIS is based on the same land-use types used by WRF.

2.3 Results

2.3.1 Observational Comparisons: Ozone

The SRVx was deployed in the Chesapeake Bay for ten daytime cruises during the DISCOVER-AQ Maryland campaign extending from July 11, 2011 through July 20, 2011. This overlapped with four flights of the NASA P3-B (a four-engine turboprop capable of long duration flights of 8-12 hours), three flight days (2 flights per day) of the UC-12B King Air (a twin-engine turboprop capable of 6 hour flights), and three flight days (2 flights per day) of the University of Maryland (UMD) Cessna 402B (a twin-piston engine, unpressurized aircraft) (Table 2-1). The SRVx docked each night in Annapolis, MD and had different cruise route each day (Figure 2-2).

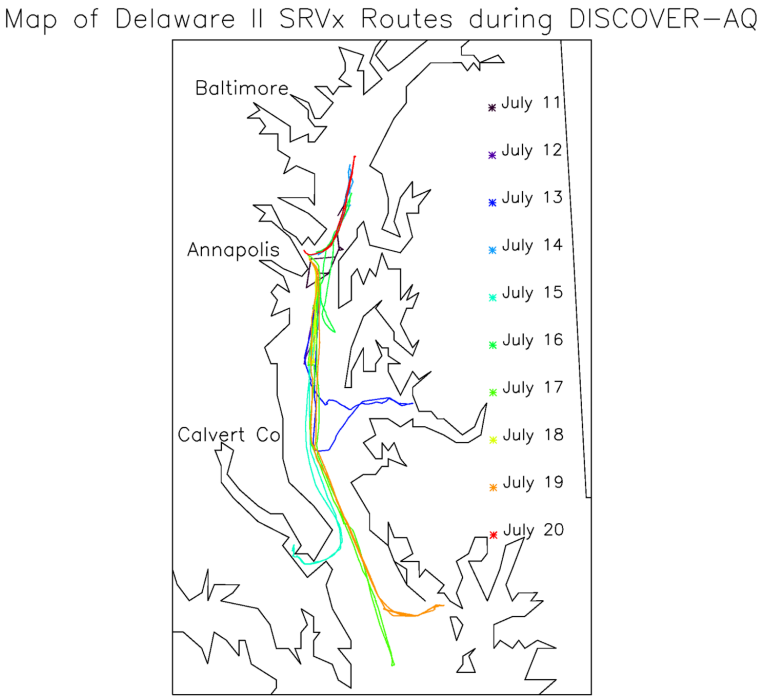

Figure 2-2. Map of NOAA Delaware II SRVx routes from July, 11, 2011 through July 20, 2011

The instruments were running while the SRVx was in port overnight in Annapolis, MD, but the data are subject to frequent local emissions. A time series of O_3

for the 10-day period can be seen in Figure 2-3.

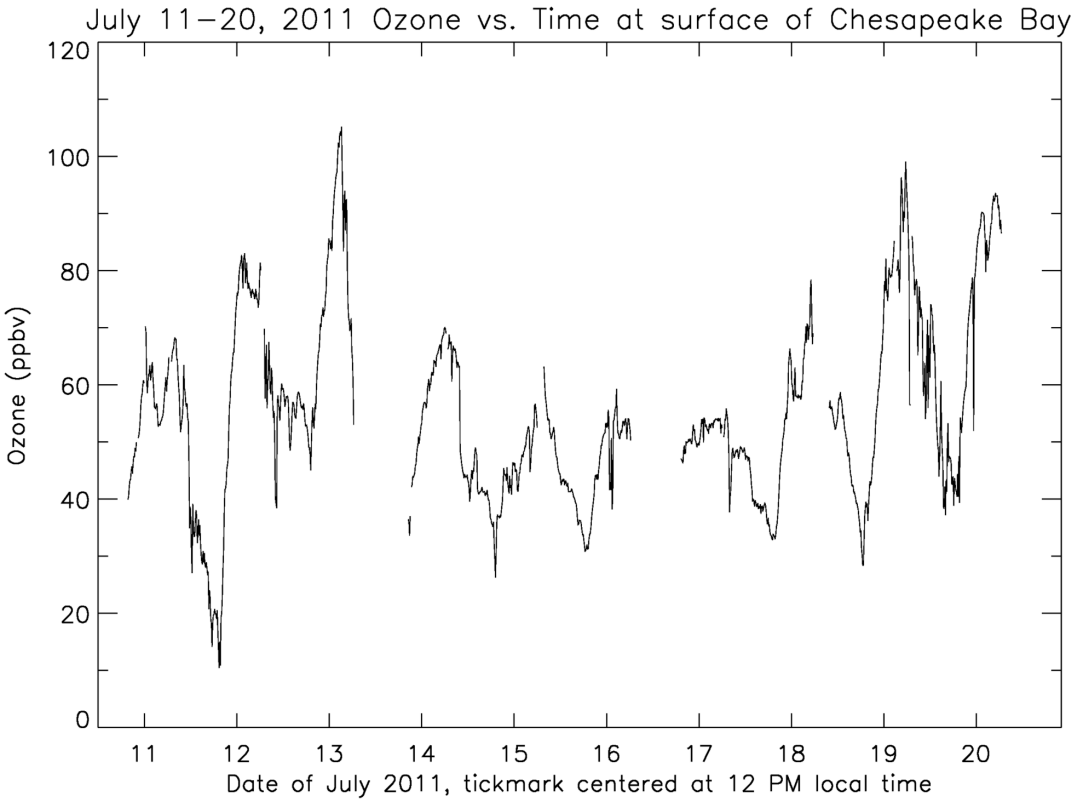

Figure 2-3. Ozone concentration (ppbv) as a function of time from July 11, 2011 through July 20, 2011. Map routes for each specific day can be seen in Figure 2-2. From 7 PM until 6 AM local time, the boat was docked at the US Naval Academy in Annapolis, MD.

On four days ozone exceeded the 8-hour maximum 75 ppbv NAAQS threshold on the moving vessel in the Chesapeake Bay: July 12, 13, 19 & 20. During this same time period, ground stations in the DISCOVER-AQ field campaign region (stations denoted in Table 2-2) exceeded the 75 ppbv threshold an average of 0.71 times per ground station. This alone is an indicator that the ozone may be higher near the surface of the Chesapeake Bay than nearby ground stations.

Comparing the hourly ozone at the SRVx's location and closest upwind ground station reinforces the idea that higher ozone concentrations exist over the Bay. The

closest upwind ground station was determined by using the backward trajectories at 10 m, 500 m, 1500 m heights ending at 1800 UTC (2 PM local time) using Global Data Assimilation System (GDAS) meteorological data in the NOAA HYSPLIT trajectory model [Draxler & Rolph, 2003]. Eight-hour maximum ozone from all relevant ground sites and the SRVx can be seen in Table 2-2.

Table 2-2. Maximum 8-hour ozone at various sites in the Maryland & Delaware region.

	Max 8 hour ozone									
Site Name	7/11/11	7/12/11	7/13/11	7/14/11	7/15/11	7/16/11	7/17/11	7/18/11	7/19/11	7/20/11
Aldino	69	66	56	51	70	59	61	88	73	77
Calvert Co.	58	71	67	49	38	37	40	57	66	59
Davidsonville	53	67	61	50	45	41	41	81	76	63
Edgewood	61	61	52	49	66	55	53	82	59	74
Essex	58	61	53	51	58	47	51	71	72	68
Fairhill	68	65	49	48	69	51	55	86	68	66
HU-Beltsville	75	63	59	61	52	49	54	75	60	80
Millington	59	68	58	54	59	46	47	62	68	68
Padonia	73	64	54	52	62	60	53	67	65	86
PG Equestrian Ctr	54	72	62	51	44	42	41	80	75	61
South Maryland	55	70	63	46	40	38	42	54	64	71
Lums Pond, DE	59	65	53	49	58	N/A	49	76	61	57
Seaford, DE	53	76	62	44	46	N/A	41	52	63	65
NOAA SRVx	58	77	85	60	50	51	52	66	80	86
Closest Ground site	58	67	62	49	38	37	40	54	64	68
Name of Closest Ground site	Calvert	Davidsonville	PG Equestrian	Lums Pond	Calvert	Calvert	Calvert	S Maryland	S Maryland	Millington

The closest upwind ground station was often only 20 to 30 km away and was chosen to ensure that comparisons were made following the same parcel of air. Figure 2-4 shows that during an exceedance day (July 13) and non-exceedance day (July 14) on the boat, the ozone near the surface of the Chesapeake Bay is uniformly higher. During the afternoon of July 13 the ozone measurement on the SRVx was 10 – 40 ppbv greater than at the Calvert County MDE site. Ozone was consistently 10 – 20 ppbv greater over the Bay than at the Essex MDE site throughout the day on July 14.

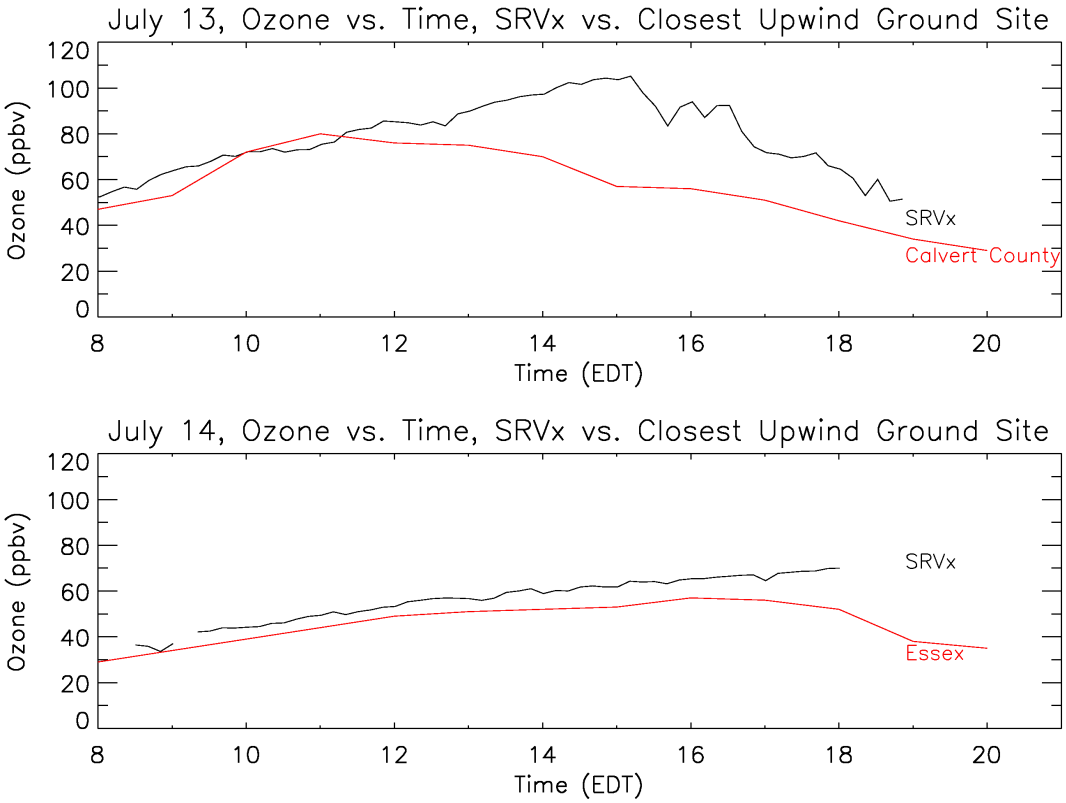

Figure 2-4. (Top) Ozone concentration on July 13, 2011 (ppbv) as a function of time at the SRVx's location and the Calvert County ground monitoring station, the closest upwind monitoring station. (Bottom) Same as (top) but on July 14, 2011 Essex was the closest upwind monitoring station

The 8-hour maximum ozone concentration over the Bay during each day of the 10-day cruise averaged 12.7 ± 6.1 ppbv higher than the closest upwind ground site. The systematic high anomaly over the Chesapeake Bay can be seen in Figure 2-5. The closest upwind ground site never experienced higher 8-hour maximum ozone and only during three days did any ground station in the region have an 8-hour maximum ozone concentration 10 ppbv higher than the SRVx's location. This was especially pronounced on July 13 when the SRVx saw an 8-hour maximum of 85 ppbv and none of the ground stations in the region exceeded the 75 ppbv NAAQS standard. When compared to 8-hour maximum ozone at the ground stations in the Baltimore "moderate" non-attainment area, the 8-hour ozone at the SRVx's location was 4.6 ± 14.3 ppbv higher suggesting that the

Chesapeake Bay has just as poor if not worse air quality than the surrounding "moderate" non-attainment area.

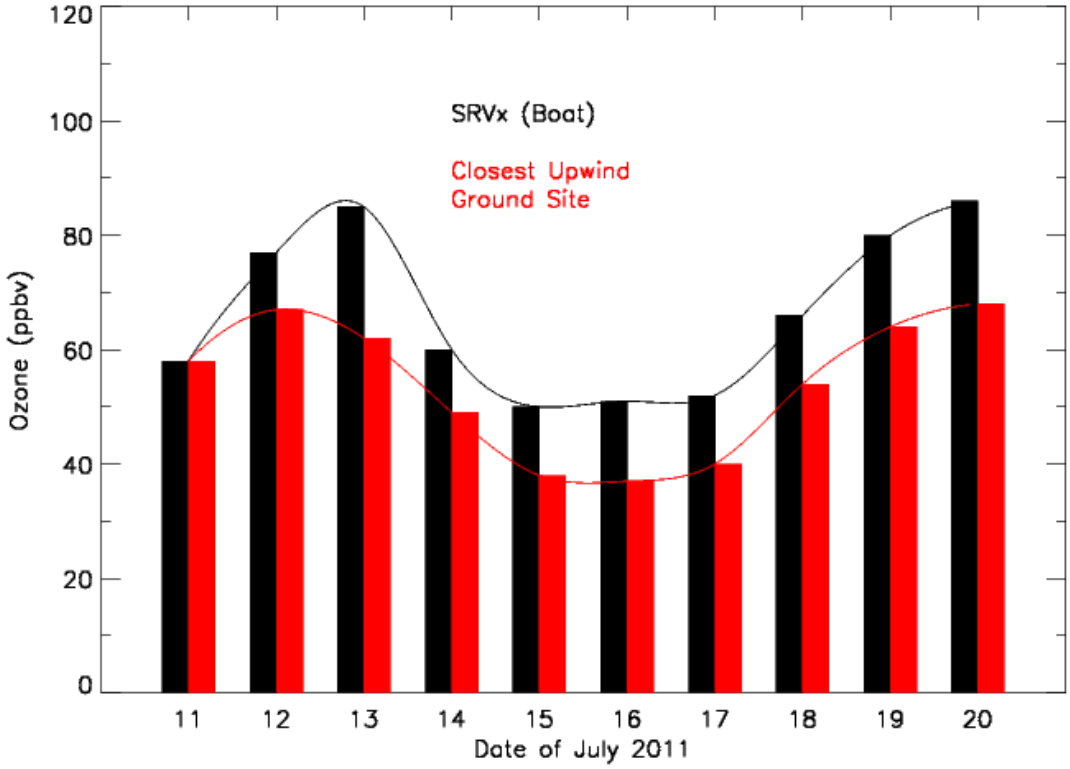

Figure 2-5. 8-hour maximum ozone concentrations (ppbv) at the SRVx's location and the closest upwind ground monitoring station from July 11, 2011 through July 20, 2011

The ozone concentration remained higher over the Chesapeake Bay later into the afternoon than over the ground stations, suggesting that there must be a mechanism to maintain high O_3 concentrations later into the day. A plot of the median hourly ozone concentrations at the SRVx's location and closest upwind ground station (Figure 2-6) illustrates the late afternoon high anomaly.

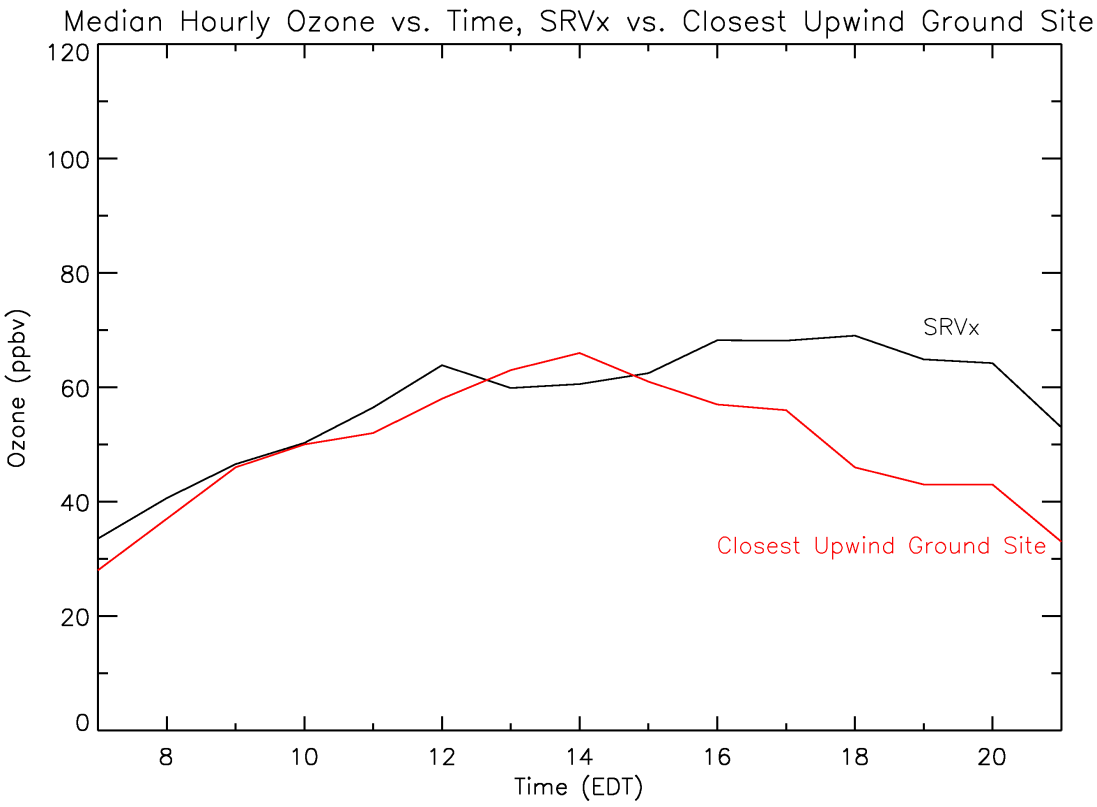

Figure 2-6. Median hourly ozone concentrations (ppbv) at the location of the small research vessel (SRVx) and the location of the closest upwind ground monitoring station from July 11, 2011 through July 20, 2011 as a function of time

Ozone concentrations over the Bay are greater and exist for longer durations than over the upwind land area due to several potential causes:

(1) A difference in ozone deposition rates over land and water;

(2) A shallower planetary boundary layer (PBL) depth over the Chesapeake Bay than the nearby land causing emissions from shipping to be trapped near the surface;

(3) Fewer fair-weather cumulus clouds over the Chesapeake Bay allowing for increased photolysis; and

(4) Decreased boundary layer venting caused by a meso-high pressure that develops over the Bay as part of the bay-breeze circulation trapping pollutants.

Furthermore, when meteorological conditions are conducive, a low-level jet can form overnight transporting polluted air over the Chesapeake Bay from the Norfolk/Virginia Beach, VA metropolitan region bypassing ground stations allowing for increased ozone production over the Bay. This phenomenon, however, was not observed during this field campaign.

2.3.2 Model Comparisons: Ozone

Our CMAQ model simulation results typically reproduce the systematically higher ozone concentrations over the Chesapeake Bay than in the Baltimore-Washington region. As shown in Figure 2-7, median ozone concentrations for the 10-day period output by both the 1.33 km and 4 km resolution CMAQ model simulations closely match the observations from the SRVx throughout the day.

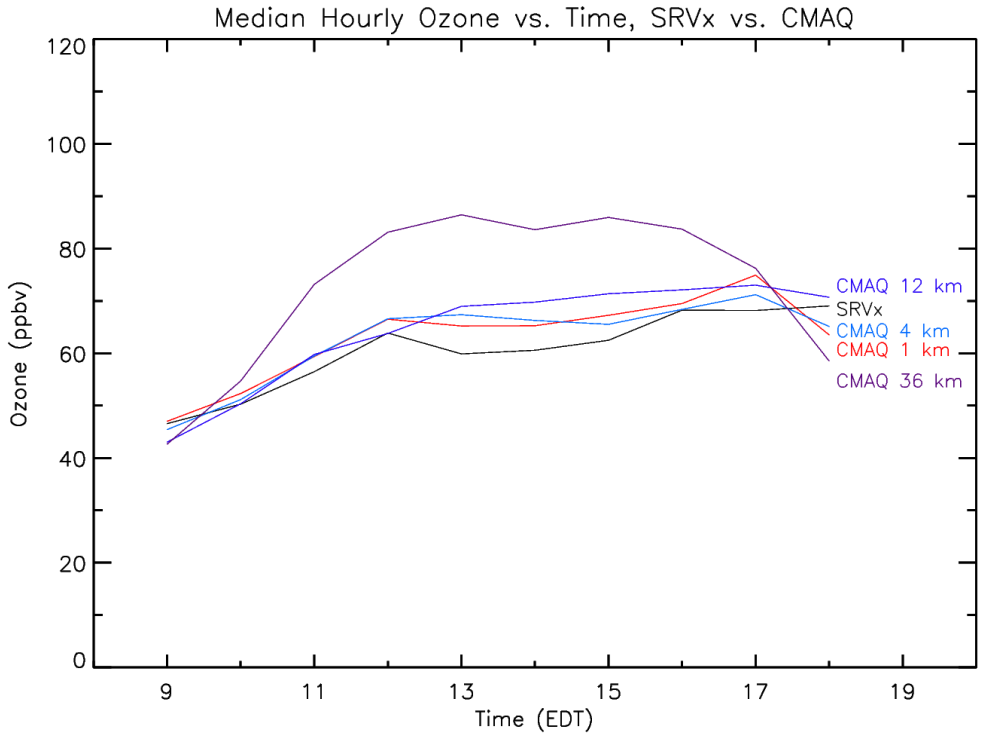

Figure 2-7. Median ozone concentrations (ppbv) at the SRVx's location and at the closest CMAQ (1.33 km) grid point for each hour from July 11, 2011 through July 20, 2011 as a function of time

Model mean bias of ozone in the 1.33 km simulation at the boat's location was 0.78 ppbv, but a root-mean square error (RMSE) of 10.14 ppbv. Table 2-3 shows the mean model bias, normalized mean bias, root-mean square error, and normalized mean error for the 1.33 km simulation.

Table 2-3. CMAQ model (1.33 km resolution) mean bias (model minus observations), normalized mean bias, root-mean square error (RMSE), and normalized mean error (NME) of ozone (ppbv) for the boat and nearby ground stations.

Location	Mean Bias (ppbv)	Normalized Mean Bias (%)	RMSE (ppbv)	NME (%)
SRVx Boat	-0.78	-1.55	10.14	20.23
Southern MD	5.00	9.98	10.69	21.33
Calvert County	4.89	9.77	10.06	20.08
Seaford, DE	2.76	5.51	9.64	19.24
PG Equestrian	0.79	1.57	11.87	23.68
Davidsonville	2.24	4.47	12.21	24.35
Beltsville	1.60	3.20	10.52	20.99
Essex	1.67	3.33	9.84	19.63
Edgewood	-1.96	-3.91	11.05	22.05
Millington	0.22	0.44	9.94	19.84
Lums Pond, DE	1.77	3.53	12.40	24.75

At a grid cell size of 12 km, the surface ozone output by the model begins to lose correlation and at a grid cell size of 36 km, there was very little correlation throughout the day; both the 12 km and 36 km model runs show a high model bias in the late morning and afternoon. Model resolution seems to play an integral role in predicting ozone concentrations over the Bay.

We conducted a validation of the 2-m temperature in the 1.33 km WRF model simulation to ensure that the meteorology is indeed representative of the actual conditions during the 10-day period. Model mean bias of 2-m temperature at the boat's location over the 10-day period was -0.52° C and a RMSE of 1.59° C, which was a lower error than the nearby BWI airport. Table 2-4 shows the hourly mean model bias and RMSE at the boat's location and the BWI airport.

Table 2-4. WRF model (1.33 km resolution) mean bias, max difference, and root-mean square error of 2-m temperature (°C) for the boat and BWI airport.

Location	Mean Bias (°C)	Max Difference (°C)	RMSE (°C)
SRVx Boat	-0.52	4.62	1.59
BWI Airport	1.24	4.20	2.35

WRF at 1.33 and 4 km resolution was able to reasonably capture wind speed and direction. For example, on July 20 the boat showed light winds that veered dramatically from the NE to SW at 1 PM local time. The WRF runs at both resolutions indicated a similar wind shift but closer to 4 PM local time. This will shift the ozone maximum by only a few hours.

Although the 1.33 km resolution CMAQ model simulation closely matched the median for the 10-day period, on certain days the model was unable to predict ozone accurately, with a high bias shown in Figure 2-8a and a low bias shown in Figure 2-8b.

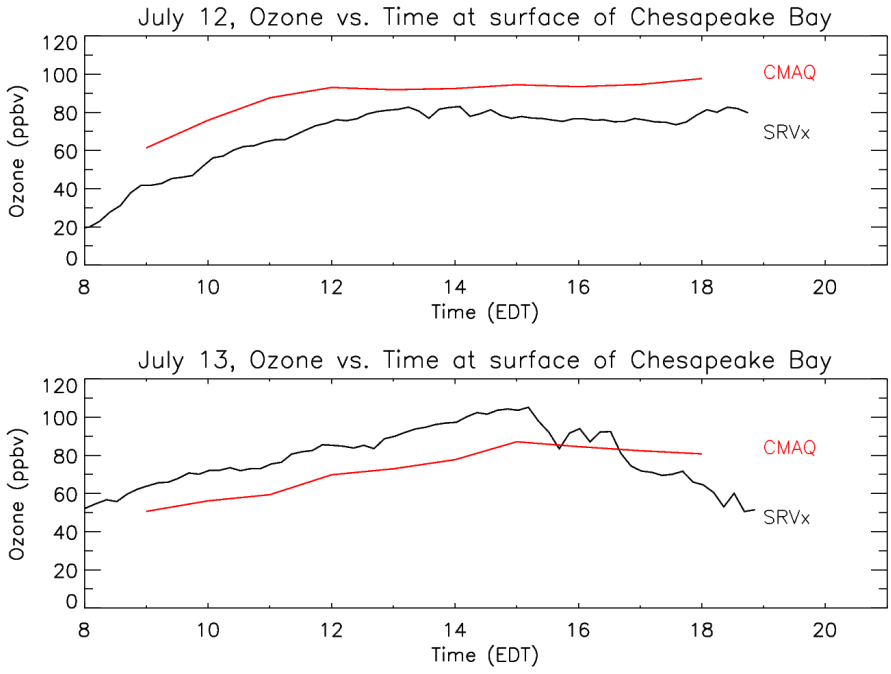

Figure 2-8. Ozone concentration (ppbv) as a function of time at the SRVx's location and at the closest CMAQ grid point on a) July 12, 2011 and b) July 13, 2011

During an exceedance day (July 12), the model had a consistent 10 – 15 ppbv high bias and on another exceedance day (July 13), the model had a 10 -15 ppbv low bias. The high bias of the model can likely be attributed to the boundary layer depths calculated by WRF and input into CMAQ, while the low bias of the model may be related to a lower temperature at the surface or perhaps a more stratified PBL inhibiting downward mixing.

Measurements of the aerosol-based boundary layer height were determined by a High Spectral Resolution Lidar (HSRL) instrument onboard the UC-12B aircraft on July 20. The HSRL dataset includes aerosol extinction at 532 nm, aerosol backscatter at 532 nm and 1064 nm and depolarization at 532 nm and 1064 nm [Hair et al., 2008] and profiles of aerosol backscatter are used to derive the mixed layer height [Scarino et al., 2013]. Observations from the HSRL were compared to the modeled boundary layer from WRF on July 20. Observations were used only for July 20 because this was the only day the SRVx was in the north part of the Chesapeake Bay and the UC-12B aircraft simultaneously conducted a flight. On July 20, the modeled boundary layer in the morning agreed to within 100 m, but in the afternoon the modeled boundary layer was 300 – 500 m lower over the Chesapeake Bay than the observed aerosol-based boundary layer (Figure 2-9). This may be causing the model to exaggerate the amount of pollutants in the lower-most part of the troposphere.

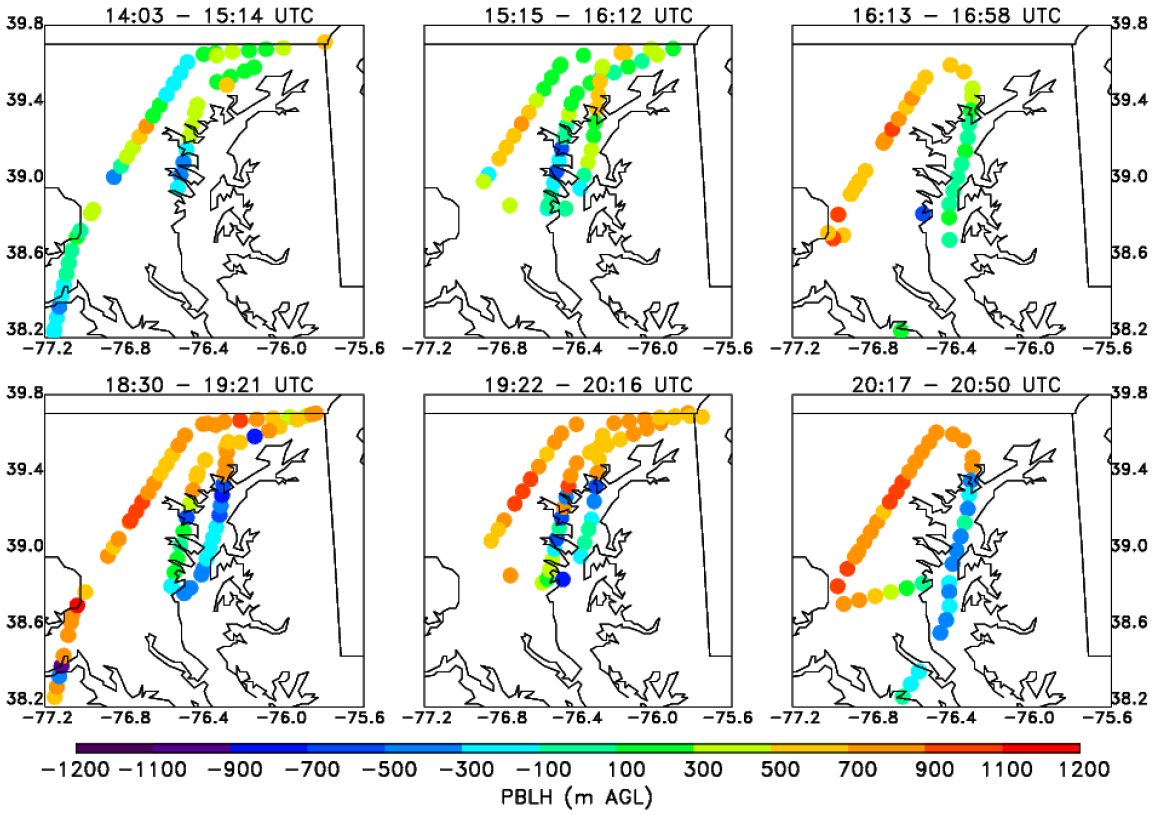

Figure 2-9. PBL depth output by WRF minus measurements of boundary layer height using a high spectral resolution lidar [HSRL) aboard the UC-12 aircraft on July 20, 2011.

2.3.3 Observational Comparisons: Total Reactive Nitrogen

Observations of reactive nitrogen species are critical since the eastern United States lies in the NO_x-limited regime of ozone production [Chameides et al., 1992; Trainer et al., 1993; Frost et al., 2006] due to the excess of largely biogenic isoprene. Accurate model output of NO_y species is especially important due to reactive nitrogen's critical role in ozone formation in the NO_x-limited regime found in eastern United States during the summer.

Observations from the SRVx were compared to the UC-Berkeley thermal dissociation laser-induced fluorescence (TD-LIF) instrument [Day et al., 2002] used on the P3-B when it flew spirals over the Chesapeake Bay. The TD-LIF does not measure

NO, so all comparisons are NOy – NO. The observations of NO_y – NO from the SRVx using a chemiluminescence instrument with external molybdenum converter are higher than the data from the TD-LIF. This is an expected outcome since NO_y concentrations decrease exponentially with height [Brent et al., 2013] due to emissions that come from the surface and relatively short lifetimes compared to other trace gases. There were no other suitable ground observations of NO_y upwind of the boat during this campaign.

2.3.4 Model Comparisons: Total Reactive Nitrogen

Observations of NO_y from the SRVx were compared to 1.33 km CMAQ results over the Bay. On each day of the 10 daytime cruises, with the exception of July 19 when the instrument was taken off-line for calibration, NO_y observations were consistently lower than the output from the nearest grid point in CMAQ. The model regularly overestimated NO_y and on July 12, it was overestimated by 100% in the mid-afternoon as shown in Figure 2-10.

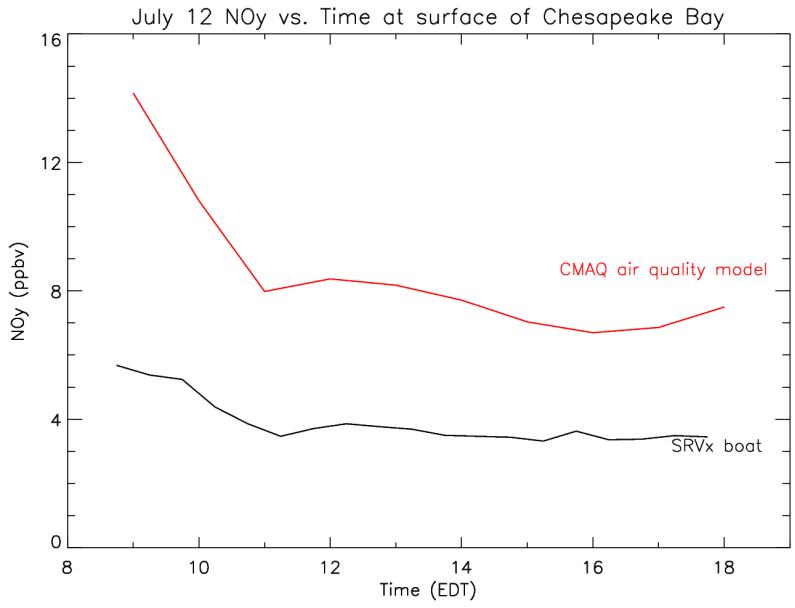

Figure 2-10. Total NO_y concentration measured on the SRVx compared to total NO_y from the closest grid point in CMAQ on July 13, 2011 as a function of time.

The data from the TD-LIF instrument [Day et al., 2002] on the P3-B aircraft during a spiral on July 20 also indicate a significant overestimate of NO_y species by CMAQ, as shown in Figure 2-11. While the vertical profiles of NO_2 and HNO_3 match well, alkyl nitrates (ANs) and peroxy nitrates (PNs) are overestimated by factors of 2 and 4 respectively. This overestimate of reactive nitrogen species has also been seen in other modeling (WRF-Chem and CMAQ) studies [Brioude et al., 2012; Yu et al., 2012].

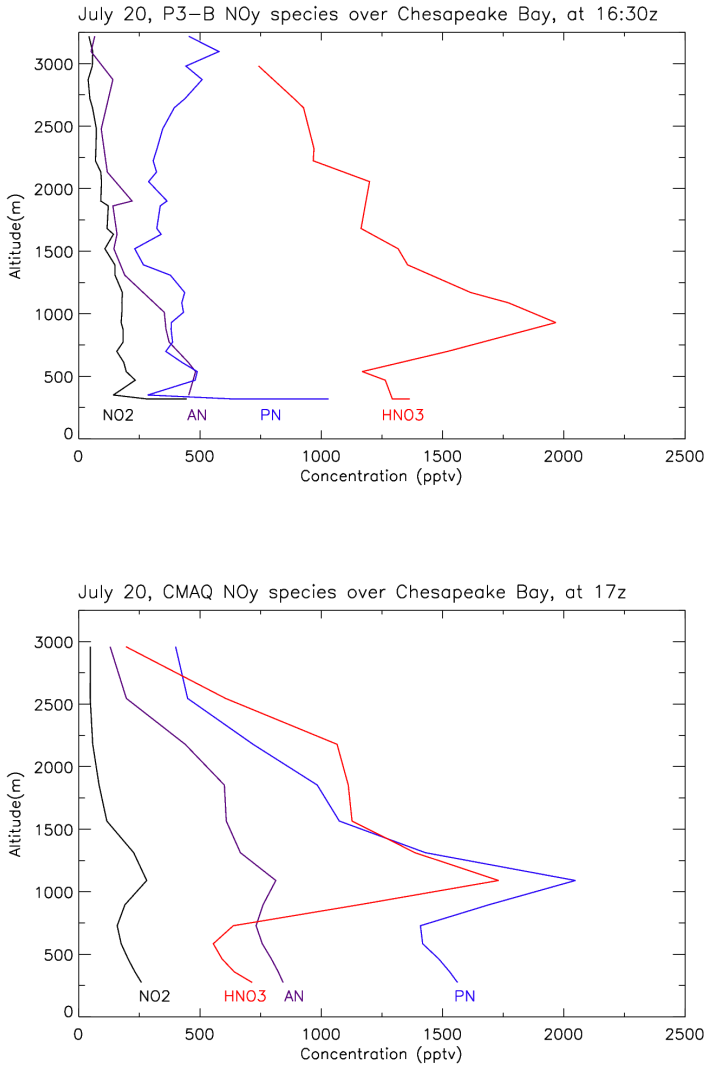

Figure 2-11. Total NO_y concentration (minus NO) split by compound (NO_2, peroxy nitrates (PN), alkyl nitrates (AN), and HNO_3 measured on the P3-B as function of altitude during the 1630 UTC spiral on July 20, 2011 over the Chesapeake Bay.

To understand whether the overestimate is an emissions issues, chemistry issue, or both, we examined the partitioning of the NO_y species. If partitioning is correct, then the issue is likely due to high emissions or low dispersion rates. To gain insight on this issue, we took the ratio of NO/NO_y during the morning hours when the two species are positively correlated and the NO measurement is above the detection limit. As seen in Figure 2-12, the NO/NO_y ratios between the model simulation and observations often lie below the 1-to-1 line.

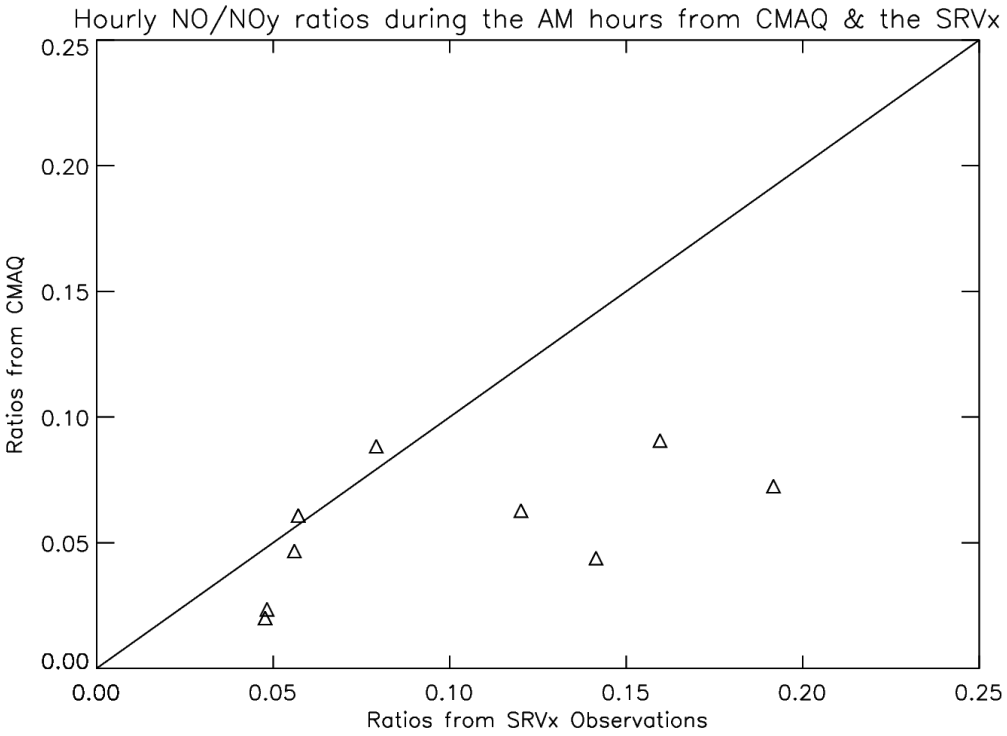

Figure 2-12. NO/NO_y ratios from 1.33 km CMAQ run vs. observations from the ship during the morning hours when NO and NO_y are positively correlated and NO is above the instrument's detection limit.

The mean of the data shows NO concentrations are 10.0% of total NO_y in the observations, while NO concentrations are 7.6% of total NO_y in the CMAQ simulation. This indicates that CB05, as employed, partitions more NO_y species as higher oxides (i.e., ANs, PNs, HNO_3) than is observed. This suggests that gas-phase chemistry scheme

(CB05) overestimates the lifetimes of higher order NO_y species such as ANs and PNs, deposition rates are too slow, or conversion rates of NO_y to NO_2 are slower than observed.

To minimize computing time, the CB05 chemical mechanism simplifies the alkyl nitrates by grouping all alkyl nitrates in a single chemical species (NTR). The lifetime of NTR calculated during a simulation of CMAQ using 2007 summer conditions, yields a lifetime of 10 days. It has been shown that isopropyl nitrate has a lifetime of 10 days [Luke et al., 1989], but higher-order alkyl nitrates have a much shorter lifetime (1-2 days) [Horowitz et al., 2007; Perring et al., 2009], due to a lack of electronegativity holding the gas phase species together. The shorter lifetimes of the high-order alkyl nitrates species are not accounted for in the CB05 gas-phase chemistry scheme. After decomposition, the alkyl nitrates split into an alkyl chain and NO_2. If the lifetime of NTR in CB05 were to be shorter, then this would yield lower concentrations of alkyl nitrates, which would be more consistent with observations.

To represent peroxy nitrates in the model, the CB05 mechanism simplifies the species into peroxyacetyl nitrates (PAN), all other higher order peroxyacyl nitrates (PANX) and peroxynitric acid (PNA), with the latter being a very small fraction of the first two at high temperatures. The summation of peroxy nitrate concentrations (PNs) in the model is higher than observed. The primary destruction of peroxyacyl nitrates is via thermal dissociation. At higher temperatures, PAN and PANX dissociate more rapidly into acetylperoxy radicals ($CH_3C(O)O_2$) and higher order acylperoxy radicals ($C_2H_5C(O)O_2$) respectively. The concentration of PAN and PANX is therefore governed by the kinetic equilibrium constant, which is a function of temperature, and the

concentrations of the products, $CH_3C(O)O_2$, $C_2H_5C(O)O_2$, and NO_2. There are stark differences in the equilibrium constant (K_{EQ}) between IUPAC [2010] and JPL [2011], with the latter being 24% less than the former (3.03×10^{-8} vs. 2.3×10^{-8}) at 298 K. The CB05 mechanism uses the higher IUPAC [2010] equilibrium constant, which favors a higher production rate of PAN. Furthermore, some studies [Turnipseed et al. 2006; Wu et al. 2012] have suggested that the dry deposition rates of PAN in the air quality models are too slow. Updating the rate constants of PAN formation as well as changing the dry deposition velocities, may better align the model output with observations.

2.4 Discussion

The observations from the SRVx show, with a 95% confidence level certainty, that ozone concentrations are elevated over the Bay when compared to upwind ground sites. The extended period of high ozone causes a larger number of days to exceed the 2008 EPA 8-hour 75 ppbv NAAQS threshold over the Bay than over nearby land areas. Here we discuss potential reasons for this phenomenon and attempt to apportion a relative importance for each mechanism.

During a day that lacks precipitation, the case for most ozone exceedance days in the Baltimore-Washington metropolitan region, ozone is primarily destroyed by the mechanisms listed in Table 2-5 [Seinfeld and Pandis, 2006]. Dry deposition (mechanism 1) is the primary mode of ozone destruction near the surface. Titration due to NO (mechanism 2) also occurs near the surface, but this serves as a reservoir for O_3 as NO_2 is re-generated. Mechanisms 3 – 5 are most prominent in the upper troposphere and isolated ocean regions where dry deposition rates are minimal.

Table 2-5. Loss mechanisms for ozone in the lower troposphere.

Mechanism 1	Dry deposition
Mechanism 2	$O_3 + NO \rightarrow O_2 + NO_2$
Mechanism 3	$O_3 + OH \rightarrow O_2 + HO_2$
Mechanism 4	$O_3 + HO_2 \rightarrow OH + 2O_2$
Mechanism 5	$O_3 + h\nu \rightarrow O_2 + O(^1D)$ at $h\nu < 320$ nm

Deposition is the primary mode of destruction in the boundary layer and occurs faster in heavily forested areas [Fowler et al., 2001; Nowak et al., 2006] than over the open ocean (e.g., Figure 2-13).

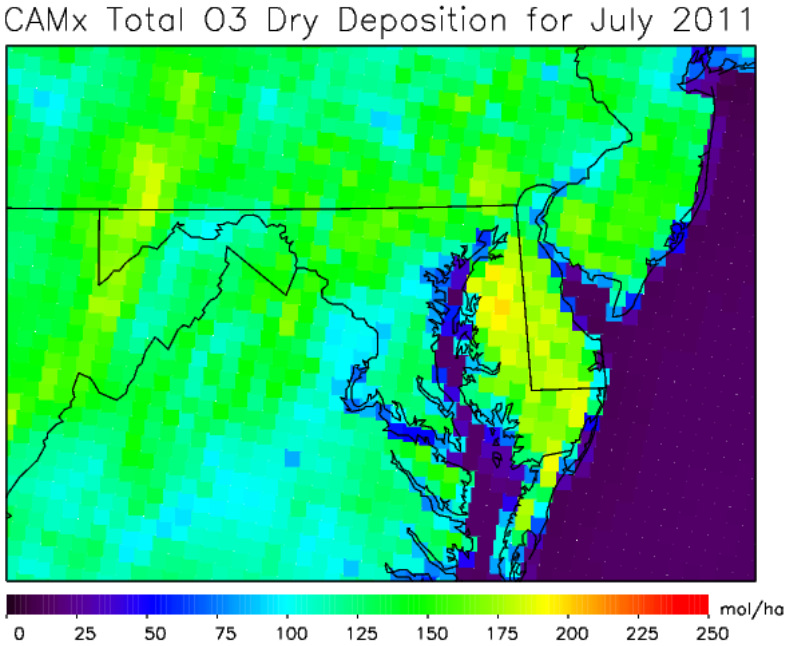

Figure 2-13. Total ozone dry deposition from CAMx during July 2011. Ozone deposition over water bodies is an order of magnitude smaller.

Differences in ozone dry deposition rates have been widely studied. A list of 24-hour-averaged dry deposition velocities from the literature is given in Table 2-6 [Wesely & Hicks 2000; Chang et al., 2004; Nowak et al., 2006].

Table 2-6. Ozone deposition velocities for various surface types.

	Forest	Coastal	Ocean
Nowak (2006)	0.5 cm/s	-	-
Wesely (2000)	0.8 cm/s	-	-
Chang (2004)	-	-	0.05 cm/s
Gallagher (2001)	-	0.148 cm/s	-

For a mix of 50% deciduous forest, 25% grass, and 25% pavement, the 24-hour averaged dry deposition velocity for ozone is 0.50 cm/s. However, estimates for dry deposition of ozone in coastal environments are 0.15 cm/s. The slower deposition velocity is due to a lack of vegetation and surface roughness in coastal areas [Gallagher et al., 2001]. To calculate the difference in ozone deposition over an hour, we can use the formula described in Table 2-7. For a boundary layer depth of 800 m, which is typical over the Chesapeake Bay during the mid-afternoon, ozone concentration would be approximately 1.6% higher after an hour than an air parcel of similar concentration over land due to slower deposition velocities over water, assuming all other environmental conditions are the same.

Table 2-7. Calculation of the difference in ozone dry deposition over land and the bay.

$$\frac{V_{d\,(land)}}{\text{PBL depth}} - \frac{V_{d\,(bay)}}{\text{PBL depth}}$$

$$\frac{18\ \text{m/hr}}{800\ \text{m}} - \frac{5.328\ \text{m/hr}}{800\ \text{m}} = 1.58\ \text{hr}^{-1}$$

If winds are from the southwest, maximizing residence time over the Bay, an air parcel that entered the southwest portion of Chesapeake Bay may have been over the Bay for approximately 5 hours. By the time an air parcel leaves the Bay, its ozone concentration theoretically could be 8% higher than transport over land.

Boundary layer height also plays a major role in determining concentrations of ozone near the surface [Rao et al., 2003]. Pollutants are primarily confined within the boundary layer due to a strong subsidence inversion during anticyclonic events. The only mechanism by which pollutants can be vented out of the boundary layer during strong anticyclonic setups is through fair-weather cumulus clouds [Dacre et al., 2007]. However, cumulus clouds are largely non-existent over the Chesapeake Bay during strong subsidence events [Loughner et al., 2011].

The boundary layer over land tends to be deeper because the surface temperature is higher over land during clear-sky conditions in the mid-afternoon. As the boundary layer depth decreases, emissions of ozone precursors, such as NO_x compounds, accumulate in a smaller volume of the atmosphere leading to higher concentrations. On July 20 between 20 – 21 UTC or 4 PM – 5 PM local time, the HSRL aboard the UC-12B aircraft measured the aerosol-based boundary layer depth to be 1000 - 1200 m over land and 400 - 600 m over the Chesapeake Bay within 10 minutes as seen in Figure 2-14.

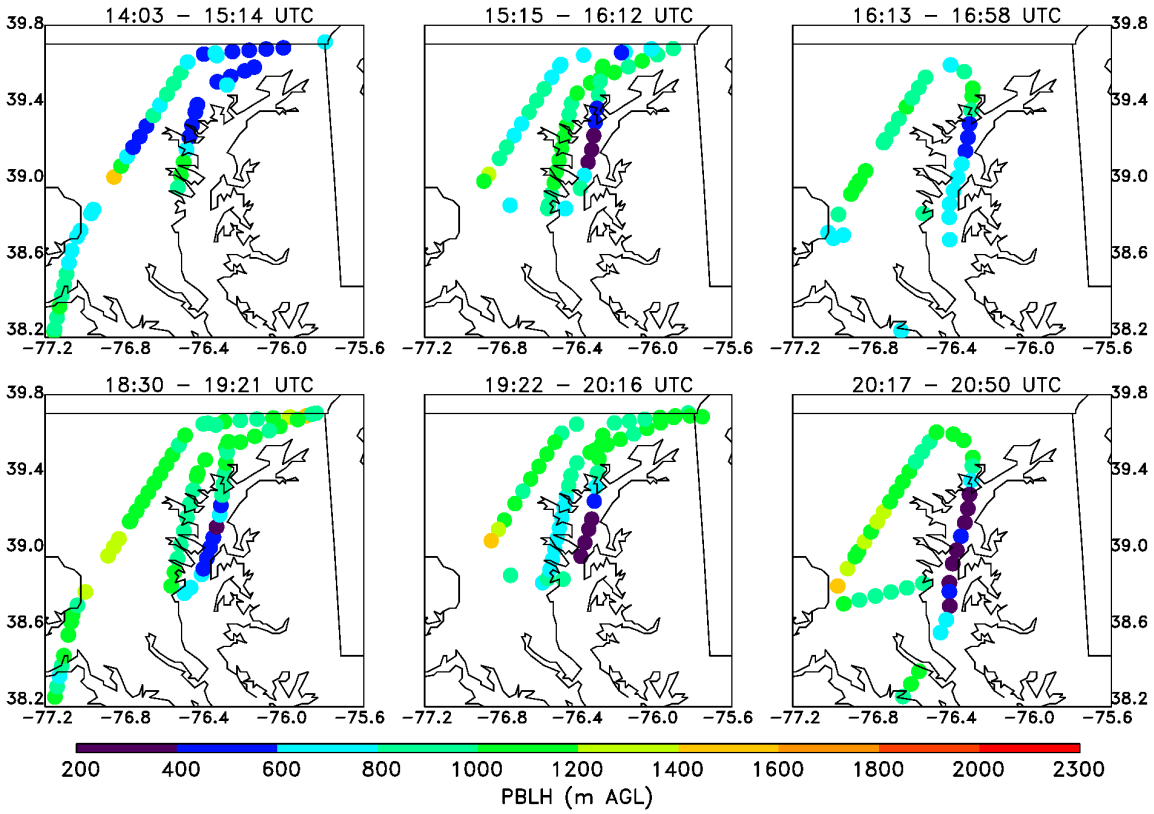

Figure 2-14. Measurements of boundary layer height using a high spectral resolution lidar (HSRL) aboard the UC-12 aircraft on July 20, 2011

If there were no boundary layer venting and environmental conditions and emissions were identical, the concentrations of NO_2 could be up to a factor of 2 higher over the Bay than over land leading to a substantial increase in O_3, since the mid-Atlantic region is in the NO_x-limited regime. However, there is likely some vertical mixing and emissions are likely lower over the Bay. Although there were no direct measurements of NO_2 at the surface of the bay during this particular campaign, data on the P3-B shows that at 0.3 km, the lowest altitude of the flight spirals, NO_2 is higher by as much as 0.5 ppbv over water than land. Using ozone efficiency rates from the DISCOVER-AQ campaign, for every 1 ppbv increase in NO_x, ozone production will increase by an average of 8.26 ppbv with a 90% confidence interval of 4.93 to 19.4 ppbv [He et al.,

2013b]; this is slightly higher than an urban study in Houston, which showed an average ozone production efficiency of 5.9 [Neuman et al., 2009].

A bay-breeze circulation often develops over the Chesapeake Bay during the late spring and early summer [Ryan et al., 1998; Stauffer et al., 2012] impacting the coastal temperature structure and associated meteorological conditions. The bay-breeze yields a meso-high pressure directly over the Chesapeake Bay, and a meso-low pressure just inland from the Bay. This creates stagnation and clear skies directly over the Bay. Fewer cumulus clouds develop over the Chesapeake Bay than over land because of the lower surface temperature, shallower boundary layer depth and relative lack of thermals over the water. Decreased cloud cover increases photolysis rates by allowing more UV radiation to reach the lowest levels of the atmosphere creating an environment more favorable for ozone production. On July 20, visible satellite imagery, seen in Figure 2-15, shows an expanse of low level, fair weather cumulus clouds over the Baltimore-Washington region, with no clouds over the Bay. Cloud coverage is estimated to be 10-30% over land and 0% over the Bay leading to a higher $j(NO_2)$ value over the Bay.

Figure 2-15. Visible image from the MODIS satellite at 1610Z (2:10 PM local time) on July 20, 2011 showing the presence of low-level cumulus clouds only over the land.

During the DISCOVER-AQ campaign, an instrument on the P3-B aircraft measured $j(NO_2)$. In the mid-afternoon, 3:30 PM local time, on July 20, 2011 when the P3-B flew at an altitude of 390 m over land in an absence of clouds, the $j(NO_2)$ rate constant was 0.0082 s^{-1}, while 30 seconds later underneath a fair-weather cumulus cloud, which was confirmed by looking at the forward camera on the P3-B, the $j(NO_2)$ rate constant dropped to 0.0043 s^{-1}. If we assume the sky over land is filled with 20% cumulus clouds and the sky over the Bay has no clouds, the average $j(NO_2)$ would be

0.0074 s^{-1} over land and 0.0082 s^{-1} over the Bay. Therefore, dissociation of NO_2 into NO and odd oxygen may be up to 10.5% faster during the mid-afternoon of a summer day.

It is estimated that NO_x emissions from barges that travel the Chesapeake Bay account for 10% of all mobile emission sources [EPA, 2010]. In March 2010, EPA adopted a regulation requiring large barges to burn cleaner fuel that which emits less NO_x when they are within 200 nautical miles of the North American coastline [EPA, 2010]. However, this regulation was not enforceable by EPA until August 2012, after the Maryland DISCOVER-AQ field study. Many large transport tankers burn bottom-of-the-barrel bunker fuel, which releases a higher proportion of NO_x than diesel fuel [Eyring et al., 2005]. To date, there has been little quantification of barge emissions [Mason et al., 2008]. Using the 8.26 ppbv O_3 per ppbv NO_x ozone production efficiency calculated during the DISCOVER-AQ campaign [He et al., 2013b], we estimate that 0.1 ppbv increase in NO_x concentrations over the Chesapeake Bay could yield a 0.8 ppbv increase in ozone, since the mid-Atlantic region is characterized by the NO_x-limited regime of ozone production.

Halogen chemistry may play a role in ozone formation over the Chesapeake Bay. Recent modeling studies suggest that Cl_2 photochemistry may result in an increase of 5–8 ppbv in daily maximum ozone levels [Finley and Saltzman 2006]. To see if more chlorine is available over the Bay, we looked at the 5-year average (between 2007 and 2011] of Cl^- dry and wet deposition at two Clean Air Status and Trends Network (CASTNET) sites in Maryland. The Blackwater National Refuge site, located on Maryland's eastern shore, is generally downwind of the Bay, while the Beltsville site is located upwind of the Bay. Dry deposition rates of Cl^- are 2.14 times higher over a 5-

year average at the Blackwater site and wet deposition rates of Cl^- are 3.62 times higher.

One factor inhibiting ozone production over the Bay is the lower tropospheric temperature profile. Coastal areas in extratropical latitudes heat up more slowly than nearby inland locations during the summer due to the influence of the cooler waters. During the 10-day campaign, temperatures on the SRVx at 2 PM local time were on average 3.4 °C cooler than the Baltimore-Washington International (BWI) airport, located 30 km inland from the Chesapeake Bay.

The dissociation of PAN into NO_2 has a strong temperature dependence (Seinfeld and Pandis, 2006]. A calculation of the rate constant using IUPAC [2010] shows that PAN dissociates 1.66 times quicker at 304.3 K than 300.9 K. The quicker dissociation of PAN at higher temperatures over land shifts the equilibrium reaction towards NO_2, the primary precursor to ozone in the NO_x-limited regime over the Mid-Atlantic. However, the dissociation of PAN is slower over the Bay, keeping more NO_2 tied up as PAN, and thereby decreasing O_3 production.

2.5 Conclusions

Observations from the NOAA SRVx vessel during the DISCOVER-AQ and GEO-CAPE CBODAQ campaigns show with a certainty exceeding the 2-sigma level, that daytime ozone concentrations are elevated over the Bay when compared to the closest upwind ground station. We posit that this high anomaly is influenced by a number of mechanisms, in approximate descending order:

- Shallower boundary layers trapping shipping emissions near the surface
- Higher photolysis rates due to clear skies over the bay

- Decreased boundary layer venting due to a lack of fair-weather cumulus clouds
- Slower deposition velocity over the Bay

The ozone concentrations exhibit a high anomaly over the Bay even though temperatures are cooler and allow precursors to ozone such as PAN to remain more stable. The observed high anomaly over the Chesapeake Bay is of primary importance since many citizens spend their leisure time on or near the Chesapeake Bay during the summertime, and are exposed to the unhealthy air quality conditions. Onshore winds can bring these pollutants to local coastal and inland communities. Expanded monitoring of ozone directly over the Chesapeake Bay is needed to precisely quantify the extent of this high anomaly.

3. CAMx Model Description

The Comprehensive Air Quality Model with Extensions (CAMx) version 6.10, developed by ENVIRON [Morris et al., 2004; ENVIRON, 2014], is a 3-D photochemical air quality model that simulates tropospheric pollutants on a fixed grid. CAMx must be provided with emissions from a processing tool such as SMOKE, meteorology from WRF, photolysis rates calculated from ozone column data from satellites such as OMI, and initial and boundary conditions from a global transport model such as GEOS-Chem or MOZART. A diagram for the necessary pre-and post-processors is described in Figure 3-1.

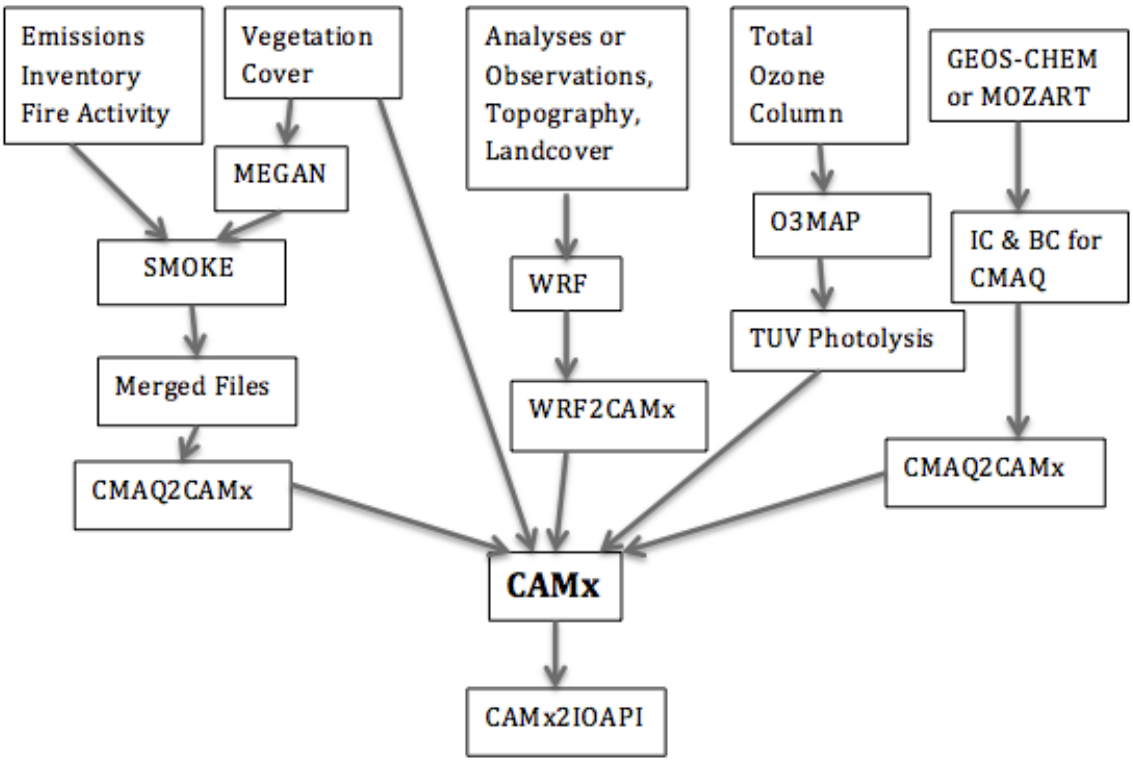

Figure 3-1. Diagram of CAMx pre- and post-processors.

3.1 CAMx Benchmark Simulation

To determine whether the model is compiled correctly, model developers provide a benchmark simulation with all input files and the expected model output. Users are requested to run the model using the provided input files and compare their model output with the model output provided by the model developers. CAMx model developers provide a benchmark simulation for June 3 & June 4, 2002, which covers the Midwestern United States.

We compare model output from our compiled version of CAMx v6.10 to the output from the model developers' version of CAMx v6.10 using the same Portland Group Fortran (PGF) compiler. In Figure 3-2, we compare surface ozone for all grid points (92 x 113 model domain) for all 48 hours of the simulation (499,008 points total). The slope of the linear least squares fit is 0.99999893 and the r^2 is 0.999533.

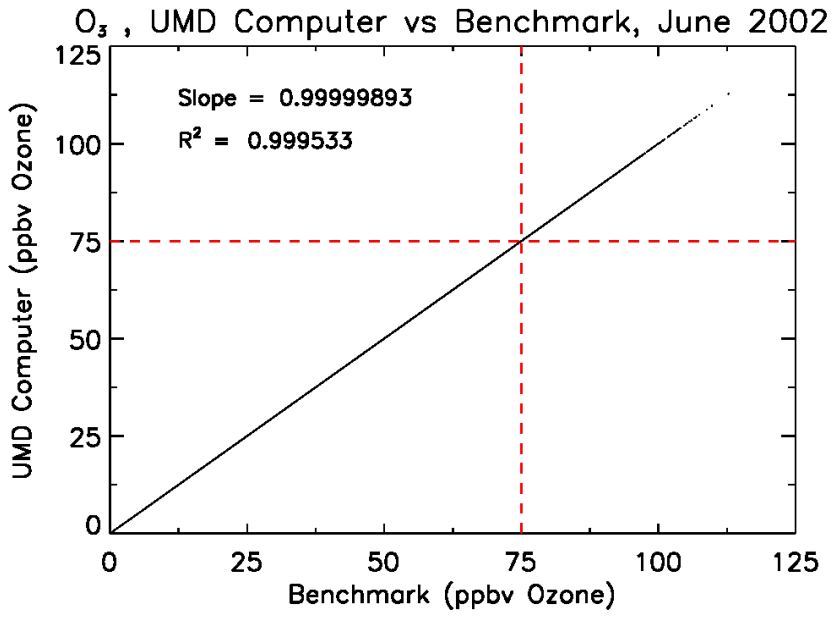

Figure 3-2. Surface ozone from the CAMx v6.10 12 km simulation June 3 & June 4, 2002 for the Midwestern United States from the University of Maryland computer system compared to the benchmark simulation.

In Figure 3-3, we compare surface NO_2 and SO_2 from the same benchmark simulation. The slope of the linear least squares fit for NO_2 is 1.0000001 and the r^2 is 0.999805. The slope of the linear least squares fit for SO_2 is 1.0000004 and the r^2 is 0.999483.

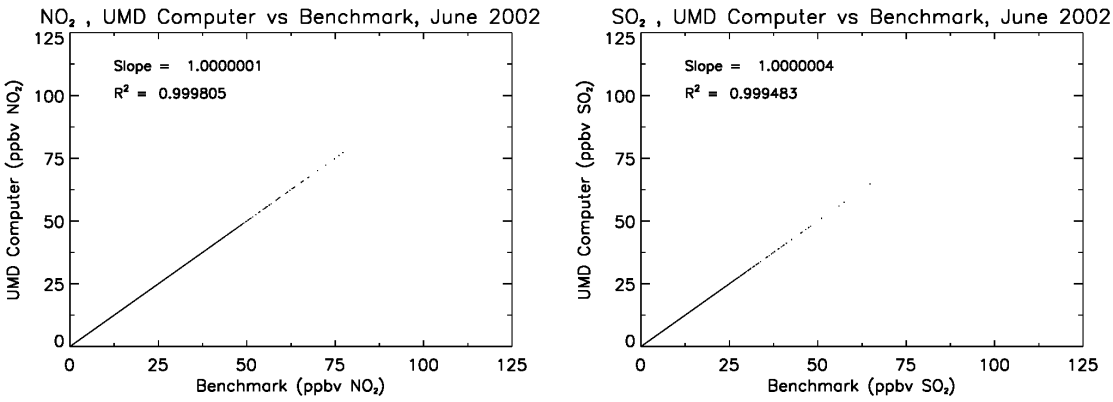

Figure 3-3. Surface NO_2 and surface SO_2 from the CAMx v6.10 12 km simulation June 3 & June 4, 2002 for the Midwestern United States from the University of Maryland computer system compared to the benchmark simulation.

The model is compiled correctly on the University of Maryland's computer system because there is excellent model agreement between our simulation and the simulation provided by model developers.

3.2 CAMx Model Set-Up

The studies described in this dissertation focus on month-long simulations of July using CAMx version 6.10 with 35 vertical layers and 12 km horizontal resolution. The baseline simulation is conducted for July 2011, using emissions and meteorological fields prepared for this summer. We also present simulations conducted using retrospective emissions for July 2002 based on July 2011 meteorology, and projected emissions for July 2018 based on July 2011 meteorology. The model domain covers the area depicted in Figure 3-4, split into 12 km x 12 km grid cells (not shown).

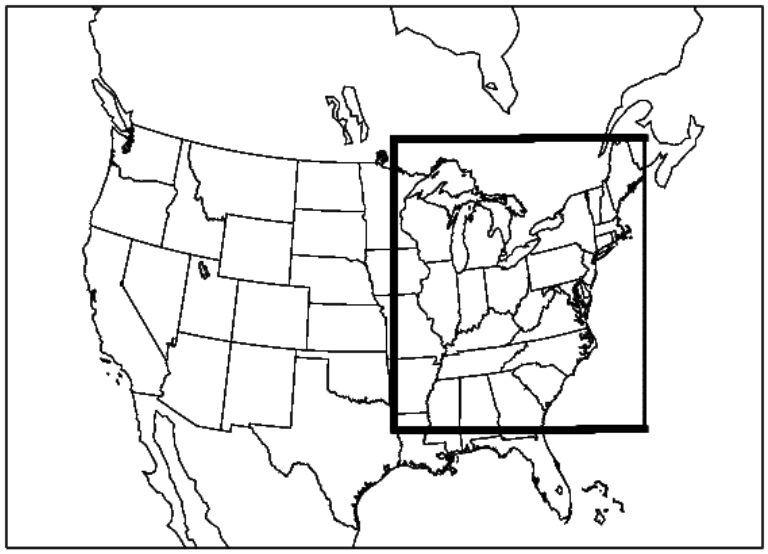

Figure 3-4. CAMx v6.10 model domain as denoted by the dark black line, 12 km horizontal resolution

3.2.1 Meteorology

WRF v3.4 was used to simulate the meteorology [EPA, 2014d] for this modeling study [Skamarock et al., 2008]. The WRF model domain encompasses the Continental United States (CONUS) at a horizontal resolution of 12 km with 35 vertical levels from the surface to 50 millibars (mbar). The 12 km North American Model (NAM) analysis provided by the National Climate Data Center (NCDC) was used for the WRF initial and outermost lateral boundary conditions. When NAM data were unavailable, the 40km Eta Data Assimilation System (EDAS) analyses from the National Canter for Atmospheric Research (NCAR) were used. Data were quality controlled and compared to observations, showing excellent agreement [EPA, 2014d]. The Group for High Resolution Sea Surface Temperatures (GHRSST) provided sea surface temperatures (SSTs) at 1 km resolution [Stammer et al., 2003]. High resolution SSTs are critical for warm, shallow, coastal waters that influence the strength of bay and sea breezes. The WRF model was re-initialized every 5 days for the 2011 calendar year and run in 132-

hour increments; the first 12 hours of each simulation were used for spin-up of the model meteorology. The WRF simulation was conducted off-line. Meteorological data were fed to CAMx v6.10 at hourly intervals.

3.2.2 Emissions

Anthropogenic emissions input files for CAMx v6.10 were created with the Sparse Matrix Operator Kernel Emissions (SMOKE) modeling system [Houyoux and Vukovich, 1999] and converted to CAMx-ready format through the 'cmaq2camx' pre-processor. We use the 2011 National Emissions Inventory (NEI) as compiled by EPA for the baseline simulation [EPA, 2014e]. Mobile emissions estimates from cars, trucks, and motorcycles were computed with the Motor Vehicle Emission Simulator 2010b (MOVES2010) [Kota et al., 2012]. Point sources were vertically distributed based on the meteorology, stack height, as well as the temperature and velocity of pollutants exiting the stacks. Emission estimates for a hypothetical 2002 scenario using 2011 meteorology were made using the 2002 NEI. The Mid-Atlantic Regional Air Management Association (MARAMA) has provided anthropogenic emission projections for July 2018 based upon EPA recommendations [EPA, 2014e]. Emissions for the July 2002 and 2018 model simulations were based on meteorology from July 2011. Biogenic emissions were calculated using Biogenic Emissions Inventory System (BEIS) version 3.14 [Pouliot and Pierce, 2009] and were identical in each of the three model simulations.

3.2.3 Boundary conditions

The boundary conditions were initialized using the GEOS-Chem v8-03-02 global chemistry model [Bey et al., 2001] at a horizontal resolution of 2.5 × 2.0°. The 'geos2cmaq' pre-processor [Henderson et al., 2014] assigns the value of the closest

global model grid point to each boundary grid cell of the 12 km regional model. Boundary condition files were converted to CAMx-ready files using the 'cmaq2camx' pre-processor [ENVIRON 2014]. Henderson et al. [2014] analyzed the accuracy of ozone boundary conditions for a CONUS model domain using OMI and TES; they found good agreement of ozone in the mid- and upper-troposphere (above 700 mbar) during the month of August 2006 – 2010 and a consistent underestimate closer to surface (below 700 mbar) during the same time period. Furthermore, Fiore et al. [2014] showed that observed mid-tropospheric ozone from the TES and OMI satellites in rural locations at our model domain boundary agreed to within 5 ppbv in GEOS-Chem, at a 2 × 2.5° resolution, during the summer of 2006. We also describe a sensitivity study in which we use a 2.5 × 1.9° MOZART-4 simulation [Emmons et al., 2010] to initialize trace gases along the CAMx lateral boundaries. The 'mozart2camx' pre-processor [ENVIRON 2014] interpolates the global model data to the closest 12 km regional model grid cell.

3.2.4 CAMx model platform set-up

All 35 vertical layers from the WRF simulation were passed to the CAMx regional model. Horizontal and vertical advection were calculated using the Piecewise Parabolic Method (PPM) [Colella and Woodward, 1984]. Vertical eddy diffusion was calculated using K_z-theory [O'Brien, 1970]. We use the Carbon Bond 05 (CB05) gas-phase chemistry with Coarse-Fine (CF) aerosols [Yarwood et al., 2005] calculated with the Euler-backward iterative (EBI) solver. Photolysis rates were calculated using the Tropospheric Ultraviolet-Visible (TUV) radiation model by the discrete-ordinates method; ozone columns used in the photolysis rate calculations were based on retrievals from the Ozone Monitoring Instrument (OMI) satellite. Model simulations started on

June 25, 2011 using initial conditions provided by the MOZART-4 global model; we allow for 6 days of spin-up of CAMx. After the 6-day spin-up, less than 0.1% of the initial conditions remain in the model domain. The simulation begins on July 1, the first day of the DISCOVER-AQ Maryland campaign. Table 3-1 describes the CAMx options chosen for our baseline simulation.

Table 3-1. CAMx version 6.10 Model Options

Horizontal resolution	12 km
Vertical Layers	35
Start Date	June 25, 2011
Days of Spin-up	6
Photolysis rate calculation	TUV, Discrete-ordinates method
Dry deposition model	Zhang et al. [2003]
Advection solver	Piecewise Parabolic Method
Vertical eddy diffusion	Kz-theory
Chemistry solver	Euler-backward iterative (EBI)
Gas-phase chemistry	CB05
Aerosol mechanism	Coarse-fine (CF)

The Ozone Source Apportionment Technology (OSAT), an add-on software package for CAMx [ENVIRON 2014], allocates ozone at receptor source locations to upwind source regions (i.e., states, cities, etc.) and types (mobile, point, etc.). Collet et al. [2014] document how OSAT differs from a zero-out method – a scenario in which anthropogenic emissions from a single region or sector are completely eliminated. Particularly useful for this dissertation, OSAT tracked boundary conditions and initial conditions as separate group categories. We also use the Chemical Process Analysis (CPA) probing tool to calculate production and loss rates of ozone and some of its precursors. A detailed description of the OSAT, APCA, and CPA software can be found in Chapters 3.6 – 3.8 and in the CAMx User's Manual [ENVIRON, 2014].

3.3 Vertical Diffusion Parameterizations

CAMx has the option to be run with K_z-theory vertical eddy diffusion, instead of the computationally intensive ACM2 parameterization scheme. At the top of the planetary boundary layer (PBL), as seen in Figure 3-5, there are narrow but strong pulses of vertical motion, which are averaged out by the large scale-subsidence surrounding these pulses. While the average vertical diffusion may in fact be small in magnitude, K_z-theory does not account for these strong pulses of vertical motion. These strong pulses of vertical motion, known as boundary layer venting, often occur via shallow cumulus clouds [Loughner et al., 2011] during a typical afternoon day. Furthermore, K_z-theory cannot account for vertical transport during deep vertical convection due to its assumption of slow vertical diffusion above the PBL. However, significant air pollution episodes tend to occur during extremely stable synoptic conditions; K_z-theory is often adequate in much of the PBL and the free troposphere. When running the K_z-theory option in CAMx, a 24-hour simulation at 12 km resolution of the eastern United States can be completed in 35 minutes, while an identical run with the ACM2 parameterization takes 90 minutes.

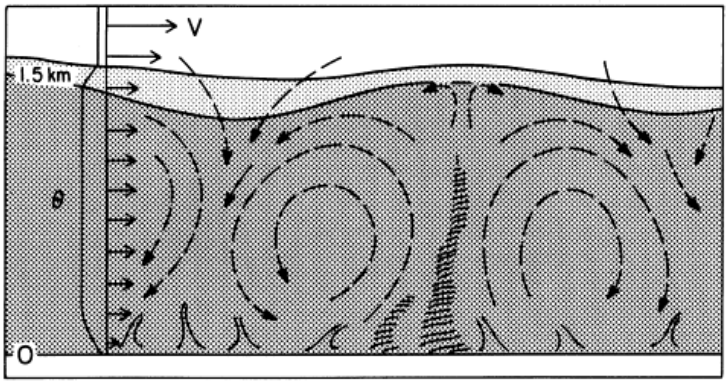

Figure 3-5. Eddy diffusivity in the planetary boundary layer (PBL) during a typical air pollution episode. Figure from Kaimal and Finnigan, 1994

Boundary layer venting is poorly handled by model parameterizations [Castellanos et al., 2011; Loughner et al. 2011; Solazzo et al., 2013]. The Asymmetric Convective Mechanism 2 (ACM2) [Pleim et al. 2007] tries to mitigate the issue with deep vertical convection by apportioning some of the mass from the lowest layers of the atmosphere directly to the upper layers, bypassing the middle layers, as shown in Figure 3-6. While this is physically unfeasible, it can be an adequate approximation during convection when quick vertical movement can displace air parcels upward within minutes. Despite the advantages of the ACM2 parameterization, it still cannot accurately represent boundary layer venting in fair-weather cumulus clouds [Loughner et al. 2011].

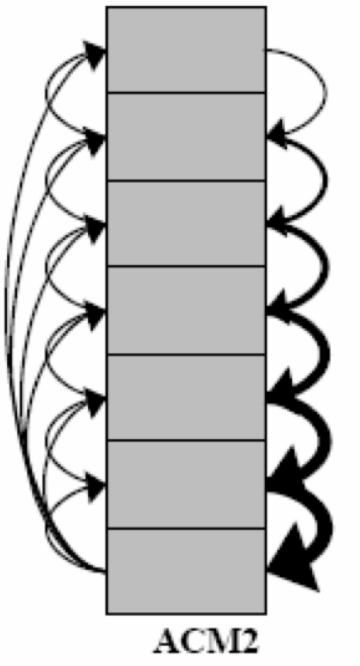

Figure 3-6. ACM2 Vertical Diffusion Parameterization, from Pleim et al. [2007].

Two different simulations of CAMx were compared to evaluate the effect of vertical parameterization schemes on surface ozone. A difference plot, shown in Figure 3-7, displays the adjustment in mid-afternoon surface ozone due to changing vertical parameterization schemes from K_z-theory to ACM2 . Anomalies are primarily

constrained to urban centers, where ozone mixing ratios are up to 5 ppbv lower in the mid-afternoon. We hypothesize that this is due to the faster venting of fresh emissions in the urban centers when using the ACM2 parameterization.

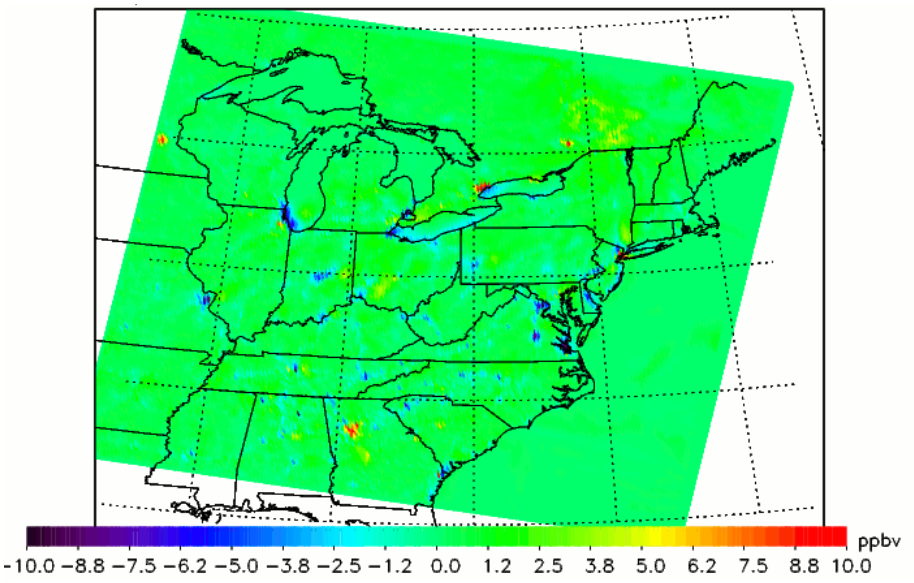

Figure 3-7. CAMx simulation shown for July 9, 2007 at 2 PM local time displaying the surface ozone difference (ppbv): CAMx(ACM2) – CAMx(K-theory).

We can also use CO – a pollutant with a lifetime of approximately one month – as a tracer to diagnose vertical mixing in air quality models. In the left side of Figure 3-8, we show observations of CO binned by altitude, while the center and right panels show model data from CAMx and CMAQ respectively. Particularly important to this Chapter, the CAMx baseline simulation uses K_z-theory to calculate vertical diffusion, while CMAQ uses the ACM2 parameterization for vertical diffusion. Both models are initialized with the identical emissions, meteorology, boundary conditions, and gas-phase chemistry.

CAMx with K_z-theory vertical diffusion appears to be a better representation of the atmosphere, especially in the lowest altitudes. CAMx captures the median value of CO observations quite well (~5 ppbv underestimate) below two kilometers above ground

level. CMAQ has a ~25 ppbv underestimate below two kilometers. Between two and five kilometers, both models underestimate CO mixing ratios – which is probably due to an underestimate of CO in the boundary conditions.

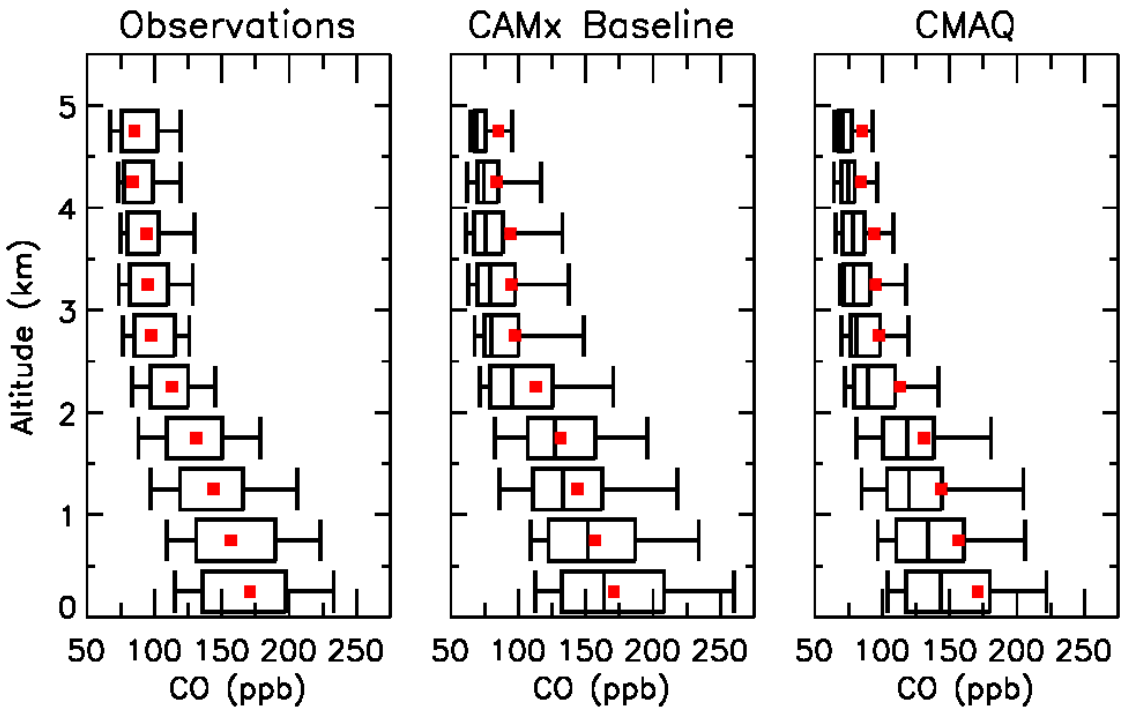

Figure 3-8. Vertical profiles of CO binned in 500 m intervals, showing the 5th, 25th, 50th, 75th and 95th percentiles. The left side panel shows one-minute averaged data from the P3-B aircraft, center panel shows a baseline simulation using CAMx v6.10, and the right side panel shows a baseline simulation using CMAQ v5.02. Model data are matched spatially and temporally. Red dots indicate median values of the CO observations at each altitude.

At quick glance, it appears that CMAQ has lower CO mixing ratios than CAMx at all vertical levels. However, this is not the case. In Figure 3-9, I show a difference plot of CO between CMAQ and CAMx following the P3-B flight path for two days during the DISCOVER-AQ campaign. On July 5 and July 21, CMAQ calculates CO mixing ratios 10 – 50 ppbv lower than CAMx in the PBL (below 3 km). Above the PBL (above 3 km) including the lower stratosphere (10 – 15 km), CMAQ calculates CO mixing ratios 0 – 10 ppbv higher than CAMx. These plots clearly indicate that CAMx calculates higher CO

mixing ratios below 5 km, while CMAQ calculates higher CO mixing ratios above 5 km (including the lower stratosphere; 10 – 15 km). This is consistent with the ACM2 parameterization, which quickly transports mass from the surface to the highest levels of the model.

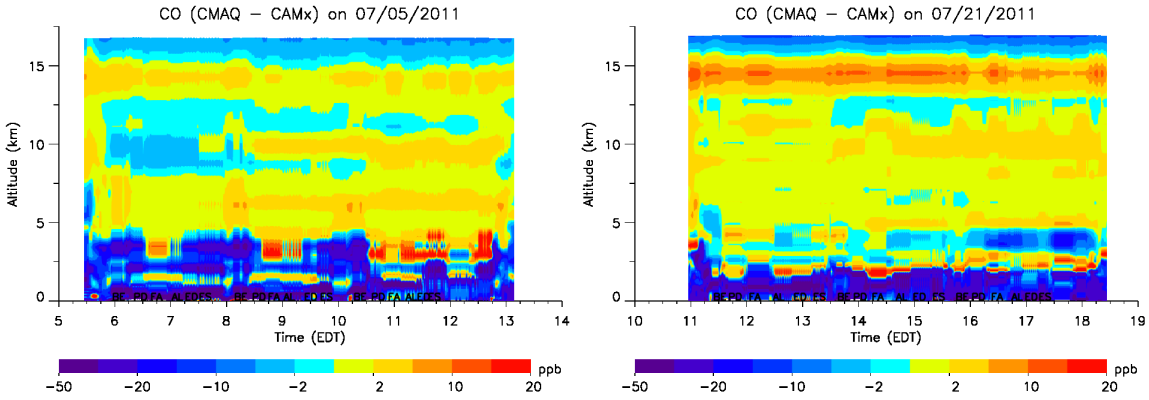

Figure 3-9. Difference (CMAQ – CAMx) curtain plots showing the vertical profiles of CO following the P3-B flight path on (left) July 5, 2011 and (right) July 21, 2011.

3.4 Gas-Phase Chemical Mechanisms: CB05 & CB6

The option to use CB6 gas-phase chemistry is an advantageous feature of CAMx. CB6 has 62 more gas-phase reactions, 5 more photolysis reactions, 26 more gas-phase species, and 5 more emissions species than CB05 (Table 3-2) [Yarwood et al., 2010]. Most of the additional species in CB6 are higher-order hydrocarbons, which had been previously lumped into other carbon bond groups. The 5 new "emission species" are propane (PRPA), benzene (BENZ), ethyne (ETHY), acetone (ACET), and higher ketones (KET).

Table 3-2. Differences between CB05 and CB6 gas-phase mechanisms. Table taken from Yarwood et al., 2010.

	CB05	CB6
Gas-phase reactions	156	218
Photolysis reactions	23	28
Gas-phase species	51	77
Emissions species for ozone	16	21

The new CB6 gas-phase mechanism also updated rate-constants of several important reactions [Yarwood et al., 2010]. They include:

(1) $$OH + NO_2 + M \rightarrow HNO_3 + M$$

(2) $$HCHO + h\upsilon \rightarrow HO_2 + CO$$

(3) $$NO_2 + h\upsilon \rightarrow NO + O$$

(4) $$N_2O_5 + H_2O_{(l)} \rightarrow 2HNO_{3(l)}$$

The rate constant in Reaction 1 increases by 5% as per the recommendation from IUPAC 2010 [Atkinson et al., 2010]. This reaction rate change leads to a shorter lifetime of NO_2 and therefore lowers ozone production. The photolysis rate in Reaction 2 increases by 23% as per the recommendation of NASA Jet Propulsion Lab (JPL) [Sander et al., 2006]. This leads to a greater source of the HO_2 radical and an increase in ozone production. The photodissociation of NO_2, Reaction 3, increases by 7%, based on a comprehensive laboratory study of NO_2 cross-sections by Shetter et al. [2003]. It is unclear from the provided references why this reaction rate was altered. Reaction rate 3 will also cause an increase in ozone production efficiency. Reaction rate 4 decreases by 80%, which is due to a change in accommodation coefficient based on Evans and Jacob [2005]. This leads to less NO_x removal during the nighttime via HNO_3 and an increase in ozone production the following day when N_2O_5 is photolyzed back to NO_x.

Due to the aforementioned changes, the CB6 gas-phase mechanism causes maximum 8-hour ozone to increase across the modeling domain in the summertime model runs [Yarwood et al., 2010]. We plot a difference plot between CB6 and CB05 using our CAMx model platform to confirm this, as seen in Figure 3-10. Studies have

shown CB6 to be more accurate when compared to photochemical smog chambers [Yarwood et al., 2010].

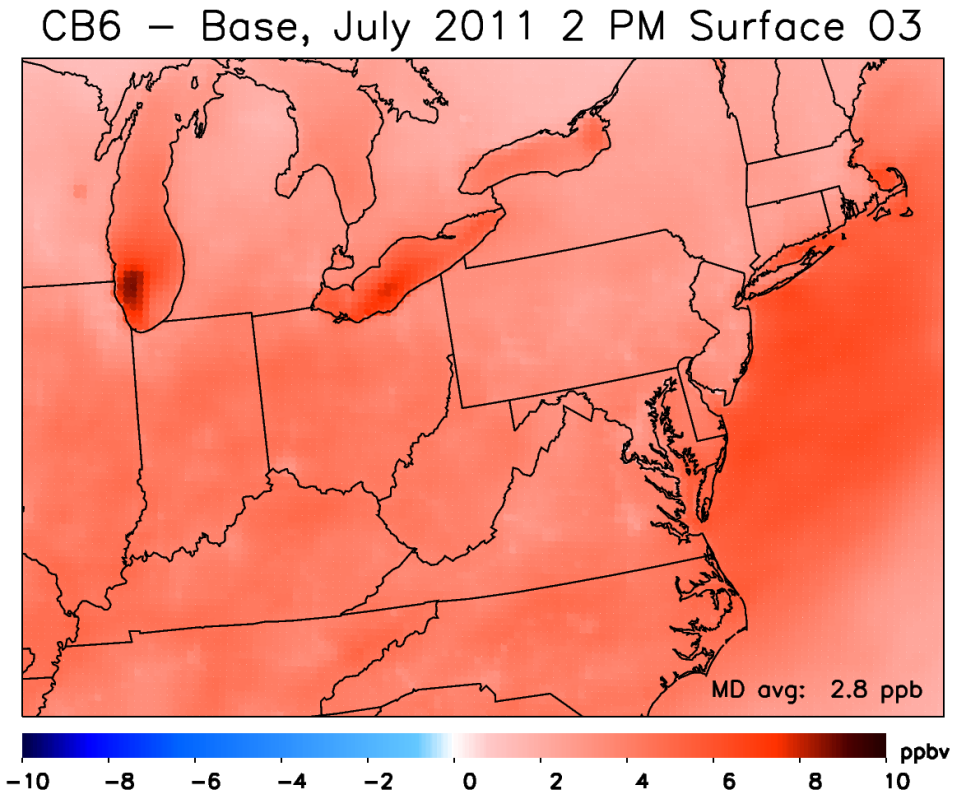

Figure 3-10. CAMx simulation shown for July 2011 at 2 PM local time displaying the surface ozone difference (ppbv): CAMx(CB6) – CAMx(CB05).

3.5 Alkyl Nitrate Chemistry

An issue not addressed in CB05 or CB6 is the proper formation of alkyl nitrates from biogenic VOCs such as isoprene and pinene. This update was instituted in CB6 Revision 2 (CB6r2) [Hildebrant-Ruiz and Yarwood, 2013].

3.5.1 Sources of Alkyl nitrates

Alkyl nitrates are almost exclusively secondary pollutants, which means that they are not directly emitted into the atmosphere; methyl, ethyl, and propyl nitrates are emitted by oceans in extremely low quantities [Neu et al., 2008] and are not important to the sum of alkyl nitrates found on land [Perring et al., 2013]. Instead alkyl nitrates are produced

by the OH-initiated oxidation of hydrocarbons in the presence of NO_x during the daytime or by the NO_3-initiated oxidation of alkenes at night. The daytime reactions are shown below:

(1) $R(alkane) + OH \rightarrow R*(one\ less\ H) + H_2O$

(2) $R* + O_2 \rightarrow RO_2*$

(3a) $RO_2* + NO \rightarrow RO* + NO_2$ OR

(3b) $RO_2* + NO \rightarrow RONO_2$

Alkyl nitrates, $RONO_2$, are formed only when the RO_2 radical "sticks" to the NO molecule (i.e., reaction 3b) instead of oxidizing NO to NO_2 (i.e., reaction 3a). Reaction 3b consists of a rearrangement in which the R-O-O grouping reorders to R-O-NO_2 when reacting with NO. The branching ratio, $k_{3b}/(k_{3a} + k_{3b})$ defined as α (alpha), varies depending on the R-functional group; the larger the branching ratio, the more alkyl nitrates are formed. As seen in Table 3-3, larger molecules typically have higher branching ratios. Alkanes typically have a branching ratio two times higher than alkenes with the same number of carbon atoms.

Table 3-3. Branching ratios of selected alkanes and alkenes from laboratory studies from Perring et al. [2013].

Alkanes	
	Branching Ratio
Ethane (C2)	1.9%
Propane (C3)	3.6%
Octane (C8)	22.6%
Decane (C10)	41.7%

Alkenes	
	Branching Ratio
Ethene (C2)	0.86%
Propene (C3)	1.5%
MVK (C4)	11.0%
Isoprene (C5)*	7.0%

Branching ratios, as with kinetic rate constants, have a strong dependence on pressure and temperature. The branching ratio will decrease at higher temperatures and low pressures (Table 3-4). Thus, the branching ratio is essentially constant throughout the lower troposphere when temperature decreases rapidly with height.

Table 3-4. Branching ratio of n-pentane as a function of temperature and pressure from laboratory studies from Perring et al. [2013].

Branching ratio of n-pentane		
	284 K	300 K
1000 mbar	0.15	0.125
800 mbar	0.13	0.1
500 mbar	0.1	0.085

3.5.2 Isoprene nitrates

Perhaps the most important alkene in the Baltimore/Washington metropolitan area is isoprene, due to its large natural source from oak, hickory and other decidious trees [Rasmussen, 1972]. The branching ratio of isoprene varies between 4 – 12 % [Perring et al., 2013], and has been estimated as 7% by much of the literature [Perring et al., 2010; Farmer et al., 2011]. The difficulty in uniquely identifying the branching ratio is due to eight different isomers of isoprene nitrates which each have a slightly different yield [Perring et al., 2013]. The CB05 gas-phase mechanism estimates the branching ratio of isoprene as 8.8% (see reaction 145 in Yarwood [2005]).

3.5.3 Branching ratio of Alkyl nitrates

The average branching ratio (α) in a region can be calculated from observations and model output by plotting O_x ($\Sigma O_3 + NO_2$) vs. Σ alkyl nitrates [Perring et al., 2010]. The slope of a plot of O_x vs. Σ Alkyl nitrates can be set to the following ratio, seen at the end of the derivation.

$$P(O_x) = \Sigma_i \gamma_i (1 - \alpha_i) k_{OH+RHi} [OH][RH_i]$$

$$P(\Sigma ANs) = \Sigma_i \alpha_i k_{OH+RHi} [OH][RH_i]$$

$$\frac{P(O_x)}{P(\Sigma ANs)} = \frac{\Sigma_i \gamma_i (1 - \alpha_i) k_{OH+RHi} [OH][RH_i]}{\Sigma_i \alpha_i k_{OH+RHi} [OH][RH_i]} = \frac{\bar{\gamma}\,(1 - \bar{\alpha}\,)}{\bar{\alpha}}$$

$$\frac{O_x}{\Sigma ANs} = \frac{\bar{\gamma}\,(1 - \bar{\alpha}\,)}{\bar{\alpha}}$$

The variable γ is defined as the O_x yield per VOC oxidation and is typically 2 for most VOC reactions that produce ozone. A slope of 60 corresponds to a branching ratio of 3.2%, while a slope of 20 corresponds to a branching ratio of 9.1%. Observational studies have yielded branching ratios between 6.5% and 10.5% [Rosen et al, 2004; Perring et al., 2009; Perring et al., 2010], using the above formulation. Studies have also found that the branching ratio is higher for airmasses with fresh emissions [Perring et al., 2010]. The branching ratios of complex anthropogenic hydrocarbons are higher [Perring et al., 2010].

In order to determine the branching ratio in the eastern United States, we plot O_x vs. Σ alkyl nitrates from observations measurements during DISCOVER-AQ. As seen in Figure 3-11 on the next page, DISCOVER-AQ observations yield a slope of 25.8. The branching ratio for the DISCOVER-AQ observations is calculated using the equation at the top of this page, assuming γ to be 2; the branching ratio is α = 7.2%. This value lies within the range – albeit the lower end – suggested by the observational study in Perring

et al. [2010]. A plot of the same paramters using CMAQ model results at the same grid points yields a slope of 15.5 and a corresponding branching ratio of $\alpha = 11.7\%$. This lies outside the range suggested by Perring et al. [2010] signifying that the branching ratio in CB05 may need to be lower.

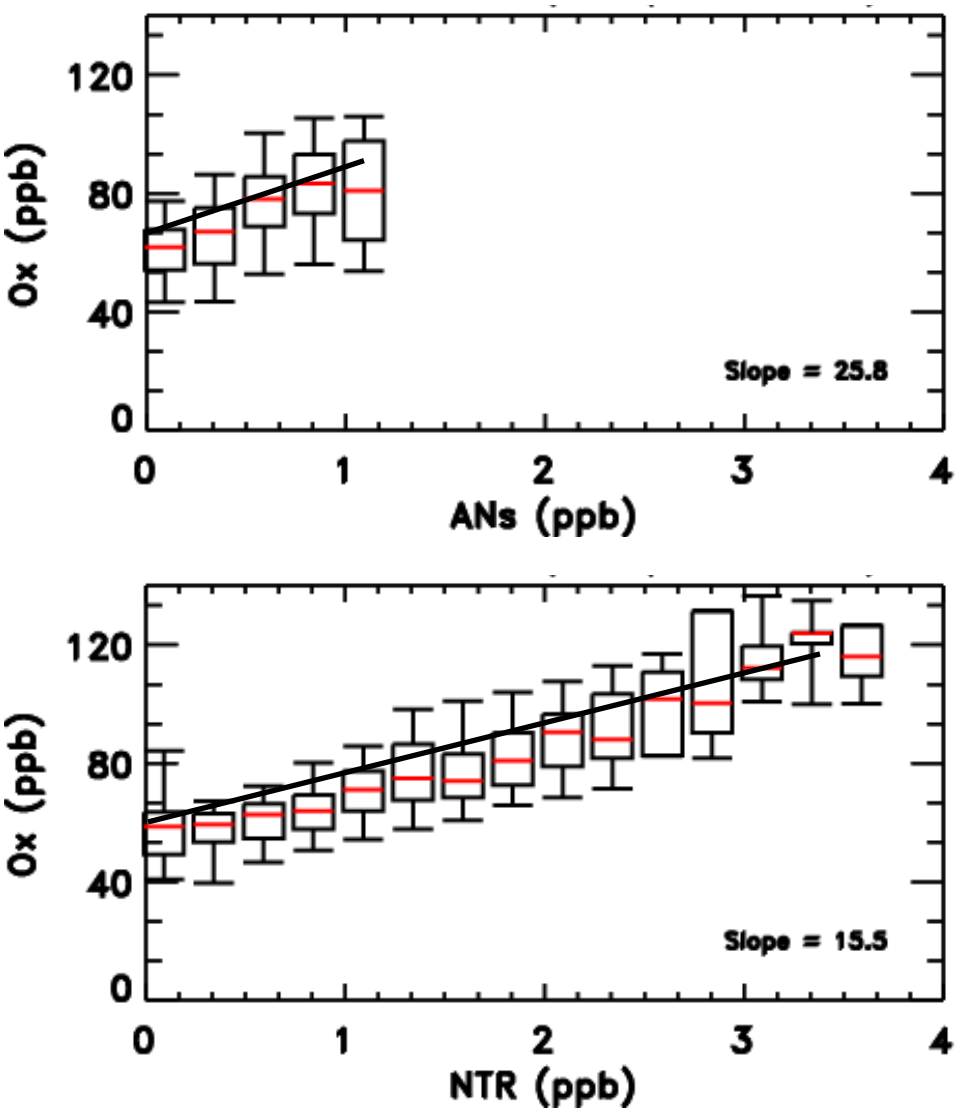

Figure 3-11. Plot of O_x (O_3 + NO_2) vs. Alkyl nitrates using (top) DISCOVER-AQ observations and (bottom) CMAQ 12 km. Slope of the best-fit line can be used to calculate branching ratio. Figure courtesy of Linda Hembeck.

3.5.4. Sinks of alkyl nitrates

Alkyl nitrates can be removed by: (1) dry/wet deposition, (2) photolysis which yields NO_2 and the original RO-functional group, or (3) attack by OH yielding HNO_3 or regenerating NO_2 [Perring et al., 2013]. CB05, without modification, has deposition being the quickest removal mechanism of alkyl nitrates, which has been calculated to be roughly 3 days (1000 m boundary layer and ~0.4 cm/s deposition velocity). Removal by photolysis and OH currently yield lifetimes of 10 days ($j_{NTR} \approx 1.1 \times 10^{-6}\ s^{-1}$) [Canty et al., 2015] and 14 days ($k_{NTR+OH}[OH] \approx 8 \times 10^{-7}\ s^{-1}$) respectively. Literature [Turnipseed et al. 2006; Horowitz et al., 2007; Wu et al., 2012] suggests that these deposition velocities for $RONO_2$ and RO_2NO_2 are too slow.

The photolysis of alkyl nitrates in CB05 is assumed to be of isopropyl nitrate, which has a longer lifetime than most alkyl nitrates. The removal by reaction with OH has been updated in CB6, and yields a reaction rate (k_{NTR+OH}) that is 4.5 times faster; yielding a new lifetime of only 3 days. In CB6, attack of NTR by OH yields HNO_3 and higher-order aldehydes. This will reduce the concentrations of NTR due to the faster deposition velocity of HNO_3. In CB6, the photolysis rate of NTR remains unchanged.

3.5.5 Alkyl nitrates in CB6r2

In the CB05 gas-phase chemistry, alkyl nitrates ($RONO_2$) are grouped into a single family of species called NTR [Yarwood et al., 2005]. For simplicity, NTR was given characteristics of isopropyl nitrates, a well-studied group of alkyl nitrates [Luke et al., 1989]. Removal of isopropyl nitrates by photolysis and OH reactions currently yield lifetimes of 10 days ($j_{NTR} \approx 1.1 \times 10^{-6}\ s^{-1}$) and 14 days ($k_{NTR+OH}[OH] \approx 8 \times 10^{-7}\ s^{-1}$) respectively. A trace gas with a photochemical lifetime of ten days will not contribute significantly to ozone photochemistry since most photochemical reactions take place on

the order of hours. At the time CB05 was developed (i.e., 2005), this was the state of science.

Since 2005, there has been an improvement in our understanding of how organic nitrates react in the atmosphere (see Chapters 3.3.1 – 3.3.4). Hildebrandt-Ruiz and Yarwood [2013] recently updated alkyl nitrate chemistry in the CB6r2 gas-phase chemistry mechanism. The updates more explicitly represent alkyl nitrates in regional air quality models. CB6r2 splits the CB05 alkyl nitrate grouping (NTR) into three separate families: alkyl nitrates that exist primarily in the gas phase (NTR1), larger multifunctional alkyl nitrates that partition to organic aerosol (NTR2) and isoprene nitrates, which react rapidly with OH (INTR). The sinks of the alkyl nitrate species are listed below [Hildebrandt-Ruiz and Yarwood, 2013].

(3-1a) $NTR1 + h\upsilon \rightarrow NO_2$

(3-1b) $NTR1 + OH \rightarrow NTR2$

(3-2) $NTR2 + H_2O_{(aerosol)} \rightarrow HNO_3$

(3-3) $INTR + OH \rightarrow 0.63\,XO_2 + 0.37\,XO_2\mathrm{H} + RO_2 + 0.444\,NO_2 + 0.185\,NO_3 + 0.104\,INTR + 0.592\,FORM + 0.331\,GLYD + 0.185\,FACD + 2.7\,PAR + 0.098\,OLE + 0.078\,ALDX + 0.266\,NTR2$

Reactions 3-1a and 3-3 recycle a portion of the alkyl nitrates back to NO_2, which can participate in ozone production. This better represents how alkyl nitrates can contribute to ozone formation. Typical daytime (8 AM – 8 PM) mixing ratios of NTR1, NTR2, and INTR in the mid-Atlantic are 0.3 ppbv, 0.9 ppbv and 0.1 ppbv respectively.

Spatial plots are shown below in Figure 3-12. In Chapter 5, I show that alkyl mixing ratios calculated using CB6r2 better agree with observations than CB05.

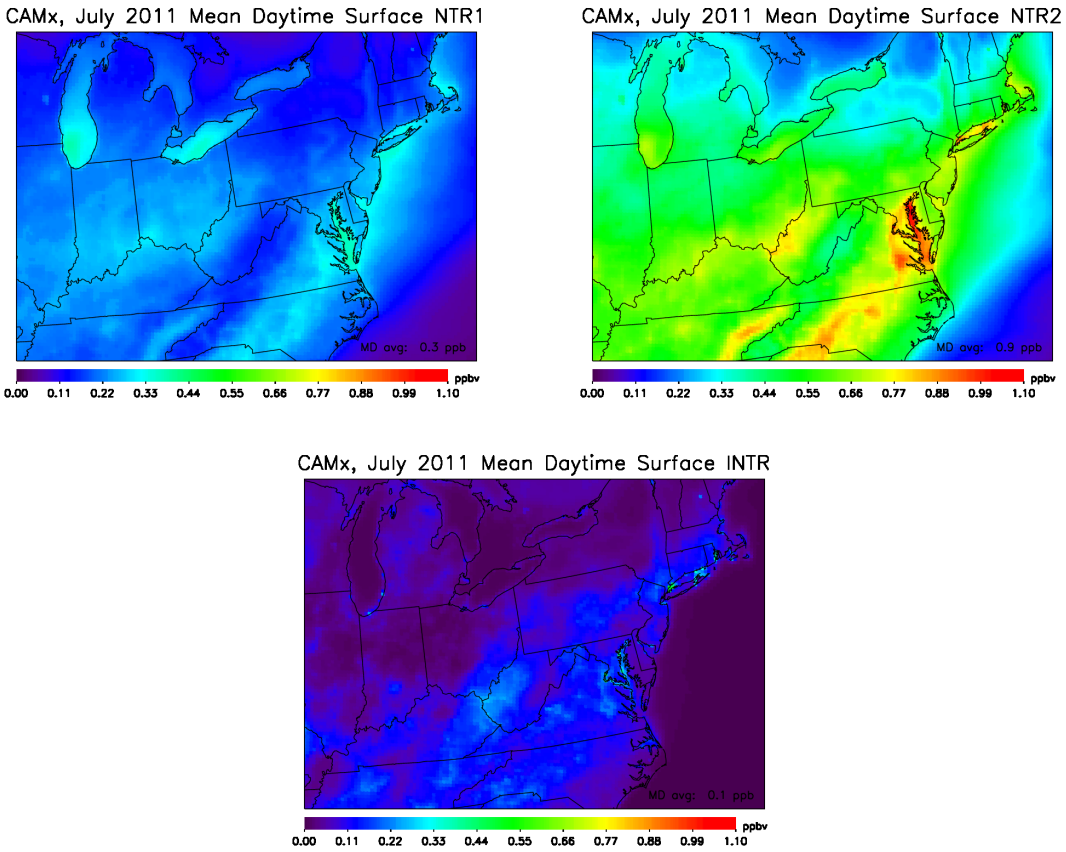

Figure 3-12. Mean daytime (8 AM – 8 PM) mixing ratios of (top left) NTR1, (top right) NTR2, and (bottom center) INTR at the surface in the eastern United States during July 2011.

3.6 Ozone Source Apportionment Tool (OSAT)

CAMx also has the capability to perform source apportionment using Ozone Source Apportionment Technology (OSAT), described in the User's Guide [ENVIRON, 2014]. This software provides a method for estimating the contributions of multiple source areas to ozone formation. An example of output from OSAT is shown in Figure 3-13. Ozone production from each states' emissions can extend well beyond their borders (up to 100's of km, perhaps even 1000 km) showing that transport of emissions can play a large role in ozone production in downwind locations.

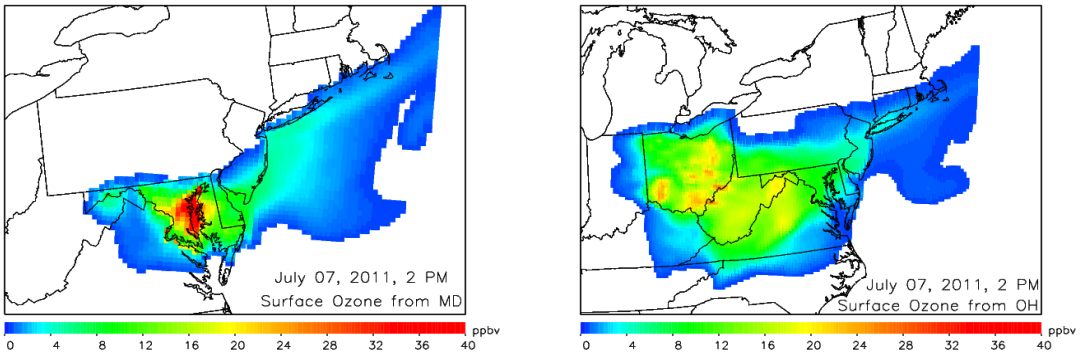

Figure 3-13. An example of surface ozone attributed to the emissions from (left) Maryland and (right) Ohio, at 2 PM on July 7, 2011.

OSAT uses four passive tracers to track ozone and its precursors. The four tracers are: N_i (NO_x tracer for source grouping *i*), V_i (VOC tracer, weighted by number of carbons, for source grouping *i*), $O3N_i$ (tracer of ozone formation under NO_x-limited conditions for source grouping *i*), $O3V_i$ (tracer of ozone formation under VOC-limited conditions for source grouping *i*). The ozone at any grid box from source region *i* is the sum of $O3N_i$ and $O3V_i$. This methodology can also estimate the fractions of ozone arriving at the grid cell that are formed under VOC- or NO_x-limited conditions.

The amount of N_i tracer at each grid box and each time step is equal to the amount of N_i tracer from the previous time step plus the amount of N_i emissions during the time

step plus the CAMx-predicted chemical destruction of NO_x (a negative value) weighted by the N_i tracer contribution to the total of all N_i tracers:

$$N_i^{new} = N_i^{old} + N_i^{emissions} + \Delta NO_x \frac{N_i^{old}}{\Sigma N_i^{old}}$$

The amount of V_i tracer at each grid box and each time step is equal to the amount of V_i tracer from the previous time step plus the amount of V_i emissions during the time step plus the CAMx-predicted chemical destruction of VOCs (a negative value) weighted by the V_i tracer contribution to the total of all V_i tracers. A weighting factor based on the OH-reactivity (kOH_i) of each V_i is used to distinguish the reactivity of each VOC:

$$V_i^{new} = V_i^{emissions} + V_i^{old} + \Delta VOC \frac{V_i^{old} \, x \, kOH_i}{\Sigma V_i^{old} \, x \, kOH_i}$$

OSAT then determines whether the grid box is VOC- or NO_x-limited based on Sillman's [1995] P_{H2O2}/P_{HNO3} indicator. When NO_x concentrations are low, the HO_2 radical will find another HO_2 radical, instead of a NO molecule. Termination proceeds via the following reaction, producing H_2O_2:

$$HO_2 + HO_2 \rightarrow H_2O_2 + O_2$$

When NO_x concentrations are high, the OH radical will quickly find a NO_2 molecule, instead of a VOC molecule. Termination proceeds via the following reaction, producing HNO_3:

$$OH + NO_2 + M \rightarrow HNO_3 + M$$

The model needs a specific ratio between the production of H_2O_2 and the production of HNO_3 to determine which reaction dominates at each time step. Sillman [1995] showed that if:

$P_{H2O2}/P_{HNO3} > 0.35$ then the grid box is NO_x-limited (or VOC-saturated)

$P_{H2O2}/P_{HNO3} \leq 0.35$ then the grid box is VOC-limited (or NO_x-saturated)

where P represents the production rates of the H_2O_2 and HNO_3 respectively.

OSAT, as designed, does not assign ozone production to the "transition" region – conditions that arise when the ratio of the H_2O_2 and HNO_3 production rates are between 0.3 and 0.6 [Sillman, 1995]; in OSAT, ozone production is either NOx or VOC- limited. If the grid box is NO_x-limited, then all of the ozone production is attributed to $O3N_i^{new}$:

$$O3N_i^{new} = O3N_i^{old} + PO_3 \frac{N_i^{old}}{\Sigma N_i^{old}}$$

If the grid box is VOC-limited, then all of the ozone production is attributed to $O3V_i^{new}$:

$$O3V_i^{new} = O3V_i^{old} + PO_3 \frac{V_i^{old} \, x \, MIR_i}{\Sigma V_i^{old} \, x \, MIR_i}$$

where MIR represents the maximum incremental reactivity factor [Carter,1994], which approximates the ozone forming potential of various VOCs based on kinetic and mechanistic reactivity effects.

Four reactions are responsible for the chemical destruction reactions and are ordered based on importance: $O(^1D) + H_2O$, $HO_x + O_3$, $O_3 + VOC$, $O(^3P) + VOC$. The amount of ozone chemically destroyed is calculated using integrated reaction rates for these four groups of reactions.

$$DO_3 = k_{O(^1D)+H_20}[O(^1D)][H_2O] + k_{HO2+O3}[HO_2][O_3] + \Sigma k_{O_3+VOC}[O_3][VOC] + \Sigma k_{O(^3P)+VOC}[O(^3P)][VOC]$$

Ozone chemical destruction is then allocated across all ozone tracers based on a weighted average:

$$O3N_i^{new} = O3N_i^{old} + DO_3 \frac{N_i^{old}}{\Sigma N_i^{old}}$$

$$O3V_i^{new} = O3V_i^{old} + DO_3 \frac{V_i^{old}}{\Sigma V_i^{old}}$$

A graphical interpretation of the OSAT tagging process is outlined in Figure 3-14.

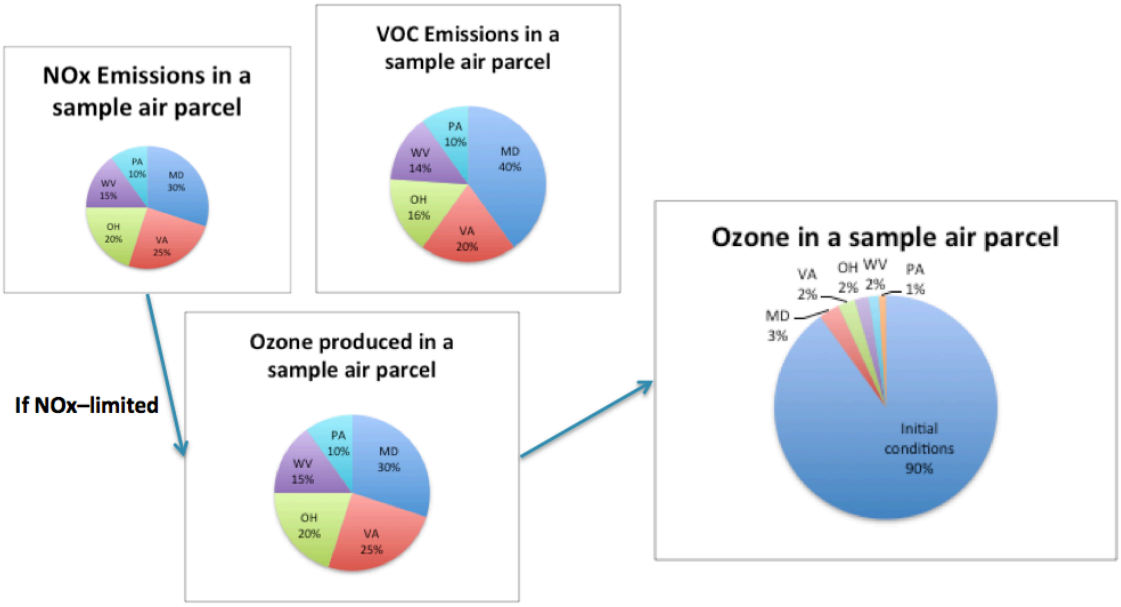

Figure 3-14. Schematic of the OSAT tagging process at the first model time step.

3.7 Anthropogenic Precursor Culpability Assessment (APCA)

A shortcoming of the OSAT software is its inability to attribute ozone in anthropogenic/biogenic interactions to the controllable (i.e., anthropogenic) source. For example, if biogenic VOCs react with NO_x in a NO_x–saturated production environment to create ozone (e.g., downtown Baltimore), OSAT would determine that the non-controllable biogenic VOCs are responsible. While this may be true from a scientific perspective, this masks the real reason why ozone was produced: NO_x concentrations were large. Instead, the APCA software attributes anthropogenic/biogenic interactions to

the controllable, anthropogenic source. Biogenic VOCs are only responsible for ozone production when reacting with biogenic sources from NO_x.

Using APCA, instead of OSAT, causes more ozone formation to be attributed to anthropogenic sources and less to biogenic sources, as shown in Figure 3-15. In the left side panel, we use OSAT to attribute ozone to different source sectors. During the late morning (~11 AM) approximately 15 ppbv of ozone is attributed to biogenic sources. In the right side panel, we use APCA. During the late morning (~11 AM) only 2 ppbv of ozone is attributed to biogenic sources. At this location, we can presume that environmental conditions during the late morning are NO_x-saturated and that OSAT attributes ozone to the biogenic source. When switching to APCA we show a better conceptual representation of the anthropogenic sources responsible for the ozone formation. It is also important to denote that calculations of total ozone (i.e. the top of bar) and boundary condition ozone (i.e., black bar) are not affected by the probing strategy utilized.

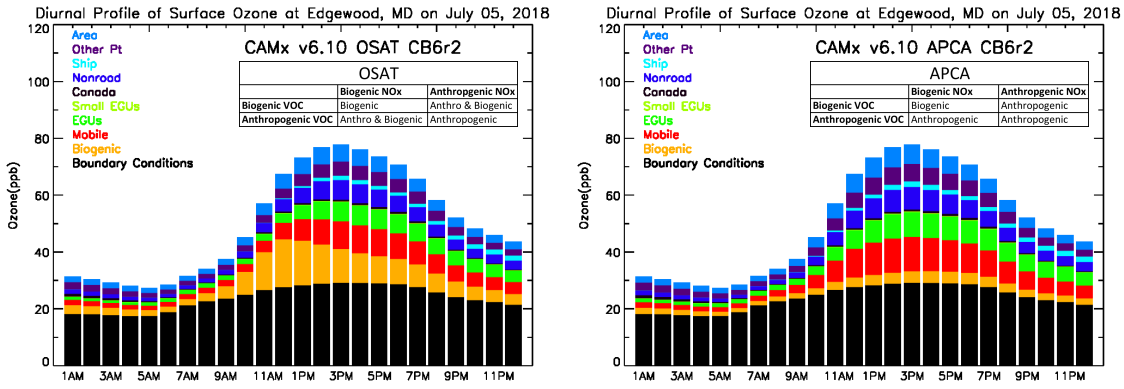

Figure 3-15. Diurnal pattern of ozone source attribution at the Edgewood, MD site for the July 5, 2018 projected scenario using (left) OSAT and (right) APCA.

APCA is particularly useful in calculating ozone attribution to grouped source sectors. In Figure 3-16, we show APCA ozone attribution to on-road and off-road mobile sources (i.e., cars and trucks), electricity generating units, non-road mobile sources (i.e., construction vehicles, farm equipment, recreational marine, etc.), and large marine vessels (C3 marine).

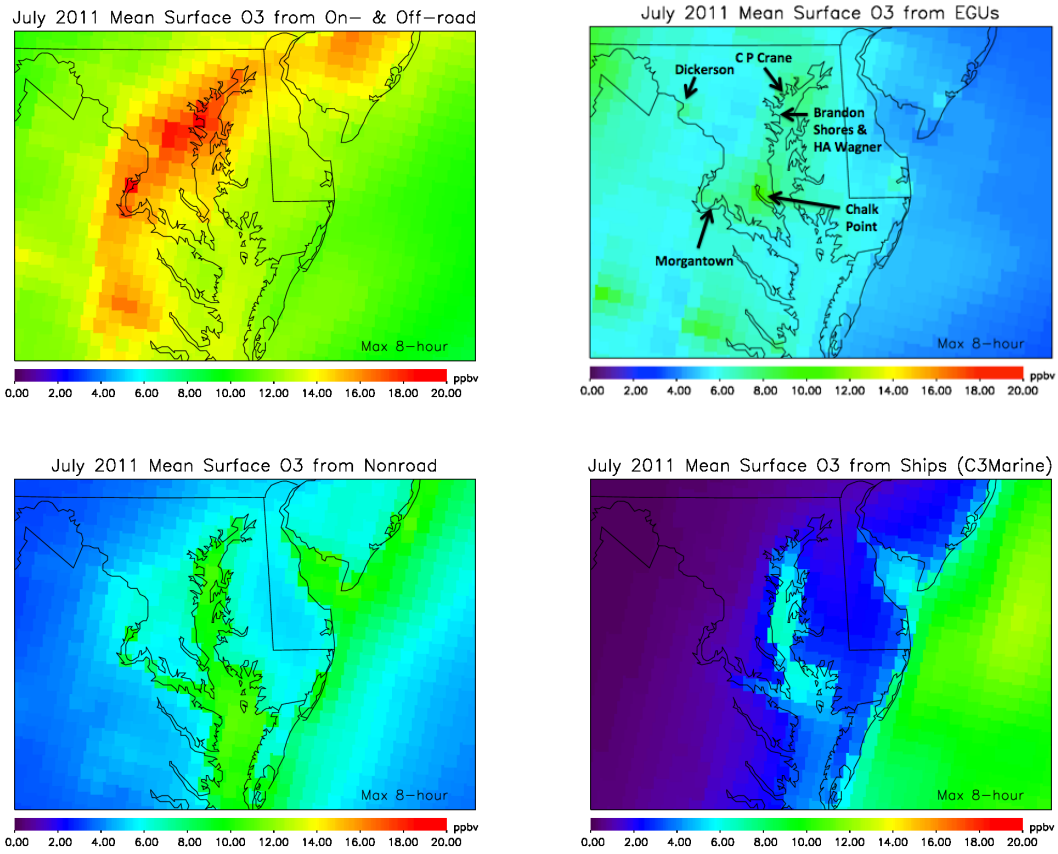

Figure 3-16. APCA source attribution during the mean 8-hour maximum ozone in the July 2011 baseline simulation for the following source sectors (top left) on- and off-road mobile sources (top right) electricity generating units (bottom left) nonroad mobile sources and (bottom right) large marine vessels.

3.8 Chemical Process Analysis (CPA)

The chemical process analysis (CPA) software uses integrated reaction rates to provide information on how specific model calculations were obtained. For example, the $NO + HO_2 \rightarrow NO_2 + OH$ is an O_x production pathway. The model can integrate the

reaction rate (i.e., $\int_{t_o}^{t_f} k_t[NO]_t[HO_2]_t \ dt$) to calculate how much NO_2 has been produced from this reaction throughout each time step. In Figure 3-17, we show July 2011 monthly mean O_x production rates in the eastern United States, in which the NO + HO_2 reaction is the dominant ozone production pathway. O_x production rates are highest in urban centers, such as Washington DC, Charlotte, Cincinnati, and Chicago, where hourly O_x production rates exceed 15 ppbv per hour. Over the state of Maryland, O_x production rates averaged 8.1 ppbv per hour. The CPA software can be particularly useful when diagnosing how ozone production and loss rates change over time (see Chapter 6).

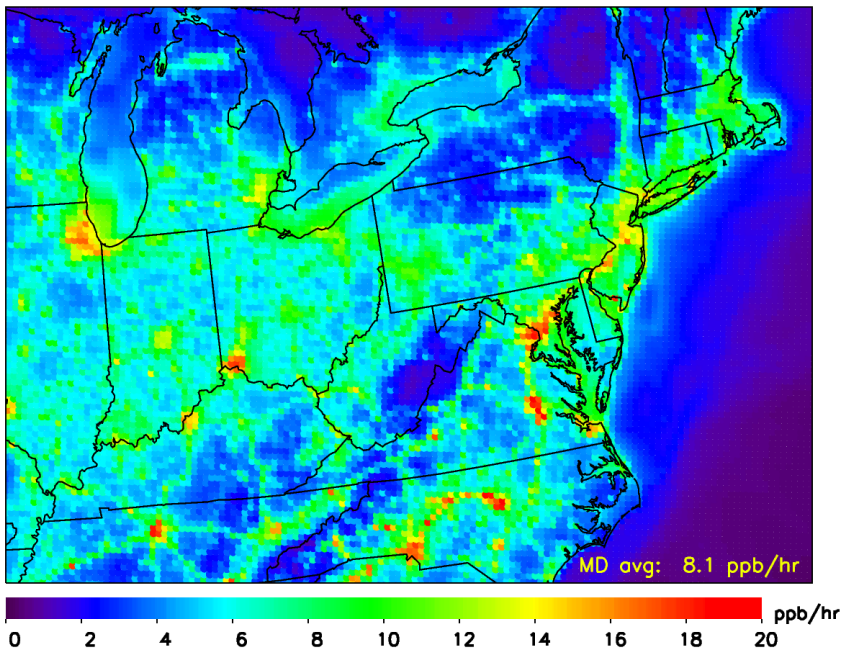

Figure 3-17. Mean daytime (8 AM - 8 PM) July 2011 O_x production rates (ppbv/hr) in the eastern United States using Chemical Process Analysis (CPA) software.

3.9 2007 Test Model Simulations

To better understand the model, we conduct quick test simulations that focus on the July 6-10, 2007 air quality episode. On July 9, 2007 the Fairhill, Maryland ozone monitoring site registered an 8-hour maximum ozone mixing ratio of 125 ppbv, well above the 80 ppbv NAAQS at the time.

A baseline CAMx v.5.40 simulation was compared to observations during July 9, 2007. We show predicted 8-hour maximum ozone from baseline simulation in Figure 3-18 compared to observations. The baseline simulation has a high bias of approximately 10 ppbv during this air quality episode. The 12-km simulation is unable to match the high spatial gradient in ozone observed along the northern Chesapeake Bay. The Bay breeze is likely contributing to the observed high ozone concentrations in Edgewood, Aldino, and Fairhill.

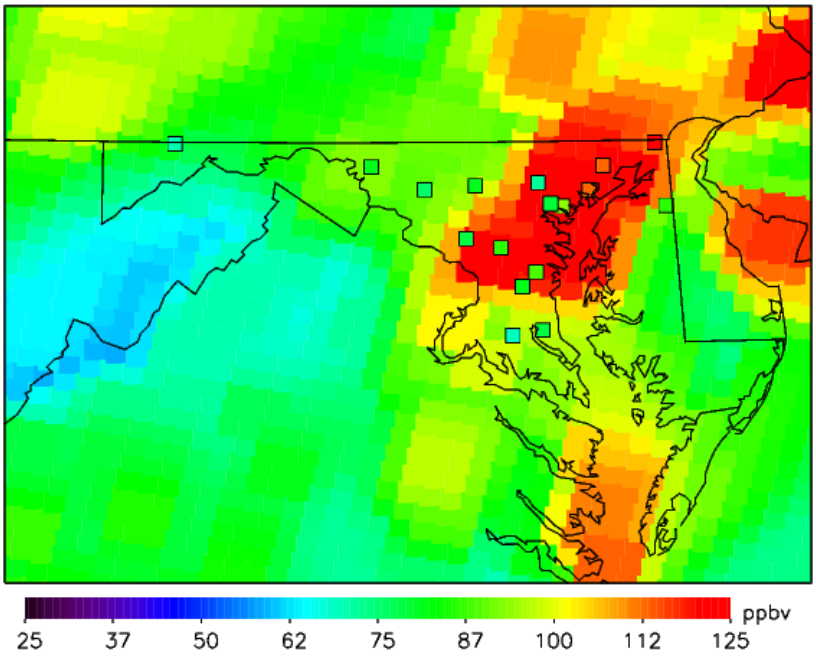

Figure 3-18. July 9, 2007 CAMx v5.40 baseline model simulation of 8-hour maximum ozone; Observations are denoted by square boxes.

Using OSAT with no modifications, we can attribute the total ozone to different regions within the modeling domain. Figure 3-19 shows a stacked bar chart of total ozone in the Baltimore region during an average July 2007 day and during three poor air quality days. During an "average day" in July 2007 roughly one-third of the ozone is attributed to the boundary conditions, one-third is attributed locally to Maryland, one-third is attributed to everywhere else in the modeling domain including the other states listed.

During the air quality episode in July 2007, local emissions are the largest contributor, while boundary conditions and everywhere else in the modeling domain have less significance. Upwind sates such as Ohio and Virginia also contribute more during the poor air quality days than during "average" days, suggesting interstate transport is playing an important role.

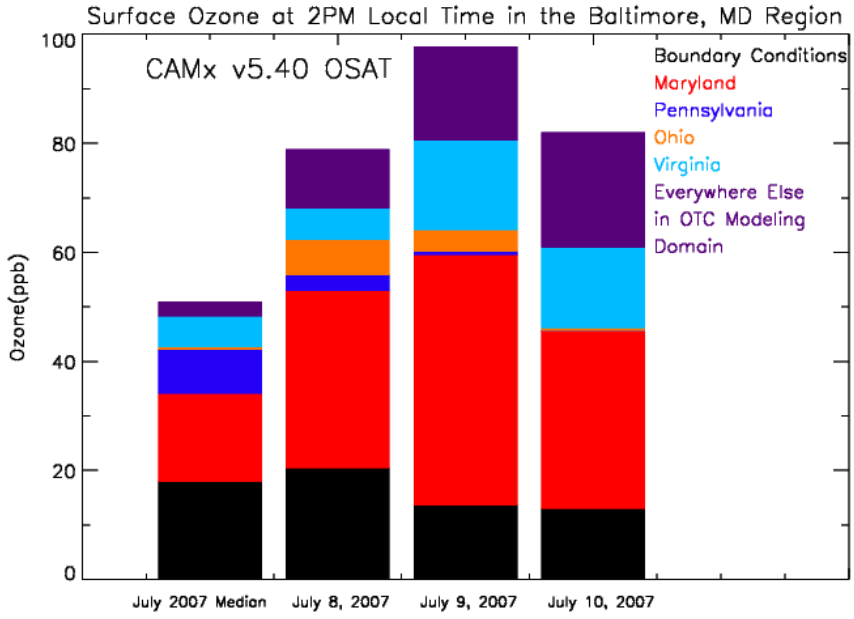

Figure 3-19. Ozone concentrations at 2PM in Baltimore, MD during the July 2007 median and three poor air quality days: July 8 – 10, 2007. Total height of the bar indicates the total mixing ratio, while individual colors represent the portion attributed to each source.

OSAT was also used to tag large individual point sources. The largest power plants, often located in rural regions, account for more than 95% of NO_x emissions in 12 x 12 km grid boxes. Figure 3-20 shows the ozone apportioned to the 10 largest point sources in the Ohio valley during a baseline simulation. Each point source generates >10 ppbv ozone locally and when combined can account for 2-3 ppbv of ozone in the Baltimore, MD region.

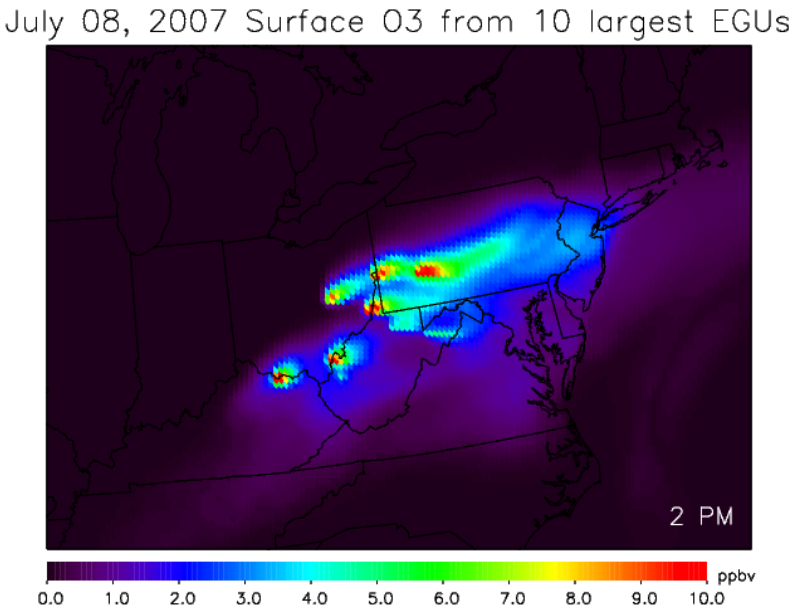

Figure 3-20. Ozone concentrations attributed to the 10 largest power plants at 2 PM during July 8, 2007, a poor air quality day.

3.10 Conclusions

CAMx has four features that can make it advantageous compared to similar Eulerian photochemical dispersion models such as CMAQ.

1. The use of eddy diffusion, K_z-theory (O'Brien, 1970) for vertical diffusion, which allows for a faster model run-time than the Asymmetric Convective Mechanism 2 (ACM2) parameterization (Pleim et al. 2007) for vertical diffusion.
2. The CB6r2 gas-phase mechanism with updated reaction rates and more detail for higher-order hydrocarbons.
3. Emissions tagging tools such as the Ozone Source Apportionment Tool (OSAT) and the Anthropogenic Precursor Culpability Assessment (APCA).
4. The Chemical Process Analysis (CPA) tool which tracks the formation and destruction rates of several important gas-phase reactions.

4. Model Evaluation

4.1 WRF Temperature Analysis

Before conducting air quality simulations, I analyzed the accuracy of the 12-km CONUS WRF v3.4 meteorology simulation for 2011 conducted by EPA [2014d] and described in Chapter 3.2. Analysis nudging for temperature, wind, and moisture was applied above the boundary layer only [EPA, 2014d]. The EPA [2014d] found a mean bias of 2-m temperature centered around zero in their 12 km CONUS simulation, but a mean temperature error of ~2 °C (i.e., for any given day the temperature averages 2° C above or below the observation, but there is no consistent bias).

Here we conduct a quick analysis of the simulation of 2-m temperature in Maryland during July 2011. In Table 4-1, we show that the majority (58.1%) of days had maximum daily temperature errors of less than 1° C. Six days had errors of 1 – 2° C, and six days had errors >2° C.

Table 4-1. Temperature error (° C) of the maximum daily temperature at the Baltimore Washington International Airport during July 2011 between observations and the WRF v3.4 simulation.

Temperature error (°C)	# Days	% of Days
0 - 1	18	58.1%
1 - 2	6	19.4%
> 2	6	19.4%
N/A	1	3.2%

While days with poor temperature performance (i.e., errors >2 °C) represent less than 20% of the total days during July, these poor performance days can sometimes occur during ozone exceedance days. We hypothesize that errors in temperature are often the result of the imprecise simulation of clouds, precipitation, and frontal boundaries. In Figure 4-1, we show two examples when WRF missed clouds and subsequently had poor

simulation of the maximum daily 2-m temperature. In the afternoon of July 6th, cloud cover from a system affecting the eastern shore of Maryland extended further to the west and affected the BWI observing station – subsequently, the high temperature on July 6th was over predicted by >2 °C. On July 25th, a cold front passed through the area during the mid-afternoon as seen in the MODIS imagery. The model did not simulate the lack of clouds in the morning, nor the quick drop in temperature following the precipitation.

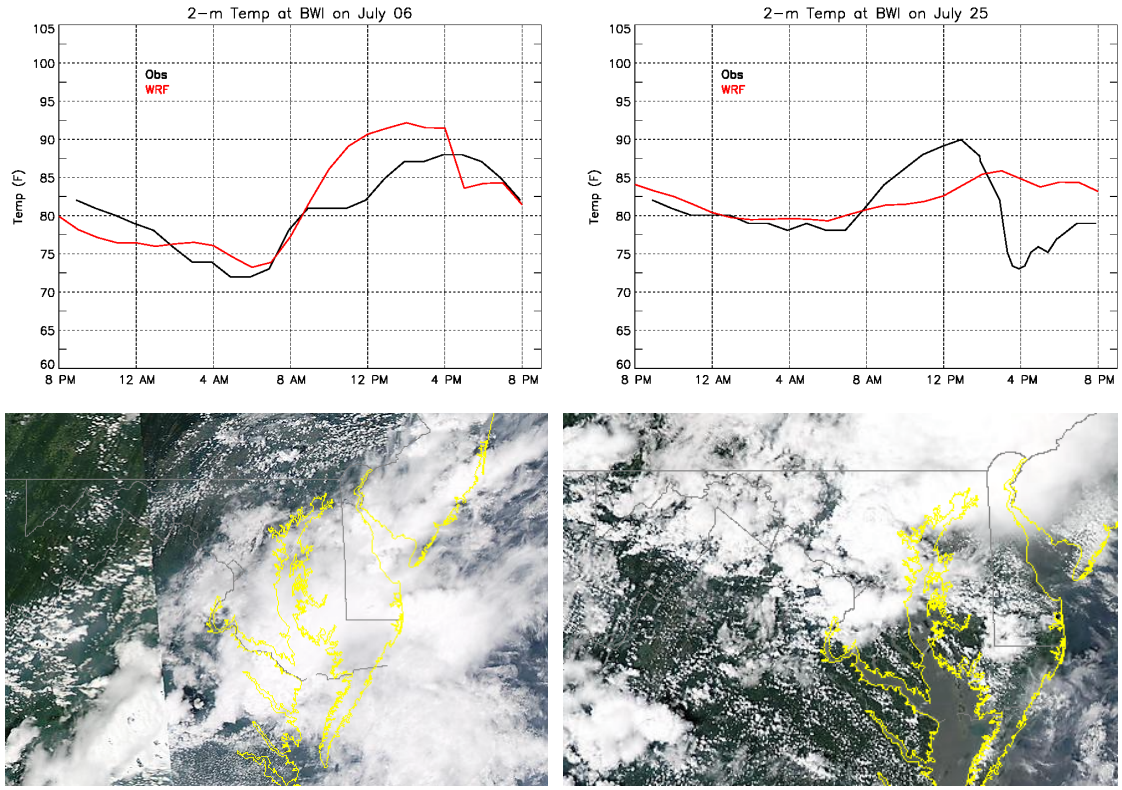

Figure 4-1. (Top) Observations of 2-m temperature compared to the same quantity from the WRFv3.4 simulation for (left) July 6, 2011 and (right) July 25, 2011. (Bottom) MODIS imagery from the Aqua overpass at ~2:30 PM local time for (left) July 6, 2011 and (right) July 25, 2011. MODIS imagery from: http://ge.ssec.wisc.edu/modis-today/

While poor simulation of the meteorology is the exception, it will cause air quality models to miscalculate ozone mixing ratios. On July 6th, 2011 CAMx predicted a widespread ozone event for the Baltimore-Washington area. Instead, only two out of

nineteen monitors exceeded the 75 ppbv NAAQS for ozone; some sites observed 8-hour maximum ozone near 40 ppbv. The two sites that did exceed the 75 ppbv threshold on July 6th – Aldino and Piney Run – are located north and west of the low pressure system that affected the Maryland coast (see left side of Figure 4-1). Figure 4-2 shows the model had an 11.9% high bias on July 6 at monitoring sites in Maryland.

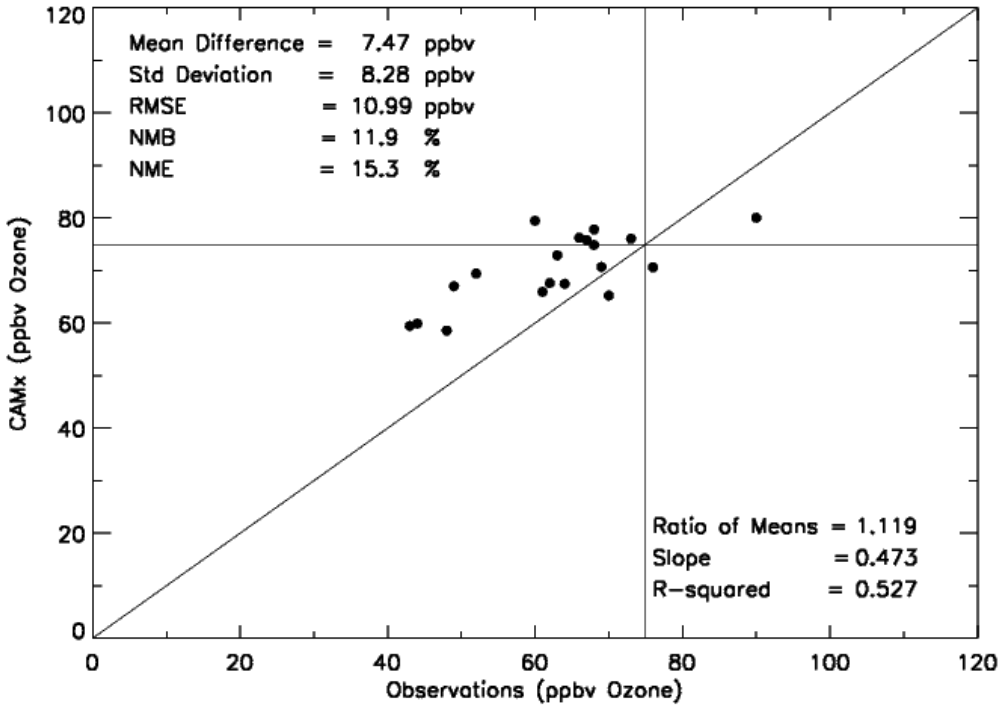

Figure 4-2. CAMx simulation of 8-hour maximum ozone compared to observations of the same value at all nineteen monitoring sites in Maryland on July 6, 2011.

The missed timing of cloud cover and frontal passages can be important issue when comparing ozone observations for individual days.

4.2 Surface Ozone

In order to better understand air quality in the mid-Atlantic, we use CAMx v6.10 to simulate tropospheric ozone in the eastern United States for the summer of 2011. In Figure 4-3 we compare simulated 8-hour daily maximum ozone mixing ratios with

observations from the Maryland Department of the Environment (MDE) monitoring sites during July 2011. We find a +1.64 ppbv mean bias in predicting surface ozone at the nineteen monitoring sites; this corresponds to a normalized mean bias of +2.6%. The standard deviation and root-mean square error are 9.27 ppbv and 9.40 ppbv respectively, indicating substantial variability in predicted ozone on daily timescales. The slope of the best-fit line is greater than one, suggesting that predictions of low ozone mixing ratios are underestimated and predictions of high ozone mixing ratios are overestimated. Further discussion of this bias is in Chapter 5.

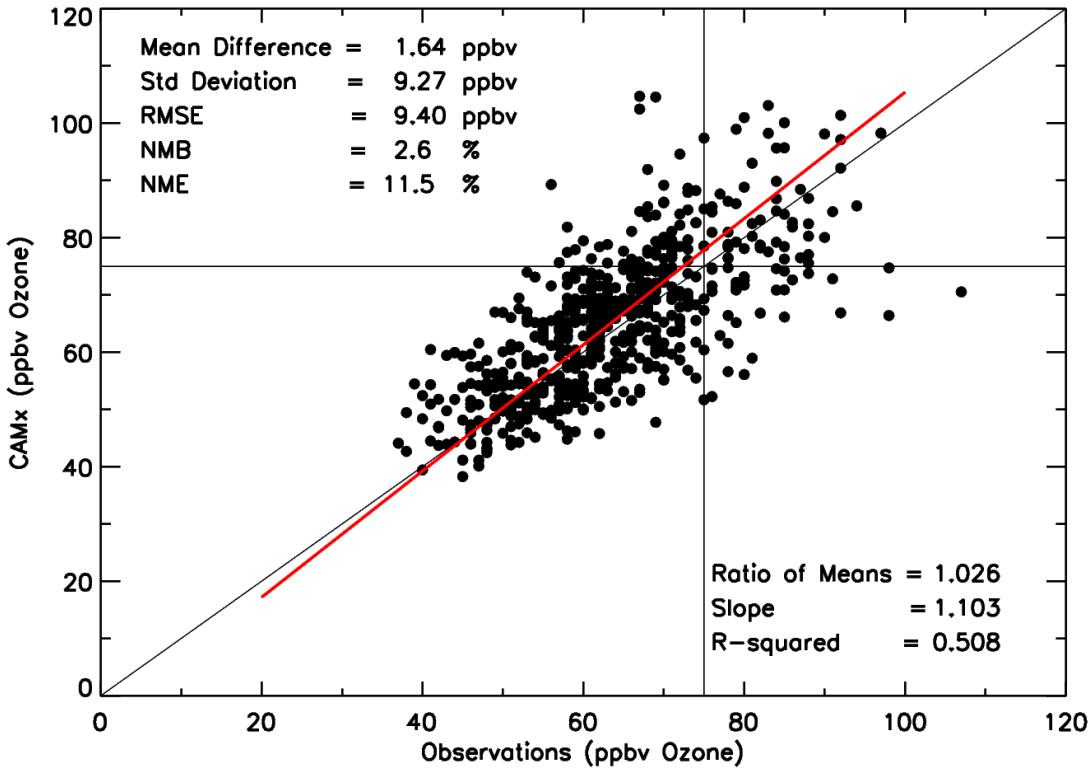

Figure 4-3. Observed 8-hour maximum ozone mixing ratios (ppbv) at the surface from the Maryland Department of the Environment vs. CAMx version 6.10 modeled 8-hour maximum ozone mixing ratios during July 2011.

We conduct a similar analysis using all CASTNET monitoring sites in the eastern United States. In Figure 4-4, we find a +7.00 ppbv mean bias in predicting surface ozone

at the nineteen monitoring sites; this corresponds to a normalized mean bias of +14.2%. Although the model calculates accurate ozone mixing ratios for an urban environment (i.e., Maryland), there is a sizable over prediction in rural locations. The slope of the best-fit line is less than one, suggesting that predictions of low ozone mixing ratios are overestimated even more often.

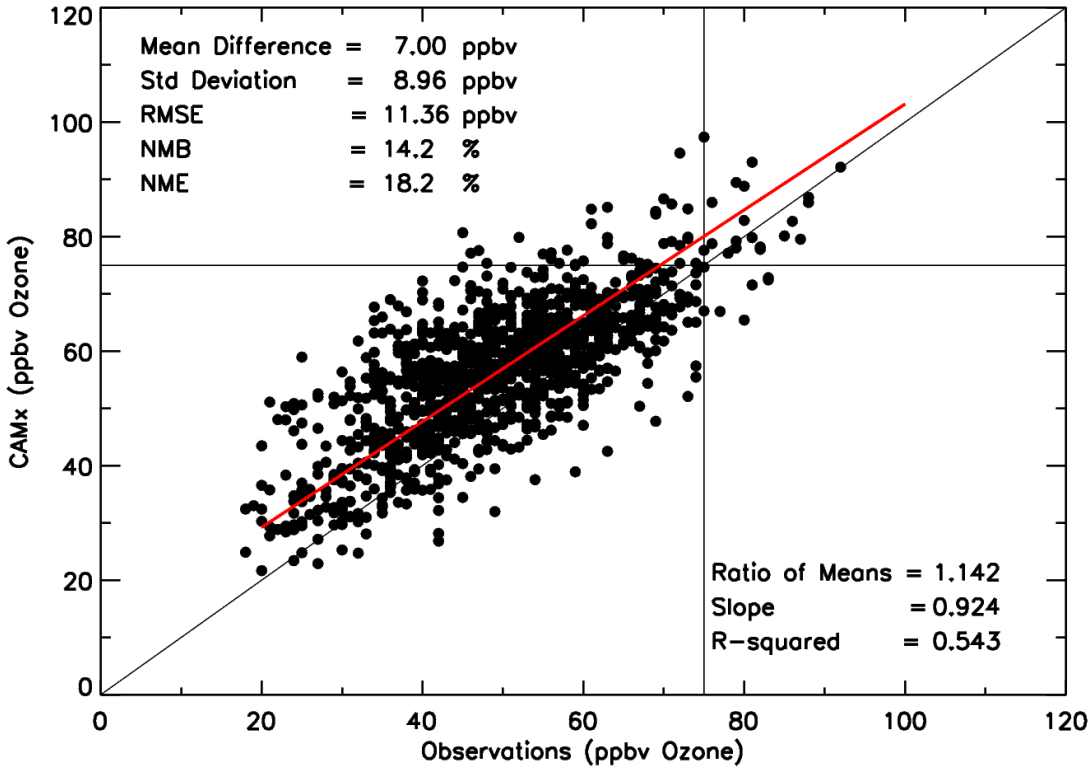

Figure 4-4. Observed 8-hour maximum ozone mixing ratios (ppbv) at the surface from the Clean Air Status & Trends Network vs. CAMx version 6.10 modeled 8-hour maximum ozone mixing ratios during July 2011.

We have also compared 8-hour maximum ozone between CAMx version 6.10 and CMAQ version 5.01. CMAQ was initialized with the same meteorology, emissions, gas-phase chemistry, and boundary conditions; differences in ozone primarily arise due to different vertical and horizontal advection/diffusion schemes; Chapter 3.2 provides a description of the CAMx model set-up. In Figure 4-5, we plot 8-hour maximum ozone

mixing ratios from CAMx v6.10 vs. CMAQ v5.01 at MDE monitoring sites during July 2011. Observed ozone mixing ratios above 75 ppbv are denoted in red. For simulated ozone mixing ratios below 75 ppbv, there is strong agreement between the two models. However, at simulated ozone mixing ratios above 75 ppbv, CMAQ calculates consistently higher ozone than CAMx.

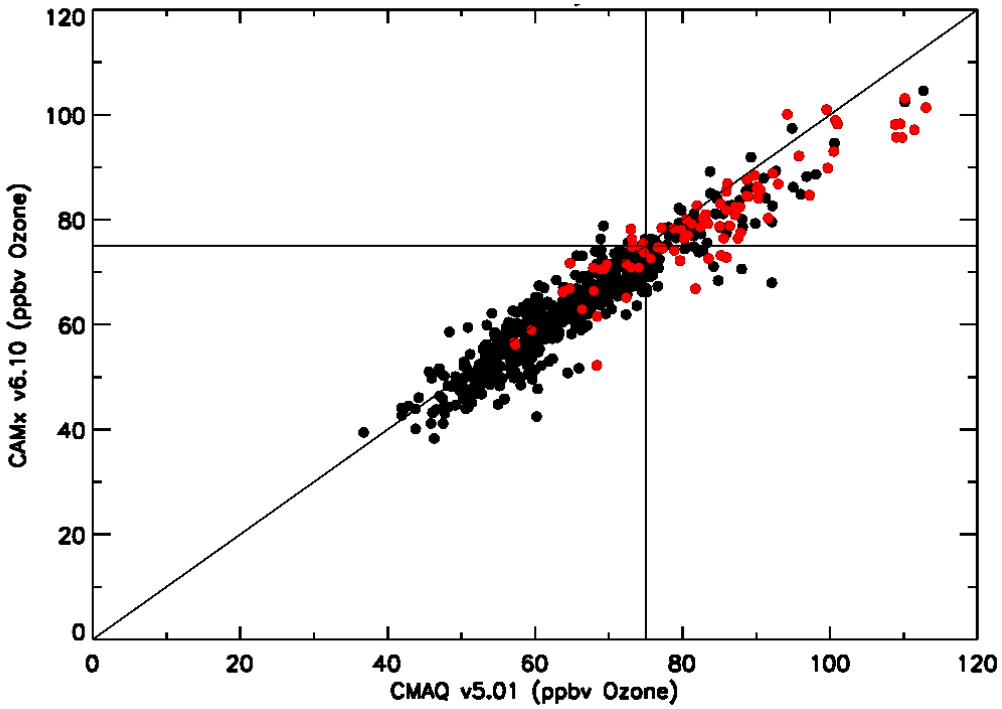

Figure 4-5. CAMx 8-hour maximum ozone mixing ratios (ppbv) vs. CMAQ version 5.01 8-hour maximum ozone mixing ratios at Maryland Department of the Environment monitoring sites during July 2011. Observed ozone mixing ratios above 75 ppbv are denoted in red.

4.3 Deposition

Acid deposition has been a long-standing issue in the eastern United States [Lehmann et al., 2005]. NO_x (emitted primarily by cars and power plants) and SO_x (emitted primarily by coal power plants) can easily transform into soluble acids such as HNO_3 and H_2SO_4. These strong acids dissolve into rainwater making it more acidic. The

increased acidity (lower pH) of rainwater can adversely affect ecosystems [Burns et al., 2008] and ruin statues, monuments, and buildings [Dolske, 1995].

Transformation to nitric acid occurs primarily through the $NO_2 + OH \xrightarrow{M} HNO_3$ reaction during the summertime in the eastern United States [Seinfeld and Pandis, 2006] . During nighttime, the $N_2O_5 + H_2O_{(l)} \rightarrow 2\ HNO_{3(l)}$ reaction can also be an important source of nitric acid [Seinfeld and Pandis, 2006]. In the mid-Atlantic, the $NO_2 + OH$ reaction dominates; please refer to Figure 6-19 in Chapter 6.

Here we evaluate the CAMx v6.10 12-km simulation for HNO_3 wet deposition during July 2011. In Figure 4-5, we compare HNO_3 wet deposition from the CAMx simulation to observations of the same quantity from NADP monitoring sites in the mid-Atlantic. For July 2011, the model appears to be accurately simulating wet deposition in urban centers. The two sites downwind of major metropolitan areas (Beltsville (MD99) downwind of Washington D.C. and Washington Crossing (NJ98) downwind of Philadelphia) agree well with the CAMx simulation. However, the simulation of HNO_3 in rural areas is mixed. The simulation of wet deposition at Piney Reservoir (MD08) in far northwestern Maryland appears to be accurate, but at most other rural locations the HNO_3 deposition is underestimated. The simulation is particularly poor at simulating HNO_3 deposition over Maryland's eastern shore and rural Virginia.

Figure 4-6 shows a peak in the deposition along the northeast side of Baltimore County. This location also corresponds (perhaps coincidentally) to the bay-breeze convergence zone during days with westerly winds [Loughner et al., 2011]. We suggest adding a monitoring site in this area to better quantify acid deposition to the Chesapeake

Bay ecosystem. This could help determine whether this is an artifact of the model or a real signal in the data.

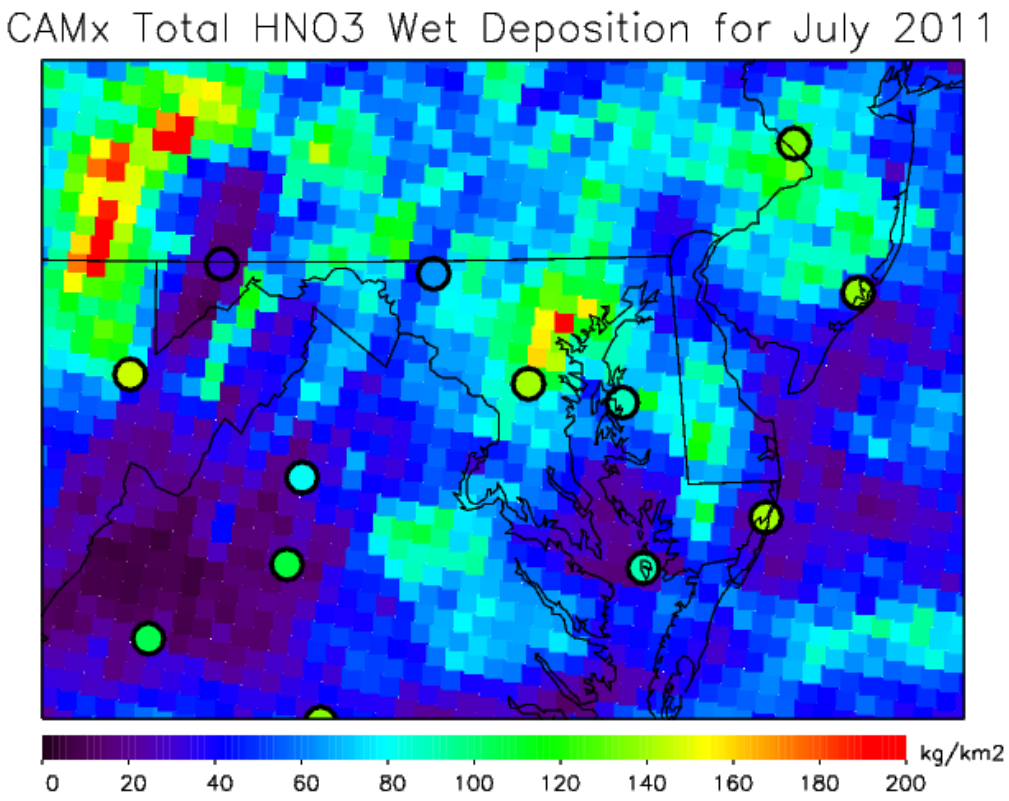

Figure 4-6. CAMx Total HNO_3 Wet Deposition (kg/km^2) during July 2011. Observations from the National Atmospheric Deposition Program (NADP) are denoted in the circles outlined in black.

4.3.1 Trends in Deposition

We have also conducted simulations for July 2002 and July 2018 using CAMx. Particularly important for this study, the meteorology – and therefore precipitation – is identical in each simulation. We have plotted the total (dry and wet) HNO_3 deposition during these two months – July 2002 and July 2018 – in Figure 4-7. The largest deposition of HNO_3 is located within and downwind of the Ohio River Valley (enhanced by emissions from power plants) and the I-95 corridor (enhanced by urban and vehicular emissions). Between 2002 and 2018, we see a 39.5% drop in total HNO_3 deposition.

While total HNO_3 deposition exceeds 400 kg/km^2 in many states throughout the eastern United States in July 2002, deposition rarely exceeds 300 kg/km^2 in any location for the July 2018 projected scenario.

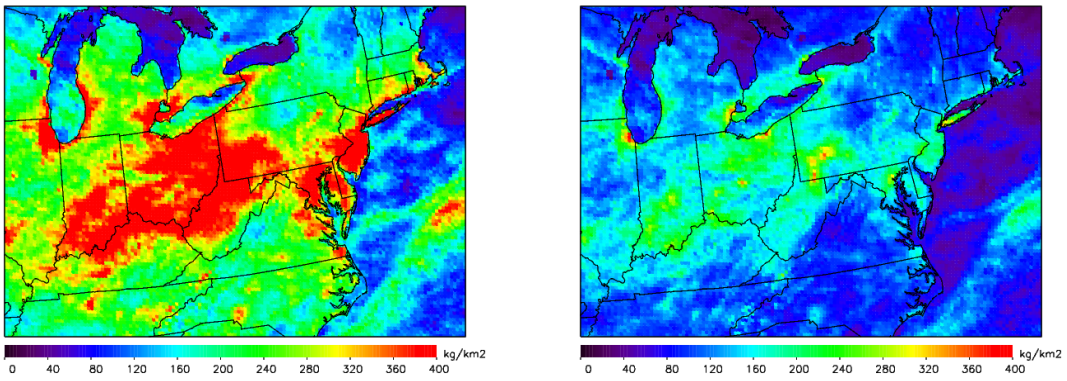

Figure 4-7. CAMx Total HNO_3 Wet and Dry Deposition (kg/km^2) during (left) July 2002 [model domain mean 185 kg/km^2] and (right) July 2018 [model domain mean 112 kg/km^2].

Although acid deposition continues to be a problem, we have seen considerable improvement over the last decade and will continue to see improvement as NO_x and SO_x emissions in the eastern United States decrease over time.

4.4 Ozone in Aloft Plumes

A prominent issue with simulating ozone in regional air quality models is the representation of ozone in aloft plumes [Castellanos et al., 2011; Solazzo et al., 2013]. To see if our model platform may be affected by poor prediction of ozone above the surface layer, we plot ozone from aircraft during the summer of 2011.

In Figure 4-8, we compare ozone from the CAMx v6.10 matched spatially and temporally to all observations from the P3-B aircraft during DISCOVER-AQ in July 2011. The data points are matched at each minute and then averaged over a ten-minute interval; model output is averaged over one hour. The P3-B measured ozone at altitudes

ranging from 300 to 3000 m above ground level. We see an underestimate of ozone mixing ratios of –6.90% at these altitudes. Although there is good prediction of ozone at the surface (see Chapter 4.2), there is an underestimate of ozone in the aloft reservoir.

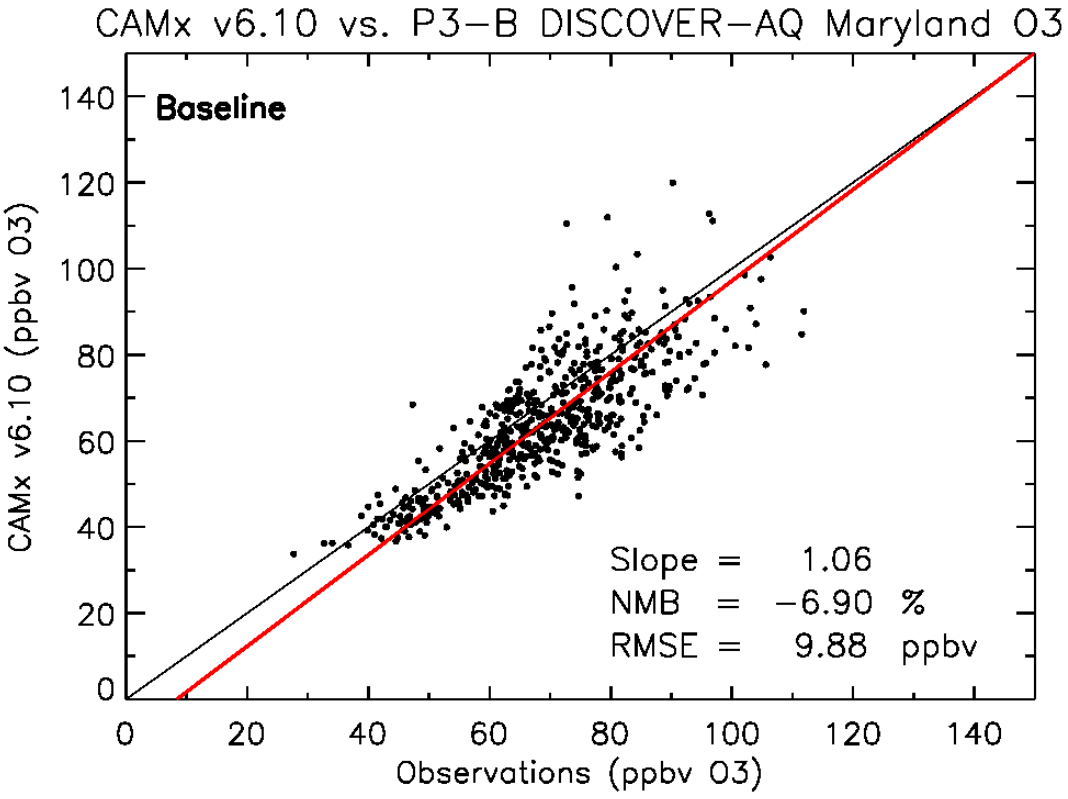

Figure 4-8. Observations of ozone measured on the P3-B aircraft (between 300 – 3000 m above ground level) during DISCOVER-AQ matched spatially and temporally to CAMx v6.10 output.

We expand on this hypothesis by analyzing data from Cessna aircraft flights. During the morning Cessna flights (Figure 4-9), CAMx underestimates the ozone below 300 m by 4.8 ppbv. There is strong agreement between 500 – 1000 m, but above 1000 m (until 2500 m, the highest altitude of the aircraft spirals), there is a continued underestimate of ozone. The peak of the underestimate is at 1300 m where the underestimate is 7.7 ppbv; the model, once again, is not capturing the aloft reservoir of ozone.

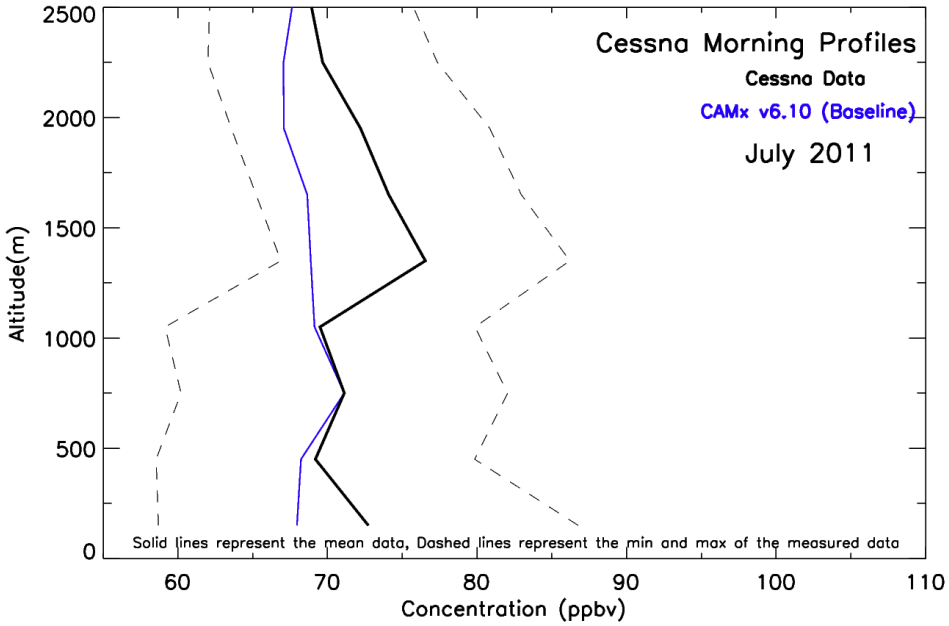

Figure 4-9. Vertical profile of ozone from the Cessna 402B aircraft (black) during ten research flights in the morning hours upwind of Baltimore, MD in the summer of 2011 (June 8, June 9, July 10, July 11, July 18, July 20, July 21, July 22, July 23, July 29). Data from CAMx 6.10 (blue) are matched temporally and spatially with the observations of ozone. Observations and model data are binned into 300 m increments. Dashed lines represent the minimum and maximum of the measured data during all ten flights.

During afternoon flights (Figure 4-10), there is excellent agreement below 300 m – CAMx has an underestimate of 0.9 ppbv – but once again there is a large underestimate of ozone aloft. The largest disagreement is at 1000 m, where there is an underestimate of 12.3 ppbv. At this altitude, the model is simulating ozone mixing ratios that are equal to the minimum ozone mixing ratio observed during all Cessna flights. In the afternoon, the models are underestimating the aloft reservoir of ozone by more than in the morning.

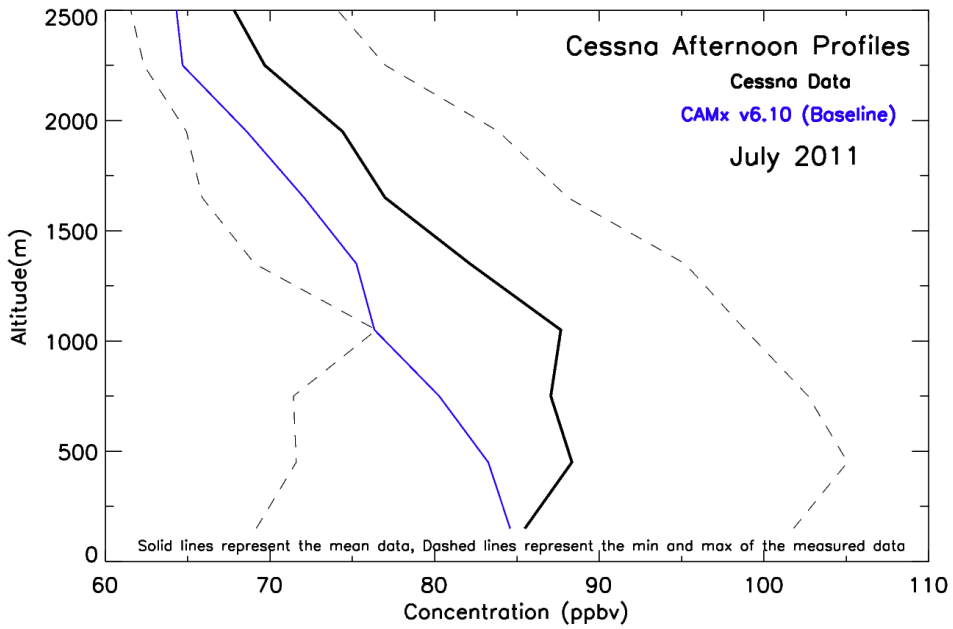

Figure 4-10. Vertical profile of ozone from the Cessna 402B aircraft (black) during ten research flights in the afternoon hours downwind of Baltimore, MD in the summer of 2011 (June 8, June 9, July 7, July 10, July 11, July 18, July 20, July 21, July 23, July 29). Data from CAMx 6.10 (blue) are matched temporally and spatially with the observations of ozone. Observations and model data are binned into 300 m increments. Dashed lines represent the minimum and maximum of the measured data during all ten flights.

A comparison to observations from ozonesondes launched from Beltsville, MD and Edgewood, MD during July 2011 (Figure 4-11) shows a similar story. CAMx and CMAQ simulations have excellent prediction near the surface, but generally have underestimates above the surface, especially in the afternoon. CMAQ generally has greater mixing ratios aloft and smaller mixing ratios at the surface; this is likely due to the ACM2 vertical diffusion parameterization used in CMAQ (described in Chapter 3.3).

During the morning ozonesonde launches at the Beltsville site, both models show a small underestimate of ozone aloft, especially between 1 – 2 km above the surface. Model prediction of the vertical structure of ozone at the Edgewood site during the morning launches is mixed; there is a consistent over prediction of 10 – 20 ppbv at the

surface, and 5 – 10 ppbv under prediction between 1.5 – 2.5 km above the surface. This seems to imply that the atmosphere is more stable (i.e., less mixed) than the model is predicting, which may be related to Edgewood's location along the Chesapeake Bay.

During the afternoon, both models simulate the mean surface values at Beltsville and Edgewood with considerable accuracy, but not there are large discrepancies aloft. At the Beltsville site, there are large underestimates of ozone aloft. Simulation of ozone aloft at the Edgewood site is better, however, there is still an underestimate of ozone mixing ratios aloft, albeit to a lesser magnitude (i.e., an underestimate of ~8 ppbv).

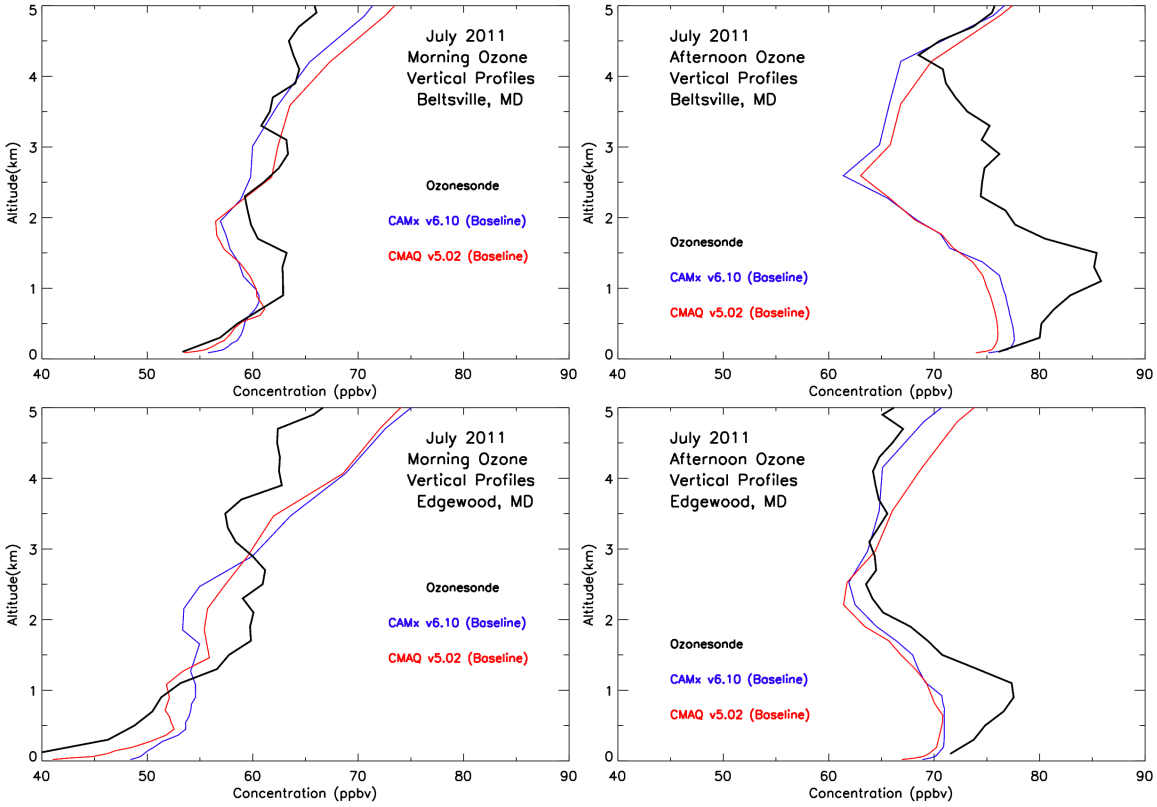

Figure 4-11. Vertical profiles of ozone from ozonesondes (black), CAMx 6.10 (blue), and CMAQ (red). Data from the models are matched temporally and spatially with the observations of ozone during July 2011. Observations and model data are binned into 300 m increments. Top row shows ozonesondes launched from Beltsville, MD and the bottom row shows ozonesondes launched from Edgewood, MD. Left panels show launches in the morning and right panels show launches in the afternoon.

While prediction of mean afternoon near-surface ozone is within +/-2 ppbv, the same cannot be said for prediction of ozone above 500 m. Both CAMx and CMAQ underestimate ozone in the afternoon aloft plume. The underestimates are largest at altitudes between 1000 – 1500 m. This has implications for the models' ability to simulate interstate transport and capture the full extent of the spatial scale of ozone events in the eastern United States.

4.5 Evaluation of Future-Year Ozone Design Values

Regional air quality models are often used to predict air quality in future years based on projected emission scenarios created from best estimates of future policy- and market-based switches. EPA recommends using a relative reduction factor (RRF) method to calculate the likeliest fourth highest daily maximum ozone mixing ratio in the future year (the NAAQS for ozone is currently based on the 4^{th} highest maximum daily 8-hour ozone) [EPA, 2014b]. The procedure is as follows:

1. Complete a simulation for a base year – in this example, the ozone season of 2011 will be the base year.
2. Conduct an analogous simulation with future year emissions and meteorology identical to the baseline year – in this example the ozone season of 2018 will be the future year. This method does not account for changes in meteorology including climate change.
3. Calculate the 8-hour maximum ozone for every day at the source receptor location – in the following example we show source receptor locations in Maryland – during the 2011 and 2018 ozone seasons.

4. Count the ten highest values in 2011 and match them temporally to the same days in the 2018 simulation (the highest value is allowed to be in an adjacent grid box, if that is the case, the value must be matched spatially as well). If the top ten values in the baseline simulation are not greater than 60 ppbv, then we are allowed to choose at least five days above a 60 ppbv. If a source receptor location does not have five days above 60 ppbv, a RRF cannot be calculated.
5. The RRF is defined as the average ozone mixing ratio of the top ten days in 2018 divided by the average ozone of the top ten days in 2011. Values are generally between 0.8 and 0.95.
6. The RRF is then multiplied by the ozone design value in the base year – a weighted 5-year running mean of the observed 4^{th} highest maximum daily ozone – to obtain the future year design value.

A limitation of using the RRF to predict future air quality is its reliance on a single year's meteorology. Interannual variability of temperature, precipitation, etc. can have a significant effect on air quality; the RRF method does not account for this. Neither can the RRF method account for climate change; for air quality projections under ten years, climate change can be considered negligible, but when projecting air quality more than ten years accounting for climate change may be necessary.

4.5.1 Prediction of 2018 Ozone Design Values

In the 2018 scenario, ozone design values are projected to decrease across Maryland – some locations may see greater decreases than others. In the first example, we use version 1 of the National Emissions Inventory (NEI) generated for 2011 and the projection for 2018. Calculated 2018 ozone design values are denoted in Table 4-2.

Fourteen of the seventeen sites listed have observed 2011 design values above the 75 ppbv 2008 NAAQS for ozone. The highest observed 2011 ozone design value is at the Edgewood source receptor: a mixing ratio of 90.0 ppbv. In 2018, the source receptor at Edgewood is the only location in Maryland that is projected to exceed the 75 ppbv 2008 standard. As discussed in Chapter 1, the ozone NAAQS was lowered to 70 ppbv in October 2015; this causes four additional sites – Davidsonville, Padonia, Essex, and Fair Hill – to be in projected non-attainment of the NAAQS in 2018.

Table 4-2. Ozone Design Values for 2011 and 2018. 2011 values are observed and 2018 values are projected based on a CAMx v6.10 simulation with version 1 NEI emissions.

Maryland Monitoring Location	County	Observed 2011 DV (ppb)	CAMx 2018 Baseline (ppb)
Davidsonville	Anne Arundel	83.0	70.7
Padonia	Baltimore	79.0	71.3
Essex	Baltimore	80.7	71.1
Calvert	Calvert	79.7	68.1
South Carroll	Carroll	76.3	66.8
Fair Hill	Cecil	83.0	70.9
Southern Maryland	Charles	79.0	67.6
Frederick Airport	Frederick	76.3	67.0
Piney Run	Garrett	72.0	61.8
Edgewood	Harford	90.0	79.0
Aldino	Harford	79.3	67.6
Millington	Kent	78.7	66.8
Rockville	Montgomery	76.3	66.9
HU-Beltsville	Prince George's	79.0	67.9
PG Equestrian Center	Prince George's	82.3	70.0
Hagerstown	Washington	72.7	63.9
Furley	Baltimore City	73.7	67.1

We then updated to a scenario that uses version 2 of the NEI emissions. There are three primary differences between the version 1 and version 2 emissions platform. In version 2, mobile emissions estimates from cars, trucks, and motorcycles are now computed with the Motor Vehicle Emission Simulator 2014 (MOVES2014) [EPA, 2014e] instead of MOVES 2010a [Kota et al., 2012]. Biogenic emissions are now

calculated using BEIS version 3.6 instead of BEIS version 3.14 [Pouliot and Pierce, 2009]. Projections for 2018 EGU emission rates are now calculated using Eastern Regional Technical Advisory Committee (ERTAC) software [MARAMA, 2013] instead of the Integrated Planning Model (IPM) [EPA, 2013b].

Projected 2018 ozone design values are denoted in Table 4-3. In 2018, the source receptor at Edgewood, MD is still the only location in Maryland to exceed the 75 ppbv standard. Edgewood is projected to be at 82.4 ppbv using CAMx and 82.1 ppbv using CMAQ. If the standard were lowered to 70 ppbv, then nine additional sites would exceed the threshold.

Table 4-3. Ozone Design Values for 2011 and 2018. 2011 values are observed and 2018 values are projected based on CAMx v6.10 and CMAQ v5.02 simulations with version 2 NEI emissions.

Maryland Monitoring Location	County	Observed 2011 DV (ppb)	CAMx 2018 Version 2 Emissions Baseline (ppb)	CMAQ 2018 Version 2 Emissions Baseline (ppb)
Davidsonville	Anne Arundel	83.0	72.4	72.3
Padonia	Baltimore	79.0	71.6	70.8
Essex	Baltimore	80.7	74.4	74.3
Calvert	Calvert	79.7	72.9	72.3
South Carroll	Carroll	76.3	68.2	68.3
Fair Hill	Cecil	83.0	74.8	74.6
Southern Maryland	Charles	79.0	70.8	70.4
Frederick Airport	Frederick	76.3	68.4	68.1
Piney Run	Garrett	72.0	62.9	61.7
Edgewood	Harford	90.0	82.4	82.1
Aldino	Harford	79.3	72.3	70.7
Millington	Kent	78.7	70.9	70.5
Rockville	Montgomery	76.3	68.1	66.5
HU-Beltsville	Prince George's	79.0	69.0	68.4
PG Equestrian Center	Prince George's	82.3	71.8	71.8
Hagerstown	Washington	72.7	65.0	64.3
Furley	Baltimore City	73.7	68.4	67.5

4.5.2 Prediction of 2011 Ozone Design Values

We can also use 2002 and 2011 simulations to verify the RRF technique. We perform a 2002 simulation using the 2002 NEI as the baseline simulation and a 2011 simulation as the "projected" scenario. We initialize both model simulations with 2011 meteorology. We then calculate "projected" ozone design values for 2011 and compare them to observed 2011 ozone design values (Table 4-4).

In most cases, the modeled ozone design value is greater than the observed ozone design value. Other studies [Gilliland et al., 2008; Zhou et al., 2013; Foley et al., 2015a, Foley 2015b] also found difficulties in simulating the response of ozone to NOx emission controls legislated by the 2002 NOx SIP Call [EPA, 2002].

Table 4-4. Ozone Design Values for 2002 and 2011. We show observed 2002 and 2011 values. We also show 2011 values based on CAMx v6.10 simulation with version 1 NEI emissions. The last column shows a difference between the model and observed values.

Maryland Monitoring Location	County	Observed 2002 DV (ppb)	CAMx 2011 DV (ppb)	Observed 2011 DV (ppb)	2011: Model - Observed (ppb)
Davidsonville	Anne Arundel	98.3	85.9	83.0	2.9
Padonia	Baltimore	88.7	79.6	79.0	0.6
Essex	Baltimore	91.3	82.4	80.7	1.7
Calvert	Calvert	N/A	N/A	79.7	N/A
South Carroll	Carroll	88.7	78.3	76.3	2.0
Fair Hill	Cecil	100.3	88.7	83.0	5.7
Southern Maryland	Charles	93.0	78.3	79.0	-0.7
Frederick Airport	Frederick	87.3	76.0	76.3	-0.3
Piney Run	Garrett	N/A	N/A	72.0	N/A
Edgewood	Harford	102.0	91.1	90.0	1.1
Aldino	Harford	98.0	87.1	79.3	7.8
Millington	Kent	95.3	84.0	78.7	5.3
Rockville	Montgomery	86.7	76.8	76.3	0.5
HU-Beltsville	Prince George's	N/A	N/A	79.0	N/A
PG Equestrian Center	Prince George's	N/A	N/A	82.3	N/A
Hagerstown	Washington	85.3	74.7	72.7	2.0
Furley	Baltimore City	N/A	N/A	73.7	N/A

Model prediction errors varied between -0.7 ppbv and +7.8 ppbv. At all but two sites in Maryland, the model using the RRF method underestimated the benefit of emission reductions. This suggests the RRF method – used to predict 2018 ozone design values – underestimates the effectiveness of pollutant control strategies.

4.6 Changing Ozone Production Rates over Time

We use the chemical process analysis (CPA) tool described in Chapter 3.8 to calculate ozone production rates for the Baltimore and New York City areas. These values do not account for deposition processes, a significant sink for O_x. In Figure 4-12, we show mean daytime (8 AM – 8 PM) net O_x (O_3+NO_y–NO) production rates for July 2002 and July 2018 at the surface. Largest net O_x production rates are in urban areas (Chicago, Washington DC, Philadelphia, New York City, etc.). Of particular interest for Chesapeake Bay ozone (Chapter 2), the highest O_x production rates are over the land, suggesting that slower loss instead of faster production of O_x is causing higher ozone directly over the Bay and other coastal areas.

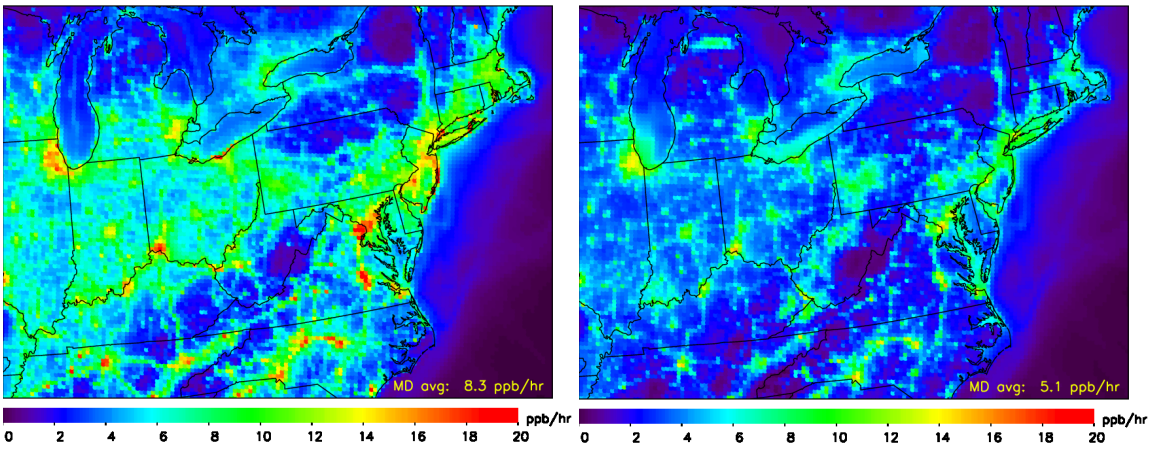

Figure 4-12. Mean daytime (8 AM – 8 PM) net O_x (O_3+NO_y–NO) production rates for July 2002 (left) and July 2018 (right) at the surface.

Ozone production rates have uniformly decreased region wide in response to reductions in NO_x and VOC emissions. In July 2002, the mean net O_x production rate in the Maryland area was 8.3 ppbv per hour. In the July 2018 projected scenario, mean net O_x production rate in the Maryland area drops to 5.1 ppbv per hour.

We then plot net O_x production as a function of NO_x mixing ratio for the Baltimore and New York City regions for July 2002 and July 2018, shown in Figure 4-13. In the Baltimore July 2002 scenario, O_x production rates increase with increasing NO_x up to ~4 ppbv. At NO_x mixing ratios above 4 ppbv, there is little dependence on the O_x production rates as a function of NO_x. In this case, the mean NO_x is 3.4 ppbv and the mean net O_x production is 12.1 ppbv per hour. In the Baltimore July 2018 scenario, NO_x is less than 5 ppbv in all locations. As a result, O_x production rates increase with increasing NO_x at all locations; this shows a NO_x-limited environment. In 2018, the mean NO_x is 1.2 ppbv and the mean net O_x production is 7.5 ppbv per hour.

The New York City area displays a different type of ozone production regime. In the July 2002 scenario, O_x increases with increasing NO_x up to ~3 ppbv. At NO_x mixing ratios above 3 ppbv (the majority of points), there is little dependence on O_x as a function of NO_x. In 2002, the mean NO_x is 9.0 ppbv (three times higher than Baltimore) and the mean net O_x production rate is 14.1 ppbv per hour (only slightly higher than Baltimore). In the July 2018 scenario, the mean NO_x has decreased considerably to 3.8 ppbv, yet there is still little dependence of O_x production rates on NO_x at mixing ratios above 2 ppbv. As a result, even in 2018, New York City remains in a mixed NO_x-limited, VOC-limited environment.

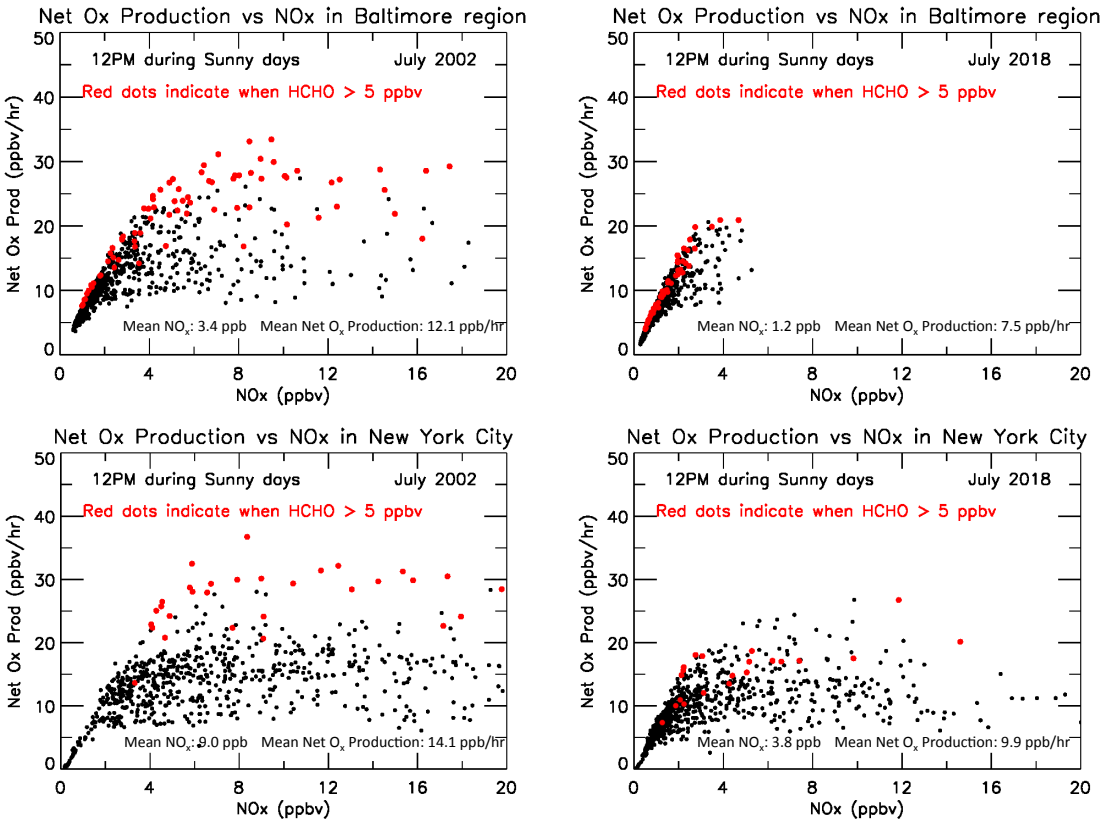

Figure 4-13. 12 PM Net O_x (O_3+NO_y–NO) production rates for July 2002 (left) and July 2018 (right) vs. NO_x during sunny days in the Baltimore region (top), and New York City region (bottom).

4.7 Ozone Transport Patterns

The Cross-State Air Pollution Rule (CSAPR) says that any state contributing more than 1% to a downwind monitor in a separate state must reduce their emissions so that the monitor will achieve attainment of the ozone NAAQS. In Figure 4-14 we show states responsible for pollution at the Edgewood, MD monitor; the states vary by transport pattern. For example, on westerly transport days, Pennsylvania is the second largest individual state (behind Maryland) contributing to the ozone problem at Edgewood. However, on southerly transport days, Virginia is the second largest contributor.

This analysis is particularly important for states that are near the 1% contribution threshold. For example, during the summer of 2011, the state of North Carolina did not contribute more than 1% towards pollution at Edgewood, but on days with southerly winds, North Carolina's contribution well exceeds the 1% contribution threshold. By constraining meteorology in future year scenarios, we make an unfair assumption that wind patterns in future years remain identical to the baseline year (in this case 2011).

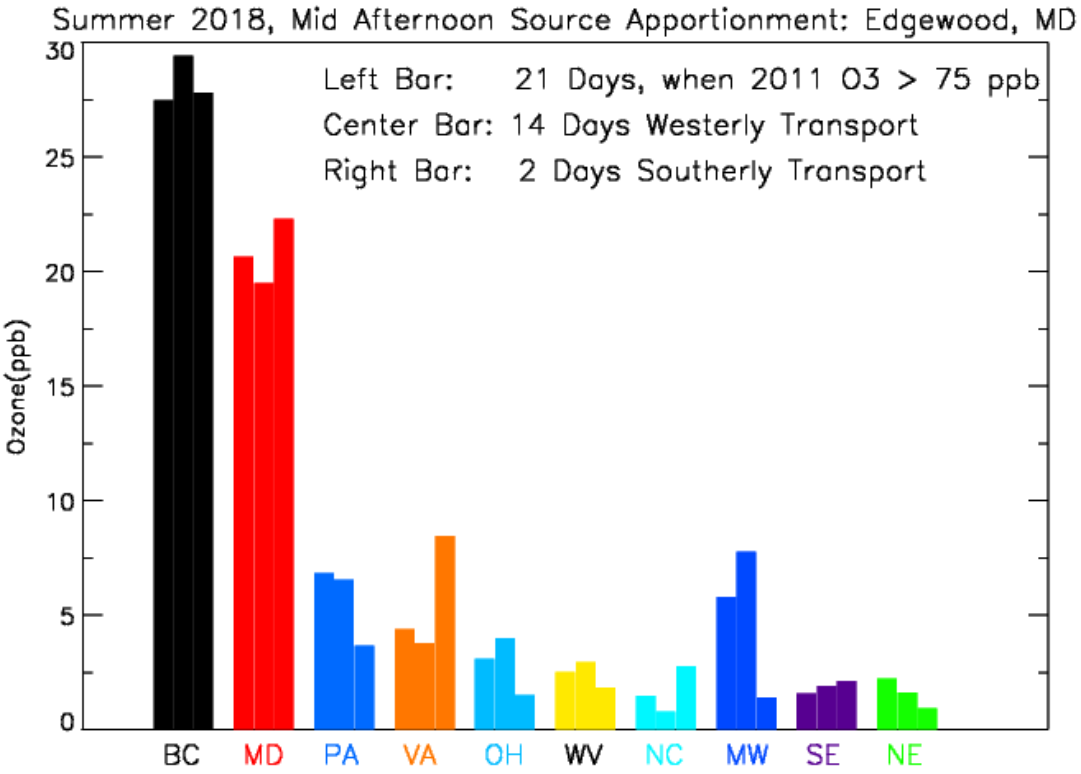

Figure 4-14. CAMv6.10 model output during (left bar; average of 21 days) all days when ozone > 75 ppbv (center bar; 14 days) only days with westerly transport and ozone > 75 ppbv (right bar; 2 days) only days with westerly transport and ozone > 75 ppbv at Edgewood, Maryland.

4.8 Conclusions

The WRF simulation used to drive the meteorology in CAMx reproduces the atmospheric conditions during July 2011 with excellent accuracy. The high temperature error is within 2 °C for more than 80% of the days during July 2011. However, for 20% of the days, high temperature errors were greater than 2 °C. I find two days, July 6th and July 25th, in which the model missed the timing of frontal systems; this directly causes poor simulation of air quality of these two days.

I show that ozone is simulated with reasonable fidelity using CAMx. At urban and suburban Maryland surface monitoring sites, the normalized mean bias in simulating ozone is +2.6 %. However, the simulation does not simulate ozone at rural sites as well; at CASTNET sites, there is a normalized mean bias of +14.2 %. Even though surface ozone in Maryland is simulated reasonably well, ozone in aloft plumes is not. Both CAMx and CMAQ have underestimates of ozone in the afternoon aloft plume. These underestimates are largest at altitudes between 1000 – 1500 m. This has implications for the models' ability to simulate interstate transport and capture the full extent of the spatial scale of ozone events in the eastern United States.

We also find that HNO_3 wet deposition in CAMx is simulated reasonably well. Observations of total HNO_3 at NADP monitoring sites in the mid-Atlantic agree well with the CAMx baseline simulation. However, there is an underestimate of HNO_3 wet deposition in most rural areas. This is consistent with the study by Canty et al. [2015], which shows an underestimate of NO_2 in rural areas. We also show trends in HNO_3 wet deposition between 2002 and 2018; HNO_3 deposition has decreased 40% over this time period.

The RRF method, as developed by EPA, has been used to predict future air quality. We show that all monitoring sites except one – Edgewood – are anticipated to be in attainment of the 2008 NAAQS for ozone (75 ppbv) by 2018. At Edgewood, ozone is projected to be 82.4 ppbv – well above the 75 ppbv standard. However, we also show that the RRF method generally underestimates the response of ozone when constrained to actual changes in emissions. We also emphasize some of the limitations with using the RRF method as designed; most notably interannual changes in meteorology (including year-to-year changes in wind patterns) are not captured.

Lastly, we show the changing ozone production rates over time using the CPA tool in CAMx. Ozone production rates have decreased region-wide in response to reductions in NO_x and VOC emissions. But perhaps more interestingly, ozone production rates in Maryland have declined faster between 2011 and 2018 than between 2002 and 2011 even though NO_x concentrations have decreased more between 2002 and 2011. However, the New York City area displays a different type of ozone production regime – one in which ozone production is sensitive to both NO_x and VOCs.

5. Enhancements to Air Quality Models

5.1 Introduction

Policymakers and regulatory agencies use regional air quality models to predict how future air quality will respond to control strategies [EPA, 2014a]. Many air quality models can skillfully simulate surface ozone in North America for focused studies of certain time periods [Hogrefe et al., 2004; Appel et al., 2007; Ferreira et al., 2011; Appel et al., 2012; Simon et al., 2012].

Despite the accurate simulation of surface ozone, most regional air quality models have difficulty simulating the response of surface ozone to past reductions in ozone precursors [Gilliland et al., 2008; Zhou et al., 2013; Foley et al., 2015a]. This may be linked to the poor simulation of trace gases that are precursors to ozone: NO_x (NO_x = $NO+NO_2$) and volatile organic compounds (VOCs) [Castellanos et al., 2011; Zhou et al., 2013]. Inaccurate simulation of precursor concentrations is particularly concerning because photochemical ozone production is sensitive to the abundance of NO_x and VOCs in the environment [Jacob et al., 2000]. For any given ozone concentration, there can be many different production pathways (e.g., empirical kinetic modeling approach (EKMA) diagrams [Kinosian, 1982; Chameides et al., 1992; Sillman, 1999]), which highlight the non-linear dependence of ozone production on NO_x and VOCs). Therefore, it is critical that air quality models are within the correct ozone production regime (i.e., NO_x-limited vs. VOC-limited) if they are used to forecast how air quality regulations will affect future ozone concentrations.

Many studies show an overestimate, by up to a factor of two, of total reactive oxidized nitrogen (NO_y) in regional air quality models compared to observations [Doraiswamy et al., 2009; Castellanos et al., 2011; Yu et al., 2012; Brioude et al., 2013; Anderson et al., 2014; Goldberg et al., 2014]. Some link the calculation of too much NO_y in air quality models to the overestimate of NO_x emissions from area sources [Doraiswamy et al., 2009], while others link it to an overestimate of NO_x emissions from commercial marine vessels [Brioude et al., 2013]. Anderson et al. [2014] suggest the discrepancy of NO_y is so large that a portion of the error must be due to an overestimate in NO_x emissions from mobile sources since they account for the majority (62%) of NO_x emissions in the 2011 National Emissions Inventory (NEI). Fujita et al. [2012] also find an overestimate of NO_x mobile source emissions in MOVES 2010a, used to develop the NEI.

A better representation of NO_y chemistry may resolve a portion of the overestimate of NO_y noted above. The Carbon Bond 6 Revision 2 (CB6r2) gas-phase chemistry has been released recently [Hildebrandt-Ruiz and Yarwood, 2013]. This updated mechanism more explicitly represents alkyl nitrates in regional air quality models and provides a significant improvement in the simulation of these compounds compared to CB05 [Hildebrandt-Ruiz and Yarwood, 2013; Canty et al., 2015]. CB6r2 splits the alkyl nitrate grouping (NTR) into three families: alkyl nitrates that exist primarily in the gas phase (NTR1), larger multi-functional alkyl nitrates that partition to organic aerosol (NTR2) and isoprene nitrates (INTR) that react rapidly with OH. NTR1 and INTR can recycle back to NO_2, but the only gas-phase sink for NTR2 is conversion to HNO_3. The CB6r2 gas-phase mechanism calculates a shorter lifetime of alkyl nitrates

and faster recycling of NO_x, which agrees better with laboratory studies [Perring et al., 2013] than CB05. In addition to improving the representation of alkyl nitrates in the regional air quality models, this change may also improve the simulation of ozone attributed to sources beyond state borders. Literature also suggests that the deposition velocities of alkyl and peroxy nitrates in air quality models are too slow [Turnipseed et al. 2006; Horowitz et al., 2007; Wu et al., 2012].

As anthropogenic sources of ozone precursors continue to decrease, biogenic emissions will play an even larger role in the ozone formation process. Two models are used to simulate biogenic emissions within regional air quality models: Biogenic Emissions Inventory System (BEIS) [Pouliot and Pierce, 2009] and Model of Emissions of Gases and Aerosols from Nature (MEGAN) [Guenther et al., 2012]. Isoprene emissions are uniformly larger in the MEGAN model within North America than in BEIS [Warneke et al., 2010; Carlton and Baker 2011].

5.2 Methods

We use the Comprehensive Air-quality Model with Extensions version 6.10 to simulate trace gas mixing ratios in the eastern United States for July 2011; Chapter 3.2 provides a detailed description of the baseline model set-up. The Anthropogenic Precursor Culpability Assessment (APCA) probing tool is used as a means to tag ozone source attribution from twelve source regions and seven source sectors. The twelve source regions are shown in Figure 5-1. The seven source sectors are listed in Table 5-1. We also use the Ozone Source Apportionment Tool (OSAT) to calculate the ozone attributed to NO_x- and VOC-limited production regimes. For a detailed description of

CAMx v6.10 and the APCA and OSAT probing tools, please refer to Chapter 3 or the CAMx User's Guide [ENVIRON, 2014].

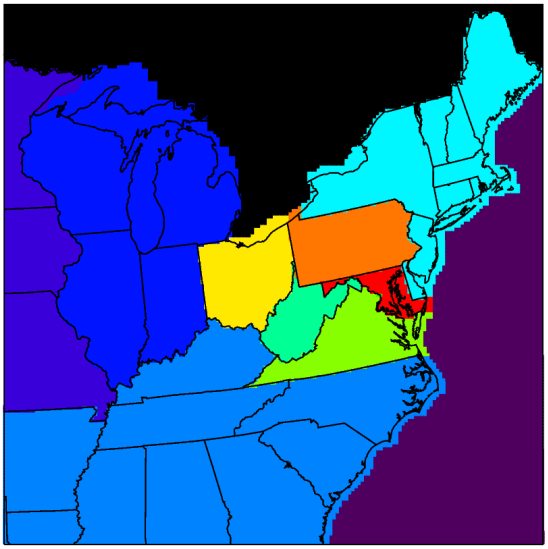

Figure 5-1. CAMx source regions for APCA tagging.

Table 5-1. CAMx source sectors for APCA tagging.

Biogenic
On-road mobile (Mobile)
Non-road mobile (Nonroad)
C3Marine (Ship)
Electric Generating Units (EGU)
Other Point sources (Other Point)
Area sources (Area)

For the modeling in this Chapter, we update the emissions to version 2 of the 2011 NEI as compiled by EPA [EPA, 2014e]. Mobile emissions estimates from cars, trucks, and motorcycles were computed with the Motor Vehicle Emission Simulator 2014 (MOVES2014) [EPA, 2014e]. Biogenic emissions in the baseline simulation were calculated using BEIS version 3.6 [Pouliot and Pierce, 2009].

5.3 Results

5.3.1 Baseline Model Simulation

During July 2011, NASA conducted a comprehensive aircraft and ground measurement campaign in Maryland called DISCOVER-AQ. This campaign provided a temporally- and spatially-rich collection of trace gas and aerosol observations throughout the lower troposphere [Crawford et al., 2014]. This dataset offers an unprecedented opportunity to compare regional air quality models to comprehensive atmospheric observations.

Figure 5-2 compares ozone from the baseline model simulation to P3-B aircraft observations. All observations were taken between altitudes of 300 – 5000 m within the Maryland air shed. We show a slope near unity (1.06) and a normalized mean bias (NMB) of –6.90% indicating a small underestimate of ozone above the surface. Because the NMB is under 10%, the baseline simulation shows good agreement with the observations of ozone. The root-mean square error (RMSE) of the baseline simulation of ozone is 9.88 ppbv.

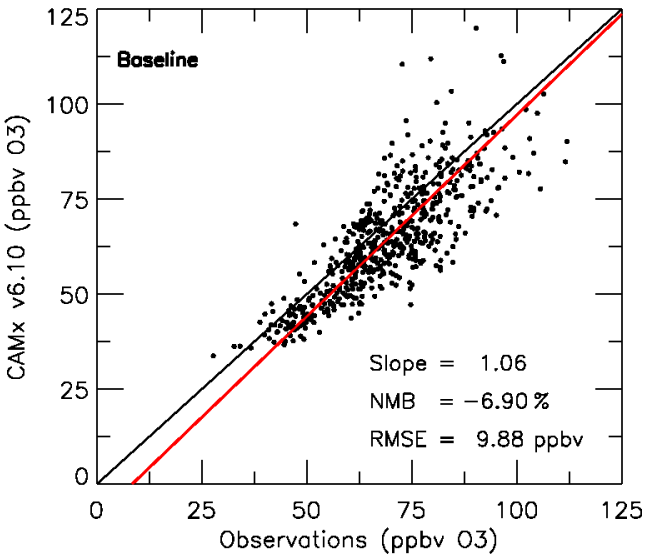

Figure 5-2. Ozone observations acquired by the P3-B aircraft during DISCOVER-AQ Maryland in July 2011 compared to model output from CAMx v6.10 at the nearest model grid point and closest hourly interval. The closest hourly model output is matched to each one-minute averaged P3-B observation; both quantities are then averaged over the same ten-minute interval. Black lines represent the 1:1 line, while red lines represent the linear best fit.

We also provide a comparison with surface observations, in Figure 5-3, which shows even better agreement with observations of ozone.

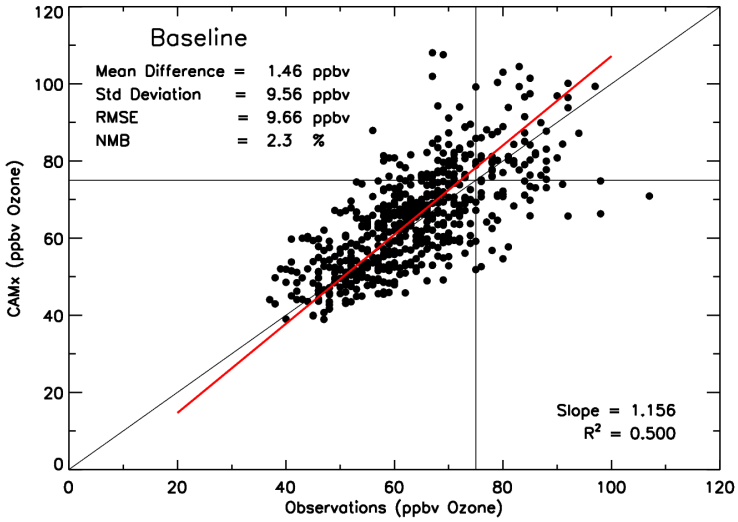

Figure 5-3. CAMx v6.10 model simulated 8-hour maximum ozone mixing ratios compared to observations of the same quantity matched spatially to monitoring sites in Maryland.

Comparing modeled NO_y and HCHO to observations of the same quantities shows large discrepancies (Figure 5-4). The model simulation overestimates NO_y by nearly a factor of two: a slope of 1.91 and a NMB of +86.2%. Conversely, the model simulation underestimates HCHO by nearly a factor of two: a slope of 0.61 and a NMB of –28.3%. Although ozone is being predicted with considerable skill, the ozone precursors (NO_y and HCHO) are not.

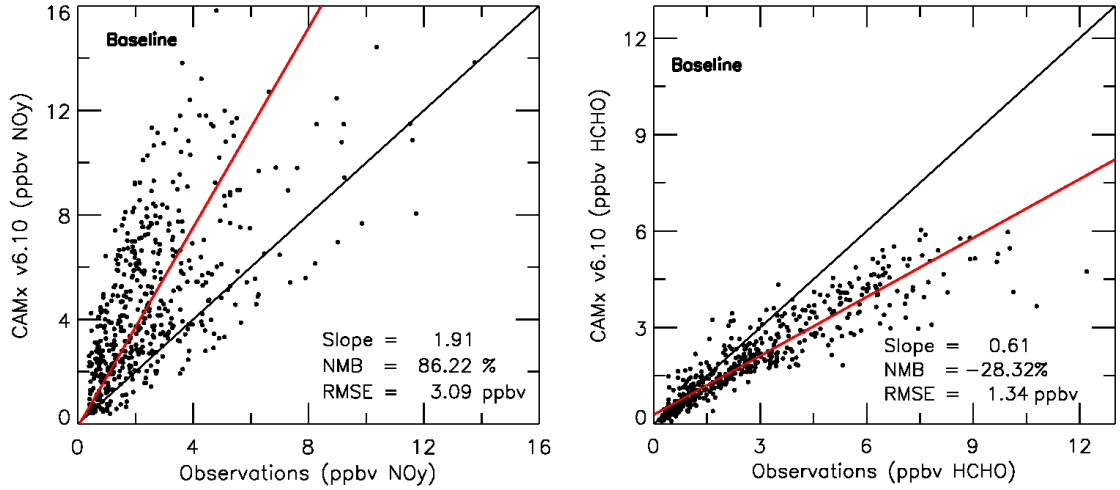

Figure 5-4. Same as Figure 5-2 except now for (left) NO_y and (right) HCHO.

In Figure 5-5, we show comparisons of NO_2, alkyl nitrates, and isoprene. In the baseline simulation NO_2 is overestimated by +28.5%. Total alkyl nitrates, represented as NTR in CB05 gas-phase chemistry are overestimated by +219%. Isoprene, represented as ISOP in CB05 gas-phase chemistry is underestimated by –38%.

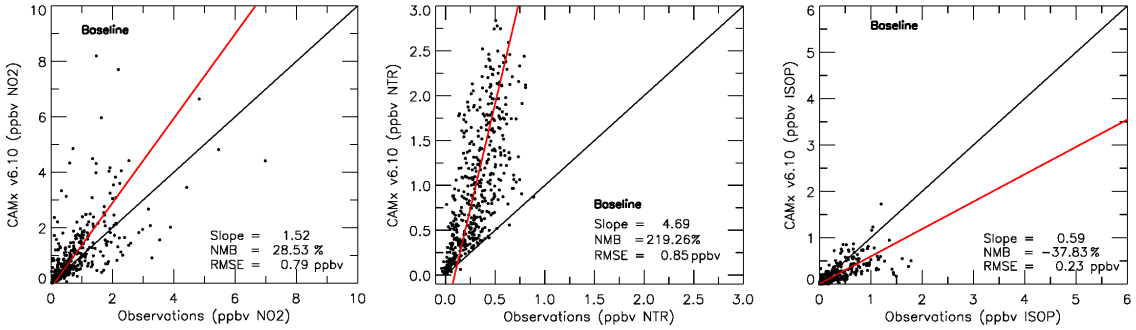

Figure 5-5. Same as Figure 5-2 except now for (left) NO_2, (center) alkyl nitrates (NTR), and (right) isoprene (ISOP).

The overestimate of NO_y and underestimate of HCHO by the baseline model simulation are more pronounced at the lowest altitudes of the P3-B aircraft spirals. In Figure 5-6, we show vertical profiles of measured ozone, NO_y, and HCHO binned in 500 m intervals and the closest CAMx model grid point, matched spatially and temporally during all flights. The median value of observed NO_y at the lowest altitude is below the 25th percentile of simulated NO_y, while the median value of observed HCHO is above the 75th percentile of simulated HCHO.

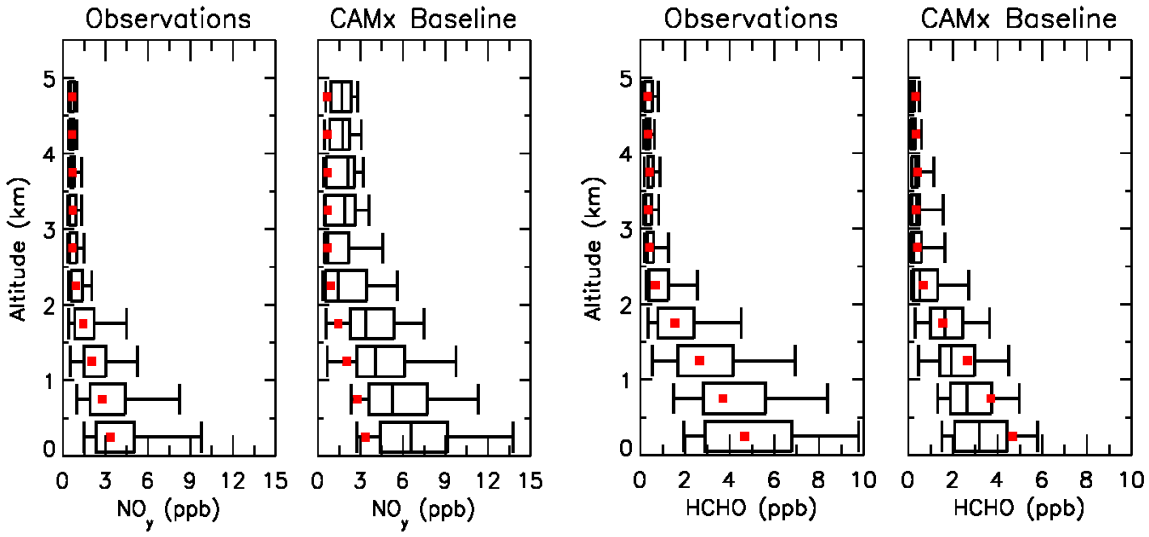

Figure 5-6. The two left panels show vertical profiles of NO_y binned in 500 m intervals, showing the 5th, 25th, 50th, 75th and 95th percentiles for (far left) observations and (middle left) baseline simulation. The right panels show vertical profiles of HCHO binned in 500 m intervals, showing the 5th, 25th, 50th, 75th and 95th percentiles for (middle right) observations and (far right) baseline simulation. Model output from CAMx v6.10 is matched spatially and temporally to the P3-B measurements at one-minute intervals. Red squares indicate the median values of the observations, which are shown on all panels to facilitate visual comparison.

We also find that ozone is underestimated for the lowest sampled altitudes, but agrees well with observations above 2.5 km (Figure 5-7); the underestimate of ozone, however, is not seen directly at the surface (Figure 5-3).

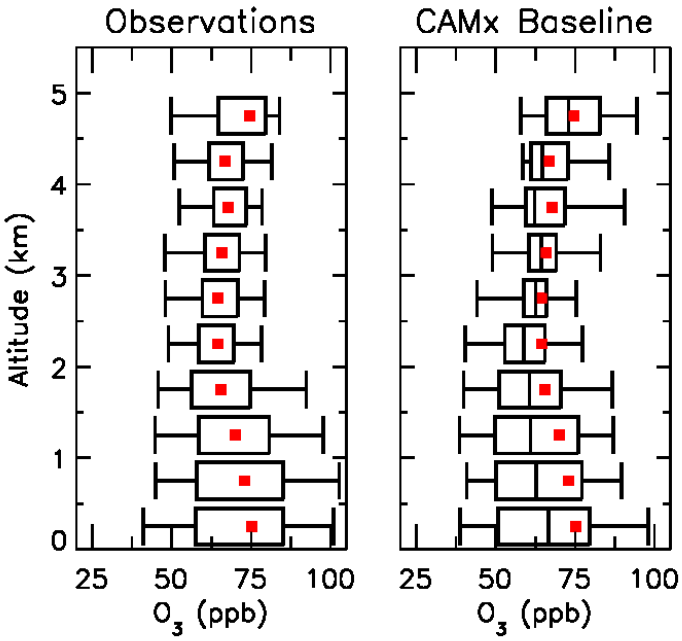

Figure 5-7. Same as Figure 5-6 except now for O_3.

5.3.2 Updated "Beta" Model Simulation

We update the model based on recommendations from recent scientific literature outlined in the Introduction (Chapter 5.1). The four changes are:

- Update the gas-phase chemistry from CB05 to CB6r2, which better represents alkyl nitrate photochemistry [Hildebrandt-Ruiz and Yarwood, 2013].
- Update the biogenic emissions from BEIS v3.6 to MEGAN v2.1, which increases isoprene emissions [Guenther et al., 2012].
- Reduce NO_x emissions from mobile sources (on-road, off-road and non-road) by 50% [Anderson et al., 2014].
- Increase the dry deposition velocities of isoprene nitrates (INTR) and multi-functional alkyl nitrates (NTR2) to be the same as nitric acid (HNO_3) [Horowitz et al., 2007].

We label the CAMx simulation with these four changes as the "Beta" simulation and compare the same trace gases (O_3, NO_y, HCHO) from this updated run to P3-B aircraft observations (Figure 5-8). The Beta simulation exhibits substantial improvement in the estimate of ozone precursors. The NMB of NO_y has improved from +86.2% to +22.4% and the NMB of HCHO has improved from –28.3% to –0.47%. The RMSE of NO_y and HCHO both improve: NO_y from 3.09 ppbv to 1.71 ppbv and HCHO from 1.34 ppbv to 0.93 ppbv. The Beta simulation yields similar predictions of ozone compared to the original calculation: the baseline has a NMB of –6.90%, whereas the Beta simulation has a NMB of –7.82%. The RMSE of the ozone degrades slightly from 9.88 ppbv to 10.53 ppbv.

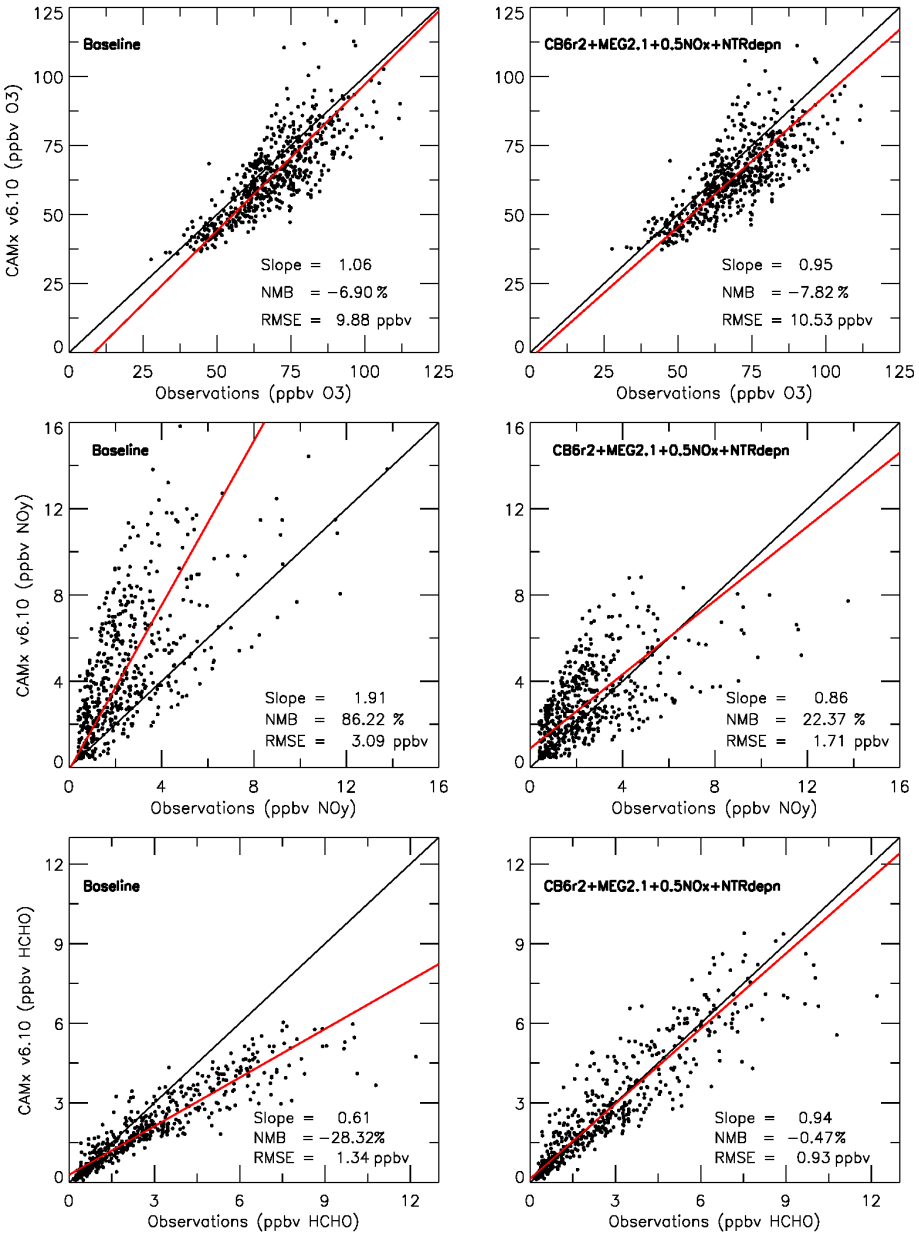

Figure 5-8. Observations acquired by the P3-B aircraft during DISCOVER-AQ Maryland in July 2011 compared to model output from CAMx v6.10 at the nearest model grid point and closest hourly interval. The closest hourly model output is matched to each one-minute averaged P3-B observation; both quantities are then averaged over the same ten-minute interval. Left panels show the baseline simulation, while right panels show the updated "Beta" simulation. Top row shows O_3, middle row shows NO_y, and bottom row shows HCHO. Black lines represent the 1:1 line, while red lines represent the linear best fit.

The Beta simulation also shows better agreement with the vertical profiles of NO_y and HCHO.

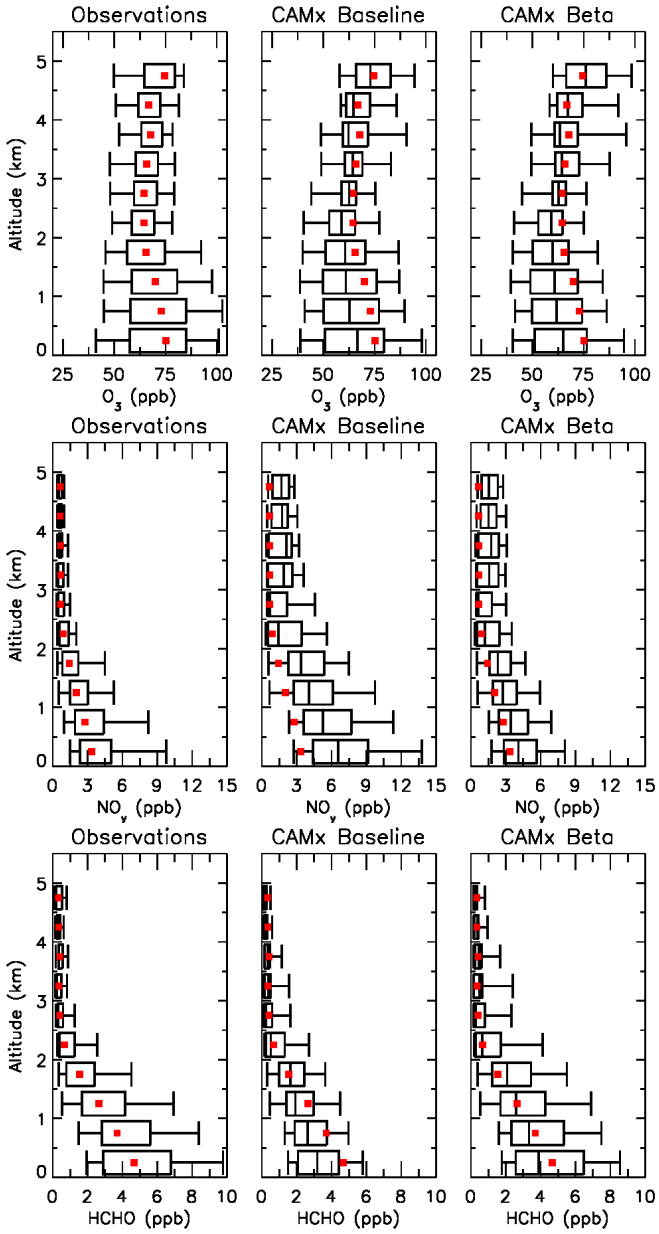

Figure 5-9. Vertical profiles of O_3, NO_y, and HCHO binned in 500 m intervals, showing the 5th, 25th, 50th, 75th and 95th percentiles. Left panels show one-minute averaged data from the P3-B aircraft, center panels show the baseline simulation, and the right panels show the updated "Beta" simulation. Model output from CAMx v6.10 is matched spatially and temporally to the P3-B measurements at one-minute intervals. Top row shows O_3, middle row shows NO_y, and bottom row shows HCHO. Red squares indicate the median values of the observations, which are shown on all panels to facilitate visual comparison.

In Figure 5-9, the median value of observed NO_y is much closer to the median value of modeled NO_y. At altitudes above 2.5 km, there is no improvement in the simulation of NO_y, likely due to an overestimate of HNO_3 within the GEOS-Chem global model used to initialize the CAMx boundaries (Figure 5-10). At these altitudes, HNO_3 is photochemically inactive and the overestimate will have minimal impact on ozone formation.

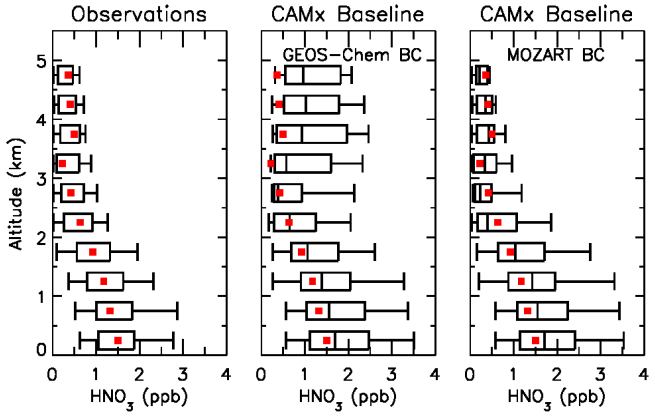

Figure 5-10. Left panel shows one-minute averaged HNO_3 observations acquired by the P3-B aircraft binned by altitude. Center panel shows the CAMx baseline simulation with GEOS-Chem v8-03-02 boundary conditions binned by altitude, and the right panel shows the CAMx baseline simulation with MOZART v4 boundary conditions binned by altitude. Model output from CAMx v6.10 is matched spatially and temporally. Red squares indicate the median values of the observations, which are shown on all panels to facilitate visual comparison.

The slight deterioration in the performance of ozone simulation in the Beta run (Figure 5-9) may be due to not enough recycling of multi-functional alkyl nitrates to NO_2 in the CB6r2 gas-phase mechanism. As seen in Figure 5-11, NO_2 is underestimated while alkyl nitrates (NTR) are overestimated in the Beta simulation.

The median value of observed HCHO is also much closer to the median value of HCHO from the Beta simulation (Figure 5-9). However, there is now a large overestimate in the simulation of isoprene (Figure 5-11), which suggests errors in the isoprene to formaldehyde conversion processes in CB6r2. Kota et al. [2015] also showed an overestimate of isoprene using MEGAN v2.1 in southeast Texas.

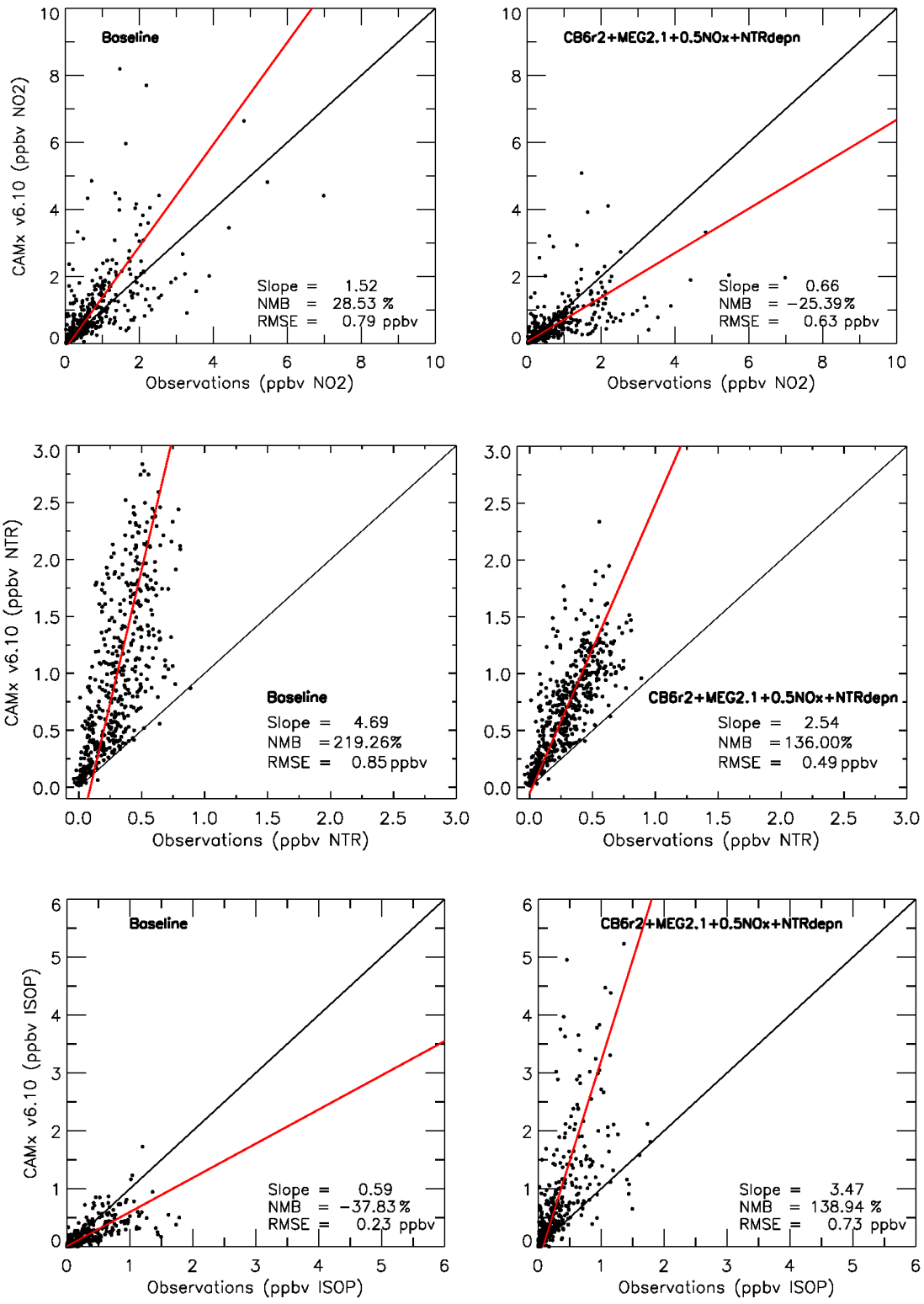

Figure 5-11. Same as Figure 5-8, but now showing: (top) NO_2, (middle) NTR, and (bottom) ISOP.

Surface ozone is simulated better in the Beta simulation (Figure 5-12).

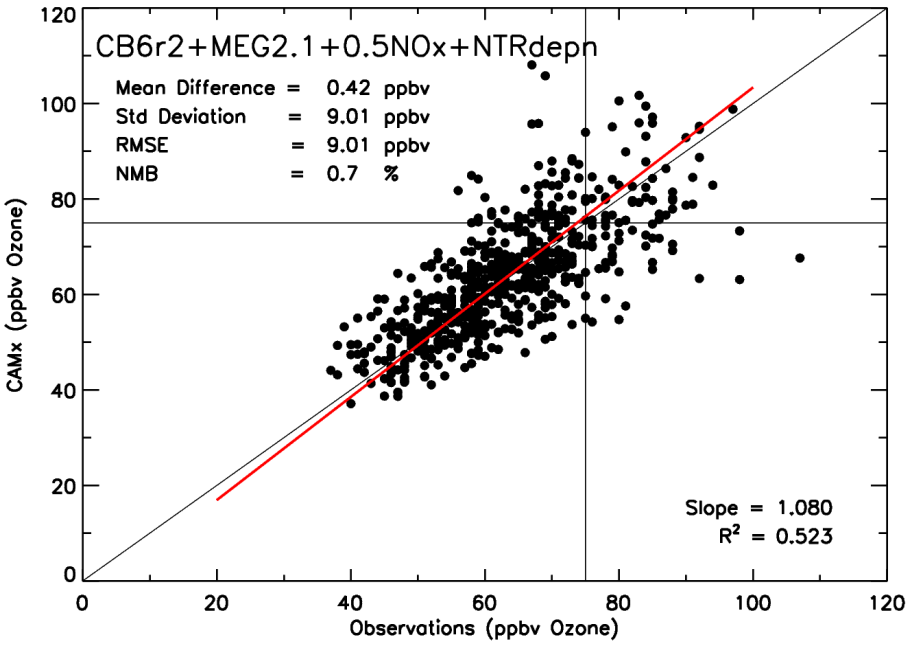

Figure 5-12. Same as Figure 5-3, but now showing comparison with the Beta simulation.

5.3.3 Changes to Ozone Attributed to Mobile & Large Point Sources

The National Emissions Inventory (NEI) shows on-road and off-road mobile source emissions account for the largest portion of the total NO_x emissions, 61% of the total (Figure 5-13). In Maryland the percentage is even larger; NO_x emissions from on-road and off-road sources account for 72% of total NO_x emissions.

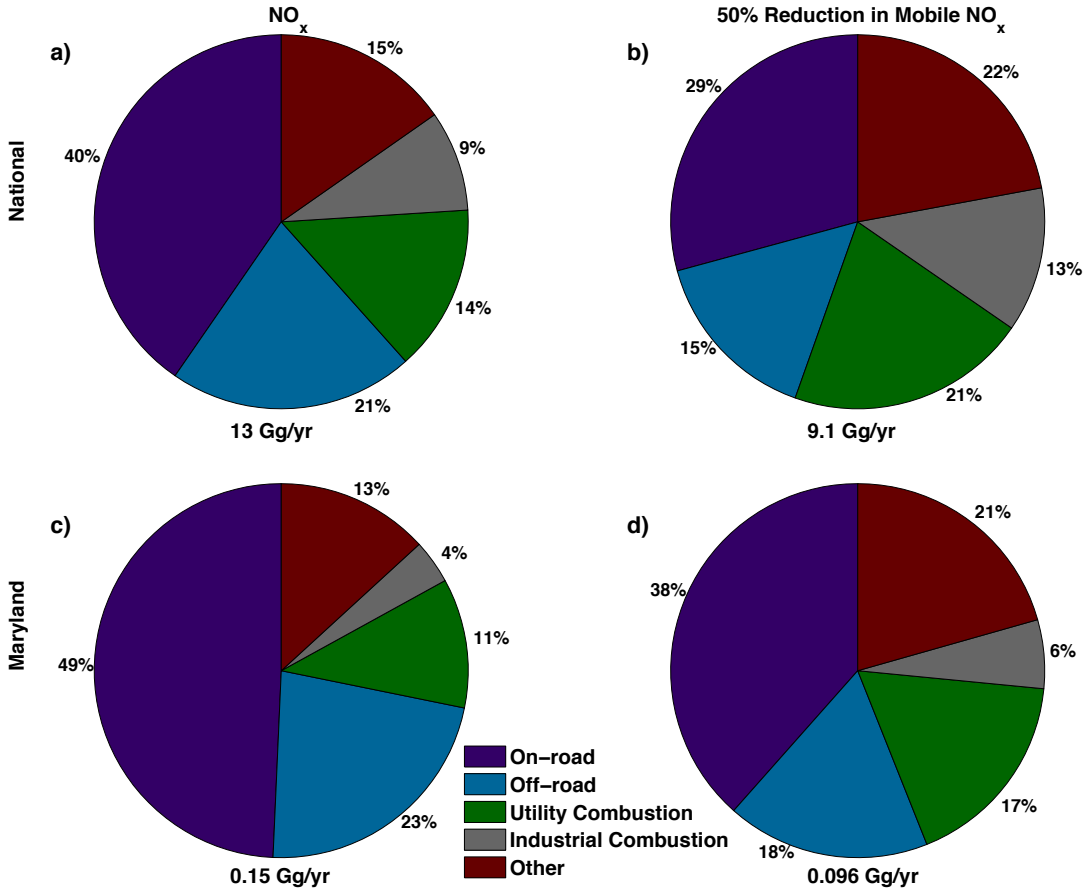

Figure 5-13. NO_x emissions sorted by sector for (left) the 2011 National Emissions Inventory and (right) a scenario with a 50% reduction in mobile (on-road and off-road) sources. Top row shows percentages for the national inventory. Bottom row shows percentages for the Maryland inventory.

Figure 5-14 depicts ozone attributed to emissions from individual states (denoted by color) as well as from various source sectors (each histogram). Results are shown for both the (left) baseline and (right) Beta simulations, for the ten worst air quality days in July 2011 at Edgewood, Maryland. We have chosen to focus on Edgewood (the location

shown as the filled circle in Figure 5-17) because this site causes the Baltimore region to be in moderate non-attainment of the 2008 NAAQS for ozone [EPA, 2014a].

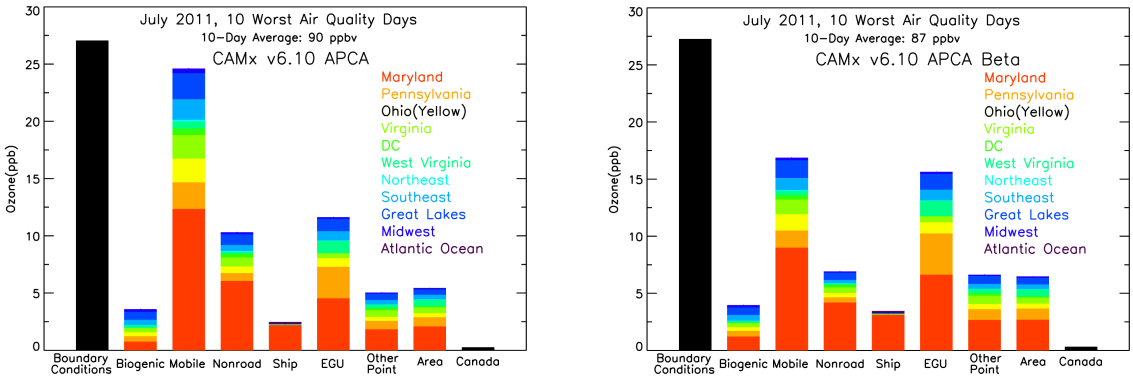

Figure 5-14. Ozone attributed to source sectors separated by state during the ten worst air quality days in July 2011 at 2 PM local time at the Edgewood, MD monitoring site which is located 30 km east-northeast of Baltimore for the (left) baseline simulation and (right) updated chemistry and emissions scenario.

In the baseline simulation (Figure 5-14, left) – generated from the NEI – on-road sources are responsible for the largest portion (24.6 ppbv) of total surface ozone. Ozone attributed to electric generating units (EGUs) accounts for the second largest single sector (11.6 ppbv) during the ten worst air quality days at Edgewood. The NEI indicates EGUs are responsible for 14% of total NO_x emissions, and 11% within the state of Maryland.

In the Beta simulation we keep emissions from EGUs identical to the baseline simulation because the NEI is developed from observed Continuous Emissions Monitoring System (CEMS) data. There is strong scientific basis [Anderson et al., 2014] to link the overestimate in NO_y to mobile source emissions since they represent more than 50% of the NO_x emissions inventory. The Beta simulation (Figure 5-14, right) attributes more ozone to EGUs and less ozone to mobile sources. While on-road mobile sources are still the primary individual source sector contributing to surface ozone, they are responsible for 7.7 ppbv less ozone compared to the baseline simulation: 24.6 ppbv to

16.9 ppbv, a drop of 31.4%. Ozone attributed to non-road sources also shows a similar percentage drop. Despite identical emissions of NO_x from EGUs in the two simulations, electricity generation is responsible for 4.0 ppbv more ozone in the Beta run, increasing from 11.6 to 15.6 ppbv, a 34.6% increase. The ozone attributed to EGU emissions shows a large increase because CB6r2 gas-phase chemistry has faster photolysis of NO_2 than CB05 and increased modeled HO_2 and RO_2 concentrations driven by greater biogenic emissions from MEGAN v2.1. This implies greater ozone production efficiency, a topic to be treated in a separate paper. For the Beta simulation, EGUs and on-road mobile sources are now responsible for roughly the same fraction of surface ozone in Maryland. The change in surface ozone attribution to on-road mobile and EGU sources for the baseline compared to the Beta simulation is similar throughout the eastern United States for July 2011 (Figure 5-15).

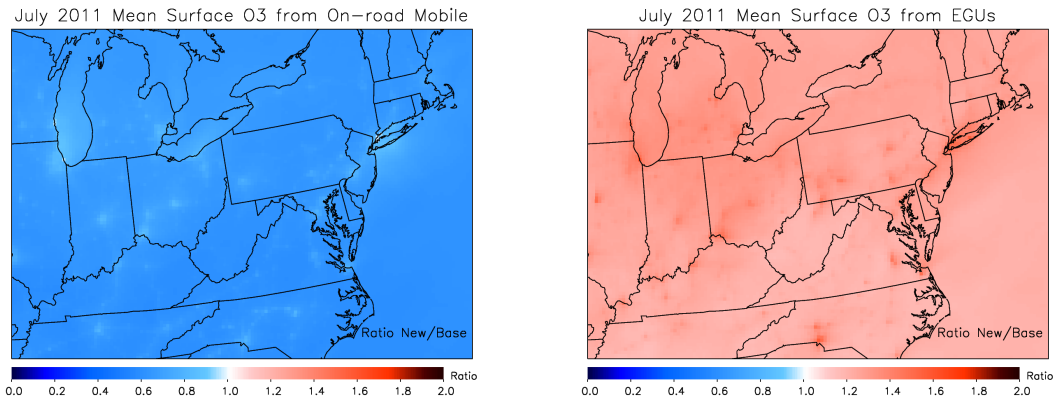

Figure 5-15. Ratio of ozone source apportionment mixing ratios from the July 2011 daytime mean updated "Beta" model divided by the same value from the baseline version of the model. Left panel shows the ratios at each model grid point from on-road mobile sources and the right panel shows ratios at each model grid point from electricity generating units (EGUs).

5.3.4 Changes to Ozone Attributed to NO_x & VOC limitations

The overestimate of NO_y and underestimate of HCHO for the baseline simulation, shown in Figure 5-4, suggests that ozone in the original model framework may be

produced in a more VOC-limited ozone production regime than occurs in the actual atmosphere, even though NO_x remains the key pollutant. We use an OSAT simulation to calculate the amount of ozone formed in NO_x-limited and VOC-limited environmental conditions. Figure 5-16 shows the percentage of ozone production attributed to a NO_x-limited ozone regime. In the baseline simulation, 65 – 85% of ozone in the Baltimore vicinity is attributed to a NO_x-limited environment.

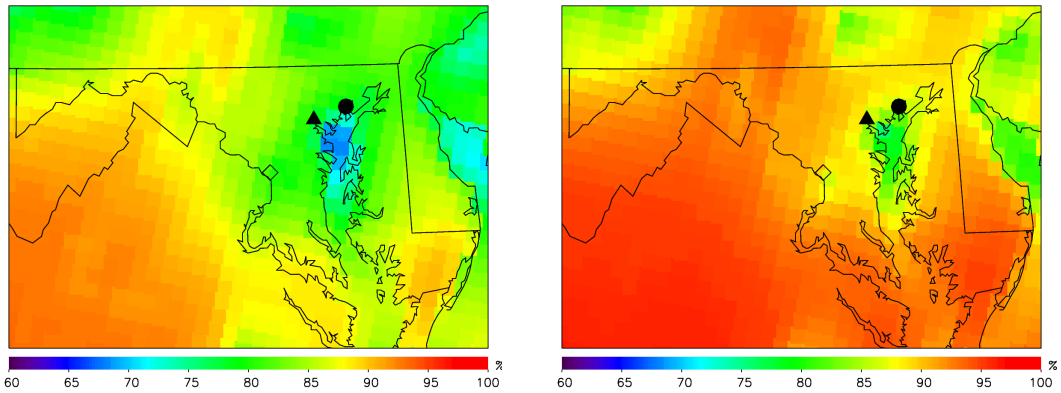

Figure 5-16. Percentage of ozone formed in a NO_x–limited production regime during the July 2011 daytime mean (8 AM – 8 PM local time) at each model grid point in the (left) baseline simulation and (right) updated chemistry and emissions scenario.

The updated Beta simulation uniformly shows more ozone production in a NO_x-limited regime. The biggest differences occur over the Chesapeake Bay. The Beta simulation shows 80 – 95% of ozone is produced in a NO_x-limited environment in the Baltimore vicinity. Instead of being in the "transition region" – the region on the EKMA diagram in which ozone production occurs due to both VOC and NO_x limitation – the area is now squarely in a region of NO_x-limited ozone production. This is consistent with observed changes in ozone resulting from NO_x emission reductions [Gilliland et al., 2008].

5.3.5 Changes to ozone source region attribution

Each incremental change to the modeling platform alters the source region attribution. Figure 5-17 shows source region attribution of surface ozone at Edgewood during the ten worst air quality in July for three simulations in three scenarios: baseline, baseline with CB6r2, and Beta. For the baseline simulation (left), Maryland is responsible for 29.9 ppbv of 90.4 ppbv of ozone, or 33.1% of the total; long-range transport accounts for the other 66.9% of the total. When changing only the gas-phase chemistry (center) more ozone is attributed to long-range transport. For the Beta simulation – reducing mobile sources of NO_x by 50%, switching to MEGAN v2.1 biogenics and increased dry deposition of alkyl nitrates – more ozone is attributed to in-state sources. In the Beta simulation, Maryland is responsible for 29.6 ppbv of the 87.5 ppbv total, which represents 33.8% – an increase over the baseline simulation. Modifications to the chemistry make ozone photochemistry more of a regional problem, while the changes to the emissions inventory and alkyl nitrate dry deposition make ozone photochemistry more of a local issue.

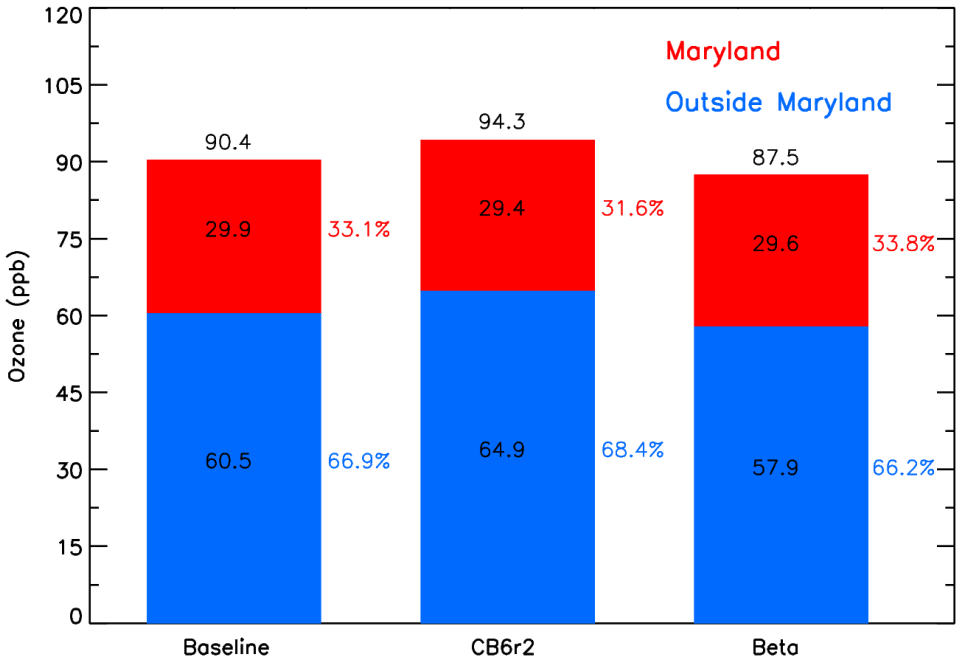

Figure 5-17. Ozone attributed to Maryland and to sources outside of Maryland during the ten worst air quality days in July 2011 at 2 PM local time at the Edgewood, MD monitoring site, located 30 km east-northeast of Baltimore, for the (left) baseline simulation (center) modified chemistry only simulation and (right) updated chemistry and emissions scenario.

5.4 Conclusions

CAMx, when modified with guidance provided by a field experiment, more realistically simulates the observed abundance of ozone precursors. We compare ozone precursors (NO_y and HCHO) and ozone measured during the July 2011 DISCOVER-AQ Maryland campaign to CAMx simulations. In the baseline simulation, there is good agreement between modeled and observed ozone, but poor agreement for NO_y and HCHO. We implemented four changes to the model: CB6r2 gas-phase chemistry, faster deposition of alkyl nitrates, reduced NO_x emissions from mobile sources, and increased isoprene emissions by switching to MEGAN v2.1 biogenic emissions. These dramatically improve the simulation of total reactive nitrogen, alkyl nitrates, and

formaldehyde. Adding more recycling of alkyl nitrates to NO_2 in CB6r2 and refining isoprene photochemistry may further improve CAMx performance.

These modifications change the attribution of ozone to different source sectors and have important policy implications. Compared to the baseline simulations, mobile source contribute 31.4% less to total ozone while EGUs contribute 34.6% more at Edgewood, Maryland. Ozone attributed to EGUs increase from 11.6 to 15.6 ppbv, while ozone attributed to mobile sources decreases from 24.6 to 16.9 ppbv. Ozone in the two model simulations is comparable and agrees reasonably well with observations, but the source attribution and targets for control strategies change substantially.

Prior research demonstrated that regional air quality models underestimate the benefit of NO_x control measures for surface ozone. If air quality models are used to forecast how future air quality regulations will affect surface ozone, they must simulate ozone within the correct production regime (i.e., NO_x-limited vs. VOC-limited). For the Baltimore area, this updated model platform increases the percentage of the ozone formed in a NO_x-limited regime from ~75 to ~85% of the total. Since the updated model platform places ozone in a more NO_x-limited regime, it is possible a simulation of surface ozone long-term trends using these changes will resolve the long-standing difficulty in simulating the response of surface ozone to past reductions in ozone precursors.

6. Increasing Ozone Lifetime in the Eastern United States

6.1. Introduction

In the United States, surface ozone concentrations began to rise in the 1950s peaking in the 1980s [Vingarzan, 2004; Oltmans et al., 2006], then declining with the most substantial decreases in the last decade [Fiore et al., 1998; Lin et al., 2001; Vingarzan, 2004; Oltmans et al., 2006; Oltmans et al., 2013] in response to emission reduction strategies of ozone precursors [He et al., 2013a; Loughner et al., 2014; Sickles and Shadwick, 2015] as required by the Clean Air Act [EPA, 2014a]. For example, in 2002, the highest ozone design value (a weighted 3-year average of the 4th highest annual 8-hour maximum ozone mixing ratio) for the Baltimore, Maryland non-attainment region was 104.0 ppbv. In 2011, the highest value ozone design value for the same region decreased to 90.0 ppbv. Urban locations in the eastern United States have seen similar surface ozone reductions during the worst air quality days [EPA, 2015b].

While many urban and suburban locations in the United States have undergone recent decreases in surface ozone concentrations, rural locations in the western United States have experienced increases [Jaffe and Ray, 2007] especially in spring [Cooper et al., 2010; Cooper et al., 2012]. Some monitors in urban city centers have also seen increases in surface ozone, presumably due to less titration of ozone by local NO_x emissions [Simon et al., 2015]. At monitors situated along the rural western North American coastline, mean annual observed ozone has been increasing at a rate of 0.34 ppbv/year since the 1980s [Parrish et al., 2009]. Cooper et al. [2012] reported an increase of ozone in the free troposphere during springtime of 0.41 ppbv/year from 1995 to 2011

at rural sites in western North America. Between 1987 and 2007, a similar positive trend of 0.31 ppbv/year was reported at the Mace Head observatory located at the westernmost coast of Ireland [Derwent et al., 2007]. While ozone mixing ratios at Mace Head have plateaued in the late 2000's, there is no indication of stabilization at rural western North American coastline monitoring sites [Parrish et al., 2009]. The increases of surface ozone in rural locations of western North America and Western Europe may be the result of a growth in the global background mixing ratio of ozone [Lin et al., 2000].

The fraction of ozone present in a given area not attributed to anthropogenic sources of regional origin is referred to as background ozone [Vingarzan, 2004]. A majority of background ozone can be attributed to uncontrollable sources such as: stratospheric intrusions [Langford et al., 2012; Lin et al., 2012a], wildfires [Val Martin et al., 2006], soil NO_x emissions [Hudman et al., 2012; Vinken et al., 2014], and lightning [Allen et al., 2012]. The remaining portion is attributed to long-range transport of ozone of anthropogenic origin. Asian anthropogenic emissions can be a meaningful contributor to North American ozone mixing ratios, especially in the elevated terrain of western North America [Jacob et al., 1999; Lin et al., 2000; Zhang et al., 2008; Cooper et al., 2010; Lin et al., 2012b; Zhang et al., 2014a; Gratz et al., 2015; Fiore et al., 2015]. Similarly, states west of the Mississippi River can be meaningful contributors to ozone pollution in the eastern United States [EPA, 2015d]. As a whole, background ozone can represent between 15 – 50 ppbv of the mean surface ozone in North America [Emery et al., 2012, Fiore et al., 2014; Lefohn et al., 2014; Dolwick et al., 2015].

Variations in tropospheric composition can alter the photochemical lifetime of ozone. On a global scale, the lifetime of tropospheric ozone is ~22 days [Stevenson et

al., 2006] calculated for the year 2000. The lifetime of ozone near the surface can be substantially shorter [Jacob 2000]. Lamarque et al. [2005] report that the global ozone lifetime has decreased by 30% since the 1930s in response to anthropogenic emissions of NO_x and VOCs. Stevenson et al. [2006] predicts mean ozone lifetime, on a global scale, will decrease by 10% between 2000 and 2030 as global emissions of anthropogenic NO_x and VOCs continue to increase. Zhang et al. [2014b] suggests that as stratospheric ozone recovers, tropospheric photolysis rates – including those that produce HO_x – will decrease, yielding a small increase in the tropospheric ozone lifetime assuming emissions remain constant. A limitation of these studies is that they were performed on global scale.

6.2. Methods

Our study focuses on three month-long simulations of July; see Chapter 3.2 for a detailed description of the model set-up. This work has been published in the *Journal of Geophysical Research – Atmospheres* [Goldberg et al., 2015]. The baseline simulation is conducted for July 2011, using emissions and meteorological fields prepared for this summer. We also present simulations conducted using July 2011 meteorology and retrospective emissions from July 2002, and conducted using July 2011 meteorology and projected emissions for July 2018. The simulations for three Julys, using identical meteorological fields, were used to assess how the relative influence of local emissions and BC_{O3} on surface ozone in the eastern United States evolves, over time, due to changes in anthropogenic emissions.

We use observations and CAMx version 6.10 (also used by EPA [2015d]) with ozone source apportionment at a high spatial and temporal resolution to quantify the role

of the long-range transport and regional anthropogenic emissions on total surface ozone mixing ratios in the eastern United States. In this chapter, we make extensive use of a quantity called boundary ozone (BC_{O3}): the sum of ozone transported across the four boundaries of our eastern United States modeling domain plus ozone formed from precursors transported across these boundaries (ozone attributed to the natural background plus Texas, California, Asia, etc.); for this reason BC_{O3} is regional in nature. We use BC_{O3} as a reactive tracer to determine how the photochemical lifetime of ozone changes as anthropogenic NO_x and VOC emissions in the eastern United States decrease. Figure 6-1 shows mean July 2011 ozone for the eastern United States from MOZART-4.

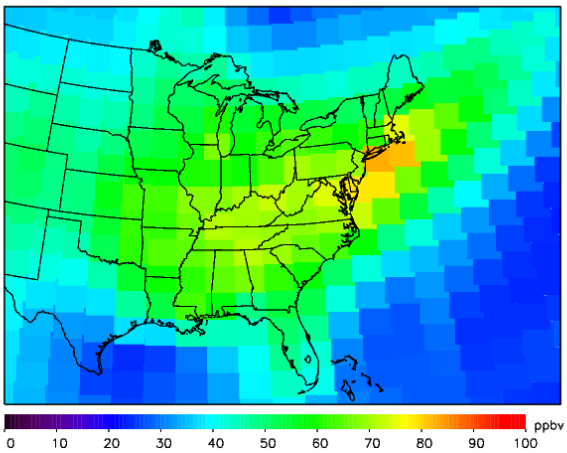

Figure 6-1. Mean ozone mixing ratios (ppbv) from the MOZART-4 global chemistry model [Emmons et al., 2010] during July 2011.

6.2.1. Uncertainty Analysis

While biogenic emissions for this study were calculated using BEIS v3.14, Chapter 5 shows better agreement of formaldehyde using emissions from the Model of Emissions of Gases and Aerosols from Nature (MEGAN) v2.1 model [Guenther et al., 2012]. Isoprene emissions are larger in the MEGAN model when compared to BEIS [Warneke et al., 2010; Carlton and Baker 2011]. Several studies also suggest an overestimate of NO_x emissions from mobile sources [Fujita et al., 2012; Anderson et al.

2014; Choi et al., 2015] using MOVES2010 [Kota et al., 2012]. Furthermore, the Carbon Bond 6 Revision 2 (CB6r2) gas-phase chemistry has been released recently [Hildebrandt-Ruiz and Yarwood, 2013]; this updated mechanism more explicitly represents alkyl nitrates in regional air quality models: an improvement over CB05 [Canty et al., 2015]. CB6r2 calculates a shorter lifetime of alkyl nitrates and faster recycling of NO_x. This may improve the simulation of ozone attributed to long-range sources. Canty et al. [2015] concluded regional air quality models underestimate the importance of interstate transport of NO_x; therefore the actual ozone mixing ratios attributed to upwind states and the boundary may be increased with respect to values found in our baseline simulation.

6.3. Results & Discussion

6.3.1. Observations of ozone

Atmospheric conditions in the eastern United States during July 2011 were conducive for poor air quality: hot temperatures with generally clear skies and a persistent subsidence inversion [Loughner et al., 2014]. Maximum 8-hour surface ozone within the state of Maryland and maximum afternoon temperature at the Baltimore-Washington International (BWI) airport during July 2011 are shown in Figure 6-2.

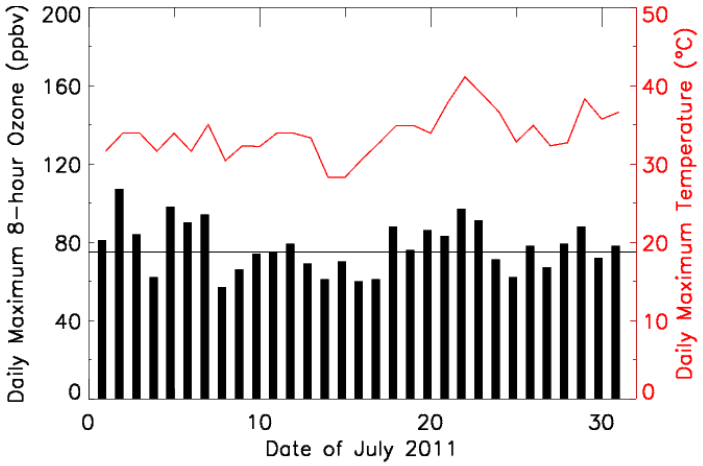

Figure 6-2. Maximum 8-hour ozone mixing ratios (ppbv) in the Baltimore non-attainment area during each July 2011 date (black bar plots, left axis) and plot of

maximum daily temperature (°C) at the Baltimore-Washington International airport (red curve, right axis).

Twenty-nine days at BWI had high temperatures above 30°C; the monthly temperature anomaly was +2.9°C compared to 1980 – 2010 climatology [NCDC, 2015]. Many of the days in July 2011 also had stagnant or southwesterly winds and clear skies, maximizing photochemical ozone production [NCDC, 2015]. Correspondingly, there were seventeen days during July 2011 when 8-hour maximum surface ozone exceeded the 75 ppbv NAAQS in the state of Maryland [Loughner et al., 2014].

Despite consistently exceeding the NAAQS during July 2011, surface ozone in the Baltimore-Washington metropolitan area has seen large decreases since the 1970's. In Figure 6-3, we plot daytime averages of carbon monoxide (CO), nitrogen dioxide (NO_2) and top and bottom third of the distribution of daytime ozone (O_3) surface mixing ratios in the Baltimore-Washington metropolitan area since 1972, a 40-year record. Instruments used to measure "NO_2" also respond quantitatively to peroxyacyl nitrate (PAN), alkyl nitrates (ANs) and other reactive nitrogen species [Fehsenfeld et al., 1987; Luke et al., 1989; Dunlea et al., 2007], but are suitable for trend work. Since the early 1970s, urban CO mixing ratios have decreased by almost two orders of magnitude and NO_2 mixing ratios have declined by one order of magnitude. Due to the nonlinearities in ozone production, ozone mixing ratios have declined at a slower rate. There has been a -0.38 ± 0.06 ppbv per year decline in the top third of monthly daytime ozone during the ozone season (April to October). Three federal regulatory measures, labeled on Figure 6-3, have contributed to the decrease in surface ozone over the past four decades: mandatory catalytic converters in automobiles, reformulated gasoline and selective catalytic reduction (SCR) scrubbing of NO_x from power plants.

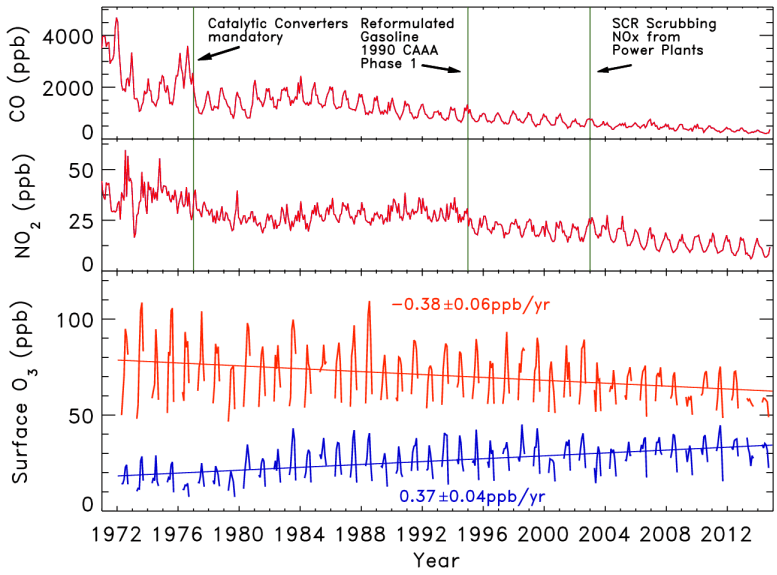

Figure 6-3. Observations at the surface of CO (top panel), NO_2 (middle panel) and the top third of the distribution of O_3 observations (red curve) and bottom third (blue curve) (bottom panel) from EPA monitoring sites in MD, DC, and Northern VA. The CO and NO_2 data are monthly averages. The ozone data are monthly daytime averages during the ozone season (Apr–Oct); colored solid lines indicate a linear fit to each of the data distributions. Vertical lines indicate the enactment of federal regulations that led to declines in CO and NO_2.

While the Baltimore-Washington metropolitan area has experienced a steady decline in the highest daytime ozone levels, the bottom third of monthly daytime ozone levels during the ozone season have been steadily rising at a rate of +0.37 ± 0.04 ppbv per year. The rise of the bottom third of the ozone distribution suggests background ozone in the Baltimore-Washington metropolitan region could be rising at a rate similar to that observed in the western United States [Parrish et al., 2009]. This is similar to what is shown by Cooper et al., [2012]; they demonstrate a statistically significant positive trend in the 5th percentile of surface ozone in Baltimore-Washington metropolitan region during spring and a weak positive trend during summer. They hypothesize that the eastern United States could be affected by an increase in the global background ozone. In this study, we expand upon the hypothesis from Cooper et al. [2012] by examining how

reductions of anthropogenic NO_x and VOC emissions in the eastern United States could be responsible for a rise in the background ozone.

It is also possible that the rise in the bottom third of the ozone distribution is due, in part, to less titration of ozone by NO_x, particularly for heavily polluted areas such as urban centers [Simon et al., 2015]. If the decline in titration of ozone by NO_x were truly responsible for a rise in the lower third of the ozone distribution, then the extremely high prior abundance of NO_2 would have been harmful to human health [Samoli et al., 2006]. Quantification of the two separate drivers of the upward trend in the bottom third ozone (i.e., rising background ozone coupled with rising influence of background ozone; less titration of ozone to very low levels) will be the subject of a future study conducted by our group.

While policy for surface ozone in the U.S. is presently focused on daily 8-hour maximum reflected by the upper-third of the surface ozone distribution, the impact of ozone on trees, plants and ecosystems is often assessed using weighted indices designed to reflect the cumulative exposures to ozone experienced during the growing season [Paoletti and Manning, 2007]. Furthermore, Bell et al. [2006] reported increased risk of premature mortality for even low levels of surface ozone. The narrowing of the surface ozone distribution, reflected by the convergence of the upper and lower thirds illustrated in Figure 6-3, suggests that improvement in air quality is overstated if based solely on the decline in daily 8-hour maximum.

6.3.2. Using CAMx OSAT to determine the role of boundary ozone

We use OSAT to determine which source regions are responsible for total surface ozone mixing ratios during July 2011. Figure 6-4 shows the source apportionment of mid-afternoon surface ozone in the Baltimore, Maryland region for the July 2011 mean and three of the observed worst air quality days during the month: July 2, July 7 and July 22. We define the Baltimore region as a 72 x 96 km rectangular box inclusive of the entire metropolitan region.

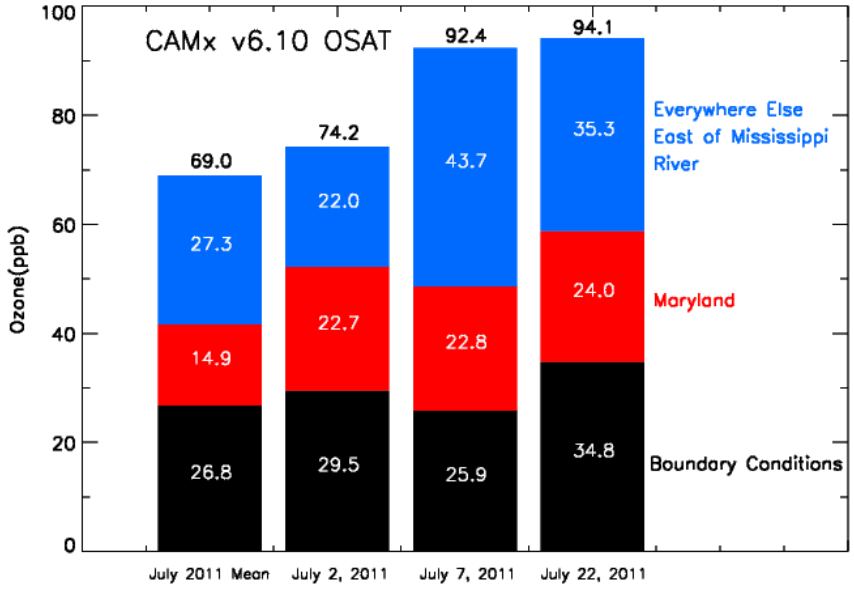

Figure 6-4. Mean ozone source apportionment (ppbv) at the surface at 2 PM EDT in a 72 x 96 km rectangular box encompassing Baltimore, MD for the July 2011 mean and the three observed worst air quality days during the month: July 2, July 7, and July 21. The black bars represent the contribution from beyond the model domain boundary, the red bars represent the contribution from the state of Maryland, and the blue bars represent the contribution from all other areas within the model domain.

For the July 2011 average, 26.8 ppbv of surface ozone, or 38.8% of the total mixing ratio in the Baltimore, Maryland region can be attributed to BC_{O3}. An EPA [2015d] modeling study using a CONUS domain during the summer of 2011 estimates boundary contribution during poor air quality days in Maryland to be 16 – 19 ppbv.

Another 27.3 ppbv, or 39.6%, is attributed to emissions of ozone precursors within the model domain boundary, but excluding the state of Maryland. Finally, 14.9 ppbv, or 21.6%, of surface ozone is attributed to the emissions of ozone precursors from sources within the state of Maryland.

The portion of ozone in the Baltimore region attributed to emission sources outside Maryland's borders but within the eastern United States model domain (blue bar) exhibits the most day-to-day variation. On July 2, 2011, a day with stagnant winds classified as a local pollution episode, the portion of ozone from within the state's border was of similar magnitude to the portion of ozone attributed to outside of Maryland's borders: 22.7 ppbv vs. 22.0 ppbv. On July 7, 2011, a day with strong westerly winds, the portion of ozone attributed to sources outside the state is 43.7 ppbv, compared to 27.3 ppbv during the July mean. These simulations suggest that the magnitude and extent of the poor air quality during the worst air quality days, the ones that qualify areas for non-attainment status, are not determined only by local sources, but instead are a combination of local production and high ozone advected downwind.

July 22 is a case study in which ozone anomalies extended beyond our model domain. While in-domain sources were still responsible for the majority of the ozone on this day, we also see an increased influence from the boundaries. On July 22, the amount of ozone attributed to BC_{O3} is increased 8.0 ppbv over the mean BC_{O3} mixing ratio. This may indicate high ozone anomalies beyond the model domain's border may be further enhancing the high mixing ratios at the surface in Maryland.

Since BC_{O3} can be a significant portion of total surface ozone, we examine the four model domain boundaries to determine which boundaries are influencing mid-

Atlantic surface mixing ratios the most. Figure 6-5 shows monthly averaged mid-afternoon ozone mixing ratios attributed to each model boundary; these are not total mixing ratios, but contributions from each of the four edges of the domain.

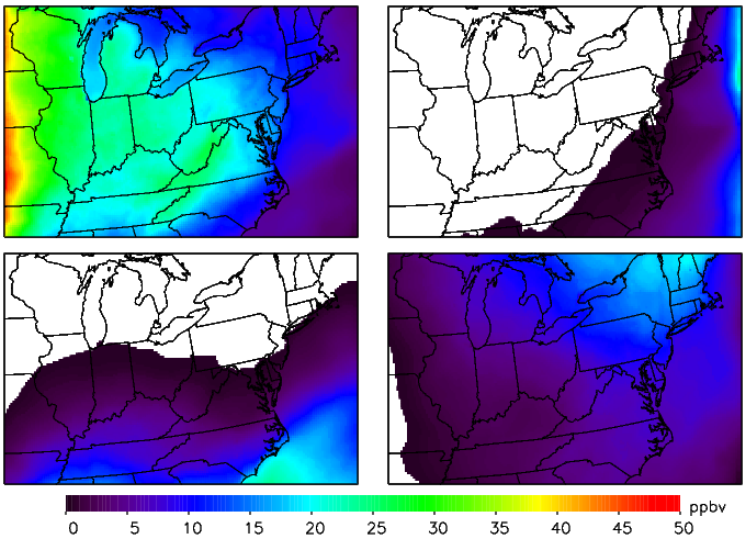

Figure 6-5. Ozone mixing ratios (ppbv) at the surface attributed to the four cardinal direction boundaries: west (top left), east (top right), south (bottom left) and north (bottom right), averaged for the entire month of July at 2 PM EDT.

The western model domain is the primary contributor to BC_{O3} in the majority of the model domain, including Maryland. Westerly winds are the dominant flow pattern in our region of study, advecting trace gases primarily from the western boundary (94° W longitude) to the east in the model domain. Meridional flow from strong cyclones or anticyclones can perturb the dominant westerly flow, but these features are not persistent enough to modify the mean zonal flow. Mixing ratios of ozone from the western model domain boundary exceed 20 ppbv at the surface in most areas. The western model boundary has the least influence on surface ozone in New York, New England and parts of Canada, where the northern boundary is the primary contributor. Ozone initialized at the southern and eastern boundaries has little effect on Maryland and much of the model domain during July 2011.

6.3.3. Role of the boundary ozone in model simulations of future years

Surface ozone concentrations during the worst air quality days in the eastern United States are projected to decrease in next decade in response to pollution control policies and market-based switches to cleaner technology. The 2018 Design Value for the most polluted monitor in the Baltimore metropolitan area – as calculated by EPA guidance [EPA, 2014b] using our CAMx simulation – is 79.0 ppbv, down from the observed 2011 Design Value of 90.0 ppbv, a reduction of 12.2%. This leaves the Baltimore area in violation of the 2008 NAAQS without further emission reduction strategies. We provide future state-by-state contribution to total surface ozone in Figure 6-6.

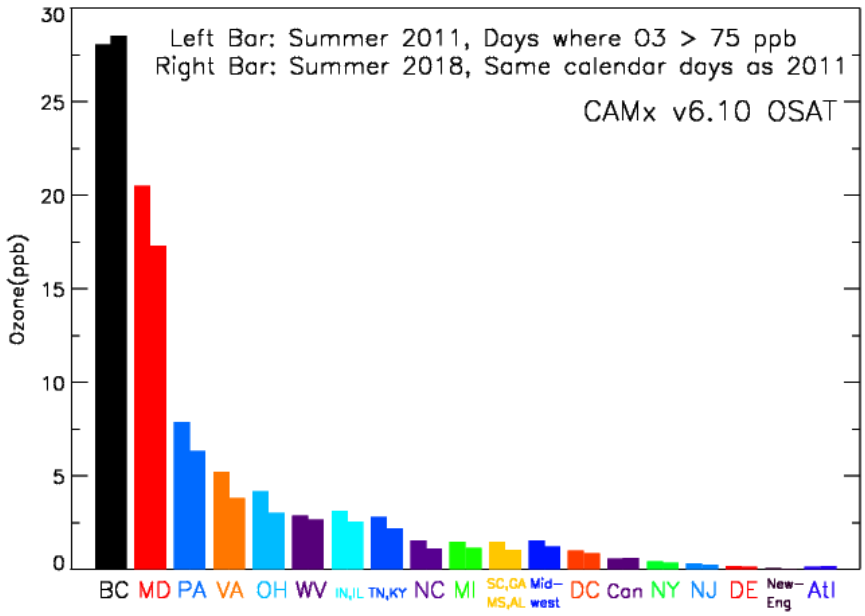

Figure 6-6. Mean ozone source apportionment (ppbv) at the surface at 2 PM EDT in a 72 x 96 km rectangular box encompassing the Baltimore, MD region for all days during the summer of 2011 (left bar) in which the ozone mixing ratio at Baltimore, MD exceeded 75 ppbv at 2 PM EDT. The projected 2018 scenario (right bar), individual days remain the same. The black bars represent the contribution from beyond the model domain boundary, the red bars represent the contribution from the state of Maryland, and other colors represent the contribution from various regions within the model domain.

We now describe a CAMx sensitivity study in which trace gas mixing ratios at the boundary for the month of July 2002 and July 2018 remain at July 2011 mixing ratios; emissions of ozone precursors within the domain vary according the respective year as described in Chapter 6.2. Figure 6-7 shows the apportionment of surface ozone in the vicinity of Baltimore from various source regions in the mid-afternoon during July 2002, 2011, and 2018; all years use 2011 meteorology.

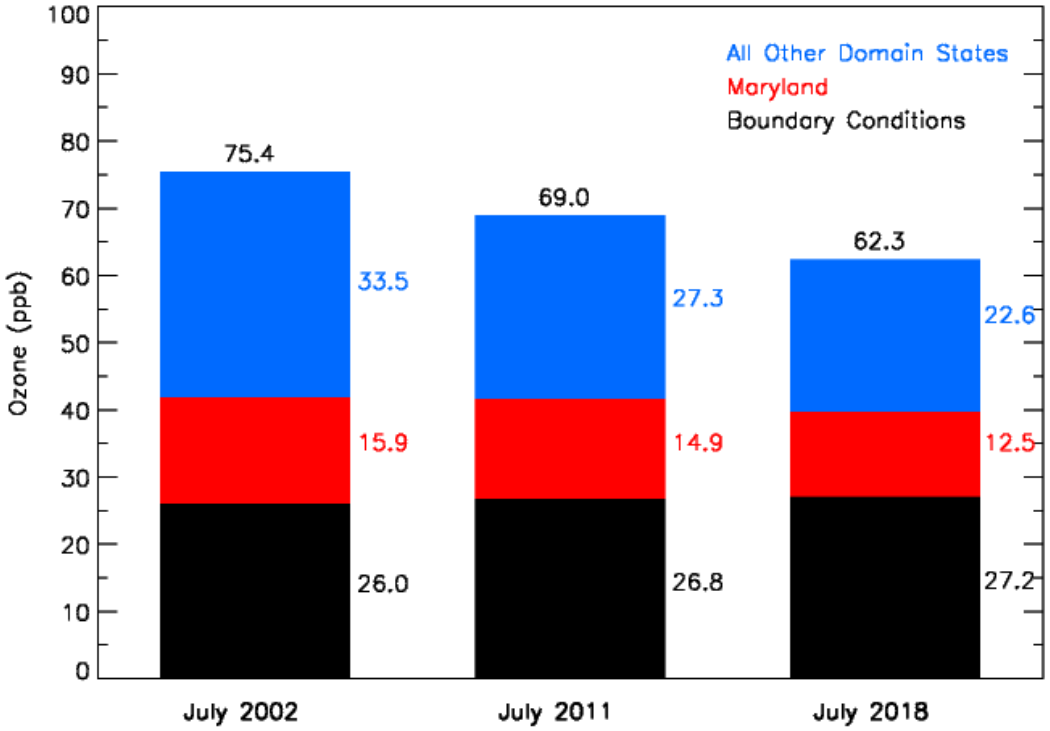

Figure 6-7. Mean ozone source apportionment (ppbv) at the surface at 2 PM EDT in a 72 x 96 km rectangular box encompassing the Baltimore, MD region for July 7, 2002, 2011 & 2018. Input emissions were calculated using the NEI for the respective year and 2011 meteorology. The black bars represent the contribution from beyond the model domain boundary, the red bars represent the contribution from the state of Maryland, and other colors represent the contribution from various regions within the model domain.

In the 2002 scenario, contribution from outside the model domain is 34.5% of the total ozone and by 2018 the percentage increases to 43.6% in Baltimore. The same tendency for BC_{O3} to have an increasing role for surface ozone is applicable to other regions in the eastern United States, such as New York City, Atlanta, and Chicago, as shown in Table 6-1.

Table 6-1. Percentage of ozone attributed to the boundary at each receptor location during the July mean of 2002, 2011, and 2018.

Metropolitan Area	2002	2011	2018
New York, NY	37.0%	41.6%	45.3%
Philadelphia, PA	38.1%	42.7%	47.6%
Baltimore, MD	34.5%	38.8%	43.6%
Washington, DC	35.9%	41.0%	46.5%

Between 2002 and 2018, there is a definitive trend for contributions from within the model domain to lose influence on total ozone during the summer. Figure 6-4 also shows that BC_{O3} increases from 26.0 ppbv in 2002 to 27.2 ppbv in 2018, a +4.6% increase over 16 years, in the Baltimore metropolitan area. This increase is also seen in other urban areas in the eastern United States as shown in Table 6-2.

Table 6-2. Portion of ozone (ppbv) attributed to the boundary at each receptor location during the July mean of 2002, 2011, and 2018.

Metropolitan Area	2002	2011	2018
New York, NY	23.9	24.6	25.9
Philadelphia, PA	26.8	27.4	27.7
Baltimore, MD	26.0	26.8	27.2
Washington, DC	27.1	27.6	28.0

We also show the same finding using CB6r2 gas-phase chemistry in Figure 6-8.

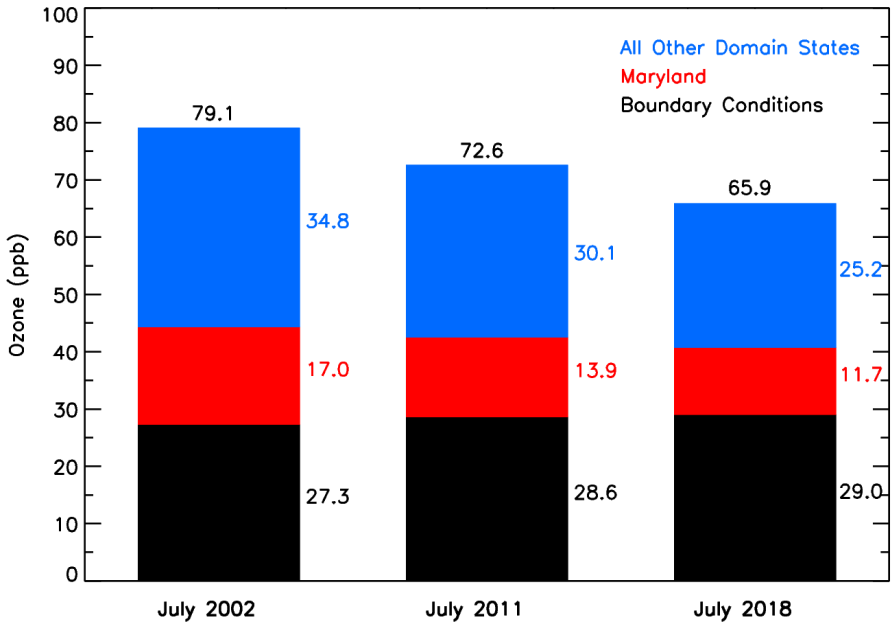

Figure 6-8. Same as Figure 6-7, but now using CB6r2 gas-phase chemistry instead of CB05.

We attribute the increase in BC_{O3} to lower O_x ($O_x = O_3 + (NO_y - NO)$) loss rates in the future. Figure 6-9 shows that in 2002, O_x loss rates in Maryland were 1.5 ppbv per hour during the daytime (8 AM – 8 PM local time). In 2018, O_x loss rates over the same timeframe are projected to be 1.2 ppbv per hour, a difference of –0.3 ppbv per hour. A reduction in O_x loss rates yields a longer lifetime of ozone in the troposphere.

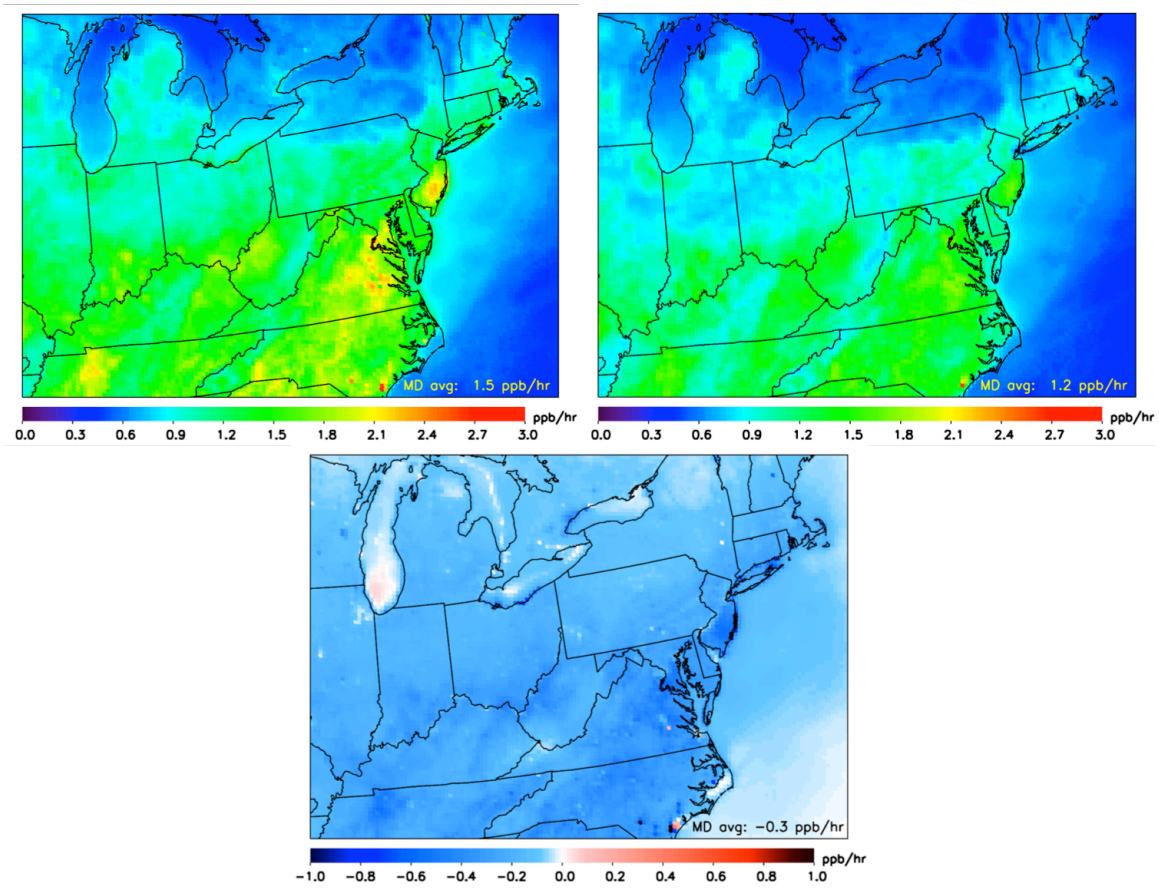

Figure 6-9. Mean daytime (8 AM – 8 PM local time) loss of O_x (O_3+[NO_y – NO]) for July 2002 (top left), July 2018 (top right), and the difference (July 2018 – July 2002) (bottom center) from the Chemical Process Analysis (CPA) probing tool in CAMx.

Our analysis suggests two reasons why O_x loss rates decline in the future: decreased removal of ozone by HO_2 and decreased removal of NO_2 by oxidation to nitrate (NO_3^-). The $HO_2 + O_3$ reaction is an important sink for ozone in non-urban, non-industrial regions and especially at altitudes above the surface layer [Wang et al., 1998]. Figure 6-10 shows a dichotomy between urban and rural regions; the highest mixing ratios of HO_2 are focused in the rural regions of the southeastern United States, while the lowest mixing ratios of HO_2 are found in major metropolitan areas.

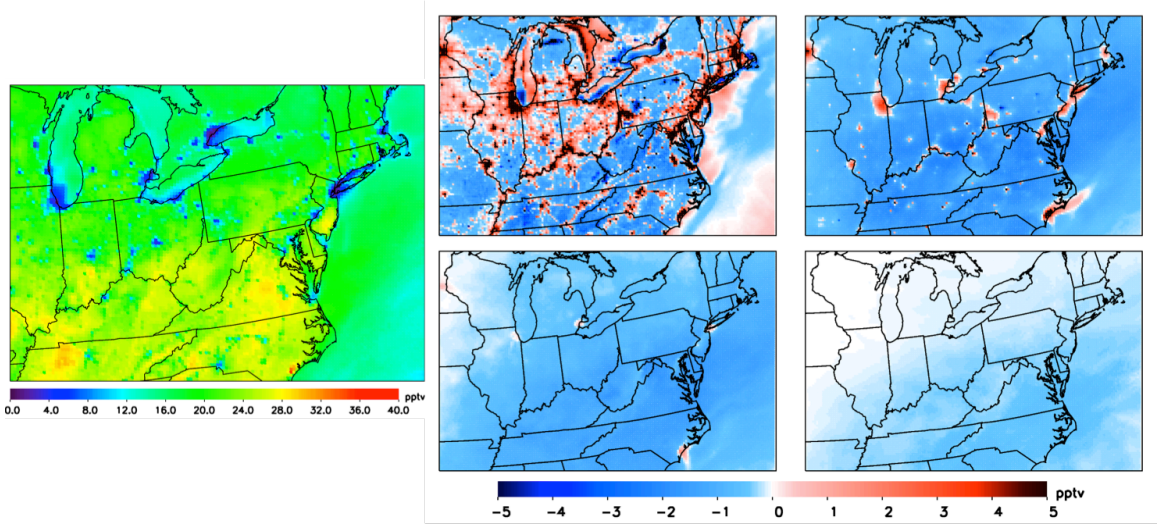

Figure 6-10. (Left) Mean July 2011 daytime (7 AM – 7 PM local time) HO_2 mixing ratios (pptv). (Right) Difference of mean HO_2 daytime (8 AM – 8 PM local time) mixing ratios (pptv) between July 2002 and July 2018: at the surface (top left panel), 1 km above the surface (top right panel), 2km above the surface (bottom left panel) and 5 km above the surface (bottom right panel).

Typical HO_2 mixing ratios in non-urban, non-industrial locations (where NO_x mixing ratios are low, < 1 ppbv) can be an order of magnitude larger in rural areas than in urban regions due to isoprene oxidation [Trainer et al., 1987]. In urban regions (where NO_x mixing ratios are high, >5 ppbv), mixing ratios of HO_2 are low because HO_2 readily reacts with NO to create NO_2 and OH, causing the $HO_2 + O_3$ reaction to be locally unimportant for the loss of ozone.

Decreased removal of ozone via chemical reaction with HO_2 in non-urban, non-industrial regions of the atmosphere is one reason why there is a decrease in O_x loss between July 2002 and 2018. Figure 6-10 also shows a plot of the difference in monthly mean HO_2 between July 2002 and 2018 for the eastern United States at the surface and three vertical layers (1, 2, and 5 km above the surface). Between 2002 and 2018, the CAMx simulation shows a 1 – 3 pptv decrease in HO_2 mixing ratios at the surface in non-urban, non-industrial locations south and west of the mid-Atlantic. This area of the mid-

Atlantic is particularly important because winds are usually from the southwest during the worst air quality episodes. Urban areas have higher future HO_2 mixing ratios due to less titration by the decreased NO_x emissions. Above the surface – especially at 1 and 2 km above the surface – the projected decrease in HO_2 is spatially uniform. Ozone above the surface layer is most affected by this decline in the abundance of HO_2. The mean change in ozone lifetime with respect to reaction with HO_2 at the surface, between 2002 and 2018, is modest: 9.21 days (k_{O3+HO2}=2.853 ppm^{-1} min^{-1}, [HO_2]=26.42 ppt) to 9.42 days (k_{O3+HO2}=2.853 ppm^{-1} min^{-1}, [HO_2]=25.84 ppt). However, 1 km above the surface, the lifetime of ozone with respect to reaction with HO_2 increases from 8.98 days to 9.48 days. In the 2002 scenario, 11.1% of ozone is removed per day via reaction with HO_2, while in the 2018 scenario, 10.5% of ozone is removed per day via reaction with HO_2, (Table 3). Even though our model simulation has a 7 ppbv rural high bias in predicting ozone, the relative change in lifetime of ozone is insensitive to the absolute concentration of ozone (within 1 sigma).

Our modeled mixing ratios of mean HO_2 agree well with measurements from Martinez et al. [2003], as shown in Figures 6-11, 6-12 and 6-13.

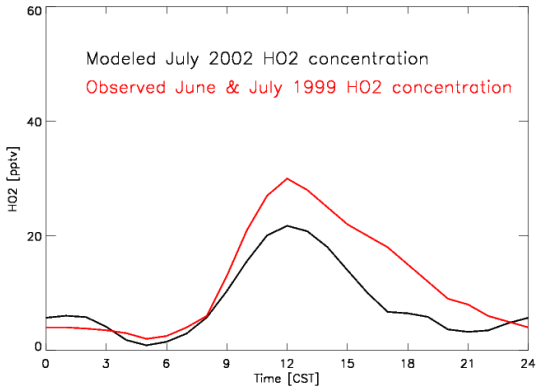

Figure 6-11. Mean modeled HO_2 mixing ratios at the Cornelia Airpark, 8 km northeast of Nashville, TN, during the July 2002 diurnal cycle. Also plotted are observations of HO_2 during June 21 – July 15, 1999 at the same location as taken from Figure 3 in Martinez et al., 2003.

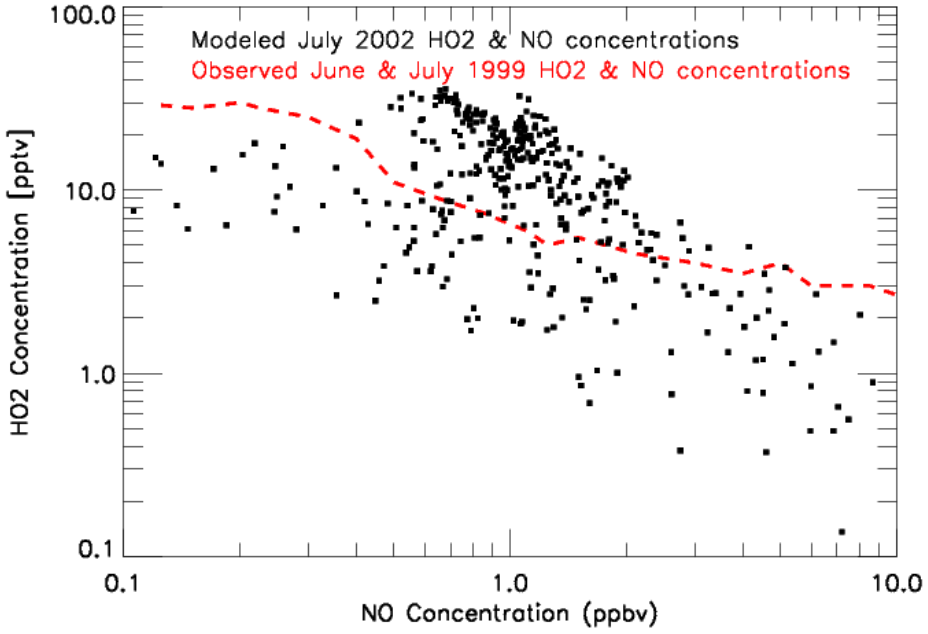

Figure 6-12. Modeled HO_2 vs. NO mixing ratios at the Cornelia Airpark, 8 km northeast of Nashville, TN, during the daytime hours (6 AM – 6 PM local time) of July 2002. Also plotted are observations of HO_2 vs. NO during June 21 – July 15, 1999 at the same location as taken from Figure 9 in Martinez et al., 2003.

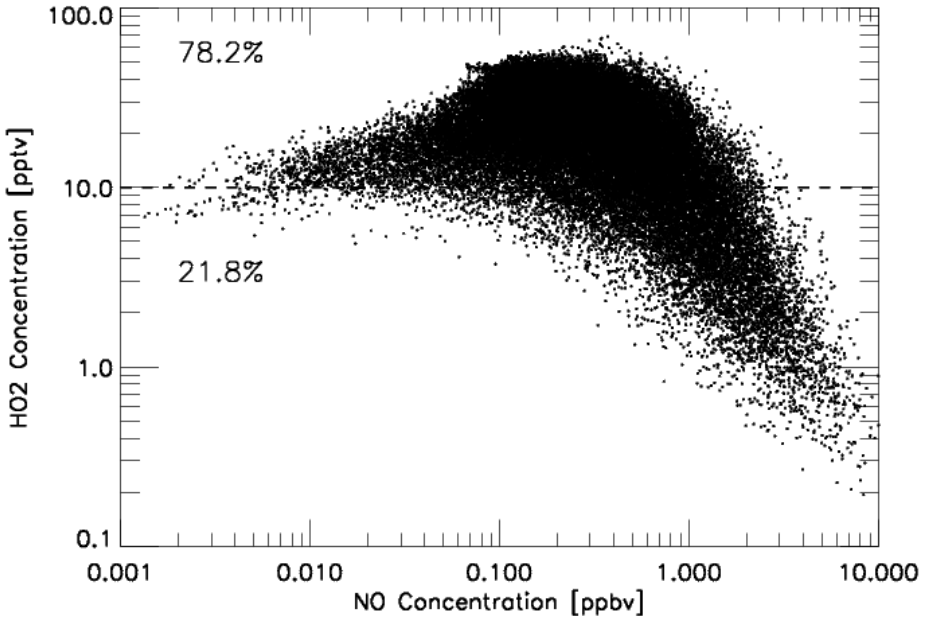

Figure 6-13. Modeled HO_2 vs. NO mixing ratios in Maryland (38 – 40° N, 75 – 78° W) during the daytime hours (7 AM – 7 PM local time) of July 2011. Percentages indicate the number of points above and below a 10 pptv HO_2 threshold; the delineation for when the reaction with O_3 is quick enough to appreciably destroy ozone.

The decreases in HO_2 above the surface layer and in rural regions are due to area wide decreases in anthropogenic emissions of NO_x and VOCs; biogenic emissions and meteorology remain identical between the two simulations. The primary sources and sinks of HO_2 are listed below [Jacob, 2000]:

Sources:

(R1) $RH + OH \xrightarrow{O_2} RO_2 + \boldsymbol{HO_2}$

(R2a) $RO_2 + NO \longrightarrow RO + NO_2$

(R2b) $RO + O_2 \longrightarrow R'CHO + \boldsymbol{HO_2}$

(R3) $RO + h\nu \xrightarrow{2O_2} 2\boldsymbol{HO_2} + R'O$

Sinks:

(R4) $\boldsymbol{HO_2} + \boldsymbol{HO_2} \longrightarrow H_2O_2 + O_2$

(R5) $\boldsymbol{HO_2} + RO_2 \longrightarrow ROOH + O_2$

(R6) $\boldsymbol{HO_2} + OH \longrightarrow H_2O + O_2$

The production of HO_2 is controlled by both VOC and NO_x emissions. Alkanes (RH) and carbonyls (R'CHO) can be direct sources of HO_2 via reactions 1 and 3. Decreased concentrations of alkanes and carbonyls will result in lower production of HO_2. NO_x emissions can also indirectly affect the HO_2 radical; lower concentrations of NO lead to slower production of HO_2 via reaction 2. The removal of HO_2 will also proceed more slowly, since the primary sink of HO_2 is the self-reaction (reaction 4). In Figure 6-14, we show a plot of the difference of HO_2 between the 2002 simulation and a sensitivity experiment in which we keep NO_x emissions in 2018 identical to 2002. The decrease of HO_2 in rural areas and above the surface is smaller than the decrease shown in Figure 6-10. Therefore, we conclude that reductions in the emissions of VOCs as well as the nonlinearities associated with declining NO_x emissions are both responsible for the

simulated decline in HO_2 that leads to an increase in the photochemical lifetime of tropospheric ozone.

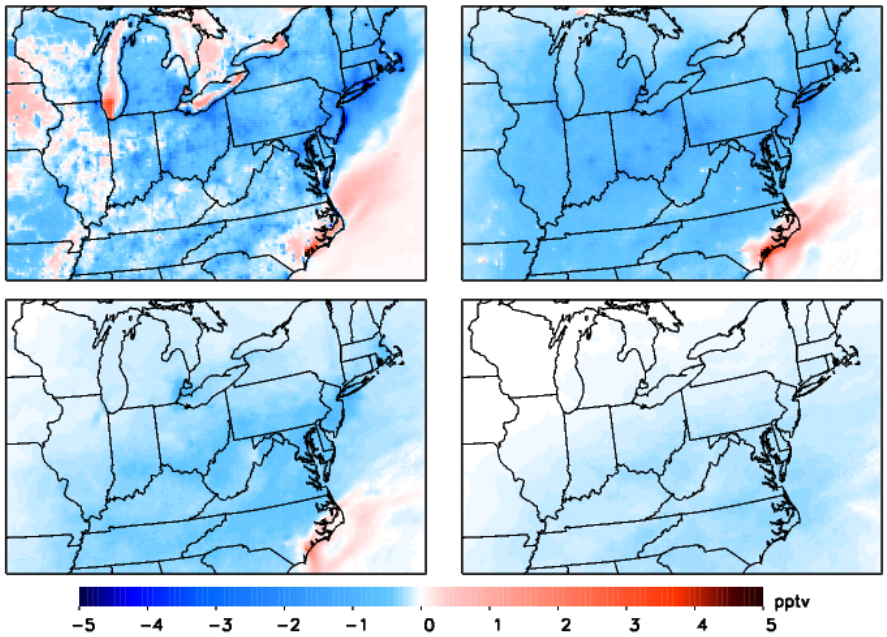

Figure 6-14. Difference of mean HO_2 daytime (8 AM – 8 PM local time) mixing ratios (pptv) between July 2002 and July 2018 with 2002 NO_x emissions: at the surface (top left panel), 1 km above the surface (top right panel), 2 km above the surface (bottom left panel) and 5 km above the surface (bottom right panel).

The second explanation for the increase in the lifetime of ozone is less removal via daytime NO_2+OH reacting to form HNO_3 as well as nighttime hydrolysis of N_2O_5. At night, reaction between ozone and NO_2 can be a sink of ozone – during the daytime, this reaction results in NO_3 being quickly photolyzed back to NO_2. The reactions proceed as follows:

(R7) $$O_3 + NO_2 \longrightarrow NO_3 + O_2$$

(R8) $$NO_3 + NO_2 + M \longrightarrow N_2O_5 + M$$

(R9) $$N_2O_5 + H_2O \xrightarrow{aerosol} 2\,HNO_3$$

As anthropogenic NO_x emissions decline, removal of ozone via NO_2+OH and N_2O_5 hydrolysis will decrease. This is normally a minor sink for ozone, but the change in NO_x between 2002 and 2018 is large enough to have a nontrivial effect. We show in Figures 6-15 and 6-16 that HNO_3 deposition has decreased domain-wide from 185 kg/km^2-month to 112 kg/km^2-month between July 2002 and 2018; calculations using equation 1 show a change in lifetime of ozone with respect to loss from nitrate formation to increase from 19.2 days to 28.6 days (PBL=1000 m, $[O_3]_{2002}$ = 43.1 ppbv, $[O_3]_{2018}$ = 38.8 ppbv).

$$\tau_{O3} = \frac{[O_3]*PBL_{depth}}{[HNO_3]_{deposition}} \qquad (1)$$

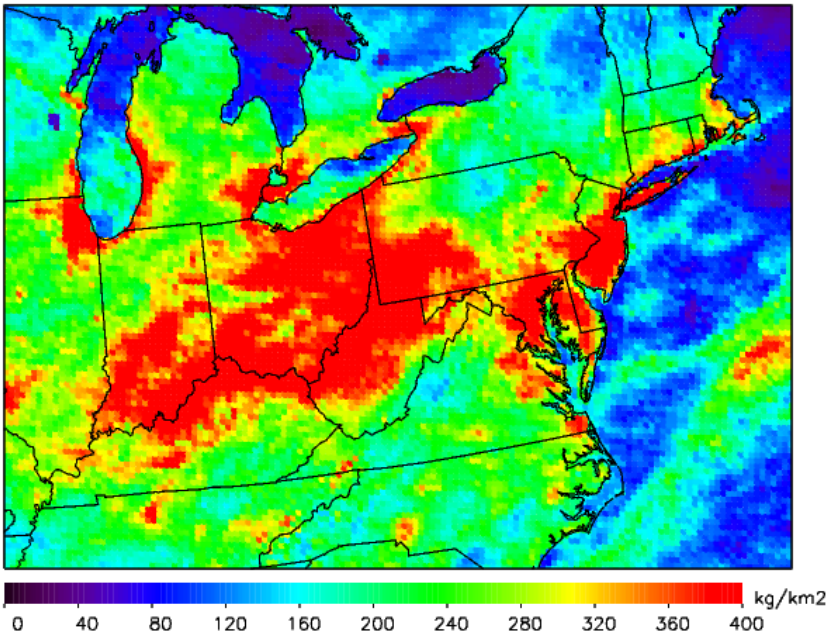

Figure 6-15. July 2002 HNO_3 deposition (kg/km^2). Model domain mean is 185 kg/km^2.

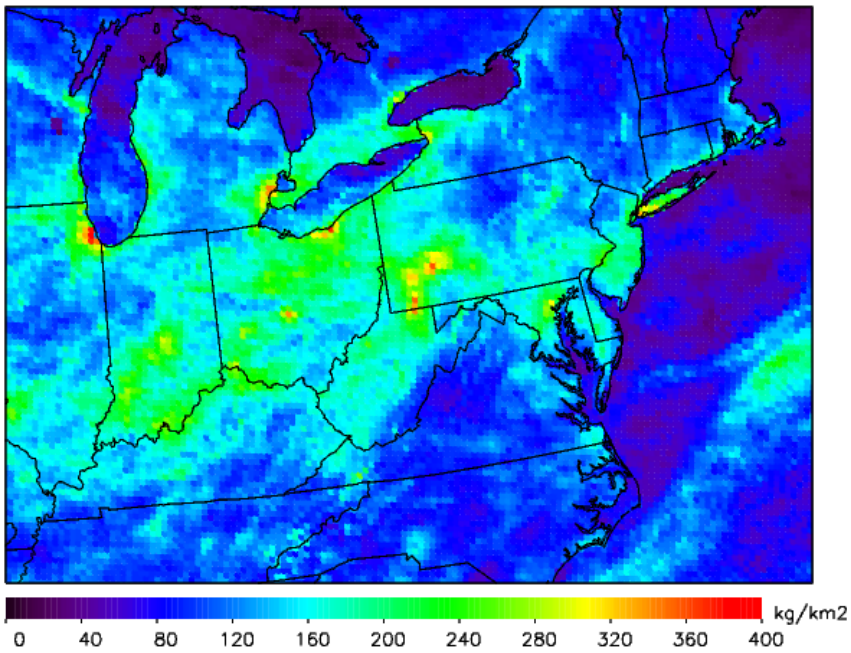

Figure 6-16. July 2018 HNO_3 deposition (kg/km^2). Model domain mean is 112 kg/km^2.

In the 2002 scenario, 5.2% of ozone is removed per day, while in the 2018 scenario, 3.5% of ozone is removed per day, as seen in Table 6-3.

Table 6-3. The percentage (%) of ozone lost per day due to two changing sinks of ozone in July 2002 and July 2018, and the change between the two years.

Ozone Loss	2002	2018	Δ
Loss by HO_2 per day	11.1	10.5	+0.6
Loss by HNO_3 per day	5.2%	3.5%	+1.7

Between these two explanations – less removal of ozone by HO_2 and by NO_2 through nitrate formation – we have accounted for the increase of the ozone lifetime. The change with respect to the HO_2 sink yields a +0.6% change per day and the change with respect to the nitrate sink represents a +1.7% change per day. Taken together this is a 2.3% per day increase in the lifetime of ozone. Typically air parcels travel for one to

three days in the model domain before reaching the east coast of the United States – where our modeling study is focused. This yields a +4.6% change over a 2-day period, which reconciles the +4.6% change found in our modeling study. Table 6-4 and figures in the supplementary material (Figures 6-17 – 6-21) show changes in termination rates of HO_2 and HNO_3. In each case, termination rates have weakened yielding a longer lifetime of O_x.

Table 6-4. The production and loss rates (ppbv/hr) of five important reactions during July 2002 and July 2018. HO_2 production, HO_2 termination, and NO_2+OH termination rates were calculated for the daytime mean (8 AM – 8 PM local time). NO_3+Organics termination and N_2O_5+Water termination were calculated for the nighttime mean (8 PM – 8 AM). The last column shows a difference between the 2002 and 2018 means.

Chemical Process Analysis	2002	2018	Δ
HO_2 production	2.20	1.80	–0.40
HO_2 termination	1.60	1.30	–0.25
HNO_3 from NO_2+OH	0.40	0.20	–0.20
HNO_3 from NO_3+Organics	0.03	0.01	–0.02
HNO_3 from N_2O_5 + Water	0.11	0.02	–0.09

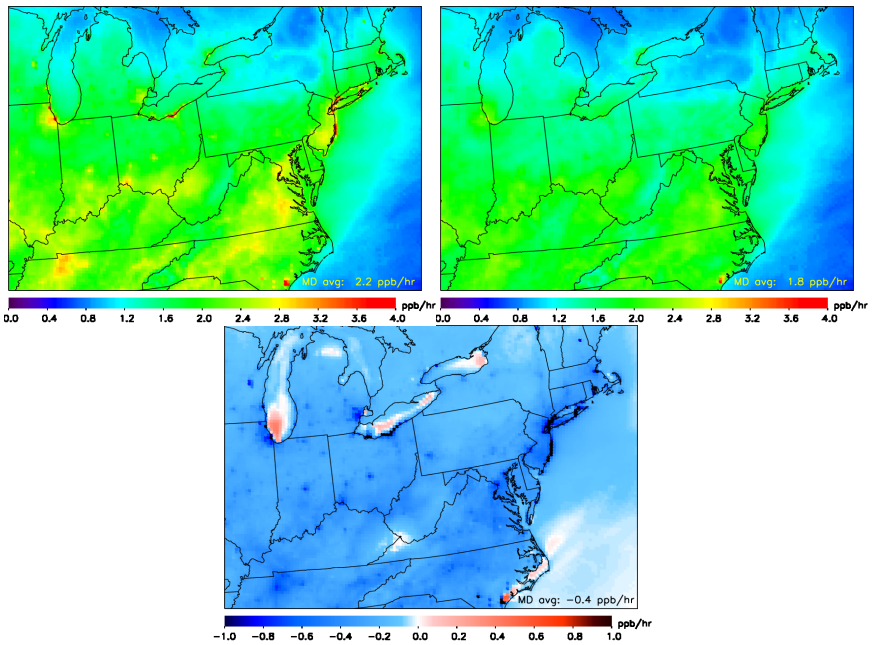

Figure 6-17. Daytime (8 AM – 8 PM local time) HO_x (HO_2+OH) Production for July 2002 (top left), July 2018 (top right), and the difference (July 2018 – July 2002) (bottom center) from the Chemical Process Analysis (CPA) probing tool in CAMx.

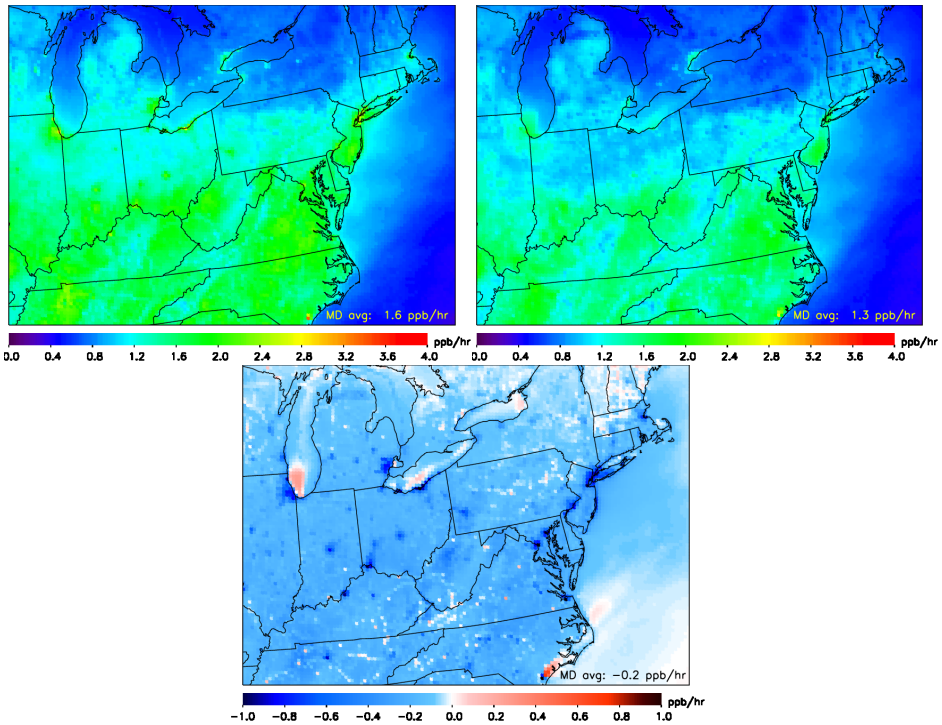

Figure 6-18. Daytime (8 AM – 8 PM local time) HO_x (HO_2+OH) Loss for July 2002 (top left), July 2018 (top right), and the difference (July 2018 – July 2002) (bottom center) from the Chemical Process Analysis (CPA) probing tool in CAMx.

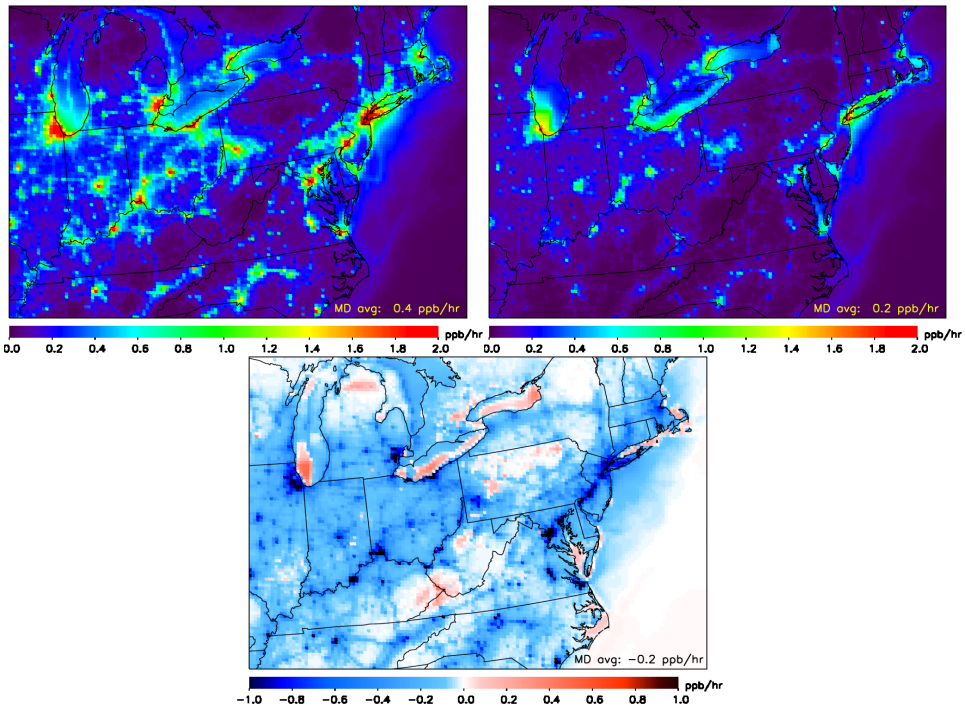

Figure 6-19. Daytime (8 AM – 8 PM local time) HNO_3 produced from NO_2 + OH for July 2002 (top left), July 2018 (top right), and the difference (July 2018 – July 2002) (bottom center) from the Chemical Process Analysis (CPA) probing tool in CAMx.

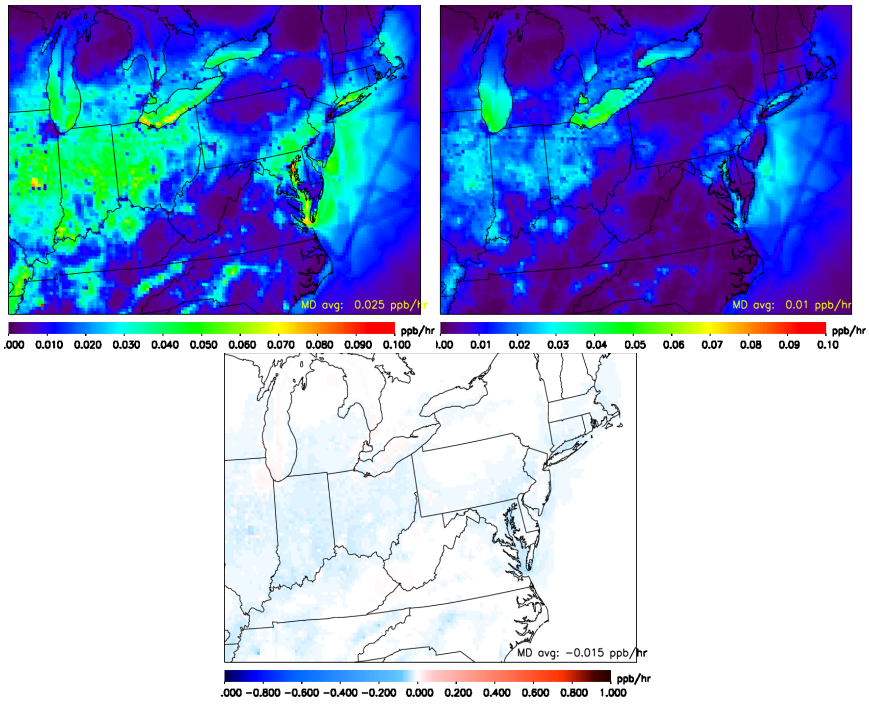

Figure 6-20. Nighttime (8 PM – 8 AM local time) HNO_3 produced from NO_3 + Organics for July 2002 (top left), July 2018 (top right), and the difference (July 2018 – July 2002) (bottom center) from the Chemical Process Analysis (CPA) probing tool in CAMx.

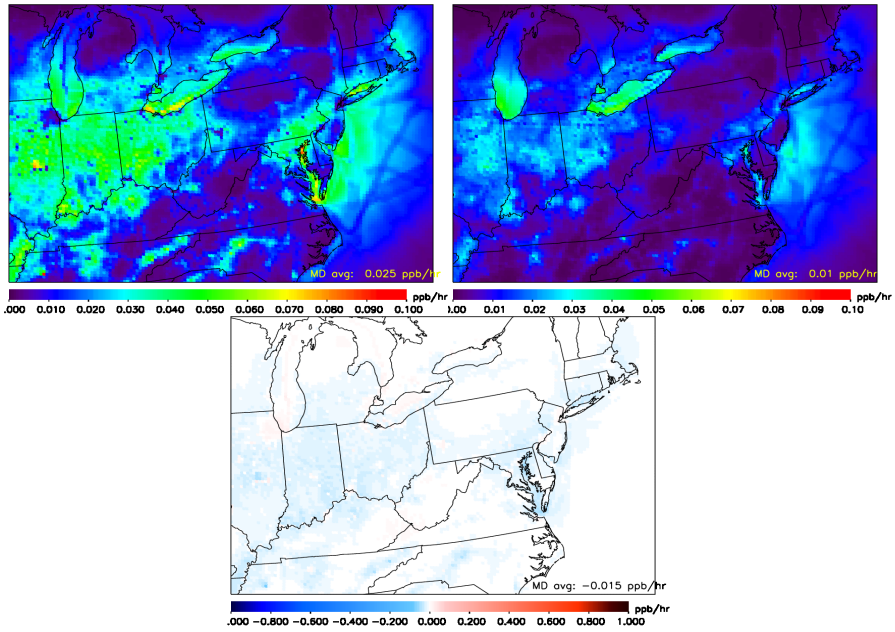

Figure 6-21. Nighttime (8 PM – 8 AM local time) HNO_3 produced from N_2O_5 + Water for July 2002 (top left), July 2018 (top right), and the difference (July 2018 – July 2002) (bottom center) from the Chemical Process Analysis (CPA) probing tool in CAMx.

6.3.4 Role of ozone above the surface

Ozone can also be tagged in individual plumes above the surface. Figure 6-22 depicts average hourly ozone source apportionment in an aloft plume 500 – 2000 m above ground level (agl) between 39° and 40° N along 78° W on July 7, 2011. The tagged plume was upwind of Maryland on July 7: a day with large interstate transport as denoted in Figure 6-4. The ozone in the aloft plume is near 75 ppbv overnight and into the early morning. The air containing high ozone can mix down in the morning leading to rapid spikes when the nocturnal boundary layer breaks up. The diurnal cycle of total ozone aloft shows a much weaker daily cycle than during a day: a 10 ppbv change between the morning minimum and afternoon maximum. When total mixing ratios are at a minimum just after sunrise (7 AM), BC_{O3} is at a maximum.

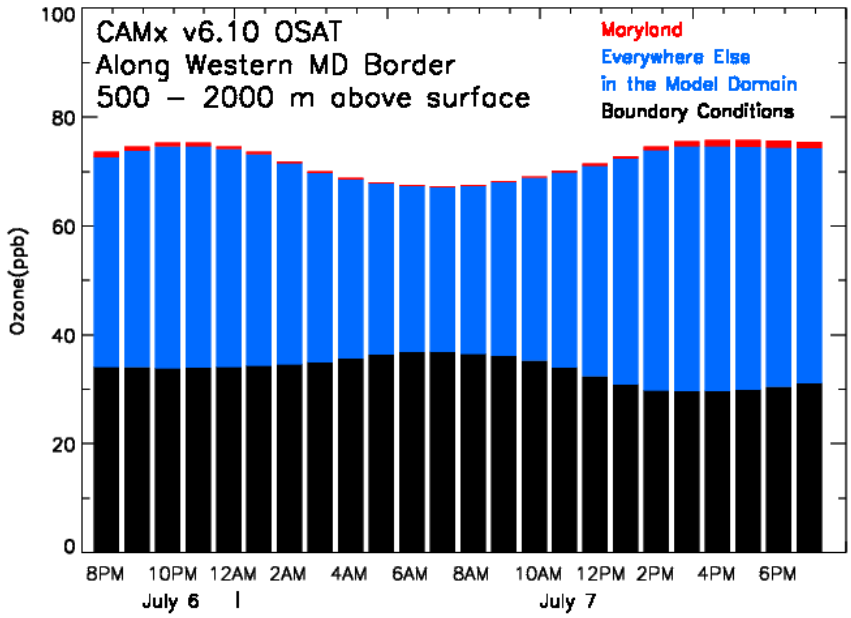

Figure 6-22. Ozone source apportionment (ppbv) between 500 – 2000 m above the surface in a 12 x 180 km "wall of cells" representing the western border of Maryland during July 7, 2011, a day with westerly transport, confirmed by HYSPLIT. Black bars represent the contribution from beyond the model domain boundary, blue bars represent the contribution from states within the model domain besides Maryland, and red bars represent the contribution from Maryland.

We suggest the following conceptual model: Overnight, the ozone mixing ratio in the residual layer, 500 – 2000 m agl, decreases slowly due to a lack of photochemical production. In contrast, ozone attributed to the boundary increases due to easier mixing from the free troposphere. At approximately 8 AM when the nocturnal temperature inversion breaks up, the residual layer (pollution from the previous day's PBL) mixes into the newly formed PBL, decreasing the portion attributed to the boundary, but increasing the portion attributed to sources at or near the surface. At the same time, precursors from upwind states, essentially dormant overnight, can begin to react to photochemically produce ozone. In this scenario, much of the boundary ozone at the surface mixes down from aloft instead of being horizontally advected from the model domain boundary. Quantifying and verifying the ozone aloft is (500 – 2000 m agl) is of critical importance as these can affect peak daytime mixing ratios in downwind locations.

6.3.5. Initialization with different global models

With the increased role of BC_{O3} in the past decade, the choice of boundary initialization has become more important. A sensitivity study [Akritidis et al., 2013] using a 50 km × 50 km regional model showed time invariant chemical boundary conditions do not capture the seasonal variability of ozone. Adding seasonal variability improved correlation and reduced the mean bias; adding interannual variability did not improve correlation, but did improve the mean bias. Boundary conditions can be essential for accurate prediction in regional air quality models [Tang et al., 2007; Tang et al., 2009].

There are two global models commonly used to initialize the trace gases at the boundary of regional air quality models: GEOS-Chem [Bey et al., 2001] and MOZART-4

[Emmons et al., 2010]. Figure 6-23 shows mean July monthly ozone mixing ratios in GEOS-Chem and MOZART-4 along our model domain boundary. In the mid-troposphere, 2 – 7 km above the surface (roughly 800 – 300 hPa), the ozone concentration is much higher in GEOS-Chem, especially at the western boundary. Mean GEOS-Chem mixing ratios in the mid-troposphere often exceed 90 ppbv at the western boundary, while MOZART-4 mixing ratios average 50 ppbv. Taking a closer look, between 0 – 2 km above ground surface there is a lot of variability between the two global models, but there is no consistent bias. Between 2 – 7 km, GEOS-Chem has mixing ratios stunningly higher than MOZART at all boundaries, but most notably at the western boundary. Above 8 km, primarily in the lower stratosphere, the mean ozone mixing ratios from MOZART and GEOS Chem agree once again.

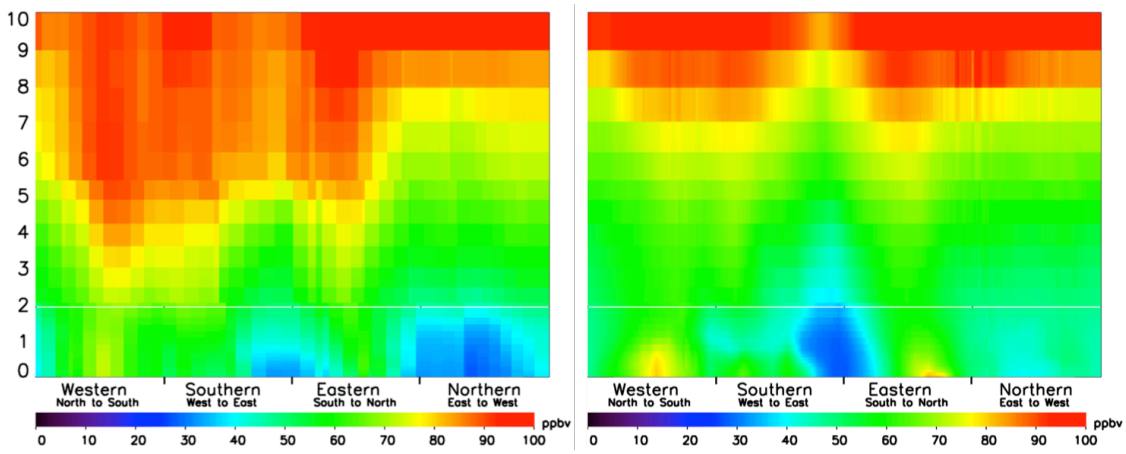

Figure 6-23. Ozone mixing ratios (ppbv) from the surface to 10 km following the model domain boundary (as shown in Figure 3-4) for the July 2011 mean. (right) same as left but now using the MOZART-4 global model.

The different boundary initializations can significantly alter the simulation of ozone in Maryland. In Figure 6-24, we plot mean vertical profiles of ozone from ozonesondes [Thompson et al., 2014] and from CAMx initialized with both global models. Simulation of mean near-surface ozone is quite good, within 1-2 ppbv, but the

lines diverge above 200 m. There is a striking underestimate of ozone (>10 ppbv) between 200 m and 2,000 m agl by both simulations. Between 2,000 m and 5,000 m agl, CAMx initialized with GEOS-Chem simulates uniformly greater mixing ratios than CAMx initialized with MOZART-4. We posit two explanations for the poor prediction of ozone above the surface: inadequate vertical mixing of ozone and its precursors, which has been known to be a problem [Solazzo et al., 2013; Castellanos et al., 2011], and/or the underestimate of ozone at the boundary, which we show to be the principal contributor to ozone mixing ratios above 500 m.

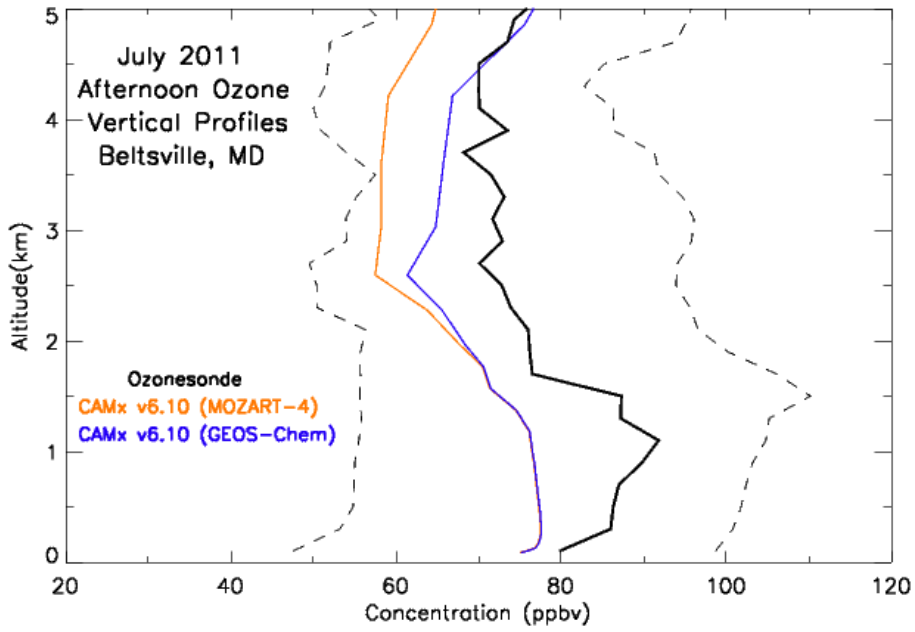

Figure 6-24. Mean vertical profiles of ozone (black curve) observed from the ozonesondes launched from Beltsville, MD [Thompson et al., 2014], (orange curve) CAMx simulation using MOZART-4 as boundary conditions and (blue curve) CAMx simulation using GEOS-Chem as boundary conditions at the closest model grid point.

6.4. Conclusions

Surface ozone in the northeastern United States is projected to decline due to reductions in anthropogenic nitrogen oxide (NO_x) and volatile organic compound (VOCs) emissions driven by air quality regulations and market-based fuel switches. However, using observed values in the Baltimore-Washington metropolitan area, we find surface ozone during relatively clean summertime days (the 33rd percentile) to be rising at a rate of +0.37 ± 0.04 ppbv/year. This finding comes in stark contrast to the steady decreases in total surface ozone observed during the worst air quality days. NO_x and VOC emissions reductions contributed to the decreases during the worst air quality days [e.g., Loughner et al., 2014], but the reasons for the increase during clean days are still unclear [Lin et al., 2000; Cooper et al., 2012]. We suggest that decreasing NO_x and HO_2 in rural areas and aloft plumes are causing an increase in the lifetime of ozone. This allows ozone to be transported greater distances than a decade ago.

The model indicates boundary ozone (BC_{O3}), defined here as ozone entering our eastern United States modeling domain, is 38.8% of the total surface ozone in Maryland during an average day in July 2011. The values of BC_{O3} predicted by OSAT, between 25 and 35 ppbv, are close to the estimated hemispheric background mixing ratios in the absence of North American anthropogenic emissions [Emery et al., 2012; Fiore et al., 2014].

Predictions from CAMx show the portion attributed to BC_{O3}, beyond the control of the eastern United States, will become a larger share as anthropogenic NO_x and VOC emissions in our model domain decrease. Between July 2002 and July 2018, BC_{O3} rises from 34.5% to 43.6% of the total surface ozone in Baltimore. Similar increases are seen in other metropolitan areas in the eastern United States.

Not only has BC_{O3} increased by percentage, but also in an absolute sense, from 26.0 to 27.2 ppbv between July 2002 and July 2018. This increase cannot be attributed to international transport, meteorological differences, or the stratosphere because we initialize the boundary and meteorology identically in each simulation; it must be a result of the changes to the emissions within our model domain.

Two processes that are sinks for ozone: O_3+HO_2 and nitrate formation are becoming less effective at removing odd oxygen; this is increasing the lifetime of ozone in the domain. The increased lifetime of ozone associated with these two sinks is +4.6% over a 16-year period, and can account for the +4.6% change in BC_{O3} over the same 16-year period. The longer lifetime of ozone will increase the spatial and temporal scale of ozone pollution, which adds urgency to control ozone precursors on a regional scale especially when the standard is tightened in future years. Decreasing anthropogenic VOC and NO_x emissions in the eastern United States has had the unintentional consequence of weakening two ozone destruction pathways.

These results also point out the importance of evaluating the global models used to initialize the boundaries of regional air quality models. We show substantial variance in ozone mixing ratios between the GEOS-Chem and MOZART-4 global models; differences of >30 ppbv ozone exist in the free troposphere. This variability leads to 1 – 2 ppbv differences in surface ozone prediction averaged over an entire month with greater inconsistency at the surface during individual days. Regional air quality simulations must initialize boundaries with the most accurate data possible because ozone coming from the boundary is a significant and likely growing contributor to policy-relevant surface concentrations.

7. Recommendations for Future Research

Chapter 2 describes first-time measurements of ozone taken directly over the Chesapeake Bay. Our experiment was also the last known time ozone measurements were taken over the Bay. Long-term measurements of surface ozone, NO_2, NO_y and formaldehyde over the Bay are needed to see if high levels of ozone and its precursors persist over time. Since 2013, ozone mixing ratios at the coastal location – Edgewood, MD – have been under the 75 ppbv NAAQS standard. It is unclear whether ozone mixing ratios over the Bay have continued to be above 75 ppbv. Long-term measurements of ozone over the Chesapeake Bay will be particularly important because the Bay becomes the center of outdoor leisure activities during the summer. It is critical to notify the public when participation in activities on or the near the Bay exposes people to poor air quality.

Chapter 2 also illustrates that 4-km horizontal simulations better resolve small-scale features such as the Bay breeze. We suggest conducting a 4-km horizontal simulations focusing on cities located near Bays, Sounds and/or Great Lakes (e.g., Baltimore near the Chesapeake Bay, New York City near the Long Island Sound, and Chicago near Lake Michigan) using CAMx and ozone source apportionment software to better understand the sources of ozone over these regions. The model run can be compared to any additional measurements of trace gases in these regions.

Reproducing the vertical profile of ozone and its precursors in model simulations remains an issue. In Chapter 4.4, we show an underestimate of ozone pollution above the surface, but within the boundary layer (i.e., 300 – 2000 m agl). For future work, we

suggest two modifications, which may improve the vertical representation of pollutants in regional air quality models. Increasing modeled HO_2 and RO_2 concentrations in the aloft plume will increase ozone productions rates; the ozone production efficiency in aloft plumes is too low [Hembeck et al., in prep.]. We can increase RO_2 and HO_2 concentrations by switching to biogenic emissions from MEGAN v2.1, which has greater emissions of isoprene. We also suggest implementing a parameterization that will cause faster one-way vertical mixing between the surface and the lower most layers of the PBL, because the precursors to RO_2 and HO_2 (i.e., short-lived VOCs) may be staying too close to the surface in model simulations.

The scientific understanding of gas-phase alkyl nitrates has significantly advanced in the past decade. However, few of these advances have made their way into regulatory air quality models. The CB6r2 gas-phase mechanism provides a better representation of alkyl nitrates than CB05 (see Chapter 3.3 and Chapter 5), but there is still room for improvement. When using CB6r2 gas-phase chemistry, an overestimate of alkyl nitrates remains. In CB6r2, NTR2 does not recycle back to NO_2, which may be an oversimplification; adding in recycling of NTR2 may improve the simulation of alkyl nitrates and ozone. It is also possible that portions of multi-functional alkyl nitrates, represented as NTR2, are measured as nitric acid in the DISCOVER-AQ dataset. More laboratory experiments are needed to confirm the recycling rate of multi-functional alkyl nitrates.

Anderson et al., [2014] describe an overestimate of NO_x emissions by the NEI. Because mobiles sources – cars, trucks, construction vehicles, etc. – are responsible for the bulk of NO_x emissions in the eastern United States, they must be overestimated. For

simplicity sake, in this dissertation, we cut the all NO_x mobile source emissions by 50%. This is certainly an over simplification. There is evidence that MOVES – the mobile source emission calculator – has difficulty in the temporal allocation of emissions during rush hour [Tracey Holloway, personal communication]. There is also evidence that vehicle type and age are first-order estimates [Jin Lin, personal communication]. A 50% across-the-board cut in mobile source NO_x emissions does not address any of these issues. A portion of the overestimate of NO_x is also likely due to area sources. Furthermore, recent work by MDE [Bull and Ashenafi, personal communication], suggests that NO_x emissions from electricity peaking units during the hottest summer days are not accounted for in the 2011 NEI. A better representation of NO_x emissions inventory, beyond a 50% across-the-board cut, is needed.

Canty et al., [2015] describe the difficulty in simulating the biogenic precursors to ozone (i.e., formaldehyde, isoprene, methyl vinyl ketone, etc.). In this dissertation, we show that BEIS biogenic emissions cause regional air quality models to underestimate formaldehyde and isoprene. Transitioning to MEGAN v2.1 biogenic emissions improves the simulation of formaldehyde, but the simulation of isoprene is now grossly overestimated. This suggests deficiencies in the conversion of isoprene to formaldehyde. Marvin et al. [in prep.] show that CB05 and CB6r2 underestimate formaldehyde when constrained to isoprene, but the master chemical mechanism (MCM) v3.3 – a complex and detailed mechanism – is able to simulate formaldehyde with better fidelity. Revising CB6r2 to better represent isoprene chemistry should help better simulate formaldehyde, RO_2, and hence ozone.

In Chapters 4.5 and 6, we show a future year model simulations. To conduct these future year scenarios, we were provided boundary conditions identical to the baseline year. As anthropogenic emissions of ozone precursors decline over time, ozone crossing the model domain boundary will become more influential. We suggest conducting any future year modeling scenarios, with boundary conditions representative of the future year.

8. Summary and Concluding Remarks

8.1 Summary

I have been involved with three primary research projects over the past five years, summarized here briefly and described below in more detail.

- During July 2011, measurements of ozone are consistently 10% - 20% higher over the Chesapeake Bay than nearby ground sites; a lower boundary layer, reduced afternoon cloud cover, slower dry deposition rates, and ship emissions contribute to the local maximum of ozone over the Bay.
- There is a significant overestimate of NO_y and an underestimate of HCHO in our baseline air quality model simulation. We implement a new model framework that better captures observations and the response of ozone to reductions of ozone precursor emissions; EGUs are responsible for a larger portion of the ozone than the baseline version, while attribution to mobile sources is less.
- Two primary gas-phase sinks for odd oxygen ($O_x \approx NO_2 + O_3$), attack by hydroperoxyl radicals (HO_2) on ozone and formation of nitrate, weaken with decreasing pollutant emissions; this unintended consequence of air quality regulation causes atmospheric pollutants to last longer, and indicates that pollutant transport between states and countries will likely play a greater role in the future as emissions continue to decline.

Regional air quality models, such as CAMx and CMAQ, indicate decidedly higher ozone near the surface of large interior water bodies, such as the Great Lakes and Chesapeake Bay. In order to test the validity of the model output, we performed surface measurements of ozone (O_3) and total reactive nitrogen (NO_y) on the 26-m Delaware II NOAA Small Research Vessel experimental (SRVx), deployed in the Chesapeake Bay for ten daytime cruises in July 2011 as part of NASA's GEO-CAPE CBODAQ oceanographic field campaign in conjunction with NASA's DISCOVER-AQ air quality field campaign. During this 10-day period, the EPA O_3 regulatory standard of 75 ppbv averaged over an 8-hour period was exceeded four times over water while ground stations in the area only exceeded the standard at most twice. This suggests that on days when the Baltimore/Washington region is in compliance with the EPA standard, air quality over the Chesapeake Bay might exceed the EPA standard. Ozone observations over the Bay during the afternoon were consistently 10% - 20% higher than the closest upwind ground sites during the 10-day campaign; this pattern persisted during good and poor air quality days. A lower boundary layer, reduced cloud cover, slower dry deposition rates, and other lesser mechanisms, contribute to the local maximum of ozone over the Chesapeake Bay. Observations from this campaign were compared to a CMAQ simulation at 1.33 km resolution. The model is able to predict the regional maximum of ozone over the Chesapeake Bay more accurately, but NO_y mixing ratios are severely overestimated by all model simulations suggesting that the input emissions estimates and CB05 gas-phase mechanism need re-evaluation.

The CAMx regional air quality model was assessed and enhanced with data from NASA's 2011 DISCOVER-AQ field campaign. Comparisons show the baseline model

overestimates NO_y by +86.2% and a model underestimate of formaldehyde (HCHO) by –28.3%. We present a new model framework that better captures observations and hopefully the response of ozone to reductions of precursor emissions. We implemented four changes to the model, based on these comparisons: CB6r2 gas-phase chemistry, faster dry deposition of alkyl nitrates, reduced NO_x emissions from mobile sources, and increased formaldehyde from biogenic hydrocarbons. Using the anthropogenic precursors culpability assessment (APCA) software, we show that the updated model platform allocates surface ozone to different source regions and sectors. More ozone is now attributed to electricity generating units (EGUs) while less ozone is attributed to mobile sources. Furthermore, there are changes to the ozone production environment. In the baseline version, the modeled ozone responds to anthropogenic reductions in NO_x and VOCs. In the Beta version of the model, the model responds more to NO_x emission reductions. The model will yield lower ozone mixing ratios when subjected to the same reductions in NO_x emissions; the baseline model underestimates the effectiveness of anthropogenic NO_x reductions.

Measures to control surface ozone rely on quantifying production attributable to local vs. regional (upwind) emissions. Again using CAMx, I simulate the relative contribution of local (i.e., within a particular state) and regional sources of surface ozone in the eastern United States (66 – 94° W longitude) for July 2002, 2011, and 2018. To determine how emissions and chemistry within the domain affect the production, loss, lifetime, and transport of trace gases, I initialized the model with identical boundary conditions in each simulation. The photochemical lifetime of ozone has increased as emissions have decreased. The contribution of ozone from outside the domain (boundary

condition ozone, BC_{O3}) to local surface mixing ratios increases in an absolute sense by 1 – 2 ppbv between 2002 and 2018 due to the longer lifetime of ozone. The photochemical lifetime of ozone lengthens because the two primary gas-phase sinks for odd oxygen ($O_x \approx NO_2 + O_3$) – attack by hydroperoxyl radicals (HO_2) on ozone and formation of nitrate – weaken with decreasing pollutant emissions. The relative role of BC_{O3} will also increase. For example, BC_{O3} represents 34.5%, 38.8%, 43.6% of surface ozone in the Baltimore, MD region during July 2002, 2011, and 2018 means respectively. This unintended consequence of air quality regulation impacts attainment of the NAAQS for surface ozone because the spatial and temporal scales of photochemical smog increase; the influence of pollutants transported between states and into the eastern US will likely play a greater role in the future.

8.2 Concluding Remarks

In this dissertation, I have used measurements and numerical simulations to investigate photochemical smog in the eastern United States. I demonstrated that ozone concentrations are consistently higher over the Chesapeake Bay than over the surrounding land areas and showed how PBL dynamics, cloud cover, loss rates, and ship emissions contribute to this local maximum. These results help explain why coastal areas such as Edgewood, MD have unusually high ozone concentrations.

I have employed the chemical transport model CAMx to explore the sources and lifetime of ozone in Maryland. The baseline model platform simulates ozone with reasonable fidelity, but the simulation of its main precursors NOx and VOCs has considerable error. When guided by observations from DISCOVER-AQ and RAMMPP field experiments, we implement changes that improve the simulation of the ozone

precursors. This means that the model will more likely get ozone right for the proper reasons and improves the ability of modelers to predict the impact of emissions reductions.

I also used CAMx to show that the photochemical lifetime of ozone is increasing as anthropogenic emissions of NO_x and VOCs decrease in the eastern United States. This unintended consequence of air quality regulation may impact attainment of the NAAQS for surface ozone because once emitted, pollutants are lasting longer in the atmosphere than a decade ago and will continue to do so as emissions decrease. As a result, pollutants transported between states and countries will likely play a greater role in the future. Regional emission reduction strategies – in addition to local strategies – will be needed for a continued decline in ozone concentrations.

9. References

Akritidis, D., Zanis, P., Katragkou, E., Schultz, M. G., Tegoulias, I., Poupkou, A., . . . Karacostas, T. (2013). Evaluating the impact of chemical boundary conditions on near surface ozone in regional climate-air quality simulations over Europe. *Atmos. Res.*, *134*, 116-130. doi:10.1016/j.atmosres.2013.07.021

Allen, D. J., Pickering, K. E., Pinder, R. W., Henderson, B. H., Appel, K. W., & Prados, A. (2012). Impact of lightning-NO on eastern United States photochemistry during the summer of 2006 as determined using the CMAQ model. *Atmos Chem Phys*, *12*(4), 1737-1758. doi:10.5194/acp-12-1737-2012

AMEC Environment & Infrastructure. (2013). *Clean Air Status and Trends Network (CASTNET) 2011 Annual Report*.

Anderson, D. C., Loughner, C. P., Diskin, G., Weinheimer, A., Canty, T. P., Salawitch, R. J., . . . Dickerson, R. R. (2014). Measured and modeled CO and NOy in DISCOVER-AQ: An evaluation of emissions and chemistry over the eastern US. *Atmos. Environ.*, *96*, 78-87. doi:10.1016/j.atmosenv.2014.07.004

Anenberg, S. C., Horowitz, L. W., Tong, D. Q., & West, J. J. (2010). An Estimate of the Global Burden of Anthropogenic Ozone and Fine Particulate Matter on Premature Human Mortality Using Atmospheric Modeling. *Environ. Health Perspect.*, *118*(9), 1189-1195. doi:10.1289/ehp.0901220

Angevine, W. M., Senff, C. J., White, A. B., Williams, E. J., Koermer, J., Miller, S. T. K., . . . Downs, T. (2004). Coastal boundary layer influence on pollutant transport in New England. *Journal of Applied Meteorology*, *43*(10), 1425-1437. Retrieved from http://journals.ametsoc.org/doi/abs/10.1175/JAM2148.1

Appel, K. W., Gilliland, A. B., Sarwar, G., & Gilliam, R. C. (2007). Evaluation of the Community Multiscale Air Quality (CMAQ) model version 4.5: Sensitivities impacting model performance Part I - Ozone. *Atmos. Environ.*, *41*(40), 9603-9615. doi:10.1016/j.atmosenv.2007.08.044

Appel, K. W., Chemel, C., Roselle, S. J., Francis, X. V., Hu, R.-M., Sokhi, R. S., . . . Galmarini, S. (2012). Examination of the Community Multiscale Air Quality (CMAQ) model performance over the North American and European domains. *Atmospheric Environment*, *53*, 142-155. Retrieved from http://researchprofiles.herts.ac.uk/portal/files/737785/906093.pdf

Atkinson, R.A., Baulch, D. L., Cox, R. A., Crowley, J. N., Hampson, R. F., Hynes, R. G., … Troe, J. (2010). Evaluated kinetic and photochemical data for atmospheric chemistry - IUPAC subcommittee on gas kinetic data evaluation for atmospheric chemistry. Retrieved from http://www.iupac-kinetic.ch.cam.ac.uk/index.html

Beaver, M. R., St, C., JM, Paulot, F., Spencer, K. M., Crounse, J. D., LaFranchi, B. W., . . . Wennberg, P. O. (2012). Importance of biogenic precursors to the budget of organic nitrates: observations of multifunctional organic nitrates by CIMS and TD-LIF during BEARPEX 2009. *Atmos Chem Phys*, *12*(13), 5773-5785. doi:10.5194/acp-12-5773-2012

Bell, M. L., McDermott, A., Zeger, S. L., Samet, J. M., & Dominici, F. (2004). Ozone and short-term mortality in 95 US urban communities, 1987-2000. *JAMA-J. Am. Med. Assoc.*, *292*(19), 2372-2378.

Bell, M. L., Peng, R. D., & Dominici, F. (2006). The exposure-response curve for ozone and risk of mortality and the adequacy of current ozone regulations. *Environmental health perspectives*, 532-536. Retrieved from http://www.jstor.org/stable/3650933

Bey, I., Jacob, D. J., Yantosca, R. M., Logan, J. A., Field, B. D., Fiore, A. M., . . . Schultz, M. G. (2001). Global modeling of tropospheric chemistry with assimilated meteorology: Model description and evaluation. *J. Geophys. Res.-Atmos.*, *106*(D19), 23073-23095.

Bloomer, B. J., Vinnikov, K. Y., & Dickerson, R. R. (2010). Changes in seasonal and diurnal cycles of ozone and temperature in the eastern US. *Atmos Environ*, *44*(21-22), 2543-2551. doi:10.1016/j.atmosenv.2010.04.031

Bowman, L. D., and R. F. Horak. (1972). A continuous ultraviolet absorption ozone photometer, Rep. ISA AID 72430, pp. 103-108, Instrum. Soc. of Am., Pittsburgh, PA

Brent, L. C., Thorn, W. J., Gupta, M., Leen, B., Stehr, J. W., He, H., . . . Dickerson, R. R. (2013). Evaluation of the use of a commercially available cavity ringdown absorption spectrometer for measuring NO2 in flight, and observations over the Mid-Atlantic States, during DISCOVER-AQ.

Brioude, J., Angevine, W. M., Ahmadov, R., Kim, S. W., Evan, S., McKeen, S. A., . . . Trainer, M. (2013). Top-down estimate of surface flux in the Los Angeles Basin using a mesoscale inverse modeling technique: assessing anthropogenic emissions of CO, NOx and CO2 and their impacts. *Atmos. Chem. Phys.*, *13*(7), 3661-3677. Retrieved from http://dx.doi.org/10.5194/acp-13-3661-2013

Burns, D. A., Blett, T., Haeuber, R., & Pardo, L. H. (2008). Critical loads as a policy tool for protecting ecosystems from the effects of air pollutants. *Front. Ecol. Environ.*, *6*(3), 156-159. doi:10.1890/070040

Byun, D., & Schere, K. L. (2006). Review of the governing equations, computational algorithms, and other components of the Models-3 Community Multiscale Air Quality (CMAQ) modeling system. *Applied Mechanics Reviews*, *59*(1/6), 51. Retrieved from http://dns2.vbird.org/teach/Modeling and analysis/CMAQ-2006.pdf

Canty, T. P., Hembeck, L., Vinciguerra, T. P., Anderson, D. C., Goldberg, D. L., Carpenter, S. F., . . . Dickerson, R. R. (2015). Ozone and NOx chemistry in the eastern US: evaluation of CMAQ/CB05 with satellite (OMI) data. *Atmospheric Chemistry and Physics*, *15*, 10965-10982.

Carlton, A. G., & Baker, K. R. (2011). Photochemical Modeling of the Ozark Isoprene Volcano: MEGAN, BEIS, and Their Impacts on Air Quality Predictions. *Environ. Sci. Technol.*, *45*(10), 4438-4445. doi:10.1021/es200050x

Carter, W. P. L. (1994). Development of ozone reactivity scales for volatile organic compounds. *Air & Waste*, *44*(7), 881-899. Retrieved from http://www.tandfonline.com/doi/pdf/10.1080/1073161X.1994.10467290

Castellanos, P., Marufu, L. T., Doddridge, B. G., Taubman, B. F., Schwab, J. J., Hains, J. C., . . . Dickerson, R. R. (2011). Ozone, oxides of nitrogen, and carbon monoxide during pollution events over the eastern United States: An evaluation of emissions

and vertical mixing. *J Geophys Res-atmos*, *116*, ARTN D16307. doi:10.1029/2010JD014540

Castellanos, P., Stehr, J. W., Dickerson, R. R., & Ehrman, S. H. (2009). The sensitivity of modeled ozone to the temporal distribution of point, area, and mobile source emissions in the eastern United States. *Atmos Environ*, *43*(30), 4603-4611. doi:10.1016/j.atmosenv.2009.05.045

Chameides, W. L., Fehsenfeld, F., Rodgers, M. O., Cardelino, C., Martinez, J., Parrish, D., . . . Zimmerman, P. (1992). Ozone precursor relationships in the ambient atmosphere. *Journal of Geophysical Research: Atmospheres (1984–2012)*, *97*(D5), 6037-6055. Retrieved from http://onlinelibrary.wiley.com/doi/10.1029/91JD03014/full

Colella, P., & Woodward, P. R. (1984). The piecewise parabolic method (PPM) for gas-dynamical simulations. *J. Comput. Phys.*, *54*(1), 174-201.

Collet, S., Minoura, H., Kidokoro, T., Sonoda, Y., Kinugasa, Y., Karamchandani, P., . . . DenBleyker, A. (2014). Future year ozone source attribution modeling studies for the eastern and western United States. *J. Air Waste Manage. Assoc.*, *64*(10), 1174-1185. doi:10.1080/10962247.2014.936629

Collet, S., Minoura, H., Kidokoro, T., Sonoda, Y., Kinugasa, Y., & Karamchandani, P. (2014). Evaluation of light-duty vehicle mobile source regulations on ozone concentration trends in 2018 and 2030 in the western and eastern United States. *J. Air Waste Manage. Assoc.*, *64*(2), 175-183. doi:10.1080/10962247.2013.845621

Cooper, O. R., Gao, R. S., Tarasick, D., & Leblanc…, T. (2012). Long-term ozone trends at rural ozone monitoring sites across the United States, 1990 2010. *Journal of Geophysical …*. Retrieved from http://fallmeeting.agu.org/2012/files/2012/12/AGU_Fall_2012_Cooper_poster.pdf

Cooper, O. R., Parrish, D. D., Stohl, A., Trainer, M., Nedelec, P., Thouret, V., . . . Avery, M. A. (2010). Increasing springtime ozone mixing ratios in the free troposphere over western North America. *Nature*, *463*(7279), 344-348. doi:10.1038/nature08708

Crawford, J. H., Dickerson, R. R., & Hains, J. (2014). DISCOVER-AQ: Observations and early results. *Environmental Manager*, 8-15.

Crutzen, P. J. (1970), The influence of nitrogen oxides on the atmospheric ozone content, *Quart. J. Royal Meteo. Society*, *96*(408), 320-325.

Dacre, H. F., Gray, S. L., & Belcher, S. E. (2007). A case study of boundary layer ventilation by convection and coastal processes. *Journal of Geophysical Research*, *112*(D17), D17106. Retrieved from http://cree.rdg.ac.uk/~sws05hd/ventilation.pdf

Day, D. A., Dillon, M. B., Wooldridge, P. J., Thornton, J. A., Rosen, R. S., Wood, E. C., & Cohen, R. C. (2003). On alkyl nitrates, O-3, and the "missing NOy". *J Geophys Res-atmos*, *108*(D16), ARTN 4501. doi:10.1029/2003JD003685

Day, D. A., Wooldridge, P. J., Dillon, M. B., Thornton, J. A., & Cohen, R. C. (2002). A thermal dissociation laser-induced fluorescence instrument for in situ detection of NO2, peroxy nitrates, alkyl nitrates, and HNO3. *J Geophys Res-atmos*, *107*(D5-6), ARTN 4046. doi:10.1029/2001JD000779

Delany, A. C., Melchior, F. L., & Wartburg, A. F. (1982). Modification of a commerical NOx detector for high sensitivity. *Review of Scientific Instruments*, *53*(12), 1899-1902. Retrieved from http://ieeexplore.ieee.org/xpls/abs_all.jsp?arnumber=4984356

Derwent, R. G., Simmonds, P. G., Manning, A. J., & Spain, T. G. (2007). Trends over a 20-year period from 1987 to 2007 in surface ozone at the atmospheric research station, Mace Head, Ireland. *Atmos. Environ.*, *41*(39), 9091-9098. doi:10.1016/j.atmosenv.2007.08.008

Dolske, D. A. (1995). Deposition of atmospheric pollutants to monuments, statues, and buildings. *Sci. Total Environ.*, *167*, 15-31.

Dolwick, P., Akhtar, F., Baker, K. R., Possiel, N., Simon, H., & Tonnesen, G. (2015). Comparison of background ozone estimates over the western United States based on two separate model methodologies. *Atmos. Environ.*, *109*, 282-296. doi:10.1016/j.atmosenv.2015.01.005

Doraiswamy, P., Hogrefe, C., Hao, W., Henry, R. F., Civerolo, K., Ku, J.-Y., . . . Demerjian, K. L. (2009). A diagnostic comparison of measured and model-predicted speciated VOC concentrations. *Atmos. Environ.*, *43*(36), 5759-5770. doi:10.1016/j.atmosenv.2009.07.056

Draxler, R. R., & Rolph, G. D. (2003). HYSPLIT (HYbrid Single-Particle Lagrangian Integrated Trajectory) Model. NOAA Air Resources Laboratory, Silver Spring, MD. *J Access via NOAA ARL READY Website (http://www. arl. noaa. gov/ready/hysplit4. html)*.

Dye, T. S., Roberts, P. T., & Korc, M. E. (1995). Observations of transport processes for ozone and ozone precursors during the 1991 Lake Michigan Ozone Study. *Journal of applied meteorology*, *34*(8), 1877-1889. Retrieved from http://cat.inist.fr/?aModele=afficheN&cpsidt=3608003

Edwards, P. M., Brown, S. S., Roberts, J. M., & Ahmadov…, R. (2014). High winter ozone pollution from carbonyl photolysis in an oil and gas basin. *Nature*. Retrieved from http://www.nature.com/nature/journal/v514/n7522/abs/nature13767.html

Emery, C., Jung, J., Downey, N., Johnson, J., Jimenez, M., Yarvvood, G., & Morris, R. (2012). Regional and global modeling estimates of policy relevant background ozone over the United States. *Atmos. Environ.*, *47*, 206-217. doi:10.1016/j.atmosenv.2011.11.012

Emmons, L. K., Walters, S., Hess, P. G., Lamarque, J.-F., Pfister, G. G., Fillmore, D., . . . Laepple, T. (2010). Description and evaluation of the Model for Ozone and Related chemical Tracers, version 4 (MOZART-4). *Geoscientific Model Development*, *3*(1), 43-67. Retrieved from http://www.geosci-model-dev.net/3/43/2010/gmd-3-43-2010.pdf

ENVIRON. (2014). *CAMx Version 6.10 User's Guide*.

EPA. (1991). Highlights of the 1990 Clean Air Act Amendments. Retrieved October 2015, from http://www2.epa.gov/aboutepa/highlights-1990-clean-air-act-amendments

EPA. (2002). Approval and Promulgation of Implementation Plans: South Carolina: Nitrogen Oxides Budget and Allowance Trading Program. Retrieved from http://www.gpo.gov/fdsys/pkg/FR-2002-06-28/pdf/02-16270.pdf

EPA. (2008). National Ambient Air Quality Standards for Ozone. Retrieved October 2015, from http://www3.epa.gov/ttn/naaqs/standards/ozone/fr/20080327.pdf

EPA. (2010). Designation of North American Emission Control Area to reduce emissions from ships. Retrieved from http://www.epa.gov/otaq/regs/nonroad/marine/ci/420f10015.htm

EPA. (2013a). National Ambient Air Quality Standards for Particulate Matter; Final Rule. Retrieved October 2015, from http://www.gpo.gov/fdsys/pkg/FR-2013-01-15/pdf/2012-30946.pdf
EPA. (2013b). Documentation for EPA Base Case v5.13 using the Integrated Planning Model. Retrieved December 2015, from http://www.epa.gov/sites/production/files/2015-07/documents/documentation_for_epa_base_case_v.5.13_using_the_integrated_planning_model.pdf
EPA. (2014a). Air Quality Designations for the 2008 Ozone National Ambient Air Quality Standards. Retrieved from http://www.epa.gov/oaqps001/greenbk/hindex.html
EPA. (2014b). Draft Modeling Guidance for Demonstrating Attainment of Air Quality Goals for Ozone, PM2.5, and Regional Haze. Retrieved January 2015, from http://www3.epa.gov/ttn/scram/guidance/guide/Draft_O3-PM-RH_Modeling_Guidance-2014.pdf
EPA. (2014c). Identification of Nonattainment Classification and Deadlines for Submission of State Implementation Plan (SIP) Provisions for the 1997 Fine Particle (PM2.5) National Ambient Air Quality Standard (NAAQS) and 2006 PM2.5 NAAQS; Final Rule. Retrieved October 2015, from http://www.gpo.gov/fdsys/pkg/FR-2014-06-02/pdf/2014-10395.pdf
EPA. (2014d). Meteorology Technical Support Document - Meteorological Model Performance for Annual 2011 WRF v3.4 Simulation. Retrieved from http://www.epa.gov/ttn/scram/reports/MET_TSD_2011_final_11-26-14.pdf
EPA. (2014e). Technical Support Document (TSD) Preparation of Emissions Inventories for the Version 6.0, 2011 Emissions Modeling Platform.
EPA. (2015a). National Ambient Air Quality Standards for Ozone. Retrieved October 2015, from http://www3.epa.gov/airquality/ozonepollution/pdfs/20151001fr.pdf
EPA. (2015b). Ozone Design Values. Retrieved October 2015, from http://www3.epa.gov/airtrends/values.html
EPA. (2015c). Cross-State Air Pollution Rule (CSAPR). Retrieved October 2015, from http://www3.epa.gov/crossstaterule/basic.html
EPA. (2015d). Air Quality Modeling Technical Support Document for the 2008 Ozone NAAQS Transport Assessment. Retrieved October 2015 from http://www.epa.gov/airtransport/O3TransportAQModelingTSD.pdf
Evans, M. J., & Jacob, D. J. (2005). Impact of new laboratory studies of N2O5 hydrolysis on global model budgets of tropospheric nitrogen oxides, ozone, and OH. *Geophysical Research Letters*, *32*(9). Retrieved from http://dash.harvard.edu/bitstream/handle/1/3988779/Jacob_NewLaboratory.pdf?sequence=1
Eyring, V., Köhler, H. W., Van Aardenne, J., & Lauer, A. (2005). Emissions from international shipping: 1. The last 50 years. *Journal of Geophysical Research: Atmospheres (1984–2012)*, *110*(D17). Retrieved from http://www.agu.org/journals/jd/jd0517/2004JD005619/2004jd005619-t04.txt
Fann, N., Lamson, A. D., Anenberg, S. C., Wesson, K., Risley, D., & Hubbell, B. J. (2011). Estimating the national public health burden associated with exposure to

ambient PM2. 5 and ozone. *Risk Analysis*, *32*(1), 81-95. Retrieved from http://www.scientificintegrityinstitute.org/Fann010112.pdf

Farmer, D. K., Wooldridge, P. J., & Cohen, R. C. (2006). Application of thermal-dissociation laser induced fluorescence (TD-LIF) to measurement of HNO3, Sigma alkyl nitrates, Sigma peroxy nitrates, and NO2 fluxes using eddy covariance. *Atmos Chem Phys*, *6*, 3471-3486.

Farmer, D. K., Perring, A. E., Wooldridge, P. J., Blake, D. R., Baker, A., Meinardi, S., . . . Cohen, R. C. (2011). Impact of organic nitrates on urban ozone production. *Atmos Chem Phys*, *11*(9), 4085-4094. doi:10.5194/acp-11-4085-2011

Fehsenfeld, F. C., Dickerson, R. R., Hubler, G., Luke, W. T., Nunnermacker, L. J., Williams, E. J., . . . Delany, A. C. (1987). A ground-based intercomparison of NO, NOx, and NOy measurement techniques. *JGR. Journal of geophysical research. Part D, Atmospheres*, *92*(12), 710-722. Retrieved from http://cat.inist.fr/?aModele=afficheN&cpsidt=7550774

Ferreira, J., Rodriguez, A., Monteiro, A., Miranda I, A., Dios, M., Souto, J. A., . . . Borrego, C. (2011). Air quality simulations for North America-MM5-CAMx modelling performance for main gaseous pollutants. *Atmospheric Environment*. Retrieved from http://www.sciencedirect.com/science/article/pii/S135223101101079X

Finley, B. D., & Saltzman, E. S. (2006). Measurement of Cl2 in coastal urban air. *Geophysical research letters*, *33*(11), L11809. Retrieved from http://www.ess.uci.edu/researchgrp/esaltzman/files/FinleySaltzmanGRL06.pdf

Fiore, A. M., Oberman, J. T., Lin, M. Y., Zhang, L., Clifton, O. E., Jacob, D. J., . . . Milly, G. P. (2014). Estimating North American background ozone in U.S. surface air with two independent global models: Variability, uncertainties, and recommendations. *Atmos. Environ.*, *96*, 284-300. doi:10.1016/j.atmosenv.2014.07.045

Fiore, A. M., Jacob, D. J., Logan, J. A., & Yin, J. H. (1998). Long-term trends in ground level ozone over the contiguous United States, 1980-1995. *J. Geophys. Res.-Atmos.*, *103*(D1), 1471-1480.

Foley, K. M., Hogrefe, C., Pouliot, G., Possiel, N., Roselle, S. J., Simon, H., & Timin, B. (2015a). Dynamic evaluation of CMAQ part I: Separating the effects of changing emissions and changing meteorology on ozone levels between 2002 and 2005 in the eastern US. *Atmos. Environ.*, *103*, 247-255. doi:10.1016/j.atmosenv.2014.12.038

Foley, K. M., Dolwick, P., Hogrefe, C., Simon, H., Timin, B., & Possiel, N. (2015b). Dynamic evaluation of CMAQ part II: Evaluation of relative response factor metrics for ozone attainment demonstrations. *Atmos. Environ.*, *103*, 188-195. doi:10.1016/j.atmosenv.2014.12.039

Fowler, D., Flechard, C., Cape, J. N., Storeton-West, R. L., & Coyle, M. (2001). Measurements of ozone deposition to vegetation quantifying the flux, the stomatal and non-stomatal components. *Water, Air, and Soil Pollution*, *130*(1-4), 63-74. Retrieved from http://link.springer.com/article/10.1023/A:1012243317471

Franklin, M., Zeka, A., & Schwartz, J. (2007). Association between PM2. 5 and all-cause and specific-cause mortality in 27 US communities. *Journal of Exposure Science and Environmental Epidemiology*, *17*(3), 279-287. Retrieved from http://www.calcontrk.org/CARBdocs/JESEE_2005.pdf

Frost, G. J., McKeen, S. A., Trainer, M., Ryerson, T. B., Neuman, J. A., Roberts, J. M., . . . Habermann, T. (2006). Effects of changing power plant NOx emissions on ozone in the eastern United States: Proof of concept. *J. Geophys. Res.-Atmos.*, *111*(D12). doi:10.1029/2005JD006354

Fujita, E. M., Campbell, D. E., Zielinska, B., Chow, J. C., Lindhjem, C. E., DenBleyker, A., . . . Lawson, D. R. (2012). Comparison of the MOVES2010a, MOBILE6. 2, and EMFAC2007 mobile source emission models with on-road traffic tunnel and remote sensing measurements. *Journal of the Air & Waste Management Association*, *62*(10), 1134-1149. Retrieved from http://www.feat.biochem.du.edu/assets/publications/Van_Nuys_tunnel_study_JAWMA_2012.pdf

Gallagher, M. W., Beswick, K. M., & Coe, H. (2001). Ozone deposition to coastal waters. *Quarterly Journal of the Royal Meteorological Society*, *127*(572), 539-558. Retrieved from http://onlinelibrary.wiley.com/doi/10.1002/qj.49712757215/abstract

Gego, E., Gilliland, A., Godowitch, J., Rao, S. T., Porter, P. S., & Hogrefe, C. (2008). Modeling analyses of the effects of changes in nitrogen oxides emissions from the electric power sector on ozone levels in the eastern United States. *J. Air Waste Manage. Assoc.*, *58*(4), 580-588. Retrieved from http://dx.doi.org/10.3155/1047-3289.58.4.580

Gilliland, A. B., Hogrefe, C., Pinder, R. W., Godowitch, J. M., Foley, K. L., & Rao, S. T. (2008). Dynamic evaluation of regional air quality models: assessing changes in O 3 stemming from changes in emissions and meteorology. *Atmospheric Environment*, *42*(20), 5110-5123.

Godowitch, J. M., Hogrefe, C., & Rao, S. T. (2008). Diagnostic analyses of a regional air quality model: Changes in modeled processes affecting ozone and chemical-transport indicators from NO_X point source emission reductions. *Journal of Geophysical Research: Atmospheres (1984–2012)*, *113*(D19).

Godowitch, J. M., Pouliot, G. A., & Rao, S. T. (2010). Assessing multi-year changes in modeled and observed urban NO_X concentrations from a dynamic model evaluation perspective. *Atmospheric Environment*, *44*(24), 2894-2901.

Goldberg, D. L., Vinciguerra, T. P., Hosley, K. M., Loughner, C. P., Canty, T. P., Salawitch, R. J., & Dickerson, R. R. (2015). Evidence for an increase in the ozone photochemical lifetime in the eastern United States using a regional air quality model. *Journal of Geophysical Research: Atmospheres*, doi: 10.1002/2015JD023930

Goldberg, D. L., Loughner, C. P., Tzortziou, M., Stehr, J. W., Pickering, K. E., Marufu, L. T., & Dickerson, R. R. (2014). Higher surface ozone concentrations over the Chesapeake Bay than over the adjacent land: Observations and models from the DISCOVER-AQ and CBODAQ campaigns. *Atmospheric Environment*, *84*, 9-19. Retrieved from http://www.atmos.umd.edu/~dgoldb/Goldberg_et_al_2014.pdf

Gratz, L. E., Jaffe, D. A., & Hee, J. R. (2015). Causes of increasing ozone and decreasing carbon monoxide in springtime at the Mt. Bachelor Observatory from 2004 to 2013. *Atmos. Environ.*, *109*, 323-330. doi:10.1016/j.atmosenv.2014.05.076

Grell, G. A., Knoche, R., Peckham, S. E., & McKeen, S. A. (2004). Online versus offline air quality modeling on cloud-resolving scales. *Geophysical research letters*, *31*(16). Retrieved from http://onlinelibrary.wiley.com/doi/10.1029/2004GL020175/full

Guenther, A. B., Jiang, X., Heald, C. L., Sakulyanontvittaya, T., Duhl, T., Emmons, L. K., & Wang, X. (2012). The Model of Emissions of Gases and Aerosols from Nature version 2.1 (MEGAN2.1): an extended and updated framework for modeling biogenic emissions. *Geosci. Model Dev.*, *5*(6), 1471-1492. doi:10.5194/gmd-5-1471-2012

Hair, J. W., Hostetler, C. A., Cook, A. L., Harper, D. B., Ferrare, R. A., Mack, T. L., . . . Hovis, F. E. (2008). Airborne high spectral resolution lidar for profiling aerosol optical properties. *Applied Optics*, *47*(36), 6734-6752. Retrieved from http://www.patarnott.com/atms360/pdf_atms360/LidarMexicoCity.pdf

He, H., Stehr, J. W., Hains, J. C., Krask, D. J., Doddridge, B. G., Vinnikov, K. Y., . . . Worden, H. M. (2013a). Trends in emissions and concentrations of air pollutants in the lower troposphere in the Baltimore/Washington airshed from 1997 to 2011. *Atmospheric Chemistry and Physics Discussions*, *13*(2), 3135-3178. Retrieved from http://www.atmos-chem-phys-discuss.net/13/3135/2013/acpd-13-3135-2013.pdf

He, H., Hembeck, L., Hosley, K. M., Canty, T. P., Salawitch, R. J., & Dickerson, R. R. (2013b). High ozone concentrations on hot days: The role of electric power demand and NOx emissions. *Geophys. Res. Lett.*, *40*(19), 5291-5294. doi:10.1002/grl.50967

He, H., Loughner, C. P., Stehr, J. W., Arkinson, H. L., Brent, L. C., Follette-Cook, M. B., . . . Martins, D. K. (2014). An elevated reservoir of air pollutants over the Mid-Atlantic States during the 2011 DISCOVER-AQ campaign: Airborne measurements and numerical simulations. *Atmospheric Environment*, *85*, 18-30. Retrieved from http://www.atmos.umd.edu/~russ/he_etal_reservoir_2014.pdf

Henderson, B. H., Akhtar, F., Pye, H. O. T., Napelenok, S. L., & Hutzell, W. T. (2014). A database and tool for boundary conditions for regional air quality modeling: description and evaluation. *Geoscientific Model Development*, *7*(1), 339-360. Retrieved from http://www.geosci-model-dev.net/7/339/2014/gmd-7-339-2014.pdf

Hildebrandt-Ruiz, L., & Yarwood, G. (2013). *Interactions between organic aersol and NOy: influence on oxidant production*.

Hintsa, E. J., Allsup, G. P., Eck, C. F., Hosom, D. S., Purcell, M. J., Roberts, A. A., . . . Mulhall, P. A. (2004). New Ozone Measurement Systems for Autonomous Operation on Ocean Buoys and Towers. *Journal of Atmospheric and Oceanic Technology*, *21*(7), 1007-1016. Retrieved from http://journals.ametsoc.org/doi/abs/10.1175/1520-0426(2004)021<1007:NOMSFA>2.0.CO;2

Hogrefe, C., Biswas, J., Lynn, B., Civerolo, K., Ku, J. Y., Rosenthal, J., . . . Kinney, P. L. (2004). Simulating regional-scale ozone climatology over the eastern United States: model evaluation results. *Atmos. Environ.*, *38*(17), 2627-2638. doi:10.1016/j.atmosenv.2004.02.033

Horowitz, L. W., Fiore, A. M., Milly, G. P., Cohen, R. C., Perring, A., Wooldridge, P. J., . . . Lamarque, J. F. (2007). Observational constraints on the chemistry of isoprene nitrates over the eastern United States. *J Geophys Res-atmos*, *112*(D12), ARTN D12S08. doi:10.1029/2006JD007747

Houyoux, M. R., & Vukovich, J. M. (1999). Updates to the Sparse Matrix Operator Kernel Emissions (SMOKE) modeling system and integration with Models-3. *The Emission Inventory: Regional Strategies for the Future*, *1461*. Retrieved from

http://citeseerx.ist.psu.edu/viewdoc/download?doi=10.1.1.41.5939&rep=rep1&type=pdf

Hudman, R. C., Moore, N. E., Mebust, A. K., Martin, R. V., Russell, A. R., Valin, L. C., & Cohen, R. C. (2012). Steps towards a mechanistic model of global soil nitric oxide emissions: implementation and space based-constraints. *Atmospheric Chemistry and Physics*, *12*(16), 7779-7795. Retrieved from http://www.atmos-chem-phys.net/12/7779/2012/acp-12-7779-2012.pdf

Jacob, D. J. (2000). Heterogeneous chemistry and tropospheric ozone. *Atmospheric Environment*, *34*(12), 2131-2159. Retrieved from http://www.cee.mtu.edu/~reh/papers/pubs/non_Honrath/jacob00.pdf

Jacob, D. J., Logan, J. A., & Murti, P. P. (1999). Effect of rising Asian emissions on surface ozone in the United States. *Geophys. Res. Lett.*, *26*(14), 2175-2178.

Jaffe, D., & Ray, J. (2007). Increase in surface ozone at rural sites in the western US. *Atmospheric Environment*, *41*(26), 5452-5463. Retrieved from http://www.atmos.washington.edu/jaffegroup/publications/Jaffe_2007_O3trends.pdf

Jerrett, M., Burnett, R. T., Pope III, C. A., Ito, K., Thurston, G., Krewski, D., . . . Thun, M. (2009). Long-term ozone exposure and mortality. *New England Journal of Medicine*, *360*(11), 1085-1095. Retrieved from http://www.nejm.org/doi/full/10.1056/nejmoa0803894

Kaimal, J. C., & Finnigan, J. J. (1994). *Atmospheric boundary layer flows: their structure and measurement*. Oxford University Press.

Kinosian, J. R. (1982). Ozone precursor relationships from EKMA diagrams. *Environ. Sci. Technol.*, *16*(12), 880-883.

Kleinman, L. I., Daum, P. H., Imre, D. G., Lee, J. H., Lee, Y.-N., Nunnermacker, L. J., . . . Newman, L. (2000). Ozone production in the New York City urban plume. *Journal of Geophysical Research*, *105*(D11), 14495-14,511. Retrieved from http://www.ecd.bnl.gov/pubs/BNL66342.pdf

Koo, B., Kumar, N., Knipping, E., Nopmongcol, U., Sakulyanontvittaya, T., Odman, M. T., . . . Yarwood, G. (2015). Chemical transport model consistency in simulating regulatory outcomes and the relationship to model performance. *Atmos. Environ.*, *116*, 159-171. doi:10.1016/j.atmosenv.2015.06.036

Kota, S. H., Schade, G., Estes, M., Boyer, D., & Ying, Q. (2015). Evaluation of MEGAN predicted biogenic isoprene emissions at urban locations in Southeast Texas. *Atmos. Environ.*, *110*, 54-64. doi:10.1016/j.atmosenv.2015.03.027

Kota, S. H., Ying, Q., & Schade, G. W. (2012). *MOVES vs. MOBILE6. 2: Differences in Emission Factors and Regional Air Quality Predictions*. Paper presented at Transportation Research Board 91st Annual Meeting, Washington DC, January 22–26, 2012, paper 12-4438.

Lamarque, J. F., Hess, P., Emmons, L., Buja, L., Washington, W., & Granier, C. (2005). Tropospheric ozone evolution between 1890 and 1990. *J. Geophys. Res.-Atmos.*, *110*(D8). doi:10.1029/2004JD005537

Langford, A. O., Brioude, J., Cooper, O. R., Senff, C. J., Alvarez, R. J., II, Hardesty, R. M., . . . Oltmans, S. J. (2012). Stratospheric influence on surface ozone in the Los Angeles area during late spring and early summer of 2010. *J. Geophys. Res.-Atmos.*, *117*. doi:10.1029/2011JD016766

Lefohn, A. S., Emery, C., Shadwick, D., Wernli, H., Jung, J., & Oltmans, S. J. (2014). Estimates of background surface ozone concentrations in the United States based on model-derived source apportionment. *Atmos. Environ.*, *84*, 275-288. doi:10.1016/j.atmosenv.2013.11.033

Lehmann, C. M. B., Bowersox, V. C., & Larson, S. M. (2005). Spatial and temporal trends of precipitation chemistry in the United States, 1985-2002. *Environ. Pollut.*, *135*(3), 347-361. doi:10.1016/j.envpol.2004.11.016

Levelt, P. F., Van den Oord, G. H. J., Dobber, M. R., Malkki, A., Visser, H., de Vries, J., . . . Saari, H. (2006). The Ozone Monitoring Instrument. *IEEE Trans. Geosci. Remote Sensing*, *44*(5), 1093-1101. doi:10.1109/TGRS.2006.872333

Levy, I., Makar, P. A., Sills, D., Zhang, J., Hayden, K. L., Mihele, C., . . . Brook, J. (2010). Unraveling the complex local-scale flows influencing ozone patterns in the southern Great Lakes of North America. *Atmospheric Chemistry and Physics*, *10*(22), 10895-10915. Retrieved from http://www.atmos-chem-phys.net/10/10895/2010/acp-10-10895-2010.pdf

Li, X., & Rappenglück, B. (2014). A WRF–CMAQ study on spring time vertical ozone structure in Southeast Texas. *Atmospheric Environment*. Retrieved from http://www.sciencedirect.com/science/article/pii/S135223101400630X

Lin, C. Y. C., Jacob, D. J., & Fiore, A. M. (2001). Trends in exceedances of the ozone air quality standard in the continental United States, 1980-1998. *Atmos. Environ.*, *35*(19), 3217-3228.

Lin, C. Y. C., Jacob, D. J., Munger, J. W., & Fiore, A. M. (2000). Increasing background ozone in surface air over the United States. *Geophys. Res. Lett.*, *27*(21), 3465-3468.

Lin, M., Fiore, A. M., Horowitz, L. W., Cooper, O. R., Naik, V., Holloway, J., . . . Pollack, I. B. (2012). Transport of Asian ozone pollution into surface air over the western United States in spring. *Journal of Geophysical Research*, *117*(null), D00V07. Retrieved from http://www.ldeo.columbia.edu/~amfiore/publications/lin2011.pdf

Lin, M., Fiore, A. M., Cooper, O. R., Horowitz, L. W., Langford, A. O., Levy, H., II, . . . Senff, C. J. (2012). Springtime high surface ozone events over the western United States: Quantifying the role of stratospheric intrusions. *J. Geophys. Res.-Atmos.*, *117*. doi:10.1029/2012JD018151

Liu, S. C., & Trainer, M. (1988). Responses of the tropospheric ozone and odd hydrogen radicals to column ozone change. *Journal of Atmospheric Chemistry*, *6*(3), 221-233. Retrieved from http://link.springer.com/article/10.1007/BF00053857

Loughner, C. P., Allen, D. J., Pickering, K. E., Zhang, D. L., Shou, Y. X., & Dickerson, R. R. (2011). Impact of fair-weather cumulus clouds and the Chesapeake Bay breeze on pollutant transport and transformation. *Atmos Environ*, *45*(24), 4060-4072. doi:10.1016/j.atmosenv.2011.04.003

Loughner, C. P., Tzortziou, M., Follette-Cook, M., Pickering, K. E., Goldberg, D., Satam, C., . . . Montzka, D. D. (2014). Impact of bay breeze circulations on surface air quality and boundary layer export. *Journal of Applied Meteorology and Climatology*, 2014). Retrieved from http://journals.ametsoc.org/doi/abs/10.1175/JAMC-D-13-0323.1

Loughner, C. P., Duncan, B., & Hains, J. (2014). The Benefit of Historical Air Pollution Emissions Reductions during Extreme Heat. *Environmental Manager*, 34-38.

Luke, W. T., Dickerson, R. R., & Nunnermacker, L. J. (1989). Direct measurements of the photolysis rate coefficients and Henry's law constants of several alkyl nitrates. *Journal of Geophysical Research*, *94*(D12), 14905-14,921. Retrieved from http://www.agu.org/pubs/crossref/1989/JD094iD12p14905.shtml

Luria, M., Boatman, J. F., Wellman, D. L., Gunter, R. L., Watkins, B. A., Wilkison, S. W., & Van Valin, C. C. (1992). Lake Michigan ozone study (LMOS): Measurements from an instrumented aircraft. *Atmospheric Environment. Part A. General Topics*, *26*(18), 3265-3277. Retrieved from http://www.sciencedirect.com/science/article/pii/096016869290342I

MARAMA. (2013). ERTAC EGU Forecasting Tool Documentation. Retrieved December 2015, from http://www.marama.org/2013-ertac-egu-forecasting-tool-documentation

Martinez, M., Harder, H., Kovacs, T. A., Simpas, J. B., Bassis, J., Lesher, R., . . . Zamora, R. J. (2003). OH and HO2 concentrations, sources, and loss rates during the Southern Oxidants Study in Nashville, Tennessee, summer 1999. *J. Geophys. Res.-Atmos.*, *108*(D19). doi:10.1029/2003JD003551

Mason, R., Dolwick, P., Carey, P., Kinnee, E., & Wilson, M. (2008). *Emissions Processing and Sensitivity Air Quality Modeling of Category 3 Commercial Marine Vessel Emissions*. Proceedings from 17th Annual International Emission Inventory Conference, Portland, OR.

McConnell, R., Berhane, K., Gilliland, F., London, S. J., Islam, T., Gauderman, W. J., . . . Peters, J. M. (2002). Asthma in exercising children exposed to ozone: a cohort study. *The Lancet*, *359*(9304), 386-391. Retrieved from http://www.coep.pharmacy.arizona.edu/HOPE/andrea/McConnell and ozone.pdf

Mickley, L. J., Jacob, D. J., & Rind, D. (2001). Uncertainty in preindustrial abundance of tropospheric ozone: Implications for radiative forcing calculations. *J. Geophys. Res.-Atmos.*, *106*(D4), 3389-3399.

Morris, R. E., Yarwood, G., Emery, C. A., & Koo, B. (2004). *Development and application of the CAMx regional one-atmospheric model to treat ozone, particulate matter, visibility, air toxics and mercury*.

Neu, J. L., Lawler, M. J., Prather, M. J., & Saltzman, E. S. (2008). Oceanic alkyl nitrates as a natural source of tropospheric ozone. *Geophys Res Lett*, *35*(13), ARTN L13814. doi:10.1029/2008GL034189

Neuman, J. A., Nowak, J. B., Zheng, W., Flocke, F., Ryerson, T. B., Trainer, M., . . . Peischl, J. (2009). Relationship between photochemical ozone production and NOx oxidation in Houston, Texas. *Journal of Geophysical Research: Atmospheres (1984–2012)*, *114*(D7). Retrieved from http://onlinelibrary.wiley.com/doi/10.1029/2008JD011688/full

Nopmongcol, U., Emery, C., Sakulyanontvittaya, T., Jung, J., Knipping, E., & Yarwood, G. (2014). A modeling analysis of alternative primary and secondary US ozone standards in urban and rural areas. *Atmos. Environ.*, *99*, 266-276. doi:10.1016/j.atmosenv.2014.09.062

Nopmongcol, U., Koo, B., Tai, E., Jung, J., Piyachaturawat, P., Emery, C., . . . Kallos, G. (2012). Modeling Europe with CAMx for the air quality model evaluation international initiative (AQMEII). *Atmospheric Environment*, *53*, 177-185. Retrieved from http://www.mg.uoa.gr/Publications/102_Nop_AQMEII_Atm_Env_2012.pdf

Nowak, D. J., Crane, D. E., & Stevens, J. C. (2006). Air pollution removal by urban trees and shrubs in the United States. *Urban forestry & urban greening*, *4*(3), 115-123. Retrieved from http://www.fs.fed.us/ne/newtown_square/publications/other_publishers/ne_2006_nowak001p.pdf

O'Brien, J. J. (1970). A note on the vertical structure of the eddy exchange coefficient in the planetary boundary layer. *Journal of the Atmospheric Sciences*, *27*(8), 1213-1215. Retrieved from http://journals.ametsoc.org/doi/abs/10.1175/1520-0469(1970)027<1213:ANOTVS>2.0.CO;2

Oltmans, S. J. (1981). Surface ozone measurements in clean air. *Journal of Geophysical Research: Oceans (1978 2012)*, *86*(C2), 1174-1180. doi:10.1029/JC086iC02p01174

Oltmans, S. J., Karion, A., Schnell, R. C., Pétron, G., Sweeney, C., Wolter, S., . . . Helmig, D. (2014). A high ozone episode in winter 2013 in the Uinta Basin oil and gas region characterized by aircraft measurements. *Atmospheric Chemistry and Physics Discussions*, *14*(14), 20117-20157. Retrieved from http://www.atmos-chem-phys-discuss.net/14/20117/2014/acpd-14-20117-2014.html

Oltmans, S. J., Lefohn, A. S., Harris, J. M., Galbally, I., Scheel, H. E., Bodeker, G., . . . Johnson, B. J. (2006). Long-term changes in tropospheric ozone. *Atmospheric Environment*, *40*(17), 3156-3173. Retrieved from http://www.earthsystemsciences.com/papers/Oltmans_2006a.pdf

Oltmans, S. J., Lefohn, A. S., Shadwick, D., Harris, J. M., Scheel, H. E., Galbally, I., . . . Claude, H. (2013). Recent tropospheric ozone changes–A pattern dominated by slow or no growth. *Atmospheric Environment*, *67*, 331-351. Retrieved from http://www.sciencedirect.com/science/article/pii/S1352231012010394

Otte, T. L., & Pleim, J. E. (2010). The Meteorology-Chemistry Interface Processor (MCIP) for the CMAQ modeling system: updates through MCIPv3. 4.1. *Geoscientific Model Development*, *3*(1), 243-256. Retrieved from http://www.geosci-model-dev.net/3/243/2010/gmd-3-243-2010.pdf

Paoletti, E., & Manning, W. J. (2007). Toward a biologically significant and usable standard for ozone that will also protect plants. *Environ. Pollut.*, *150*(1), 85-95. doi:10.1016/j.envpol.2007.06.037

Parrish, D. D., Millet, D. B., & Goldstein, A. H. (2009). Increasing ozone in marine boundary layer inflow at the west coasts of North America and Europe. *Atmospheric Chemistry and Physics*, *9*(4), 1303-1323. Retrieved from http://www.atmos-chem-phys.net/9/1303/2009/acp-9-1303-2009.pdf

Perring, A. E., Bertram, T. H., Wooldridge, P. J., Fried, A., Heikes, B. G., Dibb, J., . . . Blake, D. R. (2009). Airborne observations of total RONO2: new constraints on the yield and lifetime of isoprene nitrates. *Atmos. Chem. Phys*, *9*, 1451-1463. Retrieved from http://atmos-chem-phys.net/9/1451/2009/acp-9-1451-2009.pdf

Perring, A. E., Bertram, T. H., Farmer, D. K., Wooldridge, P. J., Dibb, J., Blake, N. J., . . . Cohen, R. C. (2010). The production and persistence of Sigma RONO2 in the Mexico City plume. *Atmos Chem Phys*, *10*(15), 7215-7229. doi:10.5194/acp-10-7215-2010

Perring, A. E., Pusede, S. E., & Cohen, R. C. (2013). An observational perspective on the atmospheric impacts of alkyl and multifunctional nitrates on ozone and secondary

organic aerosol. *Chemical reviews*. Retrieved from http://pubs.acs.org/doi/abs/10.1021/cr300520x

Pouliot, G., & Pierce, T. E. (2009). *Integration of the Model of Emissions of Gases and Aerosols from Nature (MEGAN) into the CMAQ Modeling System*. Presented at the 18th International Emission Inventory Conference, Baltimore, MD, 2009.

Rao, S. T., Ku, J. Y., Berman, S., Zhang, K., & Mao, H. (2003). Summertime characteristics of the atmospheric boundary layer and relationships to ozone levels over the eastern United States. *Pure and Applied Geophysics*, *160*(1), 21-55. Retrieved from http://www.springerlink.com/index/1FCX7C28C40WKLC6.pdf

Rappenglück, B., Ackermann, L., Alvarez, S., Golovko, J., Buhr, M., Field, R. A., . . . Keslar, C. (2014). Strong wintertime ozone events in the Upper Green River basin, Wyoming. *Atmos. Chem. Phys.*, *14*(10), 4909-4934. Retrieved from http://dx.doi.org/10.5194/acp-14-4909-2014

Rasmussen, R. A. (1972). What do the hydrocarbons from trees contribute to air pollution. *Journal of the Air Pollution Control Association*, *22*(7), 537-543.

Ridley, B. A., Madronich, S., Chatfield, R. B., Walega, J. G., Shetter, R. E., Carroll, M. A., & Montzka, D. D. (1992). Measurements and model simulations of the photostationary state during the Mauna Loa Observatory Photochemistry Experiment: Implications for radical concentrations and ozone production and loss rates. *Journal of Geophysical Research: Atmospheres*, *97*(D10), 10375-10388. doi:10.1029/91JD02287

Rosen, R. S., Wood, E. C., Wooldridge, P. J., Thornton, J. A., Day, D. A., Kuster, W., . . . Cohen, R. C. (2004). Observations of total alkyl nitrates during Texas Air Quality Study 2000: Implications for O-3 and alkyl nitrate photochemistry. *J Geophys Res-atmos*, *109*(D7), ARTN D07303. doi:10.1029/2003JD004227

Ryan, W. F., Doddridge, B. G., Dickerson, R. R., Morales, R. M., Hallock, K. A., Roberts, P. T., . . . Civerolo, K. L. (1998). Pollutant transport during a regional O3 episode in the mid-Atlantic states. *Journal of the Air & Waste Management Association*, *48*(9), 786-797. Retrieved from http://pubs.awma.org/gsearch/journal/1998/9/ryan.pdf

Samoli, E., Aga, E., Touloumi, G., Nislotis, K., Forsberg, B., Lefranc, A., . . . Katsouyanni, K. (2006). Short-term effects of nitrogen dioxide on mortality: an analysis within the APHEA project. *Eur. Resp. J.*, *27*(6), 1129-1137. doi:10.1183/09031936.06.00143905

Sander, S.P., Friedl, R. R., Golden, D. M. , Kurylo, M. J., Moortgat, G. K., Wine, P. H., … Orkin V. L. (2006). Chemical Kinetics and Photochemical Data for use in Atmospheric Studies, Evaluation Number 15. NASA Jet Propulsion Laboratory. [Available online at http://jpldataeval.jpl.nasa.gov/download.html]

Sandermann, H. (1996). Ozone and plant health. *Annu. Rev. Phytopathol.*, *34*, 347-366.

Scarino, A. J., Obland, M. D., & Fast…, J. D. (2013). Comparison of mixed layer heights from airborne high spectral resolution lidar, ground-based measurements, and the WRF-Chem model during CalNex and CARES. *Atmospheric …*. Retrieved from http://www.atmos-chem-phys-discuss.net/13/13721/2013/acpd-13-13721-2013.pdf

Schnell, R. C., Oltmans, S. J., Neely, R. R., Endres, M. S., Molenar, J. V., & White, A. B. (2009). Rapid photochemical production of ozone at high concentrations in a rural site during winter. *Nat. Geosci.*, *2*(2), 120-122. doi:10.1038/NGEO415

Seinfeld, J. H., & Pandis, S. N. (2006). *Atmospheric Chemistry and Physics - From Air Pollution to Climate Change* (2nd ed.). John Wiley & Sons.
Shetter, R. E., Junkermann, W., Swartz, W. H., Frost, G. J., Crawford, J. H., Lefer, B. L., . . . Bais, A. (2003). Photolysis frequency of NO2: measurement and modeling during the International Photolysis Frequency Measurement and Modeling Intercomparison (IPMMI). *Journal of Geophysical Research: Atmospheres (1984–2012)*, *108*(D16). Retrieved from http://acd.ucar.edu/~cantrell/2002JD002932.pdf
Sickles, J. E., II, & Shadwick, D. S. (2015). Air quality and atmospheric deposition in the eastern US: 20 years of change. *Atmos. Chem. Phys.*, *15*(1), 173-197. doi:10.5194/acp-15-173-2015
Sillman, S. (1995). The use of NOy, H2O2, and HNO3 as indicators for ozone-NOx-hydrocarbon sensitivity in urban locations. *Journal of Geophysical Research*, *100*(D7), 14,175-14,188. Retrieved from http://www-personal.umich.edu/~sillman/web-publications/SillmanIndicators95.pdf
Sillman, S. (1999). The relation between ozone, NOx and hydrocarbons in urban and polluted rural environments. *Atmospheric Environment*, *33*(12), 1821-1846. Retrieved from http://www-personal.umich.edu/~sillman/web-publications/Sillmanreview99.pdf
Simon, H., Baker, K. R., & Phillips, S. (2012). Compilation and interpretation of photochemical model performance statistics published between 2006 and 2012. *Atmos. Environ.*, *61*, 124-139. doi:10.1016/j.atmosenv.2012.07.012
Simon, H., Reff, A., Wells, B., Xing, J., & Frank, N. (2015). Ozone Trends Across the United States over a Period of Decreasing NOx and VOC Emissions. *Environ. Sci. Technol.*, *49*(1), 186-195. doi:10.1021/es504514z
Skamarock, W. C., Klemp, J. B., Dudhia, J., Gill, D. O., Barker, D. M., Wang, W., & Powers, J. G. (2008). A description of the advanced WRF version 3. *NCAR technical note NCAR/TN/u2013475+ STR*.
Solazzo, E., Bianconi, R., Pirovano, G., Moran, M. D., Vautard, R., Hogrefe, C., . . . Galmarini, S. (2013). Evaluating the capability of regional-scale air quality models to capture the vertical distribution of pollutants. *Geosci. Model Dev.*, *6*(3), 791-818. doi:10.5194/gmd-6-791-2013
SourceWatch. (2010). Clean Air Interstate Rule. Retrieved from http://www.sourcewatch.org/index.php/Clean_Air_Interstate_Rule
Stammer, D., Wentz, F., & Gentemann, C. (2003). Validation of microwave sea surface temperature measurements for climate purposes. *J. Clim.*, *16*(1), 73-87.
Stauffer, R. M., Thompson, A. M., Martins, D. K., Clark, R. D., Goldberg, DL, Loughner, C. P., . . . Tzortziou, M. A. (2012). Bay breeze influence on surface ozone at Edgewood, MD during July 2011. *Journal of Atmospheric CHemistry*. Retrieved from http://www.springerlink.com/index/QN2HN365671270MJ.pdf
Stauffer, R. M., and A. M. Thompson (2013), Bay Breeze climatology at two sites along the Chesapeake bay from 1986–2010: Implications for surface ozone, *J. Atmos Chem*.
Stauffer, R. M., et al. (2015), Bay breeze influence on surface ozone at Edgewood, MD during July 2011, *Journal of Atmospheric Chemistry*, *72*(3-4), 335-353.
Stevenson, D. S., Dentener, F. J., Schultz, M. G., Ellingsen, K., van Noije, T. P. C., Wild, O., . . . Szopa, S. (2006). Multimodel ensemble simulations of present-day and near-

future tropospheric ozone. *J. Geophys. Res.-Atmos.*, *111*(D8). doi:10.1029/2005JD006338

Tang, Y., Carmichael, G. R., Thongboonchoo, N., Chai, T., Horowitz, L. W., Pierce, R. B., . . . Avery, M. A. (2007). Influence of lateral and top boundary conditions on regional air quality prediction: A multiscale study coupling regional and global chemical transport models. *Journal of Geophysical Research: Atmospheres (1984–2012)*, *112*(D10). Retrieved from http://onlinelibrary.wiley.com/doi/10.1029/2006JD007515/full

Tang, Y., Lee, P., Tsidulko, M., Huang, H.-C., McQueen, J. T., DiMego, G. J., . . . Stajner, I. (2009). The impact of chemical lateral boundary conditions on CMAQ predictions of tropospheric ozone over the continental United States. *Environ. Fluid Mech.*, *9*(1), 43-58. doi:10.1007/s10652-008-9092-5

Tesche, T. W., Morris, R., Tonnesen, G., McNally, D., Boylan, J., & Brewer, P. (2006). CMAQ/CAMx annual 2002 performance evaluation over the eastern US. *Atmospheric Environment*, *40*(26), 4906-4919. Retrieved from http://vigor.wustl.edu/Capita/CapitaReports/071124_DataAssimilation/CMAQ_eval/TTesche_CAMQ_CAMx_EUS Eval.pdf

Tessum, C. W., Hill, J. D., & Marshall, J. D. (2015). Twelve-month, 12 km resolution North American WRF-Chem v3.4 air quality simulation: performance evaluation. *Geosci. Model Dev.*, *8*(4), 957-973. doi:10.5194/gmd-8-957-2015

Thompson, A. M., Stauffer, R. M., Miller, S. K., Martins, D. K., Joseph, E., Weinheimer, A. J., & Diskin, G. S. (2014). Ozone profiles in the Baltimore-Washington region (2006 2011): satellite comparisons and DISCOVER-AQ observations. *Journal of Atmospheric Chemistry*, 1-30. Retrieved from http://link.springer.com/article/10.1007/s10874-014-9283-z

Thornton, J. A., Wooldridge, P. J., Cohen, R. C., Martinez, M., Harder, H., Brune, W. H., . . . Fried, A. (2002). Ozone production rates as a function of NOx abundances and HOx production rates in the Nashville urban plume. *J. Geophys. Res.-Atmos.*, *107*(D12). doi:10.1029/2001JD000932

Trainer, M., Hsie, E. Y., McKeen, S. A., Tallamraju, R., Parrish, D. D., Fehsenfeld, F. C., & Liu, S. C. (1987). Impact of natural hydrocarbons on hydroxyl and peroxy-radicals at a remote site. *J. Geophys. Res.-Atmos.*, *92*(D10), 11879-11894.

Trainer, M., Parrish, D. D., Buhr, M. P., Norton, R. B., Fehsenfeld, F. C., Anlauf, K. G., . . . Roberts, J. M. (1993). Correlation of ozone with NOy in photochemically aged air. *Journal of Geophysical Research: Atmospheres (1984–2012)*, *98*(D2), 2917-2925. Retrieved from http://onlinelibrary.wiley.com/doi/10.1029/92JD01910/full

Turnipseed, A. A., Huey, L. G., Nemitz, E., Stickel, R., Higgs, J., Tanner, D. J., . . . Guenther, A. (2006). Eddy covariance fluxes of peroxyacetyl nitrates (PANs) and NOy to a coniferous forest. *Journal of geophysical research*, *111*(D9), D09304. Retrieved from http://www.cee.mtu.edu/~reh/papers/pubs/non_Honrath/turnipseed06_2005JD006631.pdf

Tzortziou, M., Herman, J. R., Cede, A., & Loughner…, C. P. (2013). Spatial and temporal variability of ozone and nitrogen dioxide over a major urban estuarine

ecosystem. *Journal of Atmospheric …*. Retrieved from http://link.springer.com/article/10.1007/s10874-013-9255-8

Val Martin, M., Honrath, R. E., Owen, R. C., Pfister, G., Fialho, P., & Barata, F. (2006). Significant enhancements of nitrogen oxides, black carbon, and ozone in the North Atlantic lower free troposphere resulting from North American boreal wildfires. *J. Geophys. Res.-Atmos.*, *111*(D23). doi:10.1029/2006JD007530

Vingarzan, R. (2004). A review of surface ozone background levels and trends. *Atmospheric Environment*, *38*(21), 3431-3442. Retrieved from http://www.cee.mtu.edu/~reh/papers/pubs/non_Honrath/vingarzan04.pdf

Vinken, G. C. M., Boersma, K. F., Maasakkers, J. D., Adon, M., & Martin, R. V. (2014). Worldwide biogenic soil NOx emissions inferred from OMI NO2 observations. *Atmos. Chem. Phys.*, *14*(18), 10363-10381. doi:10.5194/acp-14-10363-2014

Wang, Y. H., Jacob, D. J., & Logan, J. A. (1998). Global simulation of tropospheric O-3-NOx-hydrocarbon chemistry 3. Origin of tropospheric ozone and effects of nonmethane hydrocarbons. *J. Geophys. Res.-Atmos.*, *103*(D9), 10757-10767.

Warneke, C., de Gouw, J. A., Del Negro, L., Brioude, J., McKeen, S., Stark, H., . . . Hanks, A. T. C. (2010). Biogenic emission measurement and inventories determination of biogenic emissions in the eastern United States and Texas and comparison with biogenic emission inventories. *J. Geophys. Res.-Atmos.*, *115*. doi:10.1029/2009JD012445

Wentworth, G. (2015). Impact of lake breezes on ozone and nitrgoen oxides in the Greater Toronto Area. *Atmospheric Environment*, *109*, 52-60.

Wesely, M. L., & Hicks, B. B. (2000). A review of the current status of knowledge on dry deposition. *Atmospheric Environment*, *34*(12), 2261-2282. Retrieved from http://www.cee.mtu.edu/~reh/papers/pubs/non_Honrath/wesely00.pdf

West, J. J., Szopa, S., & Hauglustaine, D. A. (2007). Human mortality effects of future concentrations of tropospheric ozone. *C. R. Geosci.*, *339*(11-12), 775-783. doi:10.1016/j.crte.2007.08.005

Wu, Z., Wang, X., Turnipseed, A. A., Chen, F., Zhang, L., Guenther, A. B., . . . Xia, B. (2012). Evaluation and improvements of two community models in simulating dry deposition velocities for peroxyacetyl nitrate (PAN) over a coniferous forest. *Journal of Geophysical Research: Atmospheres (1984–2012)*, *117*(D4). Retrieved from http://www.researchgate.net/publication/224773905_Evaluation_and_improvements_of_two_community_models_in_simulating_dry_deposition_velocities_for_peroxyacetyl_nitrate_(PAN)_over_a_coniferous_forest/file/9fcfd4fa08283764f8.pdf

Yarwood, G., Rao, S., Yocke, M., & Whitten, G. (2005). Updates to the Carbon Bond chemical mechanism: CB05. *Final report to the US EPA, RT-0400675*, *8*.

Yarwood, G., Jung, J., Whitten, G. Z., Heo, G., Mellberg, J., & Estes, M. (2010). *Updates to the Carbon Bond mechanism for version 6 (CB6)*.

Yegorova, E. A., Allen, D. J., Loughner, C. P., Pickering, K. E., & Dickerson, R. R. (2011). Characterization of an eastern US severe air pollution episode using WRF/Chem. *J Geophys Res-atmos*, *116*, ARTN D17306. doi:10.1029/2010JD015054

Yu, S., Mathur, R., Pleim, J., Pouliot, G., Wong, D., Eder, B., . . . Rao, S. T. (2012). Comparative evaluation of the impact of WRF/NMM and WRF/ARW meteorology

on CMAQ simulations for PM2. 5 and its related precursors during the 2006 TexAQS/GoMACCS study. *Atmos. Chem. Phys*, *12*, 4091-4106. Retrieved from http://www.atmos-chem-phys.net/12/4091/2012/acp-12-4091-2012.pdf

Zhang, H., Wu, S., Huang, Y., & Wang, Y. (2014). Effects of stratospheric ozone recovery on photochemistry and ozone air quality in the troposphere. *Atmos. Chem. Phys.*, *14*(8), 4079-4086. doi:10.5194/acp-14-4079-2014

Zhang, L., Jacob, D. J., Boersma, K. F., Jaffe, D. A., Olson, J. R., Bowman, K. W., . . . Weinheimer, A. J. (2008). Transpacific transport of ozone pollution and the effect of recent Asian emission increases on air quality in North America: an integrated analysis using satellite, aircraft, ozonesonde, and surface observations. *Atmos. Chem. Phys.*, *8*(20), 6117-6136.

Zhang, L., Jacob, D. J., Yue, X., Downey, N. V., Wood, D. A., & Blewitt, D. (2014). Sources contributing to background surface ozone in the US Intermountain West. *Atmos. Chem. Phys.*, *14*(11), 5295-5309. doi:10.5194/acp-14-5295-2014

Zhang, L., Jacob, D. J., Downey, N. V., Wood, D. A., Blewitt, D., Carouge, C. C., . . . Wang, Y. (2011). Improved estimate of the policy-relevant background ozone in the United States using the GEOS-Chem global model with 1/2 degrees x 2/3 degrees horizontal resolution over North America. *Atmos. Environ.*, *45*(37), 6769-6776. doi:10.1016/j.atmosenv.2011.07.054

Zhou, W., Cohan, D. S., & Napelenok, S. L. (2013). Reconciling NOx emissions reductions and ozone trends in the US, 2002-2006. *Atmos. Environ.*, *70*, 236-244. doi:10.1016/j.atmosenv.2012.12.038